

ADSORPTION PROPERTIES OF METAHALLOYSITE

A Thesis Presented for the Degree of Doctor of Philosophy
in Chemistry in the University of Canterbury, Christchurch
New Zealand

by

B. L. J. JACKSON

1971

ACKNOWLEDGEMENTS

I would like to express my thanks to Dr. A. Metcalfe for supervising this Ph.D. project. I am indebted to him for his advice and encouragement. I would also like to thank Dr. R.F.C. Claridge who acted as supervisor whilst Dr. Metcalfe was in Canada on Sabbatical leave. Further thanks are due to the technical staff of the Chemistry Department for their considerable aid in design and construction of apparatus.

The receipt of clay samples, D.T.A. curves and electron micrographs from the Pottery and Ceramics Research Association is acknowledged. The many useful discussions with the staff of this Association were greatly appreciated.

I am especially grateful to my wife and children for accepting my many absences over the past four years and to my wife for her invaluable help in proof-reading and in many other aspects concerned with the completion of this thesis.

I wish also to thank Mrs. L. Gunthorp

for her able typing of the text of this thesis and Miss K. Slocombe for typing the tables. Thanks are also due to Dr. G.J. Churchman for his help in diagram preparation.

The receipt of a Pottery and Ceramics Research Association Fellowship is most gratefully acknowledged.

ABSTRACT

The surface and porous properties of New Zealand metahalloysites, and the manner in which these properties are affected by chemical and physical treatments, have been studied by adsorption methods.

The clay mineral surface has a considerable influence on the nature of the adsorption process, polar water and ethyl chloride molecules giving rise to low pressure hysteresis not observed for the adsorption of nitrogen and argon. Low pressure hysteresis is attributed to structuring effects in the interfacial layer, desorption occurring from a layer more densely packed than during adsorption.

Treatment of the mineral with solutions of metal chlorides altered the specific surface area to a small degree while treatment with trimethylchlorosilane was found to have a considerable effect on the surface properties.

Particle morphology is found to have a significant influence on the effects which take place upon heating metahalloysite, larger changes in specific surface area occurring for material having an elongated particle shape.

Vacuum outgassing at raised temperatures causes small changes only in the specific surface area and pore size

distribution of a metahalloysite prepared by dehydrating an halloysite from TePuke.

Dehydroxylation gave rise mainly to small pores of diameter 30 - 100Å. The surface area changes, which occur as the outgassing temperature is increased, are explained by a combination of three effects, loss of strongly adsorbed water, particle coalescence and dehydroxylation.

Gravimetric water vapour sorption measurements were made on homoionic metahalloysite saturated with the exchange cations Li^+ , Na^+ , K^+ , Rb^+ , Cs^+ , Mg^{2+} , Ca^{2+} and Sr^{2+} . The size and range of the hysteresis loop is found to vary with the nature of the exchangeable ion. The relative effect of the various cations depends upon their respective polarizabilities. Li^+ and Mg^{2+} ions are anomalous in their behaviour, an effect attributed to their small size and consequent high energy of interaction with the mineral surface. This high interaction energy retards the ion hydration below that expected for the high polarizability of these ions.

A molecular adsorption model is advanced

which assumes specific site adsorption, the sites being intimately connected with the exchange cations. The completion of the various stages postulated in the model correspond closely to the points, on Jura-Harkins' plots of the experimental data, at which distinct slope changes occur, and which indicate 'phase' changes in the adsorbed film. Small highly charged ions stabilise a molecular arrangement believed to be similar to the Hendricks-Jefferson 'net' structure. The larger ions disrupt this structure and for these ions a 'phase' change is observed which corresponds with the formation of a closest-packed adsorbed layer.

The proposed adsorption model is essentially the same as that successfully used for the kaolinite-water system. That similar models can be employed to predict the nature of the adsorption of water vapour on both kaolinite and metahalloysite is an indication of the resemblance between the two mineral surfaces.

TABLE OF CONTENTS

	<u>Page</u>
<u>CHAPTER 1</u>	<u>INTRODUCTION</u>
1.1 The Nature of the Mineral	1
1.2 Nomenclature	2
1.3 Structure	2
1.4 Dehydration of Halloysite	3
1.5 Disorder in the Metahalloysite Lattice	4
1.6 Morphology	7
1.7 Rehydration of Metahalloysite	8
1.8 Occurrence	9
1.9 Laboratory Synthesis	11
1.10 General Surface Properties of Kaolin Minerals	11
1.11 Conclusions Sections 1.1 to 1.10	12
1.12 The Texture of Clay Minerals	13
1.13 The Adsorption Properties of Clay Minerals	15
1.14 The Effect of Pretreatments on the Properties of Clay Mineral	25
<u>CHAPTER 2</u>	<u>MATHEMATICAL TREATMENT</u>
	<u>OF ADSORPTION</u>
2.1 Surface Area	29

	<u>Page</u>
2.2 Pore Size Distribution and Pore Structure	45
2.3 De Boer Va/T Plots	56
<u>CHAPTER 3</u>	<u>64</u>
<u>EXPERIMENTAL</u>	
3.1 Preparation of Metahalloysite Samples	64
3.1.a Introduction	64
3.1.b Preparation of Homoionic Metahalloysites	67
3.1.c Preparation of Natural Metahalloysites	73
3.1.d Preparation of Silane-Treated Metahalloysites	74
3.1.e Preparation of Maungaparerua Metahalloysite Samples	76
3.2 Volumetric Determination of Adsorption Isotherms	79
3.2.a Apparatus	79
3.2.b Procedure	86
3.2.c Errors in Volumetric Data	95
3.3 Determination of Water Vapour Adsorption Isotherms	97
3.3.a Apparatus	97
3.3.b Operation	112
3.3.c Equilibrium Time	114
3.3.d Errors in Water Vapour Adsorption Data	115

	<u>Page</u>
3.4 Determination of Cation Exchange Capacity	117
3.4.a The Permanganate Method	117
3.4.b Atomic Absorption Method	119
3.4.c Results	121
3.5 Weight Loss Determinations	123
3.6 Infra Red Spectra	126
3.7 Differential Thermal Analysis Spectra	127
<u>CHAPTER 4</u>	<u>DISCUSSION</u>
	129
4.1 Adsorption of Polar and Non Polar Adsorbates on Metahalloysite	129
4.1.1 General Observations	129
4.1.2 Low Pressure Hysteresis	132
4.2 Adsorption of Non-polar Molecules on Metahalloysite	148
4.2.a The Type II Isotherm	148
4.2.b The Type B Hysteresis Loop	149
4.2.c Reproducibility of the Type B Hysteresis Loop	155
4.3 Weight Loss	157
4.4 The Effect of Pretreatments on the Specific Surface Area and Pore Properties of Metahalloysite	163

	<u>Page</u>
4.4.1.a Maungaparerua Metahalloysite	163
4.4.1.b TePuke Metahalloysite	167
4.4.2 The Effect of Vacuum Outgassing	
Temperature on the Specific Surface	
Area and Pore Properties of TePuke	
Metahalloysite	169
4.4.2.a Introduction	169
4.4.2.b The Specific Surface Area of	
Metahalloysite	171
4.4.2.c The Effect of Heating on the Specific	
Area of Kaolins	173
4.4.2.d The Surface Area of Homobitic TePuke	
Metahalloysite in Relation to	
Outgassing Temperature	175
4.4.2.e The Specific Surface Area of 'Natural'	
TePuke Metahalloysite in Relation	
to Outgassing Temperature	180
4.4.3 The Pore Size Distribution of	
Clay Minerals	185
4.4.3.a Introduction	185
4.4.3.b The Pore Size Distribution of TePuke	
Metahalloysite	188

	<u>Page</u>
4.4.3.c Pore Size Distribution from Water Desorption Data	200
4.5 The Adsorption of Water Vapour on Homoionic Metahalloysite	205
4.5.1 Introduction	205
4.5.2 Literature Results for the Metahalloysite-Water Vapour System	210
4.5.3 Water Vapour Adsorption on Homoionic TePuke Metahalloysite	212
4.5.4 Model for the Adsorption of Water Vapour on Metahalloysite	220
4.5.5 Conclusion to Section 4.5	232
REFERENCES	234
APPENDIX I Platinum Resistance Element Calibration Data	262
APPENDIX II Prediction of Amounts Adsorbed According to the Proposed Model for Water Vapour Adsorption	264
APPENDIX III Computer Programme for Calculation of Isotherm Data	268
APPENDIX IV Water Vapour Isotherm Data	272

CHAPTER 1 : INTRODUCTION

1.1. The Nature of the Mineral

Halloysite, a clay mineral of the kaolin family, which also contains kaolinite, dickite and nacrite, is named after Omaluis d'Halloy, the discoverer of the first recognized deposit of this material at Angleur, Belgium. The mineral exists in two forms, one more hydrous than the other. At first the less hydrated species was considered to be kaolinite (1), but Mehmel (2) later recognised it as a distinct mineral and since this time there has been considerable argument concerning its relationship to the other kaolin minerals. The chemical composition of the less hydrous form proved to be identical to that of kaolinite while the empirical formula describing the hydrated mineral required an additional two water molecules (2,3). Halloysite, or its dehydrated form, is often found to have a distinctive tubular morphology (7,69,39,70) quite different from the tabular forms characteristic of the other kaolin minerals.

1.2 Nomenclature

There has been a prolonged controversy (4) regarding the choice of names for the two hydration states of the mineral but in this study use is made of the nomenclature suggested by Mehmel (2), a choice which is in agreement with the largest proportion of investigators in the field of clay mineral research (5). Therefore the hydrated mineral, with ideal stoichiometry $\text{Al}_2\text{Si}_2\text{O}_5(\text{OH})_4 \cdot 2\text{H}_2\text{O}$, and the dehydrated form, with ideal stoichiometry $\text{Al}_2\text{Si}_2\text{O}_5(\text{OH})_4$, are respectively referred to as halloysite and metahalloysite.

1.3 Structure

Metahalloysite and halloysite are placed in the kaolin group because the sheet units, making up their crystal structures, are normal kaolinite layers, common to all members of the group. Each kaolinite unit layer is composed of a sheet of silica tetrahedra and an alumina octahedral sheet intimately connected by oxygen atoms at the apices of the silica tetrahedra (figure 1). The members of the kaolin

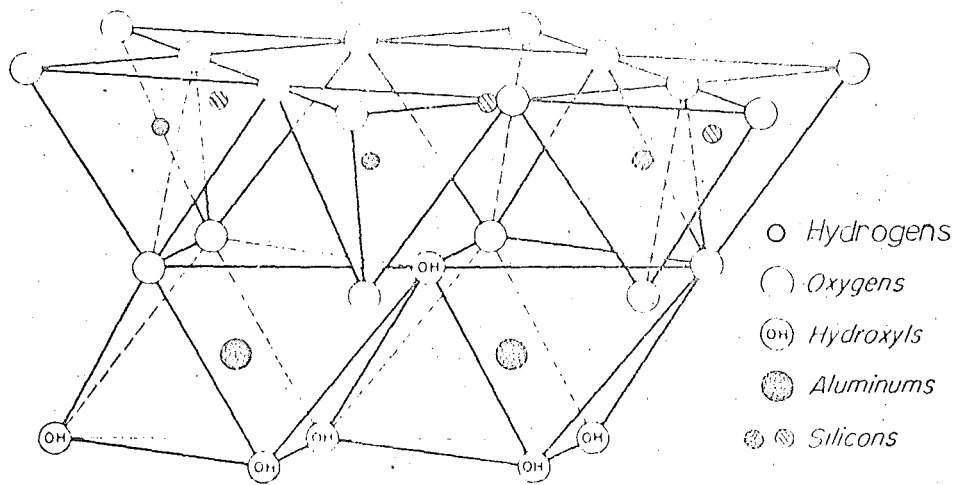
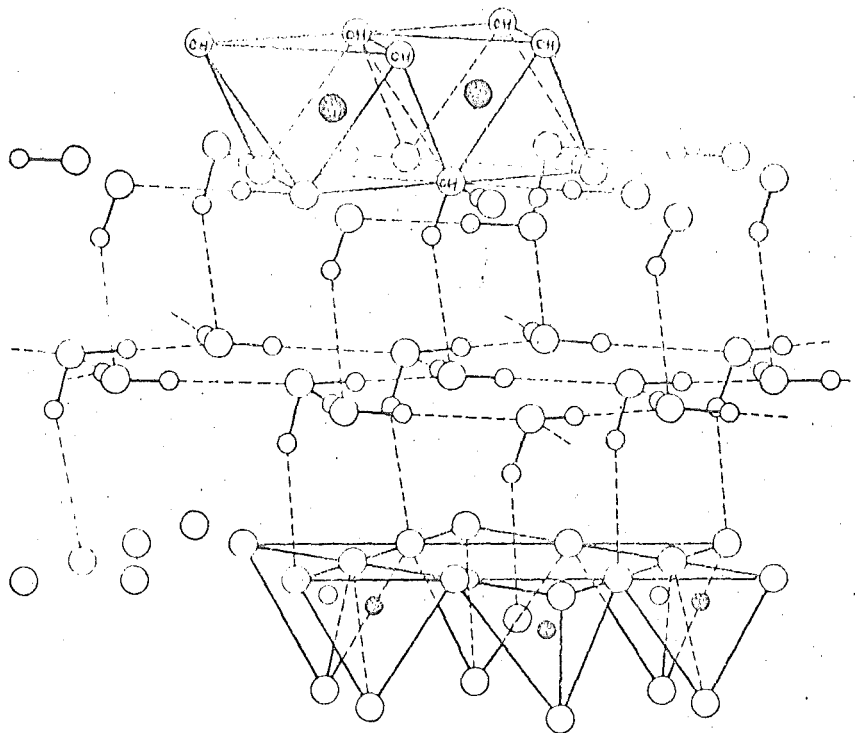


Fig. 1. Layer structure of kaolinite, after Gruner (338).



Legend as in Fig.1.

Fig. 2. Halloysite structure showing a single layer of water molecules, after Hendricks & Jefferson (8).

group differ only in the way the unit layers are stacked with respect to each other. Halloysite is a unique member of the group as it alone has a single layer of water molecules, thought to be arranged in a definite configuration (8)(figure 2), forming hydrogen bond 'bridges' between the kaolinite unit layers (6,7).

1.4 Dehydration of Halloysite

Interlayer water is easily and irreversibly lost from halloysite (7,9,98,65,66) resulting in the formation of metahalloysite and a decrease in the X-ray basal spacing from 10.1\AA to about 7.2\AA . Initiation of the dehydration process is brought about by a reduction of the relative humidity below a limiting value which depends on the origin of the mineral (10,11,12), possibly explained by different drying histories for the various deposits (10). The process, occurring by a mechanism of interstratification (13), is not complete until zero relative humidity conditions are reached (10). Temperatures up to 400°C are necessary (11,17) to remove the last, firmly bound remnants of interlayer water and to reduce the X-ray

basal spacing to the value characteristic of kaolinite, namely 7.14\AA (4).

1.5 Disorder in the Metahalloysite Lattice

Although kaolinite, the parent member of the kaolin group of minerals, and metahalloysite are very closely related on the basis of stoichiometry and structure, they have, since the time of Mehmel (2,3), generally been considered as distinct minerals. Only one technique, that of single crystal electron diffraction, is able to show a crystallographic distinction between the two minerals (22), all other methods, including X-ray diffraction (18,19,37), differential thermal analysis (4), infra-red spectroscopy (22) and solubility determinations (4,59,64), merely serving to indicate the degree of order or disorder of the crystal structure. Lack of order in the stacking of the unit layers of metahalloysite is indicated by the diffuseness and reduced number of reflections observed in the X-ray diffraction pattern for the mineral (19,37), the loss of lattice hydroxyls on heating occurring at temperatures $60-80^{\circ}\text{C}$ lower

than for kaolinites (52), a lower energy of activation for the dehydroxylation process (55 Kc/mole compared with 65 Kc/mole for kaolinite) (62), fewer broader adsorption bands in the infra-red spectrum (22) and higher solubility in acid (4) and basic (4,59,64) solutions. Lower structural perfection could be due to fewer hydroxyl groups on the outer surfaces of the layers resulting in reduced interlayer hydrogen bonding (63). It may also result from lattice distortions caused by the presence of residual water molecules between the layers or isomorphous replacements within the lattice. Lattice distortions and reduced interlayer hydrogen bonding both contribute to reduced crystal thickness and therefore smaller particle size and increased specific surface area, properties which alone might explain the observed thermal effects, the high solubility and high cation exchange capacity of metahalloysite in comparison with kaolinite. It is known (4) that solubility and cation exchange capacity increase and that the temperature of dehydroxylation decreases as the particle size and degree of crystal perfection of a kaolin mineral decrease.

Single crystal electron diffraction studies (20-25) showed that metahalloysites exhibit a degree of three dimensional structural order higher than that previously inferred from X-ray and other data. On the basis of such studies, Chukrov and Zvyagin (22) conclude that metahalloysites are structurally different from kaolinites and that they cannot be regarded as end members of the kaolinite series, the two series converging only at the extremes of structural randomness. The observed intensity data best fitted a monoclinic model, unlike the triclinic structure of kaolinite, while the diffraction patterns indicated structural order in the ac plane and random layer displacements in the b axis direction limited to multiples of $b/3$, unlike the ordered structure of kaolinite.

It is generally found that any differences between kaolinite and metahalloysite, in their spectral properties, are reduced by heating the latter mineral (53), resulting in the loss of small amounts of residual interlayer water and a concomitant increase in the structural order.

1.6 Morphology

Until recently it was generally accepted that an elongated tubular morphology for a kaolin mineral was indicative of the presence of halloysite or metahalloysite. It is now concluded (37) however, that these minerals exist in a sequence of morphological forms including tabular (34-36,38), lath-like and tubular, the cross-section of the last often being circular (7,69,39) or polygonal (7,22). While there are no definite reports of other kaolin minerals having natural tubular particles, some have been artificially prepared in the laboratory (31-33).

Various theories have been advanced to explain the circular cross-section often observed for halloysite particles and which has been quoted (27,51) as explaining the diffuse X-ray diffraction patterns observed for this mineral. Layer curvature could result from interlayer misfit due to the length discrepancy between the upper and lower plane cell dimensions of the halloysite unit layers (39), a condition which would be enhanced by the presence of interlayer water (40), or from unbalanced stresses within the unit

layers (41). Chukrov and Zvyagin (22), and Pundsack (42) consider that natural halloysite crystals are formed as solid elongated crystallites of polygonal cross-section with well developed ring fracture zones, and that hollow tubes are produced as artifacts of secondary processes, such as drying or agitation, allowing the expulsion of the inner portions of crystallites.

1.7 Rehydration of Metahalloysite

Although the halloysite to metahalloysite conversion is not appreciably reversed by a change in the physical conditions (2,3,65,66,98), it is possible to replace the interlayer water by way of an intermediate complex (14-16), washing the complex with water resulting in the formation of halloysite. It was found that interlayer penetration was achieved with polar complexing molecules only (14) and that heating the metahalloysite reduced the number of compounds giving penetration. It appears, from this evidence, that the retention of small amounts of interlayer water facilitates penetration by the molecules or ions of the

complexing agent. Kaolinites also form interlayer complexes, but with fewer compounds than metahalloysites and generally much less water is retained on washing than observed for metahalloysites (55,56). Range et al (71) have based a classification system on the different intercalation properties of the two minerals.

1.8 Occurrence

Grim (4) recognized halloysite as a rare component in weathering products and considered that peculiar conditions were necessary for its formation. A current literature survey (43) clearly indicates however, that this mineral is far more often the primary alteration product of recent chemical weathering under various climatic conditions, of a wide range of parent rocks, than is kaolinite. Occurrences of halloysite are less common, while those of kaolinites are more common with increasing depth, and therefore greater age, of deposits, observations which imply that halloysites change into kaolinites (43). It must be pointed out however, that if some of the kaolinites proved to be metahalloysites, on testing with the new

electron diffraction technique, then the above implication does not apply.

The frequent coexistence of halloysite with considerable portions of a material, known as allophane, which is amorphous to X-rays, has prompted many workers (17,46,47,60,61) to consider halloysite to be a transition form from allophane. Aomine and Wada (50) believe there is a continuous chemical transition series from allophane through halloysite to kaolinite. Because of its frequent occurrence, and since some has been shown to have considerable crystalline organization (50,52), allophanous material can be viewed as an inherent part of the clay mineral with which it is found (95). It is possible that allophane is simply very small particles of the clay mineral itself, an idea supported by grinding studies (98,101) which show a gradual break-down of crystal structure as grinding continues, with an increase in the amount of material amorphous to X-rays.

1.9 Laboratory Synthesis

Attempts at the laboratory synthesis of halloysite have been largely unsuccessful, the usual product being the more ordered kaolinite. One group (48,49) however, produced lath-shaped material which, although amorphous to X-rays, had electron diffraction patterns resembling those of halloysites, and Parham (43), by continuous leaching of feldspathic materials, produced a secondary product morphologically identical to that formed by natural weathering of identical feldspars, namely halloysite.

1.10 General Surface Properties of Kaolin Minerals

One of the main characteristics of clay minerals is the development of electrically charged particles of high surface area (67,68). Charged particles result from the isomorphous replacement of aluminiums or silicons, within the mineral lattice, by ions of lower valence. The resulting charges must be satisfied by the adsorption of the required amount of cations, which if adsorbed in an exchangeable state give rise to the cation exchange property of the mineral.

High specific surface area (m^2/g) is mainly a result of the small particle sizes observed for clay minerals but may be considerably increased by a well developed porosity.

As the kaolinite unit layer has one basal surface which is predominantly oxidic and the other mainly hydroxylic, it is reasonable to assume that particles of kaolin minerals have one face of each type, together with an indeterminate amount of edge area at which the nature of the surface is more complex.

Many physical and chemical treatments can considerably alter the surface nature of a clay mineral and make any rationalisation of the results of subsequent experiments, in terms of the natural mineral, extremely difficult. Some of the many treatments used in sample preparation, and their effects, are considered in a following section of this thesis.

1.11 Conclusions Sections 1.1 to 1.10

Although a distinct structural difference has been shown to exist between the kaolinite and

metahalloysite series of minerals, it is nevertheless reasonable to conclude that metahalloysites can be regarded as disordered kaolinites, at least in terms of chemical and surface properties. Support for this conclusion is found in the dissolution studies of Hughes and Foster (64), and in the X-ray diffraction data of Brindley et al (37). These studies reveal the existence of a continuous series of minerals, displaying increasing degrees of lattice disorder, between kaolinite and metahalloysite. The surface nature of metahalloysite is therefore expected to be largely similar to that of kaolinite, although, in view of the disordered structure of the former mineral, increased isomorphous replacements, cation exchange capacity, lattice vacancies and resultant surface imperfections are likely to be present.

1.12 The Texture of Clay Minerals

The most important quantities which describe the texture of a substance include, particle size, morphology, specific surface area and pore

volume, size and shape. Because of the small size of clay mineral particles, the determination of the first two parameters generally requires the use of electron microscopic techniques. A particle size distribution can be obtained for a sample by sedimentation procedures which, for the smaller size fractions of clay minerals, often necessitate centrifugation. However, the application of Stokes' Law requires the assumption of spherical particles and therefore, when applied to clay particles, which are non-spherical, is not expected to yield physically meaningful particle size fractions. Specific surface area and pore properties are, with certain qualifications and limitations dealt with in succeeding sections, amenable to examination by the low temperature physical adsorption of gases or vapours.

The values of the textural parameters, particularly particle size and specific surface area, are a reflection of the degree of perfection (or disorder) associated with the crystal structure of a mineral. It has been shown (73), for a

series of kaolinites and metahalloysites, that the greater the structural disorder the smaller the average particle size and the higher the specific surface area and adsorption values observed for the mineral.

1.13 The Adsorption Properties of Clay Minerals

For those systems in which no chemical reaction occurs the interaction of molecules with the surfaces of clay minerals takes place by a combination of the classical ionic, dipolar and dispersion forces. Which of these predominates in a particular system depends upon the nature of the mineral and adsorbate, and upon the pressure and temperature of the adsorbate in the vapour phase.

Generally an arbitrary distinction between physical adsorption and chemisorption is made at a heat of adsorption of 10 kcal/mole. Molecules having a permanent dipole however, may interact strongly with the electrostatic field at the surface of an ionic or polar surface, such that the field-dipole interaction is considerably larger than the

the van der Waals interaction. In these cases heat of adsorption values of 10 to 15 kcal/mole adsorbed are not uncommon, but these should not be identified with chemisorption unless further evidence indicating chemical reaction is available.

Ideally on a homogeneous surface the heat of adsorption should be constant for all fractions of surface coverage θ . The exposed surfaces of real materials however, such as clay minerals, are not energetically homogeneous. Variations in the adsorption site energy may arise from local charge imbalances, caused by isomorphous replacement of lattice ions by ions of lower charge, from the ions adsorbed to neutralise these imbalances, and from other centres of stray forces such as at the crystal edges or at crevices, faults, defects or lattice vacancies. Surface heterogeneity is manifest by a high heat of adsorption at low surface coverage, decreasing as the fraction of surface covered increases.

Various primary properties known to affect the adsorption characteristics of a clay mineral include structure, texture, cation exchange capacity,

exchangeable cation, impurities, and water content. It is generally acknowledged (72,129) that the adsorption properties of a pure clay mineral are in the main determined by its structure and specific surface area while the exchange cations cause secondary effects only. The extent of physisorption of non-polar molecules on clay minerals is entirely dependent on the area and accessibility of the solid surface and therefore, as is discussed in later sections, can be used to determine the surface area and the characteristics of the pore systems of minerals. Physical adsorption of polar molecules on clay minerals, while often dependent on the external surface, is also strongly affected by many of the other primary clay mineral properties. The effects of some of these primary properties on clay mineral adsorption are now considered in some detail as are the effects of physical and chemical pretreatments on the primary properties.

1.13.a Structure

That the structure of a clay mineral

has considerable effect on its adsorption properties is clearly illustrated by a comparison of the two-layer or non-expanding, kaolin minerals and the three-layer or expanding, montmorillonite minerals. In a crystal of the two-layer minerals the individual sheets, which present one hydroxyl and one oxygen covered face, are hydrogen bonded together and, under normal conditions, adsorbate molecules do not penetrate the sheet system, adsorption being limited to the particle surfaces. In certain circumstances however, with some polar molecules, penetration can occur with the formation of an interlayer complex (14-16,55,56). The adsorption of non-polar molecules on three-layer minerals is also limited to the particle surfaces, but the adsorption process for polar adsorbates on the expanding minerals is complicated by interlayer penetration. Such penetration is facilitated by the much weaker interlayer forces which result between the oxygen groups present on both faces of the individual mineral sheets.

1.13.b Cation Exchange Capacity

The property of cation exchange is exhibited to a greater or lesser extent by all clay minerals and is a result of cations, adsorbed to neutralise local charge imbalances, being retained in an exchangeable state. Sites for the adsorption of exchange cations can arise in three ways, isomorphous replacement, breaking of bonds, and by ionization of hydroxyl groups. The permanent lattice charge, resulting from isomorphous substitutions within the lattice, is generally considered (81) to be of much lower magnitude for kaolins than for other clay minerals. Some workers (92,116,117,127) however interpret their adsorption results in terms of the exchange cations residing on the basal surfaces of kaolin minerals and indeed only one silicon in four hundred replaced by aluminium would result in an exchange capacity of 2 meq/100gm (82). Such small amounts of replacement, difficult to detect analytically, could therefore contribute significantly to the low exchange capacity (1-10meq/100gm) observed for kaolin minerals. Some kaolins have in fact been

shown to contain isomorphous substitutions (93,119).

Broken bonds are undoubtedly formed at the edges of fractured silica-alumina sheets and could result in unsatisfied valencies balanced either by the adsorption of cations or by chemical reactions (78-80). Protons, ionized from hydroxyl groups exposed on basal planes or at crystal edges, could be replaced by cations and thus contribute to the exchange capacity.

Approximately linear relationships between specific surface area and exchange capacity have been found for kaolinite (77) and for kaolinites and metahalloysites (73), which indicates that broken bonds or hydroxyl ionization are the major contributors to the exchange capacity of these minerals. If isomorphous replacement was the sole cause of the exchange property no such relationship would be expected. Dry or wet grinding of kaolin minerals is found (105) to substantially increase their cation exchange capacities, presumably due to an increase in the number of broken bonds.

Metahalloysites are almost invariably

found to have much larger specific surface areas (76,29,128) and somewhat higher cation exchange capacities (51,76,84-86) than kaolinites, not an unexpected result considering the degree of disorder generally associated with the halloysite structure.

Various methods of determining the exchange capacity of minerals often yield quite different values for the one mineral (91), the results quoted (4,84,74) for halloysite, for example, ranging from 9 to 50 meq/100gm, although the high values may be due to the formation of interlayer complexes with the exchange agent.

Although it is possible that lattice charge imbalances contribute more to ion exchange in halloysite than in kaolinite, the evidence for one halloysite (84) indicates the absence of isomorphous substitutions and also that there are no exchangeable interlayer cations.

The exchange cations associated with the clay mineral are expected to have a small effect only on the adsorption of non-polar molecules but may exert a considerable influence on the nature of

adsorption of polar molecules. This is particularly true for the adsorption of water vapour which cations may affect in a number of ways: by their effect on the arrangement of the clay particles and on the distance by which they are separated, due to their own tendency to hydrate and by their influence on the structure, thickness and stability of the adsorbed layer. Generally the larger the cation of a given charge associated with a mineral surface the more detrimental it is to the water structure (123) and the lower the total amount of water adsorbed.

Three recent reviews (68,75,83) point out our limited knowledge of the nature of the clay-water interaction. The clay mineral-adsorbed water system is extremely complex and the state of adsorbed layer and the effects of cations on the structure of the layer are uncertain. There is however little doubt that cations do hydrate, particularly if small or highly charged. The tendency of a cation associated with a clay mineral surface to hydrate, is related not only to the size and charge of the ion but also on the strength of the ion-clay bond, the stronger the

bond the less likely is the ion to hydrate.

Exchangeable cations associated with the kaolins cause considerable modifications to the amount of water adsorbed on these minerals (45,115, 116,89,99). The order of a series of ions, placed according to the magnitude of their effect on the adsorption, varies for the different minerals and even for different deposits of the same mineral. This presumably results from the ions residing in different positions on the surfaces of the various mineral samples with a consequent variation in the strength of the ion-clay bond(118).

1.13.c Impurities

The presence of amorphous, organic or other non-clay material in a clay mineral sample can lead to serious misinterpretation of the results of adsorption measurements. Plant or animal remains in a specimen of clay may cause a considerable underestimate of the external surface area of the mineral fraction (94) as may the presence of non-clay materials such as glasses or unweathered parent rock.

The association of allophane with halloysite has already been mentioned. This amorphous material has a considerable range of silica: alumina ratios (124) and great variability of properties. Although of widespread occurrence (57,58) it is rarely considered to be of importance in accounting for the physical properties of clay minerals.

1.13.d Water Content

The adsorption properties of a clay mineral can be markedly affected by its water content, the water being associated either with the structure of the mineral or with the exchange cations. Halloysite and methalloysite^a were found (99,100) to have quite distinct adsorption characters, as were different cation modifications of kaolinite (115) when outgassed at the same temperature, or the same cation modification when outgassed at different temperatures. The latter effect results from the different cations losing their hydration water at different temperatures.

1.14 The Effect of Pretreatments on the Properties
of Clay Minerals

Many physical and chemical treatments, used in the preparation of clay mineral samples for research, cause changes in the primary properties and hence in the adsorption characteristics of the samples. It is therefore necessary to choose very carefully the treatments to which a mineral is subjected.

Generalization of published results is extremely difficult as the various mineral deposits display a high degree of individuality as a result of the mode and environment of formation. This situation is made considerably more difficult by the diversity of pretreatments used, some of which alter the physical form and even the chemical and structural nature of the mineral concerned.

Dry grinding has been found to decrease the particle size of a mineral, increase its surface area and proportion of amorphous material (101,102) and, especially with a kaolin mineral (105), to increase its cation exchange capacity. Extended periods of grinding cause the structural breakdown

of clay minerals (4, Chapter 7) both dry and wet grinding having destructive effects on the halloysite structure (103,104).

Acid treatment of kaolin minerals generally causes dissolution of a proportion of the mineral, increased surface area (106-108,125) and, at least for halloysite, a decreased cation exchange capacity (108). The latter effect results, as has been shown for hydrogen clays (109-111), from the spontaneous migration of lattice aluminium ions to the exchange positions where they replace the hydrogen ions and, due to their small size and high charge, become firmly held. Homoionic clay mineral samples are often prepared by way of the hydrogen clay, but since such a procedure results in a large proportion (about 40%) of the exchange sites being occupied by aluminium ions (112), the conclusions drawn from adsorption studies on the modified minerals must be regarded with a degree of caution.

Use of peroxide solutions of concentrations greater than six per cent, to remove organic matter, may induce exfoliation of crystals,

(94) and even simple salt solutions have been shown to cause partial breakdown of the clay mineral lattice structure (113,114). Alkaline solutions, often utilized in an attempt to remove amorphous material (96), like acid treatments, cause changes in the porosity and an increased specific surface area (120), while neutral citrate-dithionite solution for the removal of iron oxide impurities also appears to remove lattice aluminiums (121).

Heat can markedly affect the adsorption character of a mineral (122). As well as reducing the water content, an increase in the temperature generally reduces the cation exchange capacity, causing some ions to become imbedded into the lattice structure with a corresponding reduction in their effect on the adsorption properties of the mineral. The cation exchange capacity of a metahalloysite decreased from 9.5 to 7.5 meq/100gm when the temperature of the mineral was raised above 70°C (85).

The time of drying (116) and the method of storage (117) were shown to have significant effects on the extent of adsorption of a kaolinite,

slurry aging at 70°C resulting in greater adsorption and vacuo aging lower adsorption than for the initial sample.

CHAPTER 2 : MATHEMATICAL TREATMENT

OF ADSORPTION

2.1 Surface Area

From a critical survey of the literature on methods of surface area determination as applied to solids, it was decided to make use, in this study, of the gas adsorption technique based on the original volumetric method of Brunauer, Emmett and Teller (BET,130). This particular method was chosen for four reasons: its basic simplicity of application, the fact that it is theoretically more soundly based (131,132) than many other methods, because it can be made non-destructive of the sample and finally because it is the most thoroughly tested and documented of all techniques for surface area measurement, exhibiting considerable success when applied to solids in general (133,134). In spite of the development of many new techniques in recent years the BET method remains the most widely used and one of the more accurate methods

available.

When a gas is brought into contact with a solid surface it is almost universally true that molecules impinging on the surface remain for a definite time before re-evaporating. This is the phenomenon of adsorption whereby the concentration of molecules on the surface is higher than in the gas phase. Eventually a dynamic equilibrium is set up between molecules arriving and those evaporating from the surface.

By adopting a kinetic approach to the adsorption phenomenon, similar to that of Langmuir (135) for monolayer adsorption, but extending the theory to allow for the formation of multilayers of adsorbed molecules, Brunauer, Emmett and Teller derived the following expression (equation 1). This equation relates the amount of adsorbed material to the pressure of the adsorbate gas and mathematically predicts the amount of adsorbate required to cover the surface with a single layer.

$$\frac{P/P_0}{n_a (1 - P/P_0)} = \frac{C - 1}{n_m C} \cdot P/P_0 + \frac{1}{n_m C} \quad 1$$

n_a - the number of moles of gas adsorbed at pressure P ,

n_m - the number of moles of adsorbate required to cover the surface with a unimolecular layer,

P_0 - saturated vapour pressure of the adsorbate gas at temperature T ,

C - a constant given by the expression

$$C = \frac{a_1 v_2}{a_2 v_1} e^{(E_1 - L)/RT} \quad 2$$

E_1 - average heat of adsorption of the first layer,

L - heat condensation of bulk adsorbate,

R - gas constant,

T - experimental temperature,

a_1, a_2 - condensation coefficients for molecules of the first and second layers,

v_1, v_2 - oscillation frequencies of the molecules in the first and second layers.

In the derivation of the BET equation

(equation 1) several serious assumptions are made. The basic theory considers an energetically uniform solid surface covered with an array of identical adsorption sites and assumes that adsorption can occur in more than one layer. It also presumes that the adsorption sites in each individual layer are equivalent, that all layers above the first have the properties of the liquid adsorbate with a heat of condensation L , and that the first layer has a higher adsorption heat E_1 . The final assumption made is that an infinite number of layers are adsorbed at saturation, that is when the relative pressure P/P_0 is equal to unity.

It is not proposed to give a full derivation of the BET equation in this thesis and in this regard the reader is referred to the original derivation (136) and to recent books by Gregg and Sing (134) and Flood (199). It is also possible to arrive at the BET equation by a statistical mechanical treatment (138) of the same basic model.

The BET theory is open to criticism (139) on various grounds but mainly due to its over-

simplified model of the adsorption process. Most real surfaces are known to be geometrically and energetically non-uniform, due to faults, dislocations and impurities, and the heat of adsorption decreases as the surface coverage increases, rather than being a constant as postulated in the theory. Only in a few instances, for example graphitized carbon black, is a truly homogeneous surface approximated to.

In such cases however, the BET theory is not particularly successful presumably due to the neglect of lateral interactions between adsorbate molecules. Such interactions can hardly be negligible, particularly at high coverages. The postulate that the heat of adsorption in higher layers is equal to the heat of condensation is inconsistent with the neglect of lateral interactions since the neglect of these interactions requires the adsorption heat to be less than half the heat of liquefaction. Smith and Pierce (140) showed for some adsorbates on graphite that the heat of adsorption of higher layers is not equal to the heat of bulk liquefaction. Whereas the theory assumes that molecules of the n^{th} layer form

localised adsorption sites for molecules of the (n + 1)th layer, it is clear that in a close-packed layer a molecule occupies a central position in a triangular formation of molecules in the underlying layer. Two further questionable postulates are that all layers after the first are energetically equivalent (141,142), when one might expect a gradual reduction in the adsorption potential with distance from the surface, and that at saturation the number of adsorbed layers (n) is infinite when in fact there are many cases for which n is finite at $P/P_0 \approx 1.0$ (140,143-145). Finally the initial assumption of fixed adsorption sites seems unjustifiable in view of the evidence for mobility of physically adsorbed molecules (146).

In order to derive from the BET equation a value for the monolayer capacity n_m , a plot of the relative pressure P/P_0 versus the term $\frac{P/P_0}{n_a (1 - P/P_0)}$ is prepared for several experimental values of the amount adsorbed n_a at different equilibrium pressures P. This plot should be a

straight line of slope $\frac{C - 1}{n_m C}$ and intercept $\frac{1}{n_m C}$, from which data values of n_m and C can be calculated by use of expressions 3 and 4.

$$n_m = (\text{slope} + \text{intercept})^{-1} \quad 3$$

$$C = \frac{\text{slope}}{\text{intercept}} + 1 \quad 4$$

To translate n_m into surface area it is necessary to know or assume a value for the area of surface covered by a single molecule. With this knowledge the specific surface area (m^2/g) is calculated by way of equation 5.

$$\Sigma = \frac{N \times n_m \times \sigma}{m \times 10^{20}} \quad \text{m}^2/\text{g} \quad 5$$

N - Avogadro's number

m - mass of the sample in grams

σ - cross-sectional area of an adsorbate molecule (\AA^2)

The magnitude of σ may be calculated (147, 148) from relationship 6 by assuming a hexagonal close-packed adsorbed layer.

$$\sigma = 1.091 \left(\frac{M}{Nd} \right)^{2/3} \times 10^{16} \text{ \AA}^2 \quad 6$$

d - density of the adsorbate at the temperature at which it is adsorbed.

M - molecular weight of adsorbate

An average heat of adsorption for the first monolayer can be obtained from the BET C constant (expression 2) making the assumption that the pre-exponential expression $\frac{a_1 v_2}{a_2 v_1}$ in equation 2 is equal to unity. Hence

$$E_1 = L + RT \ln C \quad 7$$

The BET equation (equation 1) is most successful (134) when applied to isotherms of types II and IV in the BDDT (149) classification (figure 3). Physical adsorption on nonporous materials most commonly results in an isotherm of type II while type IV isotherms are often observed for similar adsorption on porous or compacted nonporous substances. The equation is not suited (134,140) to the analysis of isotherms of types I and III, and apparently fails for type V (150) isotherms and those containing steps (151,152). Even for type II cases the BET equation

does not predict the course of the isotherm over the entire relative pressure range (134, Chapter 2) and BET plots are usually linear only in the lower part of the range, generally for P/P_0 between 0.05 and 0.35. Analysis of data below this range is considered to give surface areas of doubtful significance (153).

Experimentally determined isotherms of type II (figure 4) often display a central, almost linear portion, the lowest point of which is identified with the completion of a monolayer (131,148) and signified as point B. Solution of equation 1 for the position of this point yields the expression

$$(P/P_0)_B = \frac{1}{1 + \sqrt{C}} \quad 8$$

indicating that point B varies with the C constant of the adsorbate-adsorbent system. For reliable results it is believed (155) that the BET equation should be applied over a range which includes point B, and since C is dependent on the adsorbate-adsorbent system it is expected that the range over which the BET equation should be applied would show a similar dependence.

From a comparison of surface areas derived using the BET method with nitrogen as adsorbate

and the geometrical areas of the same samples it is suggested (134,156) that, at least for nonporous solids, the technique leads to areas which approximate the true areas within a few per cent. Good agreement was also found between microscopic areas and those obtained by krypton adsorption (170).

The choice of adsorbate for the determination of the specific surface area of a solid substance must be very carefully made for several reasons. Firstly it should not chemically react with the solid, nor dissolve in the sample, nor should its adsorption be affected by the lattice of the solid. A marked degree of localised adsorption would mean that the molecular cross-sectional area cannot be calculated successfully from the physical properties of the adsorbate and equation 6. Secondly it should, with a given solid, yield a type II isotherm with a welldefined 'knee' indicating a relatively high BET C constant. Finally the size of the adsorbate molecule should be such that it is not sterically hindered from measuring the entire external surface.

Fig. 3 Brunauer, Deming, Deming, Teller BDDT Isotherm Classification(149)

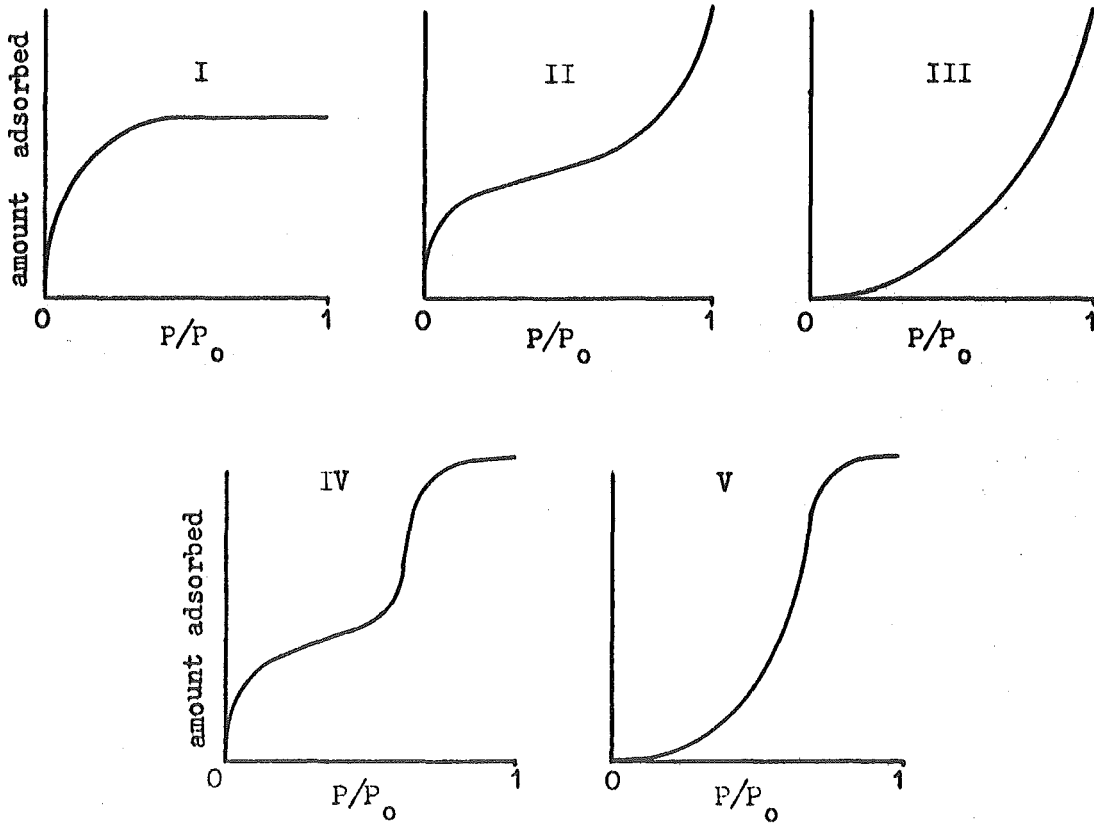
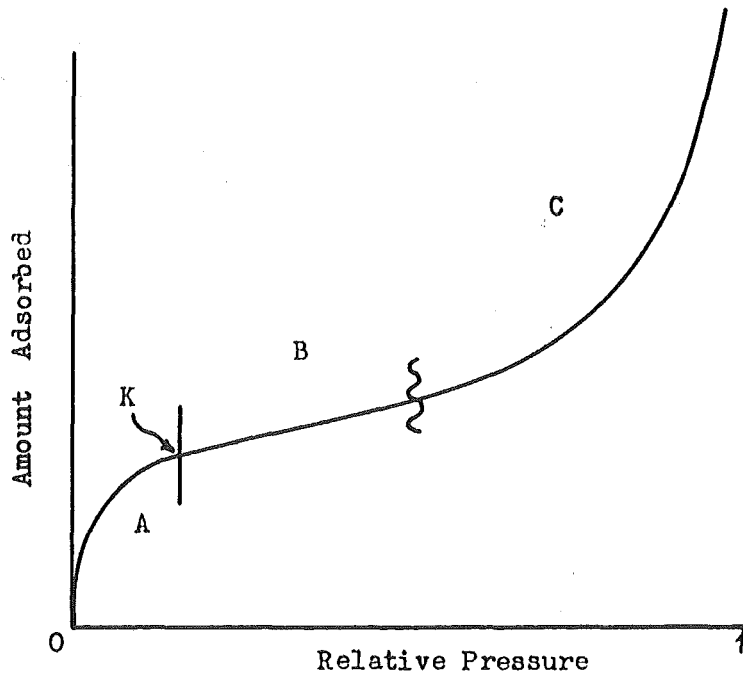


Fig. 4 The Type II Isotherm



Nitrogen, the gas used in the original work (136) and still the most commonly used, approximately fulfills the above requirements for the great majority of adsorbents. However it is known to be chemisorbed on some metals (158) and also for experimental reasons is not suited to the determination of specific surface areas smaller than about one m^2/g . In these instances the use of the noble gases is suggested (134,155,159-161).

There have been a large number of factors discussed in the literature which are believed to affect the general applicability of the BET method. Some of these factors have been mentioned in connection with the choice of adsorbate, others are concerned with effects which, although casting some doubt on the physical meaning of the areas obtained, do not invalidate the method.

It is as yet impossible to assign correct σ values (162,163) and the arbitrary assumption of such values negates the possibility of determining an absolute surface area equal to the total geometrical area. The adsorbate molecular area σ often depends

markedly on the chemical nature of the surface (132, 143, 162-172) due to localised adsorption on specific lattice sites during the formation of the first layer (162, 163, 169, 174, 175), or to other packing differences, the latter possibly arising from the polarization of non-polar adsorbate molecules by ionic surfaces (176, 177). The cross-sectional area of the nitrogen molecule has been given various values including 12.9\AA^2 and 14.2\AA^2 (166), and 20\AA^2 (162, 163). Most of the 6 values for this gas however fall between 14.5 and 19\AA^2 and the most generally accepted value is 16.2\AA^2 , that calculated from equation 6. This last value has proved to be extremely useful for surface determinations of oxides and related substances (178). Equation 6 cannot be applied to all adsorbates and is only suited to molecules which are approximately spherically symmetrical or which have little interaction with the adsorbent surface. For non-spherical molecules a knowledge of the attitude of the adsorbed species is necessary before a choice of σ can be made. A series of normal alcohols, for example, yield a more consistent set of

areas for one sample if perpendicular orientation of the adsorbed molecules is assumed than if a horizontal position is taken (179).

The cross-sectional area of the water molecule has been variously quoted as 8.0\AA^2 (180), 10.4\AA^2 (181), 11.4\AA^2 (182), 12.5\AA^2 (148) and 14.8\AA^2 (183, 184). Such variations are not unexpected in view of the highly specific adsorption characteristics of the water molecule. The σ value for the water molecule often requires large adjustments to give satisfactory agreement between the specific surface areas determined by water and nitrogen adsorption, particularly for different homoionic samples of ^Aclay mineral (45, 122, 186).

In view of the above facts it might be suggested that the noble gases with their spherical molecules should give rise to more acceptable surface areas. Further, the molecules of these gases, unlike nitrogen, lack a permanent moment. Aristov and Kiselev (187) suggested that it is unreasonable to assume a constant σ value for the nitrogen molecule since it is known to have a considerable quadrupole

moment (187-190) and is therefore expected to interact strongly with polar adsorbents. These authors propose that the value of 13.7\AA^2 for the cross-section of the argon molecule should be used as a standard.

The noble gases are not however without their limitations. There is difficulty in deciding upon the physical state of the adsorbed molecules and therefore the values of σ and the saturation pressure P_0 are in doubt (155,172,191). It is also evident that even for these spherical molecules the σ values are dependent on the surface structure of the adsorbent, the values for krypton for example mainly lying in the range 18 to 24\AA^2 (155) although for carbon surfaces 15.45\AA^2 is suggested (152). The calculated values corresponding to the liquid and solid densities are 15.2\AA^2 and 14.0\AA^2 respectively, values which lead to monolayer capacities which differ by about 10% (159,170).

More critical however, for the noble gases, is the observation that BET plots are often curved (192,193), and an effect shown to be influenced

by the porosity and chemical nature of the surface (155) and by the choice of P_0 , particularly when the BET C constant is low (194). Some plots have been determined which have several linear portions (153). Curved BET plots are seldom noted for nitrogen adsorption and those that have been (195,196) were for uniform surfaces, an indication of the neglect of lateral interaction effects between adsorbate molecules in the derivation of the BET equation.

Further factors which may limit the applicability of the BET equation include changes in the adsorbed film (197-200), which cause discontinuities in the adsorption isotherm, and that the monolayer volume is a fairly strong function of temperature (201). Phase changes are not predicted by the BET theory and, if they take place in the normal pressure range over which the BET equation is applied, are expected to give surface areas of doubtful significance (199).

The concept of specific surface area itself is in doubt for substances with pores smaller than about 20\AA radius (202-205) or for adsorbents such as zeolites which have considerable amounts of

completely enclosed surface. It is obvious that surface area values will be too low for pores approaching molecular size since in these cases the adsorbed molecules are covering larger areas of surface than signified by their σ value (206). Use of the BET equation for substances containing such micropores is suspect (207,208) as condensation occurs in small pores in the relative pressure range over which the BET plot is constructed. An extreme case is given by adsorbents which show a molecular sieve effect (209-212), adsorbates of different cross-sectional area yielding different specific surface areas for the same sample (197). Furthermore, slow surface diffusion of adsorbate into pores may result in greatly extended equilibrium times and the experimental difficulty in determining when equilibrium conditions have been reached (197, 213-215). Another experimental difficulty may arise from the effects of thermal exchange which can be appreciable in solid-gas systems and lead to temperature differences between the adsorbent and its coolant bath (193,197,216).

From the considerations outlined above it is clear that the BET procedure cannot be used uncritically, it is not successful when applied to microporous adsorbents, and to derive meaningful surface areas the utmost care must be taken in deciding upon a suitable adsorbate. Due to the inability to determine absolute σ values for molecules adsorbed on different surfaces and due to the many other physical and experimental difficulties, one must conclude that the method has its most powerful use as a tool to compare the surface areas of adsorbents of similar chemical type.

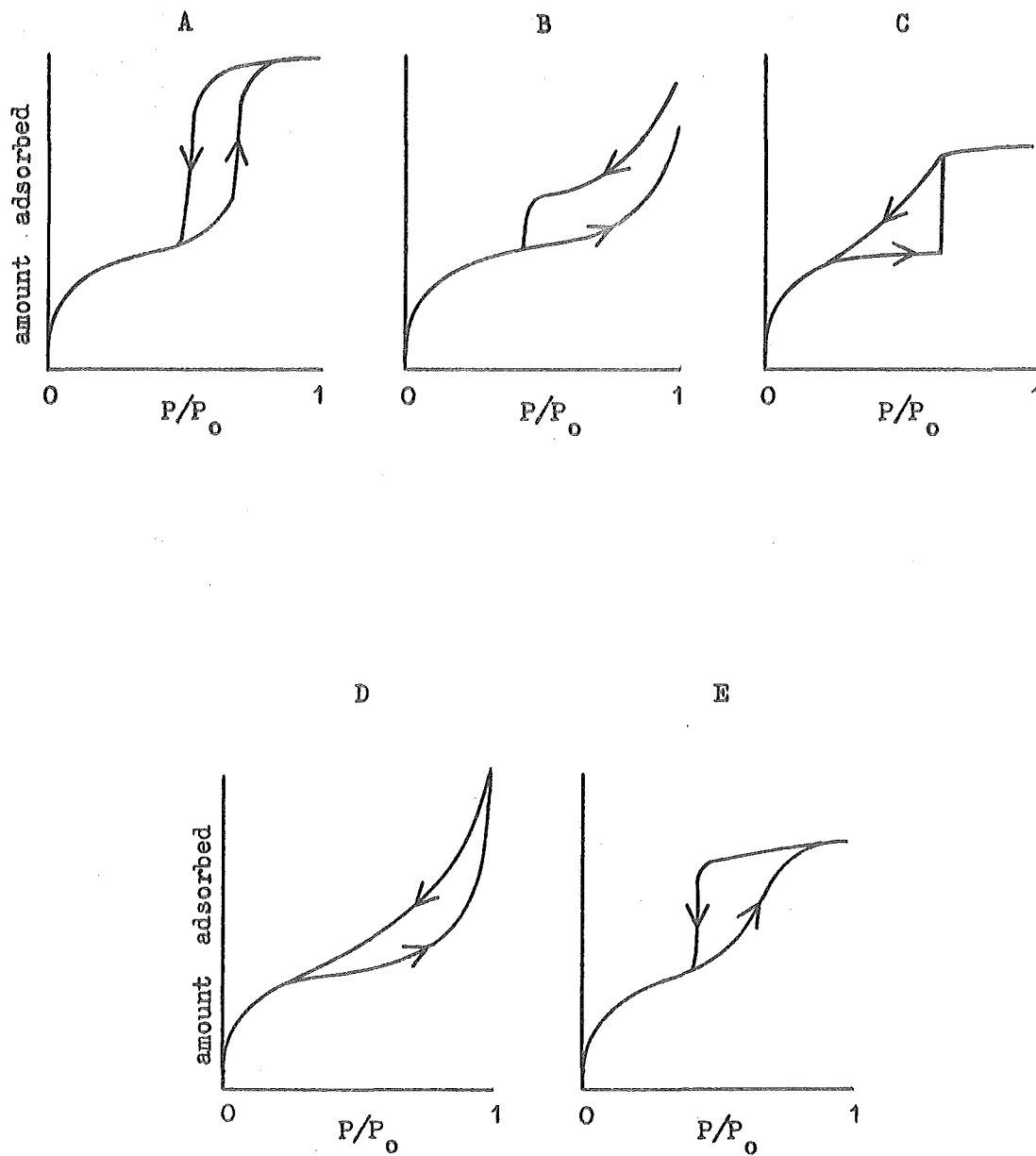
2.2 Pore Size Distribution and Pore Structure

It is possible, in certain cases, from a critical examination of the isotherm for the adsorption of an inert gas on a substance, to obtain values for the total pore volume, average pore size and pore size distribution. It is also possible to gain some insight as to the most probable pore shape. The adsorption of nitrogen at its boiling point has

been found to be a particularly useful system in such studies (217-221) and has been used successfully for clay minerals (218,222). Using the same basic, vacuum volumetric apparatus, as mentioned in the section dealing with surface area determination, a complete adsorption curve is secured by incrementally increasing the total pressure in the sample system. A similar desorption curve is determined by incrementally decreasing the pressure in the system.

A number of isotherm shapes can result from the adsorption of nitrogen on solid samples. The BDDT classification, as already mentioned elsewhere, lists five basic types (figure 3). As well as these there is the possibility that the desorption curve does not retrace the adsorption curve, which results in a hysteresis loop. De Boer (154) recognizes five fundamental hysteresis loop shapes (figure 5) and identifies each of these with certain characteristic pore shapes. Such indications of the pore shape cannot, however, be accepted as definite and other evidence from electron micrography or structural data is required to decide on the most

Fig. 5 De Boer Classification of Hysteresis Loops(154)



probable pore geometry. Further information on pore shape can often be obtained from the 't plot', a plot of volume adsorbed against the statistical thickness of the adsorbed layer on a non-porous solid. These plots are discussed in section 2.3.

Total pore volumes can be determined, with any degree of accuracy, only from isotherms of types I, IV or V of the BDDT classification (figure 3) in which the adsorption isotherm is parallel to the pressure axis as it approaches the saturation vapour pressure (173). Calculation of the pore volume from the total uptake at saturation requires the assumptions that adsorption on the outside surfaces is negligible and that the capillary condensed liquid has the same density as bulk liquid adsorbate. The latter assumption is untenable for adsorbents with very small pores, as evidence (157) indicates that, for nitrogen at least, bulk liquid properties cease to apply in pores with radius less than 18\AA . A further difficulty with small pore adsorbents, which often give rise to types I and IV isotherms, is that the pore volumes differ if measured with molecules of

different dimensions, due to a molecular sieve effect. For isotherms of types II and III the approach to the saturation pressure is asymptotic because of interparticle condensation or a considerable fraction of large pores. In cases such as these no meaningful value of the total amount adsorbed at saturation, and hence total pore volume, can be derived.

The complete range of pore sizes is conveniently classified (205) into three sections on a radius basis: micropores with radii less than about 15\AA , intermediate or transitional pores with radii between 15 and 500\AA and macropores having radii greater than 500\AA .

Pore size distributions for pores of radius $r < 1000\text{\AA}$ are obtained by the application of the Kelvin equation (equation 9) to those isotherms which display a hysteresis loop, the loop being identified with irreversible capillary condensation effects.

$$\log P/P_0 \approx \frac{-2\gamma v}{rRT} \cos \phi \quad 9$$

- P - equilibrium vapour pressure,
 P_0 - saturated vapour pressure at temperature $T(^{\circ}\text{K})$,
 γ - surface tension of adsorbate
 v - molar volume of adsorbate,
 r - pore radius (\AA),
 φ - angle of contact between the liquid and the wall of the pore.

The Kelvin equation indicates that the vapour pressure above a concave interface, as forms in a pore, is less than that above a planar liquid surface. Therefore the vapour above a curved interface of radius r is unstable, with respect to the liquid, if the pressure is greater than predicted by the equation. Thus, as the pressure of the vapour in contact with a porous substance is raised, capillary condensation is expected to occur in pores of increasing radii. If the mechanisms for adsorption and desorption are different, or if the two phenomena are controlled by evaporation from curved interfaces of different radii, a hysteresis loop results in the isotherm.

A number of methods can be used to calculate the pore size distribution from isotherm data (223), all but one of these (185) invoking the use of the Kelvin equation together with an assumed pore shape.

In order to solve the Kelvin equation for values of the pore radius, values are required for the surface tension γ and the molar volume v of the adsorbed material and for the wetting angle ϕ . Because of the absence of suitable data, the assumptions are made that the properties of the adsorbed and capillary condensed material are those of the ordinary bulk liquid, and that the angle of contact is zero. Except for very wide pores, liquids exhibiting a contact angle with the solid surface are not suitable for pore distribution analysis (224). The lower pore size limit to which the equation can be applied is set by these assumptions since the indications are that bulk properties cease to apply for nitrogen at radii less than about 18\AA (225-227). The desorption from smaller pores is governed by a process dependent on the adsorbate and the temperature

and independent of the pore size of the adsorbent (157,225). Fedyaikin (228) has shown that for porous glass the adsorbate surface tension was a function of tube radius down to 200\AA and this is likely to be true for pores smaller than this and for other substances. It is indeed doubtful (229) that the conventional thermodynamic arguments, on which the Kelvin equation is based, can be applied to curved interfaces only a few molecular diameters wide. At present it is usual to accept the physical basis of the equation but to bear in mind its probable quantitative shortcomings.

If capillary condensation was the only effect taking place on adsorption the calculation of pore size distributions would be a simple task. However, the simultaneous presence of adsorbed layers complicates the computations, making it necessary to allow for the total adsorption on the pore walls and also for the influence of adsorption on the equilibrium governing capillary evaporation and capillary condensation (224,230-236). The method of calculation is cumulative, usually beginning at

saturation and proceeding in small decrements of relative pressure, each associated with its own mean pore size as derived from the Kelvin equation. Each succeeding decrement of adsorbed volume after the first, as well as the volume desorbed from the corresponding group of pores, also includes an amount desorbed from the multilayer remaining after emptying all the previous pore ranges. The correction for thinning of the multilayer can be applied if the relationship between multilayer thickness t and the relative pressure P/P_0 is known. It has been shown (203, 237, 238) that, although different calculation methods lead to essentially the same expression, a major source of error lies in the numerical values chosen for t , considerable differences occurring among the $t/\frac{P}{P_0}$ relations used by various workers. Since the method of calculation is invariably cumulative and the errors therefore additive, the distributions in the small pore region will reflect discrepancies arising at much larger pore sizes. An absolute value for the thickness t at each pressure would considerably reduce the errors

involved but, in view of the effect of adsorbent surface on the adsorption of even spherically symmetrical molecules (discussed in section 2.1), it is obvious that absolute values of t , which can be applied to all surfaces, cannot be obtained. Thus it is necessary to resort to the use of a standard set of t values derived from the adsorption on a nonporous adsorbent chemically similar to the porous substance to be examined. As is pointed out in the section dealing with the use of t plots, t curves for nitrogen adsorption are quite similar for almost all nonporous solids and therefore pore size distributions can, with some confidence, be calculated from nitrogen data with the aid of the 'Universal isotherm' (239).

All methods of calculating pore size distributions, except the 'modelless method' (185) invoke an idealised pore model. Even the excepted method requires a pore model to convert pore volume distributions into pore area distributions and thus allow the calculation of the pore surface area for comparison with the surface area as derived by other

methods, such as the BET method (136). It is obvious, however that the pores of a real adsorbent will hardly ever conform entirely to an idealised shape and complete agreement between the cumulative surface area (S_{cum}) and the BET area (S_{BET}), often accepted as confirmation of assumed pore shape, can not be expected in view of the inherent approximate nature of every method of pore distribution calculation (232). The use of simple models has sometimes lead to an erroneous picture of the material (240).

The two most common pore shapes assumed are cylindrical and parallel plate which are usually applied, for calculation purposes, to the desorption branch. The modelless method is considered to give reliable results (241) from the desorption isotherm regardless of the pore shape. The desorption branch is believed (241-243) to represent the thermodynamic equilibrium situation, evaporation being controlled by the curvature of the meniscus which is present in a pore. The formation of the meniscus is delayed along the adsorption curve and therefore it does not represent a true equilibrium condition. The reverse

is the case for a third common pore shape, namely the ink-bottle. For such a pore the evaporation of liquid from the wide body is delayed by the presence of the small neck and for these cases the adsorption branch should be used for calculation (230,242,244). Anderson (223) however reasons that only for slit shaped pores is there a reasonable mechanism for lack of equilibrium on adsorption and that for all other pore shapes the adsorption curve should be used.

Despite the quantitative shortcomings of the resulting pore size distributions it is nevertheless felt (203) that the sorption method gives reasonably reliable information on the volume and specific surface area of transitional pores. The calculations must not however be extended below a pore size range where the assumptions underlying the Kelvin equation can no longer remain valid. The dimensions of such pores are definitely too small for the concepts of a liquid meniscus or of capillary condensation. Broekhoff and de Boer suggest that calculations should be stopped at the relative pressure

corresponding to the point of closure of the hysteresis loop (224) or to the point at which the first deviation from a linear t plot is observed (230). If a significant fraction of micropores exist in a sample then equality between S_{cum} and S_{BET} cannot be expected unless the area of such pores is calculated. The existence of micropores can be shown by a positive intercept on the volume axis of a V_a/t plot (discussed in section 2.3) and a method has been put forward extending the use of the V_a/t plot to the calculation of the distribution and areas of micropores (245,246).

2.3 De Boer V_a/t - Plots

A convenient way of examining the porous nature of a material in the pore radius range less than about 200\AA , is by the graphical comparison of an adsorption isotherm for the test substance with an isotherm for the same adsorbate on a standard non-porous solid. Differences in specific surface area are eliminated by plotting the isotherms in a reduced form, that is V/V_m against the relative pressure, where V_m is the monolayer capacity obtained

from the application of the BET equation, and V the amount adsorbed. The considerations set out in section 2.1, dealing with surface area determination, indicate that, in order to make a valid comparison of isotherms, the test and standard substances should be of similar chemical type. This is necessary to eliminate as far as possible the effects of the nature of the surface on the adsorption characteristics.

Deviations of the test isotherm from the standard may be analyzed in terms of capillary condensation effects (250,259). Concurrence of the curves is an indication that the test substance is non-porous or at least macroporous, while adsorption in excess of that observed for the standard indicates capillary condensation. Small deviations from a complex curve however are often difficult to detect (250) and a method which more clearly reveals the effects of porosity has been developed by Lippens and de Boer (249).

In the Lippens and de Boer method a t -curve is first prepared for a standard non-porous substance. This is directly obtained from the

standard reduced isotherm by choosing a value for the thickness z of an adsorbed monolayer. The thickness t of the adsorbed layer is then given by expression 10.

$$t = z \times \frac{V}{V_m} \quad 10$$

The value of the monolayer thickness z for nitrogen is calculated to be 3.54\AA (219), making the assumptions that the adsorbed liquid has the same density as normal liquid nitrogen and that hexagonal closest-packing occurs in the adsorbed phase. The thickness t is therefore a statistical thickness.

Secondly a curve is drawn which relates the values of the amount adsorbed V_a at various relative pressures on the substance under consideration, with the corresponding values of the statistical thickness from the standard t curve.

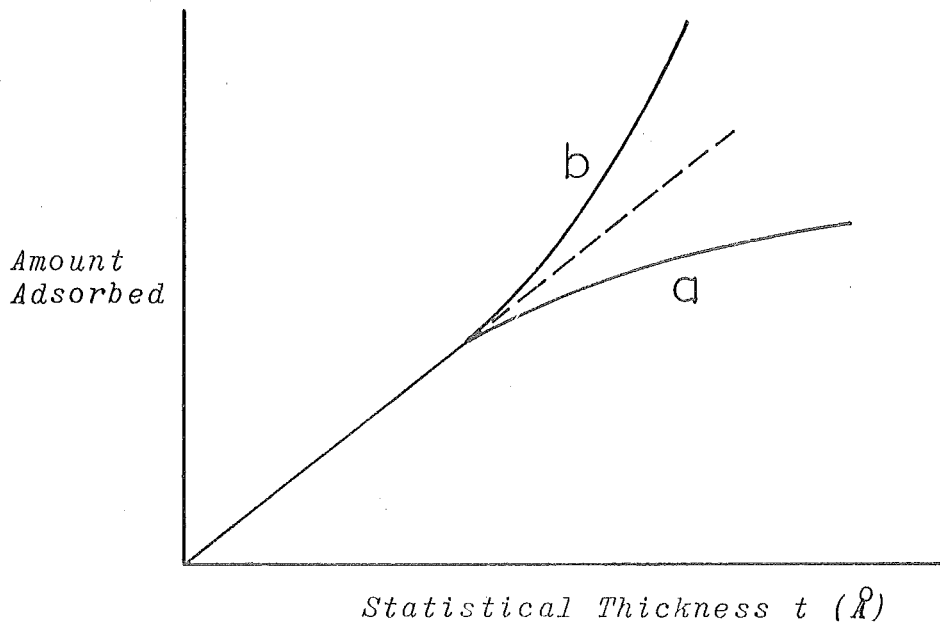
If, on the test material, normal monolayer-multilayer adsorption takes place unaffected by capillary condensation, the V_a/t plot would be a straight line passing through the origin. The slope of this line is related to the specific surface area by the expression

$$S_t \approx 15.47 V_a/t$$

11

Two types of deviation from a linear V_a/t plot are recognized (249).

Fig. 6 Deviations from Linear V_a/t Plots.



1. The slope of the curve increases (figure 6, curve b) if capillary condensation occurs, the material taking up more adsorbate than corresponds to the multilayer on a free surface.

2. A decrease in the slope (figure 6, curve c) occurs if slit-shaped pores become filled, their surface area no longer being available for adsorption. The new slope corresponds to the surface area remaining accessible.

In some cases the V_a/t plot has a positive intercept on the volume axis, the intercepted volume being identified with pore filling in narrow pores.

With the use of V_a/t plots some very striking conclusions have been drawn (219,221,246-249) concerning the pore sizes, shapes and volumes, the onset of capillary condensation and the distribution of surface area among the various pore ranges and the external surface. The method also indicates the presence or absence of reversible condensation in pores of shapes which do not give rise to hysteresis.

Several assumptions are made in the use of the method and in the derivation of quantitative information from the V_a/t plots. Surface coverage is presumed to occur by the same mechanism on all parts of the surface of the material including the micropores.

Substantial evidence has been collected (134) which shows this is not the case and Sing and coworkers (250,251) criticise, on this basis, the calculation of the specific surface area S_t from the V_a/t plot for microporous substances. It is also pointed out (249) that the use of a standard t curve imposes a certain C value which may not correspond to that for the test material. It cannot be expected therefore that S_t will always equal S_{BET} . The assumption that adsorbed and capillary condensed liquid has normal bulk liquid properties seems unreasonable in view of the evidence that at least the surface tension varies with capillary size down to 200\AA (228). This variation might also be expected to continue to smaller pore sizes.

It is often very difficult to obtain a non-porous standard substance chemically similar to the test material. In such cases one can make use of the 'Universal' isotherm, a reduced nitrogen isotherm which is approximately the same for a large number of materials (134). It is believed (239) that the coincidence of the nitrogen isotherms is due to

their measurement at a high reduced temperature whence thermal agitation smears out small attractive forces in successive adsorbed layers. Significant differences are evident between the standard t curves quoted by various workers and, although not causing important errors in pore size distribution calculations, these differences may lead to a wide disagreement in results and interpretation when used for V_a/t plots (239). The use of the universal curve may also introduce a significant surface area error as an average value of C is used rather than a standard value. There is also a possibility that the standard substances used are not truly nonporous and several authors (239,252,253) consider that the standards of de Boer and coworkers (219,220) were in fact porous.

The interpretation of V_a/t plots is not always clear-cut. This is indicated by the existence of at least three cases of linear plots which are believed due to a combination of downward deviations (decreased slope), arising from the filling of micropores, and upwards deviations

(increased slope) due to capillary condensation in transitional pores (254-256).

A V_a/t curve is of questionable meaning for the type III (257), and presumably also for type V isotherms, since the value of V_m for these isotherm shapes are as has been mentioned earlier, of doubtful validity.

Thus V_a/t plots are capable, in many cases, of yielding considerable information about the porous nature of a material. Some caution must however be taken when applying the method to microporous solids. At present the method is mainly limited to nitrogen adsorption although standard data has been recently published for water adsorption on various materials (145) and for carbon tetrachloride on nonporous silica (258).

CHAPTER 3 : EXPERIMENTAL

3.1 Preparation of Metahalloysite Samples

3.1.a Introduction

The major part of this study was carried out upon samples of metahalloysite prepared by dehydration of the parent halloysite mineral obtained from a find near TePuke, New Zealand. The deposit is described as secondary (292), water-sorted, and was probably formed as the result of weathering and/or hydrothermal action on rhyolite and andesite (10). Characterization of the parent mineral by X-ray examination (10) showed only small amounts of impurities to be present. These impurities, mainly quartz and cristobalite, were found to be most significant in the larger particle size fractions.

X-ray diffraction and weight loss techniques have been used by Hughes (10) and more fully by Churchman (13) to study the dehydration of TePuke halloysite. The reports of both of these investigations include, by way of mineral characterization, a chemical analysis, a differential

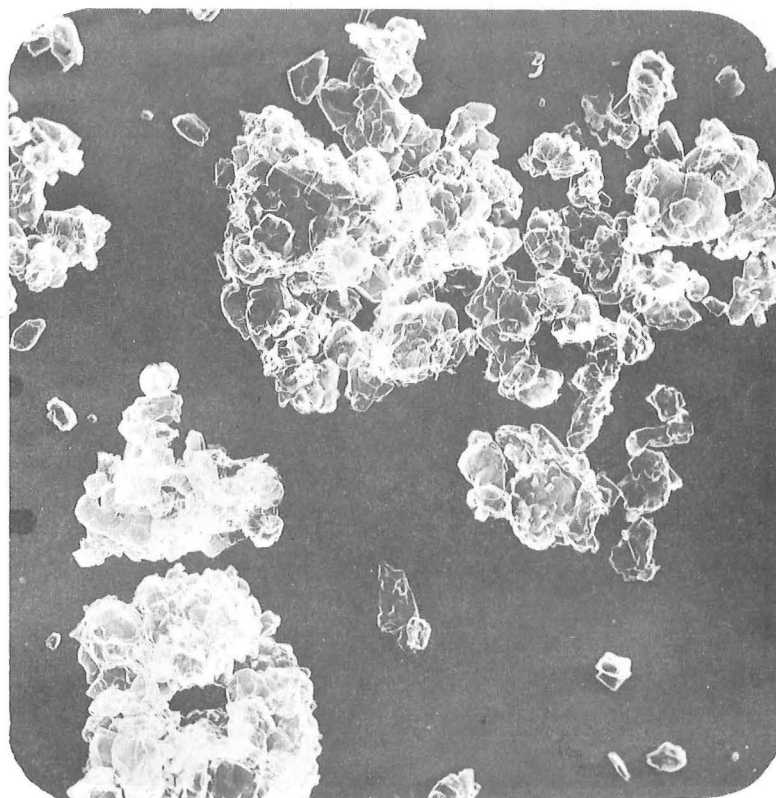
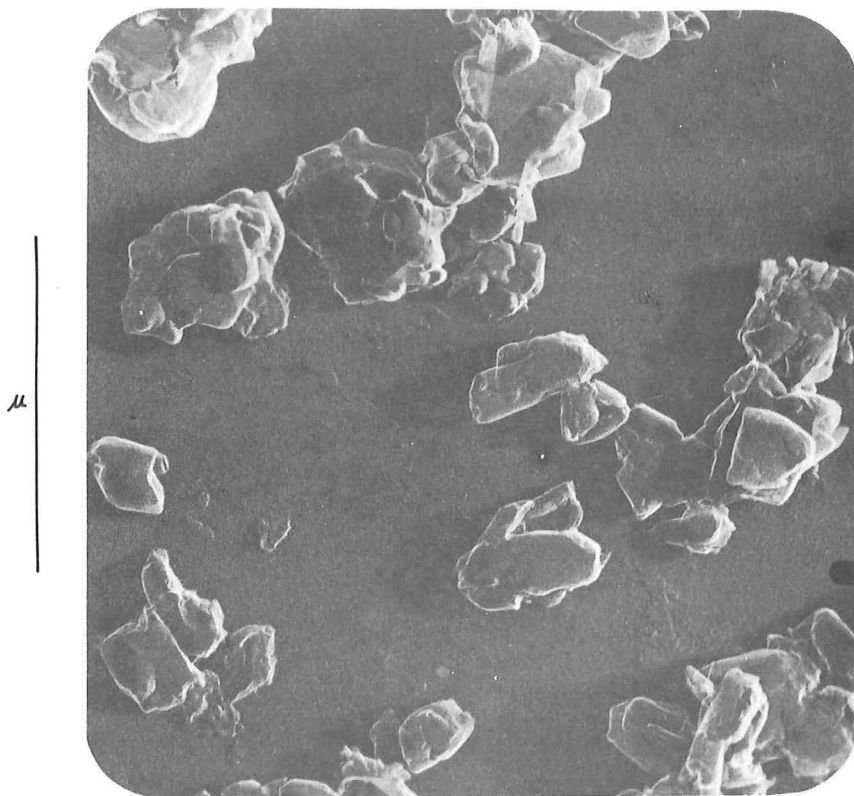


Fig. 7 Electron micrographs of 'natural' (10μ) Te Puke Metahalloysite outgassed at 110°C

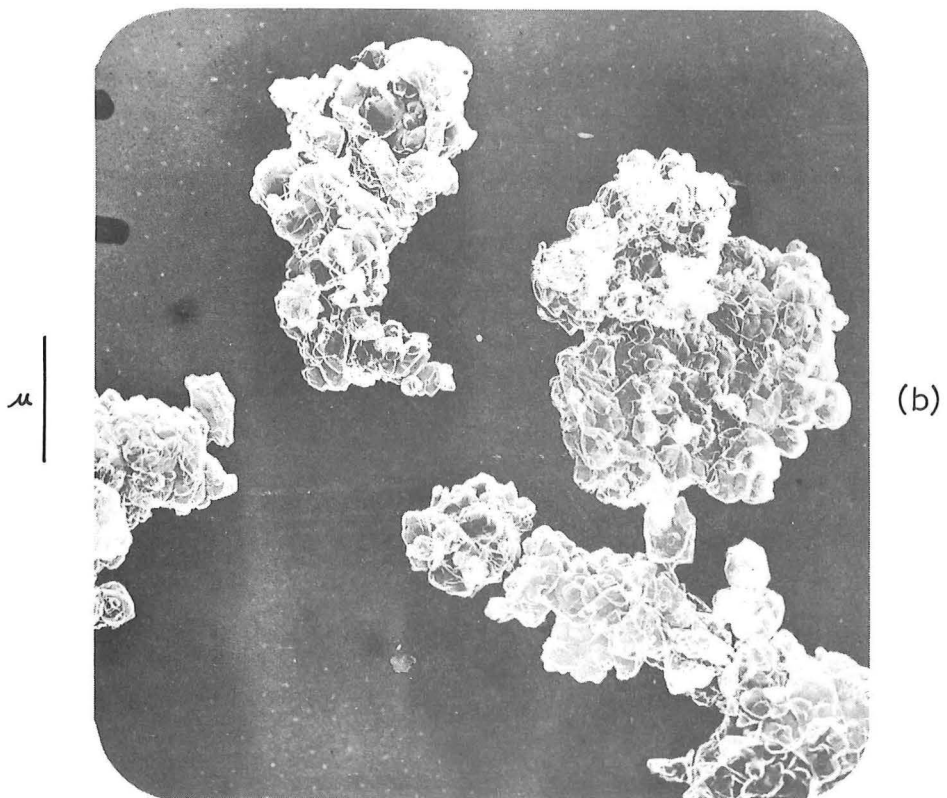
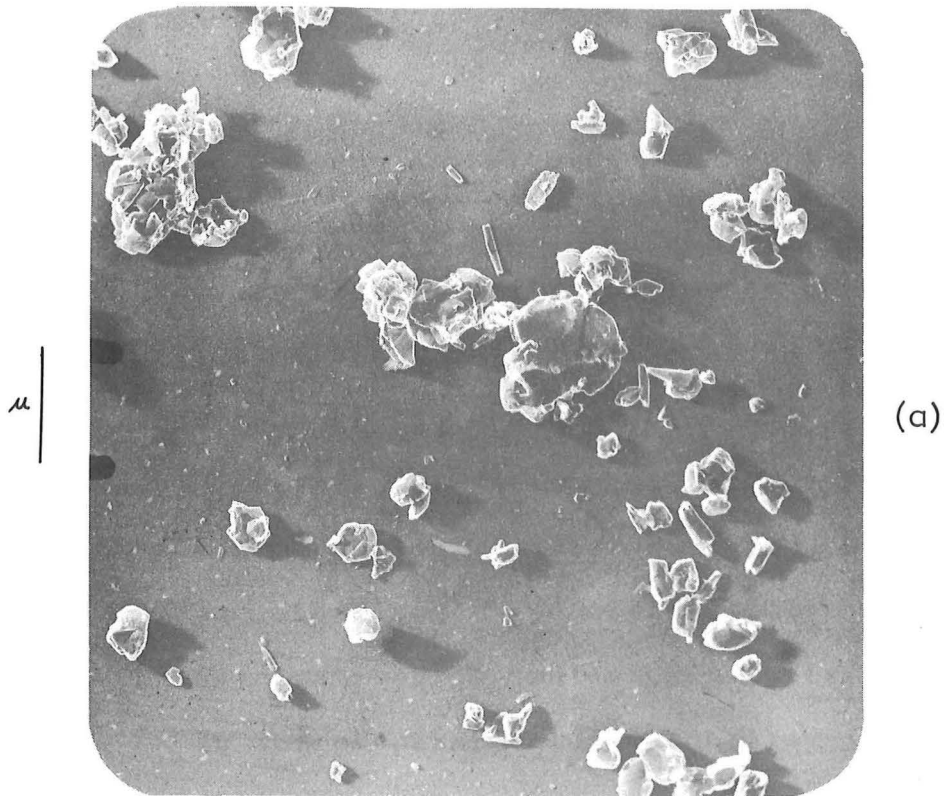


Fig. 8 Electron micrographs of 'natural' ($<10\mu$) TePuke Metahalloysite samples outgassed at (a) 350°C , (b) 500°C .

thermal analysis pattern and electron micrographs. It is generally concluded that the major mineral is halloysite but that there is little evidence of the tubular morphology typical of this mineral. The electron micrographs of the above studies and those of the present investigation (figures 7 and 8) indicate that the morphology is best described as bulky and angular, the larger 'particles' quite clearly being aggregations of smaller particles.

In the preparation of metahalloysite samples, for use in this study, due note has been taken of the fact, discussed in section 1.14, that most chemical and mechanical treatments can cause marked changes in the properties of clay minerals. In order to maintain the mineral properties as near to the natural state as possible, it was decided to use neither chemical agents for dispersion nor chemical treatments to remove organic materials. The general whiteness of the natural material is visual evidence that the content of iron and organic matter is low. The aggregate TePuke clay mineral sample had been air-dried and lightly ground before being received

for this work. Subsequent treatments were limited to, (1) agitation in water to disperse some of the larger aggregates, (2) sedimentation and centrifugation procedures to retain a limited particle size fraction and to reduce the content of non-clay impurities, and (3) the application of the disodium salt of ethylenediaminetetra-acetic acid (EDTA) to remove strongly adsorbed multivalent cations and replace them with sodium ions.

Particle size fractionation of materials such as clay minerals, which have particles of non-spherical shape or aggregates consisting of many smaller particles, cannot yield separations which are entirely meaningful in a physical sense. The procedure should however give a reasonably homogeneous clay mass, small portions of which can be accepted as representative of the whole.

In view of the purity of the parent material (10) it was decided to retain particles of equivalent spherical diameter (e.s.d.) between 1 and 20 microns (μ), thus allowing the retention of about 60% of the bulk material without the use of exhaustive

separation techniques. Utilization of smaller particle sizes would necessitate, in the cation exchange processes, extensive use of dialysis techniques which require substantial periods of time.

3.1.b Preparation of Homoionic Metahalloysites

A suspension of TePuke halloysite (30g) in distilled water (500ml.) was agitated in a dispersion cup for two minutes. The suspension was then poured into a 1l. beaker, the volume adjusted to give a sedimenting height of 10cm, the mixture stirred briskly for a few seconds and allowed to settle for 4min 40sec. Four such sedimentations were carried out on separate portions of halloysite and the resulting suspensions decanted and added together. The settled material, containing particles of e.s.d. greater than 20μ , was discarded.

The suspension containing particles of e.s.d. $< 20\mu$ was transferred to 250ml. centrifuge bottles which were filled to within 3cm. of the top. Centrifugation at 1500 rpm for six minutes, using a

MSE "Medium".centrifuge, resulted in a supernatant suspension containing particles of e.s.d. $< 1\mu$ and a settled fraction enriched with particles between 1 and 20μ e.s.d. The suspended material was decanted but retained and the settled portion redispersed by agitation with distilled water (250ml.). Centrifugation under the same conditions of speed and time, separation of suspended and sedimented material as before and a further repetition of resuspension, centrifugation and separation finally yielded a settled fraction which is signified as '1-20 μ '. All of the separated supernatant suspensions were added together and, after evaporation of the water and drying in an oven for 24 hours at 110°C , gave rise to a sample designated $< 1\mu$ metahalloysite.

The sediments from the above centrifugations were combined and the total volume made up to 500 ml. with distilled water. To this was added a solution of sodium EDTA (ANALAR, 37g.) in distilled water (450ml.) made up to pH \approx 7 (BDH narrow range pH papers) with sodium hydroxide pellets (ANALAR). The overall volume was increased to

1 litre with distilled water, the suspension agitated for 5 minutes and left for 1 hour before centrifugation at 1500 rpm for 6 minutes. A second EDTA treatment was carried out upon the sediment, using a solution of the same final concentration as in the first treatment and allowing a contact time of 4 hours. The mixture was frequently agitated during this period and finally centrifuged (1500 rpm, 6 minutes), the liquid being discarded. The settled material in each of the four 250ml. centrifuge tubes was then treated three successive times with 200ml. portions of sodium chloride solution (ANALAR, 1M). Brisk stirring of the flocculated material was carried out several times during the contact time of 2 hours after which the mixture was centrifuged (1500 rpm, 6 minutes). This treatment was followed by a series of four washings with distilled water (200ml.), each being left for 10 minutes before centrifugation. The first two centrifugations were at 1500rpm for 6 minutes, the others at 2000 rpm for 10 minutes. At this stage it is believed that the great majority of the cation exchange positions are saturated with sodium ions and

the sample is referred to as a sodium-clay.

The total sample of sodium-clay was made up to 1 litre with cooled, boiled distilled water and portions containing approximately 2g of solid (~ 70ml.) separated. These samples were centrifuged and washed twice with distilled water, centrifugation being continued for 20 minutes at 3000 rpm using a BTL 'Bench' centrifuge. All succeeding centrifuging procedures were under these conditions unless otherwise specified.

Each small sample was treated 3 times with a solution (1N, 30ml.) of the chloride of one of the group I or II metals, the contact time for the first treatment being 3 hours, the others 10 minutes, each with frequent agitation. Centrifugation between the salt treatments was at 3000rpm for 5 minutes. Repetitive washing with cooled, boiled distilled water (30ml. each washing) and centrifugation was then continued until the supernatant solution gave no silver nitrate test for chloride ions. Five washings were required to achieve this condition. Contact times for the washings varied between $\frac{1}{2}$ and

12 hours. Three further washings were carried out, contact time 3, 3 and 24 hours, before the final sediment was dried at 110°C in an oven for 48 hours and the material lightly crushed bottled and stored in a desiccator over calcium sulphate.

In this manner homoionic metahalloysite samples were prepared which, depending on the particular chloride used in the final stage of the treatment, are referred to elsewhere in this thesis as Li⁺-, Na⁺-, K⁺-, Rb⁺-, Cs⁺-, Mg²⁺-, Ca²⁺-, or Sr²⁺- metahalloysites.

Because many preparative procedures are known (section 1.14) to alter the nature of the clay mineral, several tests were carried out in conjunction with the EDTA treatment to discover whether or not it caused dissolution of the halloysite sample or formed a water stable complex with the mineral.

Dissolution of the sample was negligible since an analysis for silicon of the supernatant EDTA solution, after removal of the clay material, indicated no silicon in excess of that present as impurities in the solutions used. The method of analysis used was

that of Jackson(293) involving the colorimetric determination of molybdosilicic acid.

The results of three tests indicated that no water stable clay mineral - EDTA complex formed during EDTA treatment of halloysite. The infra-red spectrum (figure 9a) of a sample of the EDTA treated mineral was identical with the spectrum (figure 9b) of a sample in which this treatment was replaced by treatment with a solution of sodium chloride (1M), no absorptions being present in either spectrum which could be attributed to nitrogen containing species. Similarly, the differential thermal analysis curves (figure 10) of these two samples were identical, with no definite peak observable in the curve for the EDTA treated material, which might result from the thermal breakdown of organic material.

Both of the above tests are fairly insensitive to very small amounts of material such as might be present on the surface of a clay mineral after treatment with EDTA and in this regard a third more sensitive test was carried out. This involved

Fig. 9

IR Spectra of Treated Te Puke Metahalloysites

(A) 1-20 μ fraction treated with sodium chloride

(B) 1-20 μ fraction treated with NaEDTA (p71)

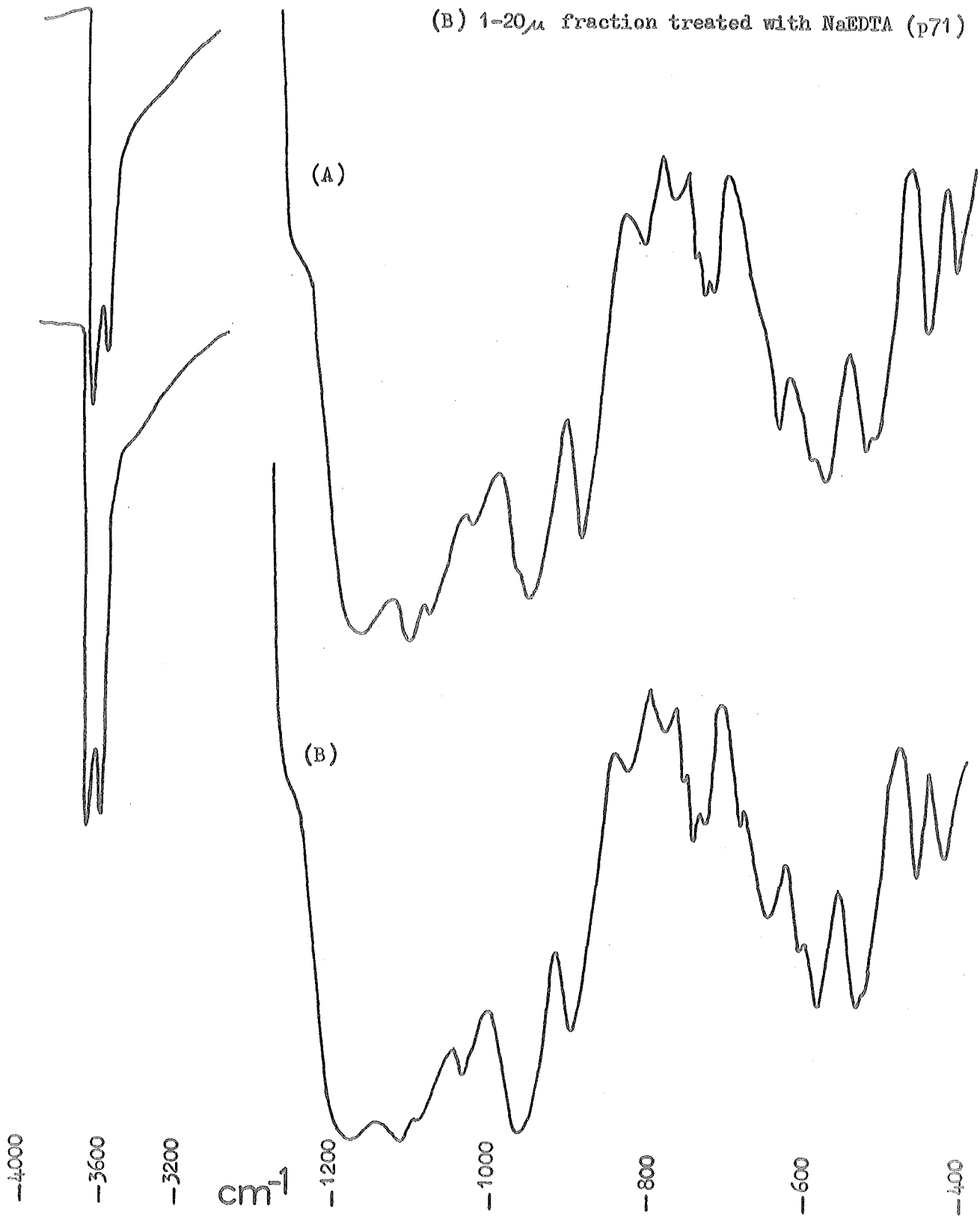
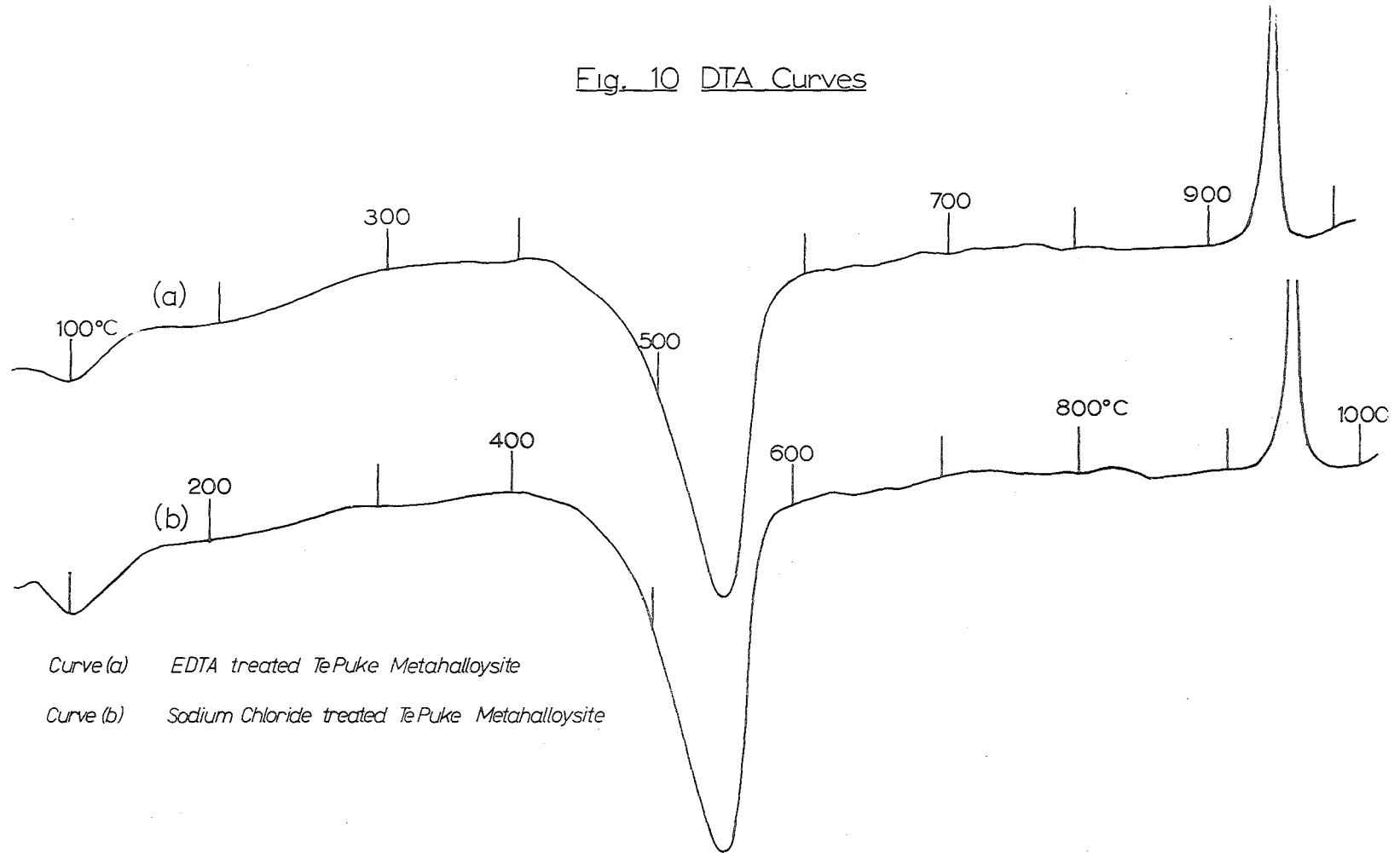


Fig. 10 DTA Curves



a chemical spot test for nitrogen as outlined by Fiegl (294). The nitrogen had first to be converted to cyanide by fusion of a small portion (0.2g) of the treated clay with twice the quantity of fusion mixture (1:1 zinc dust and sodium carbonate) in a fusion tube. The tube and contents were plunged, while still hot, into a test tube containing water (2cc). A drop of the resulting solution, after filtering, was tested according to the method of Fiegl (294). The test proved to be negative indicating the absence of nitrogen containing material.

3.1.c Preparation of Natural Metahalloysite

The term natural is not used to denote a metahalloysite formed as the result of the dehydration of an halloysite by natural processes but rather a laboratory dehydrated halloysite which has not been chemically treated and therefore retains its natural complement of exchange cations.

A quantity (100g) of TePuke halloysite was added to sufficient water (~1200ml.) in a 2 litre beaker to give^a sedimentation height of 10cm and after

brisk agitation a time of 4 minutes 40 seconds allowed for sedimentation. The suspension was decanted and the sedimentation process repeated on the settled material. The suspension from this and the previous sedimentation were combined, the mixture agitated, divided into two equal parts and the volumes adjusted to give a 10cm depth in 2 litre beakers. A settling time of 53 minutes enabled particles with e.s.d. less than 10μ to be retained as the suspended fraction. The sediment was retreated under the same conditions and the suspension retained. The final two suspensions were added together and evaporated to dryness in an oven at 110°C , the solid, lightly crushed, transferred to a smaller container and stored in a desiccator over calcium sulphate. This material is subsequently referred to as natural ($<10\mu$) metahalloysite.

3.1.d Preparation of Silane-treated Metahalloysites

A sample (3g) of natural ($<10\mu$) metahalloysite in a weighing bottle was heated in a 110°C oven overnight before treatment with 10 ml. of a solution of chlorotrimethylsilane (CTMS)

(ANALAR, 10ml.) in benzene (100ml.). This volume of silane solution was calculated to contain more than ten times the amount required to react with all of the hydroxyl groups present on the surface of the clay sample. After allowing the solvent and excess CTMS to evaporate, the weighing bottle and its contents were replaced in a 110°C oven and the weight recorded at intervals until constant (about 12 hours). A CTMS treatment was also carried out on a natural (<10 μ) sample after it had been vacuum outgassed at 400°C. These samples were not stored but were introduced immediately into sample bulbs ready for attachment to the adsorption system (section 3.2.a.viii).

One such sample of natural (<10 μ) metahalloysite, oven heated only, was accurately weighed into a tared weighing bottle, a CTMS treatment carried out and the bottle and contents reweighed after the constant weight condition had been reached. The weight increase observed was equated with the amount of CTMS retained by the clay as a result of reaction with surface hydroxyl groups.

3.1.e Preparation of Maungaparerua

Metahalloysite Samples

These samples were received as dried extruded cylinders prepared, by H.J. Percival of Victoria University, from material of two particle size ranges, separated from a bulk Maungaparerua halloysite sample. The size fractionation (295) was accomplished in another laboratory. Some of the cylinders were oven dried at 110°C and are referred to as 'unfired', others were heated to 650°C for 30 minutes and are denoted as 'prefired' (296).

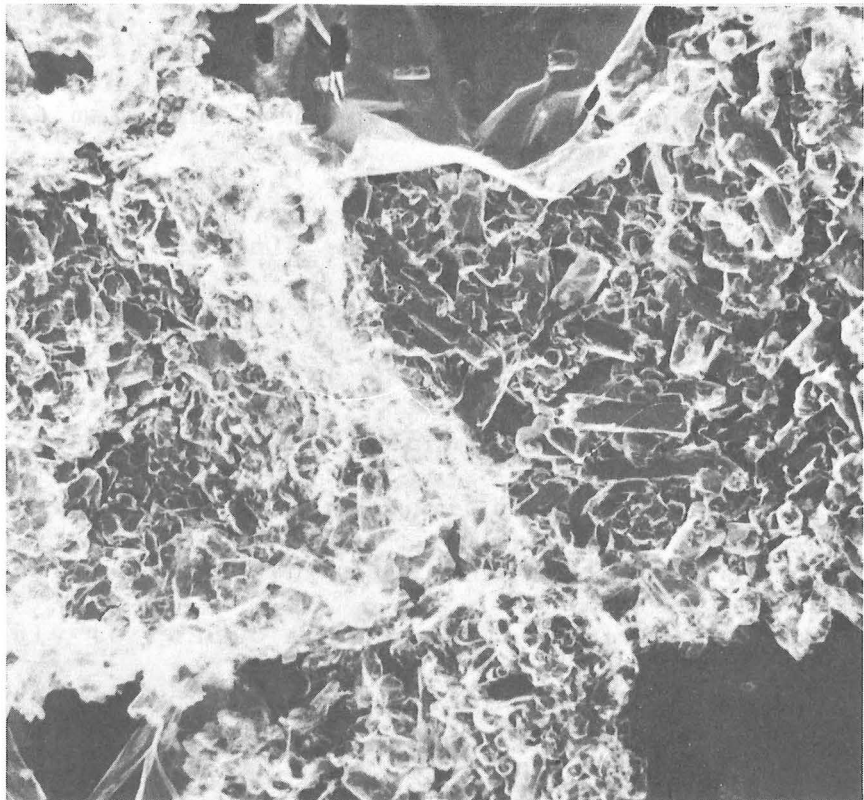
The smaller size fraction, containing particles of $< 2\mu$ e.s.d., has a predominantly tabular morphology and is specified as 'tabular', while the larger 5-10 μ fraction, denoted as tubular, has noticeably elongated particles some showing tubularity. Figure 11 contains an electron micrograph for each of these fractions. These and other micrographs presented in this thesis were kindly supplied by Professor J. Brown at the Georgia Institute of Technology.

μ |



(a)

μ |



(b)

Fig. 11 Electron micrographs of Maungapararua halloysite particle size fractions (a) $< 2\mu$ e.s.d. (b) $5-10\mu$ e.s.d.

The two morphologically different fractions of the mineral were received in a form flocculated with aluminium sulphate and the subsequent treatments adopted by Mr. Percival, for either fraction were as follows:

(1) The material was made into a 5% by weight suspension with distilled water and boiled for 5 min. with a 2% sodium carbonate solution.

(2) The suspension was centrifuged once at 2000rpm for 5 min. and the sediment divided in half.

(3) One half of the sediment was washed once or twice with distilled water until, on centrifuging, some of the material remained in suspension. This produced the 'dispersed' fraction.

(4) The second half was washed once with 1:1 acetone/H₂O to remove excess sodium ions but not enough to deflocculate the sample. The resulting material is designated as 'flocculated', and, like the final material from (3), was dried in an oven at 110°C.

(5) After drying the material was rewetted sufficiently to result in a plastic state and extruded to give cylinders of approximately 4mm.

diameter. In this way four different samples were prepared - Tubular dispersed and flocculated, Tabular dispersed and flocculated. By treating portions of each of these samples at one of the two temperatures 110°C or 650°C, there results eight different materials, the names of which are set out in full in Table 1.

Table 1. Specific Surface Area (m²/g) of Pretreated Maungaparerua Metahalloysite.

	Flocculated			Dispersed		
	Unfired 110°C	Prefired 650°C	Increase %	Unfired 110°C	Prefired 650°C	Increase %
Tabular ($< 2\mu$)	21.7 ± 0.4	23.4 ± 0.4	8 ± 4	20.4 ± 0.4 20.1 ± 0.4 20.1 ± 0.4	24.7 ± 0.5 24.9 ± 0.5	23 ± 5
Tubular (5-10 μ)	17.7 ± 0.4 17.9 ± 0.4	29.5 ± 0.5 30.1 ± 0.5	68 ± 6	16.5 ± 0.4 16.3 ± 0.4	31.6 ± 0.5	93 ± 8
Differences %	22 ± 5	27 ± 4		23 ± 5	27 ± 4	

3.2 Volumetric Determination of Adsorption Isotherms

3.2.a Apparatus

The vacuum volumetric adsorption system constructed for this investigation was a modified version of Emmett's apparatus (297) incorporating some features from that used by Salman and Robertson (298). The essential details of the apparatus are shown diagrammatically in figure 12.

(i) Vacuum System

High vacuum (HV) was generated and maintained by a rotary pump in series with a mercury diffusion pump. The pressure inside the system was read by way of a Veeco vacuum ion-gauge head inserted in the main manifold of the system, and a Veeco Vacuum Gauge type RG-21X. A rough vacuum of about 10^{-2} mm.Hg, used to adjust the levels of mercury in various parts of the apparatus, was maintained by a rotary pump.

(ii) Gas Storage Bulbs

The gas storage system consisted of four reservoirs, one for each of the gases helium, nitrogen and argon, and one for ethyl chloride stored

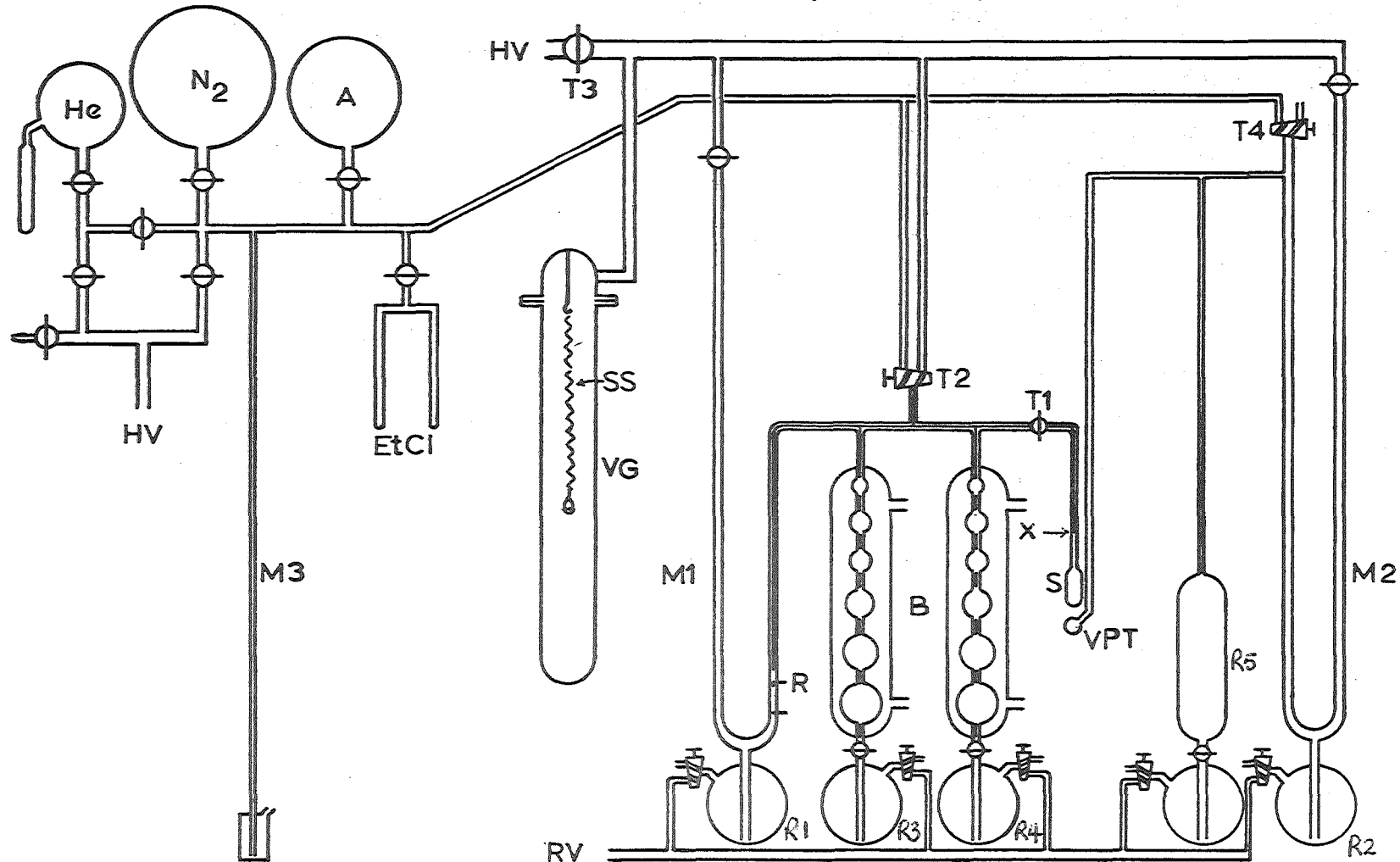
in the liquid form.

(iii) Adsorbates

Nitrogen was passed directly from a cylinder of Matheson 99.999 grade nitrogen gas into a well evacuated 5 litre storage bulb attached to the gas line (GL) of the adsorption apparatus. Argon and helium were both of Matheson research grade purity, the former quoted as having no detectable impurities, the latter a major impurity of < 5 ppm neon. These gases were entered directly into the system without further purification and stored in 2 litre flasks. The helium reservoir was fitted with a side-arm filled with molecular sieves type 5A. Several hours prior to the extraction of helium samples from the reservoir, the side-arm was cooled to liquid air temperature causing any condensable gas impurities, present in the reservoir, to be adsorbed onto the molecular sieves. The gas reservoirs were maintained at close to, or slightly above, atmospheric pressure to reduce the effects of air leakage.

Ethyl chloride (BP grade, 99.5% w/w ethyl chloride, major impurity methyl chloride) was

Fig. 12 Volumetric Adsorption System



HV high vacuum $<10^{-5}$ torr
 VG Vacuum weight loss apparatus
 B gas burettes
 S sample bulb

VPT vapour pressure thermometer
 R reference point
 RV rough vacuum $\sim 10^{-2}$
 M1-3 manometers

SS silica spiral spring

stored as liquid at 0°C over activated alumina, after vacuum distillation in situ ten times to remove air.

(iv) Vapour Pressure Thermometer

Nitrogen and argon adsorption isotherms were determined at the boiling point of liquid nitrogen. Since the saturation vapour pressure of the adsorbate is dependent upon the temperature of the thermostat bath, this must be measured at intervals throughout the isotherm determination. In the present study a value of the thermostat bath temperature was recorded in conjunction with every equilibrium isotherm point by the use of a nitrogen vapour pressure thermometer (VPT) to measure the saturated vapour pressure P_0 of nitrogen. This vapour pressure is related (299) to the temperature ($T^{\circ}\text{K}$) of the thermostat bath by the expression:

$$\log P_0 = - \frac{339.8}{T} + 7.71057 - 0.0056286T \quad . \quad 12$$

The vapour pressure thermometer consisted of a small bulb (5cc) connected to a manometer (M_2) and to a nitrogen receptacle which

could be pressurised by raising the mercury level in reservoir R5. The small bulb was placed in close proximity to the sample bulb (S).

Before the cryostat bath was raised about the sample bulb, at the commencement of an isotherm determination, about 400-500 torr of nitrogen from the storage bulb was admitted to the vapour pressure thermometer through tap T4. The pressure was then increased to around 850 torr by raising the level of mercury in R5. At this stage the liquid nitrogen bath was placed in position around the sample bulb. As the small bulb of the thermometer cooled, nitrogen condensed until the pressure in the thermometer reduced to that corresponding to the boiling point ($T^{\circ}\text{K}$) of the bath liquid, as given by equation 12. The nitrogen saturated vapour pressure P_o is the difference between the levels of mercury in the arms of manometer M2 corrected to a standard pressure at 0°C by expression 13.

$$P_s = P_{\text{obs}} \times \frac{d_T}{d_o} \quad 13$$

d_T - density of mercury at room temperature $T^{\circ}\text{C}$

d_o - density of mercury at 0°C

P_{obs} - observed pressure

P_s - standard pressure at 0°C

(v) Dosing Burettes

The burettes (B1, B2) were each constructed of a series of dosing bulbs of various sizes from 1ml. to 50ml. connected by capillary tubing. The volume of each bulb, demarcated by lines drawn with glass marking ink on the connecting tubing, was calibrated to $\pm 0.002\text{ml.}$ by mercury displacement. These burettes were then sealed into glass water-jackets and mounted onto the vacuum system. During the determination of an isotherm, the dosing bulbs were thermostated by circulation of water through the water-jackets from a large reservoir maintained at $25 \pm 0.01^{\circ}\text{C.}$

(vi) Mercury Manometers

Manometers M1 and M2 were fabricated from 10mm. internal diameter glass tubing. The mercury levels in the arms of each manometer were observed by the use of a cathetometer capable of

detecting level changes of 0.01mm.

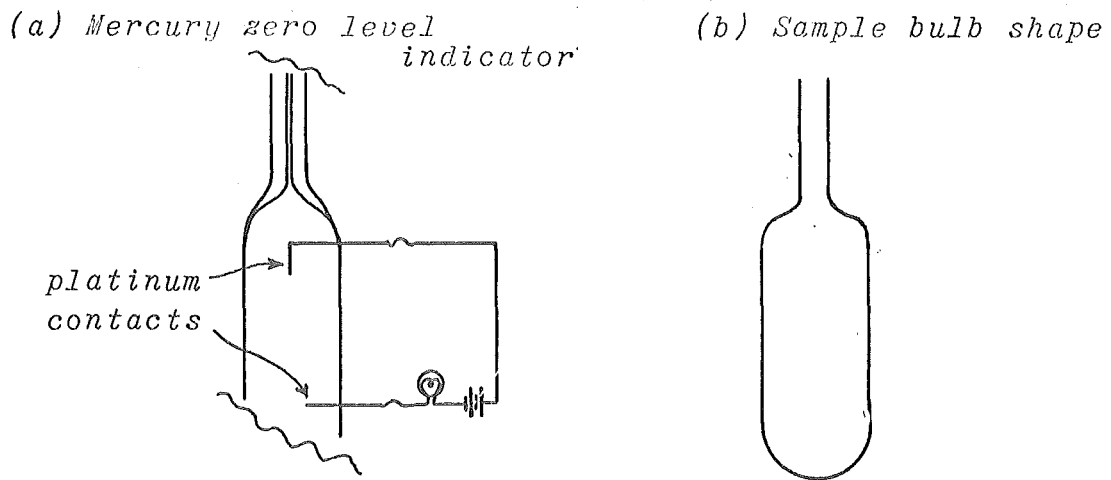
M1, used to measure the pressure inside the adsorption system, was enclosed in a sealed air jacket to reduce the effects of rapid room temperature fluctuations. An electrical circuit was included in the arm on the adsorption side of this manometer to enable the mercury in this arm to be held at a constant level and hence to allow the preservation of a constant volume in the adsorption system. The circuit consisted of a pair of tungsten wires fused into the arm so as to occupy a central position in the manometer tubing (figure 13a), connecting wires, a pair of torch batteries (1.5V) and a small light bulb. The mercury level was altered by suitable manipulation of tap T5. As the level was slowly increased the first illumination of the light bulbs indicated that the reference point at the upper tungsten contact had been reached.

(vii) Mercury Reservoirs

Mercury reservoirs R1-R5 were provided to raise or lower the levels in manometers M1 and M2 and in burettes B1 and B2, and to pressurize the

nitrogen in the vapour pressure thermometer. If increased pressure was necessary to raise the levels this was accomplished by the use of a bicycle pump.

Fig. 13 Apparatus Components



(viii) Sample Bulb

Various types of sample bulb were tested but the most satisfactory proved to be a narrow-necked straight tube (figure 13b) of just sufficient volume to accommodate the chosen clay sample. Bulbs were cleaned with permanganic acid, washed and dried in an oven. After weighing, a

clay sample was introduced, the bulb placed in an oven at 110°C for at least 4 hours, cooled in a desiccator for 15 min. and reweighed. The bulb was then sealed directly on to the adsorption system at point X.

Sample weights varied from 0.25g to 10g but most experiments were carried out on 3g samples, this amount of material having a surface area of approximately 100 square metres.

(ix) Connecting Glass Tubing

All connecting tubing within the adsorption system (figure 12) was a thick walled, narrow bore (1.5mm internal diameter) variety to keep to a minimum the volume of the system at room temperature and hence reduce the effects of changes in the ambient temperature on the pressure within the system.

3.2.b Procedure

(i) Outgassing Procedure

Prior to all isotherm or surface area determinations the clay samples were outgassed at an elevated temperature, usually 70°C, although

temperatures between 25°C and 500°C were used in particular cases. During outgassing a pressure of $<10^{-6}$ torr was maintained and at this pressure samples were outgassed for at least 4 hours at 70°C or 60 hours if a higher temperature was involved. The criterion accepted as indicating both the absence of leaks in the system and a sufficiently prolonged sample outgassing was that, on isolation of sample bulb and dosing bulb system from the pumps, by closing tap T3, the pressure did not increase to greater than 5×10^{-5} torr in 30 minutes.

Outgassing temperatures were obtained by the use of a small wire-wound furnace maintained to within 3°C of temperature by an Ether Transitrol controller equipped with a chromel-alumel thermocouple. Temperatures were measured by using a Tinsley Potentiometer (Type 4604B) and a chromel-alumel thermocouple with a cold-junction immersed in an ice bath.

It was sometimes noticed that initial evacuation of clay samples resulted in entrainment of small particles and for this reason, in later

experiments, a small glass wool plug was placed on the dosing bulb side of the sample bulb tap T1 to stop such material being spread throughout the system.

(ii) Calibration of the Free Space Volume.

The calibration of the free space volume (VFS), that volume between taps T1, T2, the top marks of the burettes and the mercury level at the reference point (R) in manometer M1, was accomplished by a helium displacement method.

With the gas burette mercury levels at the lowest marks, an amount of helium was admitted to the system through tap T2, the mercury in M1 returned to the reference point and the pressure recorded. The mercury level in one of the burettes was then raised to include the first bulb, the mercury in M1 returned to R and another pressure observed. Several more bulbs were filled in turn and the corresponding pressures recorded. Note was taken of the room temperature in conjunction with each pressure reading and the pressures corrected to standard values by the use of equation 13.

A graph of the change in volume of the system, that is the sum of the volumes of the dosing bulbs filled with mercury, versus the reciprocal of the standard pressure P_s , yields an intercept on the volume axis which equals the total volume of the dosing and free space systems.

Subtraction of the known volume of the gas burettes gives rise to the volume VFS of the free space, which in the present system was about 8ml. and could be reproducibly determined to ± 0.01 ml. Graphical calculation of VFS was carried out in some cases but more usually the computation was done by least squares regression.

(iii) Calibration of the Dead Space

The dead space (DS) is defined as the volume in the sample system up to tap T1 which is not occupied by the solid sample. This includes the pore volume of the clay material. Calibration of the dead space was achieved by helium displacement.

A small amount of helium was introduced into the adsorption system with tap T1 closed and the mercury level in the dosing bulbs increased such that

the resulting helium pressure was greater than 250 torr. This pressure was recorded. After immersing the sample bulb in the appropriate cryostat bath and allowing about 2 hours for the sample to come to thermal equilibrium with the bath liquid, tap T1 was opened and the pressure allowed to reach equilibrium ($\frac{1}{2}$ hour usually sufficient). The dead space volume is the difference in volume (at STP) of helium in the dosing bulb-free space system before and after opening tap T1, assuming that no adsorption takes place on the sample.

In the calculation of adsorption data the volume of the dead space is included in the form of a correction factor (FD) defined by expression 14, which is applied to the equilibrium pressure to determine the amount of gas in the sample bulb which remains unadsorbed.

$$FD = (VOLHE1 - VOLHE2) / PT2 \quad 14$$

VOLHE1 = volume of helium (STP) admitted

VOLHE2 = volume of helium (STP) remaining in
the dosing bulb - free space system
after opening tap T1

PT2 = the observed pressure, corrected to standard conditions, after opening tap T1.

(iv) Determination of Isotherm Data

Prior to the determination of isotherm points, the helium gas used as a calibrant, was evacuated at room temperature until a vacuum of 10^{-6} torr was obtained. Tap T1 was closed and, with the mercury in the dosing bulbs at the lowest marks, some adsorbate gas was admitted to the system through tap T2 and the pressure recorded. After placing the appropriate cryostat in position around the sample bulb and allowing at least 2 hours for thermal equilibrium to be attained, tap T1 was opened. The internal pressure was allowed to come to a constant value, the time required for this equilibration varying with the nature of the adsorbate gas and with the position of the particular point on the isotherm. Desorption points, for example, required considerably longer time intervals to reach the equilibrium condition than did adsorption points. During the course of the first isotherms determined, some

points were left for considerable times, pressure readings being taken at intervals. For only a few points in the high relative pressure region along the desorption curve were times greater than two hours necessary for equilibration. The initial adsorption point was always left for longer than two hours although subsequent adsorption points required only a half hour for $P/P_0 < 0.9$ and one hour for $P/P_0 > 0.9$.

Further adsorption points were accumulated by increasing the pressure within the system, either by raising the levels of mercury in the dosing bulbs, or through making additions of adsorbate to the system. Time was allowed for the attainment of equilibrium conditions between each volume change or adsorbate gas addition. The data recorded for each isotherm point included the equilibrium pressure, room temperatures, volume of dosing bulbs filled and, for nitrogen and argon isotherms, the saturated vapour pressure.

Desorption points were recorded after suitable increases in the volume of the system or the

removal of amounts of adsorbate gas. Addition or removal of gas was always carried out with tap T1 closed and with the mercury in the burettes at the lowest marks, this standardised procedure simplifying the computer program for the calculation of adsorption data.

For the determination of a specific surface area at least four sets of equilibrium data were recorded in the range of relative pressure P/P_0 between 0.05 and 0.30, the region to which the BET equation is best applied (see section 2.1). About 40 data points were collected for an isotherm, approximately twenty points spaced over the length of each of the adsorption and desorption curves.

(v) Calculation of Isotherm Data

All calculations, except of the free space volume VFS, are included in a computer program modified from one obtained from Dr. L.A.G. Aylmore of the University of Western Australia. The program, written in Fortran IV language for use on an IBM 360/44 computer, is contained and explained in Appendix 3. By the application of the Gas laws

the programme calculates the dead space correction factor FD , the value of the amount of gas adsorbed (as a volume at S.T.P.) at each equilibrium pressure and, providing there are sufficient points in the region $0.05 < P/P_0 < 0.30$, a value of the specific surface area. Included also are the calculation of error estimates based on the linear least squares regression computation of the specific surface area, and the correlation coefficient. Both of these error estimates are an indication of the linearity of the BET plot.

Input data for each isotherm point include, uncorrected equilibrium and saturated vapour pressures, the volume of dosing bulbs not containing mercury, room temperature, and correction factors to reduce observed pressures to standard conditions. The values of certain constants are also necessary for the calculation of isotherm data or specific surface areas, these comprising sample weight, free space volume, adsorbate molecular cross-sectional area, and a correction factor to allow for the non-ideality of the adsorbate gas.

3.2.c Errors

A general indication of the accuracy of the isotherm points derived from the present experimental system, is given by the smooth, reproducible nature of the curves obtained. The quantitative calculation of experimental errors is difficult however, especially for points after the first, since points are determined consecutively and the resulting errors are cumulative.

Application of the approximate error formulation (equation 15) of Loebenstein and Deitz (301) to the first adsorption points of various nitrogen isotherms of the present study, yields percentage errors in the number of moles adsorbed per gram of 0.16% for a 7g sample and 0.50% for a 1g sample.

$$\frac{100\delta n}{n} = \frac{100 \left[V_B \int_{P_i}^{P_e} + (V_B - 3.85V_D) \int_{P_e}^{P_i} + (P_i - P_e) \int_{V_B}^{V_D} + (3.85P_e) \int_{V_D}^{V_B} \right]}{V_B(P_i - P_e) - 3.85P_e V_D} \quad (15)$$

- P_i - initial nitrogen pressure in burette system,
- P_e - equilibrium nitrogen pressure,
- V_B - volume of nitrogen cc.(STP) in burette system,
- V_D - volume of nitrogen cc.(STP) in dead space system.

In applying expression 15 a reasonable error for the helium calibration of the dead space was accepted as 1%, i.e. $\delta V_D = 0.01 \times V_D$, and the error in pressure for the volumetric apparatus was taken as 0.002 cm, therefore $\delta_{P_i} = \delta_{P_e} = 0.002$ cm.

The linearity of the BET plot over the relative pressure range 0.05 - 0.30 is a further indication of the accuracy obtained with the adsorption system. Such plots (figures 14 and 15) are visibly linear but a clearer indication of their linearity is given by the least squares correlation coefficient calculated, in conjunction with the specific surface area, by use of the general isotherm computer programme. Of the values calculated only one was less than 0.999.

It is believed however, that a satisfactory way of specifying the overall errors, associated with the determination of isotherm data, is by the reproducibility of duplicate specific surface area determinations on the same sample, or even better, on different portions of the same material, the latter including sampling errors as well as experimental errors.

Fig. 14 BET Plots for Nitrogen Adsorption on Te Puke Metahalloysite

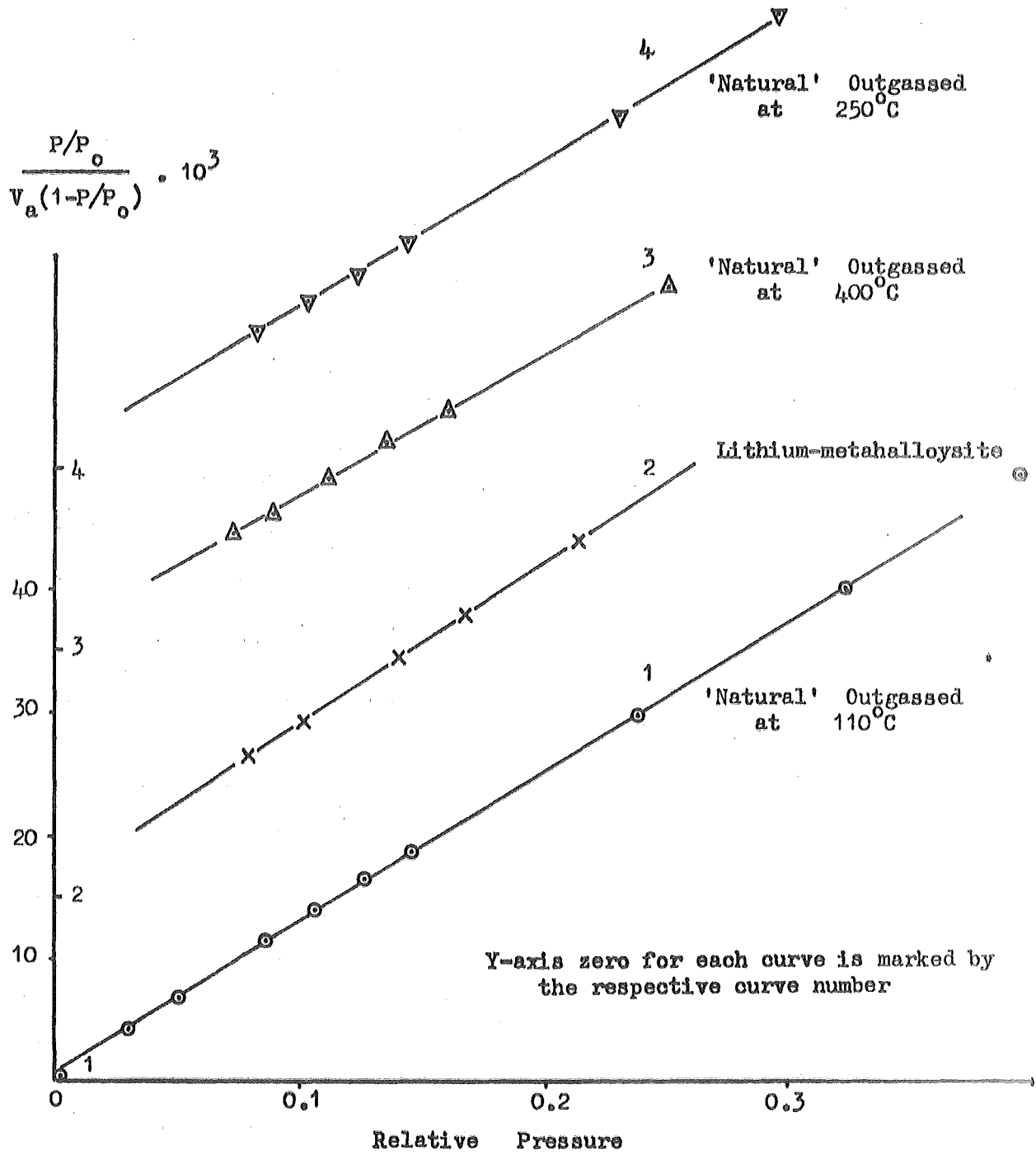
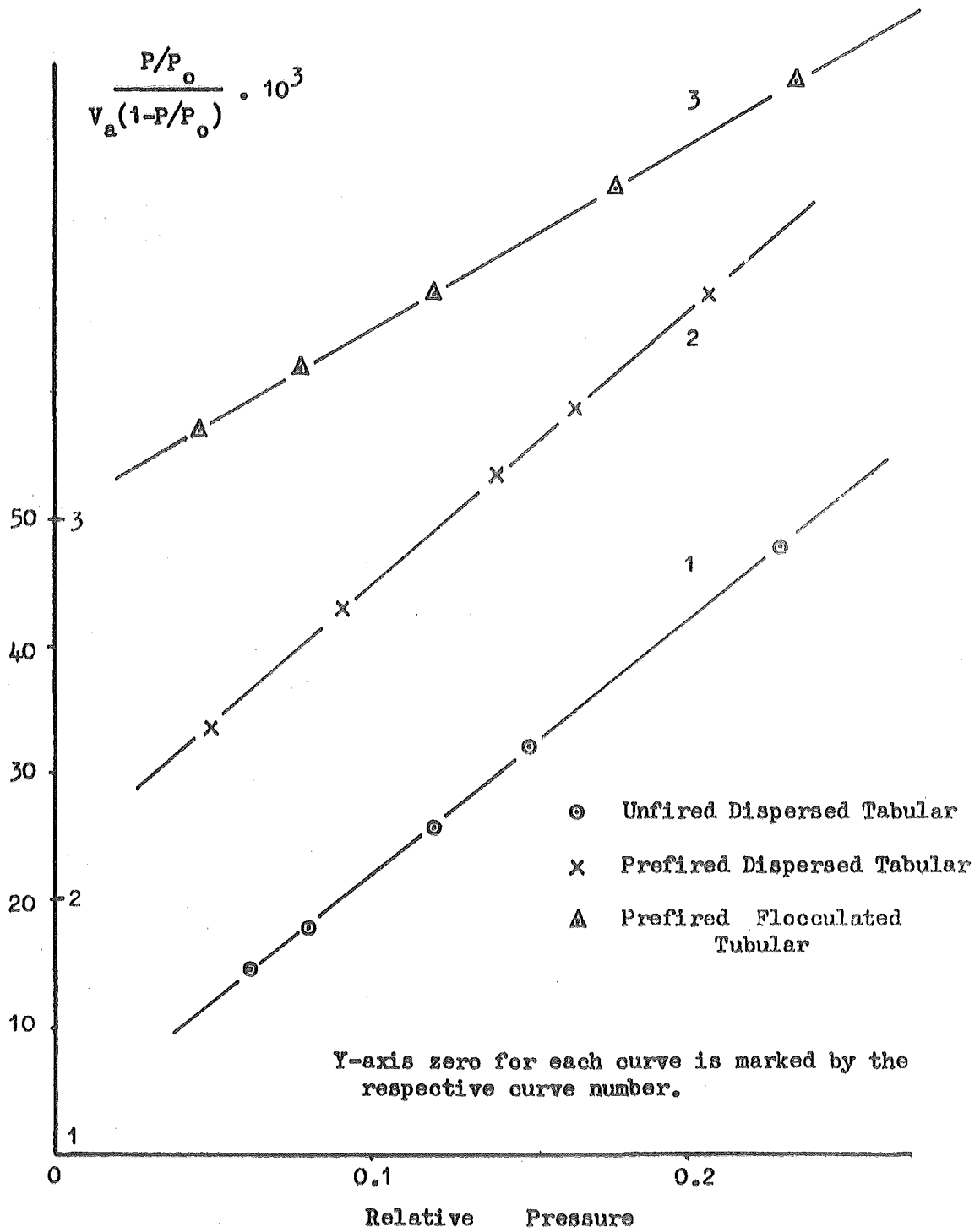


Fig. 15

BET Plots for Nitrogen Adsorption on
Maungaparerua Metahalloysite



Surface areas determined in duplicate, triplicate and, in some instances, in quadruplicate are contained in the various tables. The reproducibility for smaller sample sizes (0.2g to 0.4g) was around 2% while for the larger samples (3g - 10g) it was closer to 1%. Errors quoted with the various specific surface areas in this study are therefore the reproducibility errors rather than experimental errors, the former being some five times larger than the error calculated by the application of equation 15.

3.3 Determination of Water Vapour Adsorption Isotherms

3.3.a Apparatus

Water vapour adsorption-desorption isotherms were determined with a vacuum gravimetric apparatus employing silica spiral spring balances. In the first instance the adsorption system was contained in a thermostated air bath but certain inadequacies of this arrangement, as outlined below, led to the apparatus being rebuilt with the adsorption system immersed in

a thermostated water tank. The essential features of the apparatus remained the same however and are displayed schematically in figure 16.

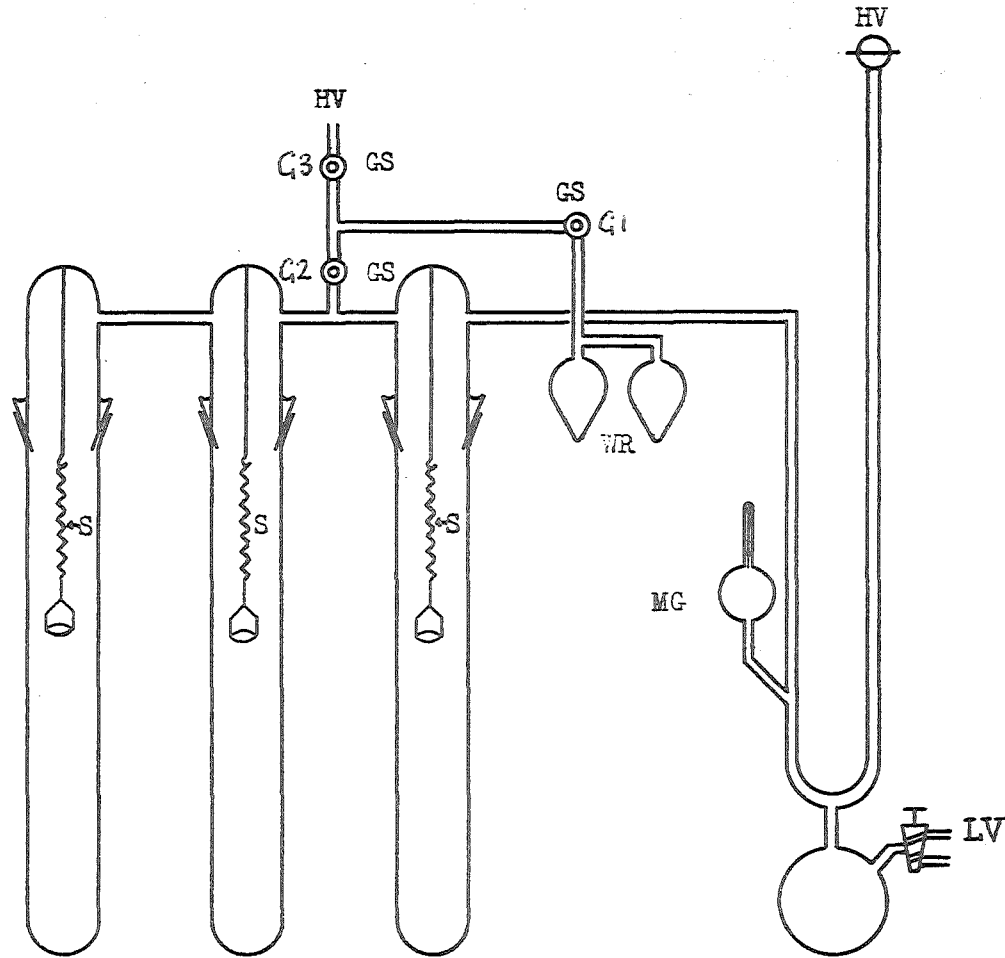
The main components of the adsorption system include: (i) high vacuum, (ii) a mercury manometer, (iii) silica spiral spring balances, (iv) adsorption tubes, (v) water reservoirs, (vi) a constant temperature bath and (vii) a platinum resistance element and precision decade bridge.

(i) High vacuum HV. A pressure of less than 10^{-5} torr was generated by a mercury diffusion pump backed by a rotary pump. The value of the pressure obtained upon evacuation was determined approximately by the use of a rough McLeod gauge included as part of the manometer system M. A vacuum causing the mercury to 'stick' at the top of the fine capillary of the gauge was accepted as indicating a pressure of lower than 10^{-5} torr.

(ii) Mercury Manometer. The manometer, constructed of 12mm internal diameter glass tubing, was used to determine equilibrium vapour pressures.

Fig. 16

Gravimetric Water Vapour Adsorption Apparatus



HV high vacuum ($< 10^{-5}$)
LV low vacuum ($\sim 10^{-2}$)
GS greaseless stopcock

S silica spiral spring
WR water reservoirs
MG McLeod gauge

The mercury levels in the manometer arms were measured reproducibly to 0.01mm by means of a travelling microscope.

(iii) Silica Spiral Spring Balances.

Silica springs of stated maximum loading capacity 1g and nominal sensitivity about 25cm/g, were obtained from Jencons (catalogue number T/A9S/72No23). Each quartz helix, together with a quartz fibre used as a reference marker, was waxed to a glass support hook attached to the upper half of an adsorption tube. Mineral samples, weighing about 500 - 700 mg, were contained in shallow one inch diameter dishes made of 0.0005 inch thick platinum sheet. Sample dishes were suspended from the lower end of the quartz spirals by way of platinum stirrups constructed of 0.0008 inch diameter wire, bent to shape and spot-welded where necessary. The dishes were cleaned between samples by washing with dilute hydrochloric acid, water and ethyl alcohol and oven dried at 110°C.

Accurate calibration of spring sensitivities

was carried out in situ using platinum weights tared on a Cahn electromicro-balance. Spring extensions were observed with the aid of travelling microscopes capable of being read to 0.01mm and, in the range calibrated, all extensions proved to be linear functions of the weight added.

The springs were calibrated at only one temperature and, as the isotherm temperature was invariably different from this, a correction must be applied to the spring sensitivity (k) to allow for the coefficient of thermal expansion of silica. The sensitivity of a quartz spring is determined by the number of turns, coil diameter, fibre thickness and the torsional modulus (Z) of the material, only the last being appreciably affected by a change in the temperature. Since the sensitivity, expressed in terms of extension per unit load, is inversely proportional to the torsional modulus, it follows that

$$\frac{\partial \ln k}{\partial T} = - \frac{\partial \ln Z}{\partial T} \quad 16$$

Integration of equation 16 and substitution of the

value for the temperature coefficient of Z, quoted (250) as $1.23 \times 10^{-4} \text{ deg}^{-1}\text{C}$, yields expression 17.

$$\log_{10} k_2 - \log_{10} k_1 = - \frac{1.23}{2.303} \times 10^{-4} (T_2 - T_1) \quad 17$$

k_1 - spring sensitivity at temperature T_1

k_2 - spring sensitivity at temperature T_2

An alteration in helix length also results upon a change in temperature due to the associated sensitivity change. The alteration in length can be calculated, according to Ernsberger (250), by the use of equation 18 which relates the length change ΔL to the temperature differential ΔT .

$$\Delta L = - 1.23 \times 10^{-4} k_2 \left(M + \frac{m}{2} \right) \Delta T \quad 18$$

M - load mass (sample, stirrup, pan).

m - spring mass.

(iv) Adsorption Tubes. The silica springs were contained inside large glass tubes (5 cm diameter, length 50 cm) fitted with Quick-fit joints (B50/42) to allow easy access to springs and samples. During operation the joints were greased with Apiezon T, a

low vapour pressure lubricant which remains usable at high temperature. All taps in the adsorption section of the system were of greaseless type to reduced as much as possible the effects of grease adsorbing on the clay samples.

Two adsorption tubes and springs were used simultaneously in the air bath while the larger size of the water bath system allowed the adsorption on three samples to be studied at any one time.

(v) Water Reservoirs. Two pear-shaped glass bulbs were used as water receptacles enabling the outgassing of the liquid by repetitive vacuum sublimation.

Prior to introduction the distilled water was brought to the boil removing a considerable fraction of the dissolved gas. The plug of tap G1 was removed and the water inserted into the reservoir system while still hot, by way of a hypodermic syringe fitted with PVC tubing. The last remnants of dissolved gas were abstracted from the liquid by a series of freeze and thaw operations pumping at high vacuum while in the frozen state

(at about 82°K), followed by a series of five vacuum sublimations pumping at high vacuum after each complete transfer of the water from one reservoir to the other. Subsequent to this procedure, and between each isotherm, the water was pumped at high vacuum for one minute.

(vi) Constant Temperature Bath

(a) Thermostated Air Bath. This consisted (figure 17) of a wooden box with removable glass windows front and back, and a glass partition in the centre around which thermostated air was circulated by means of fans mounted on the base of the box. The enclosure was also equipped with a wire mesh heating element mounted directly above the fan blades and, attached to the underside of the enclosure lid, a coil of copper tubing through which cooling water could be passed if necessary.

The first thermostating device, tested in the air bath, employed a mercury-toluene thermoregulator as the temperature sensor. In an effort to gain rapid response to temperature fluctuations, the regulator was constructed (see figure 19a) such that 80% of the

total liquid content of 50ml. was contained in narrow bore copper tubing (4mm. internal diameter).

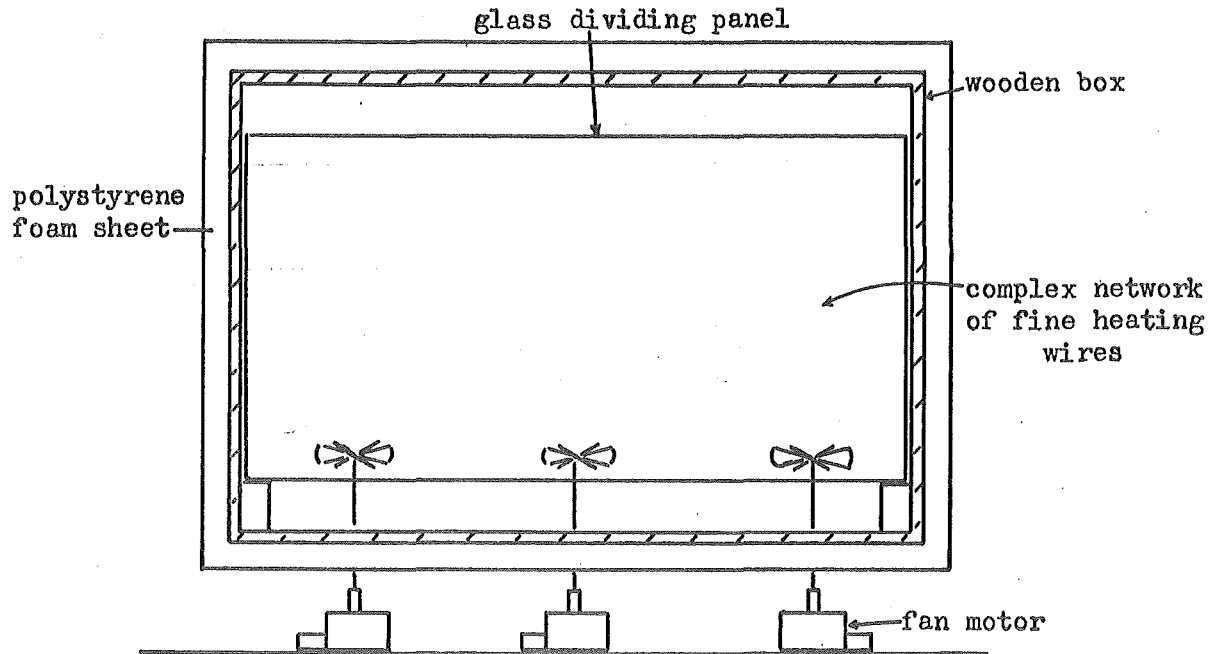
It was found impossible, using the above thermoregulator, to thermostat the enclosure to better than 0.1°C , a result, it is believed, of the large thermal lag in the regulator response. There was also a persistent temperature drift of $0.1 - 0.2^{\circ}\text{C}$ per day the cause of which is unknown.

A number of alterations were made to the enclosure and to the method of temperature control in an effort to improve the thermostating range to about $\pm 0.02^{\circ}\text{C}$ and to enable this to be maintained for considerable periods of time. In view of the extended equilibrium times observed (45,300) for the low temperature adsorption of water vapour on clay mineral systems similar to that of the present study, it was felt that a suitable thermostating system should be capable of maintaining the set temperature for at least two days without attention and without appreciable drift.

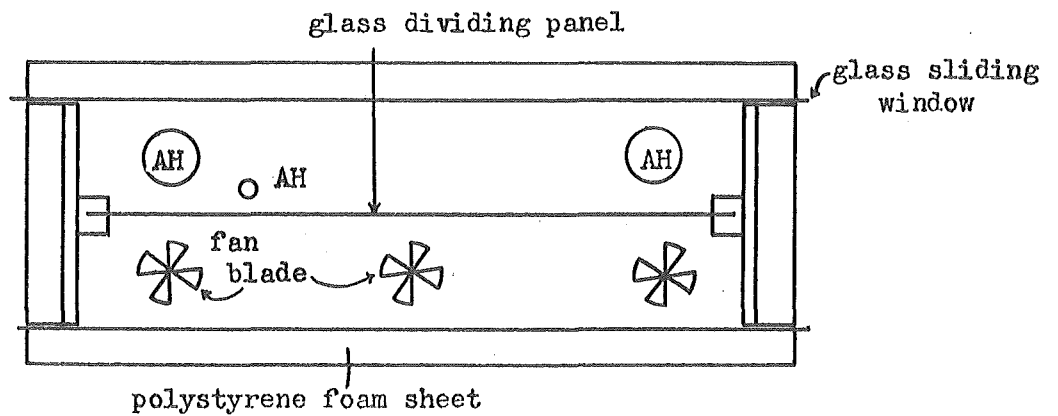
The first change made was to more efficiently insulate the enclosure by eliminating air leaks to the

Fig. 17 Thermostated Air Enclosure

(a) Side view



(b) Top view



AH holes in base allowing access to gravimetric adsorption tubes and vacuum pumps.

outside environment and by attaching polystyrene foam sheet (1 - 2 inch thick) to the outside of the box. Similar foam sheets, with appropriate slots cut to allow the manometer and spring extensions to be observed, were cemented to the glass windows.

Secondly the mercury-toluene regulator was replaced with a platinum resistance element which has a much faster response to temperature changes than the regulator. A deGussa, 100 ohm platinum in glass resistance element, with a temperature sensitivity of about $0.4 \text{ ohm}/^{\circ}\text{C}$, was employed and the small changes in resistance of the element resulting from temperature fluctuations were converted to voltage changes by the use of a strain bridge ^{and} ~~was~~ fed into a millivolt recorder (Varian) modified by (a) affixing a black perspex plate ($\frac{1}{8}'' \times 4'' \times 1\frac{1}{4}''$) to the pen holder, (b) attaching a sensitive photoelectric cell to the deck and (c) placing a small illuminated lightbulb on the deck so that the perspex plate traversed across the line between photocell and lightbulbs. The output voltage of the photoelectric cell served as an on-off

switch in the heating circuit for the enclosure.

Including the above refinements the air bath could be thermostated to $\pm 0.05^{\circ}\text{C}$ for a few hours at a time. Over longer periods however temperature variations were considerably longer, overnight fluctuations often being as much as 2°C . The delicate balance between cooling rate and heat input, set up at the thermostating temperature, could not be adjusted to allow for the large variations (up to 10°C) in room temperature which occurred overnight. Mains voltage variations may also have contributed to the observed temperature fluctuations, the variations sometimes amounting to 10% of the nominal 240 volt mains supply.

In order to test the thermostating range and degree of temperature drift in the air enclosure, a similar system to the above, involving platinum resistance element, strain bridge and millivolt recorder, was used to continuously monitor the enclosure temperature. Temperature variations as small as 0.001 could easily be distinguished on the recorder trace.

The effects of ambient temperature changes were considerably reduced by resiting the apparatus in a thermostated room, controlled to $\pm 0.5^{\circ}\text{C}$. Coincident with the shift of position, larger fan motors were fitted to the box and larger diameter, higher pitch fan blades used to increase the speed of air circulation. The large transient temperature fluctuations were considerably reduced by these changes but remained as high as 0.5°C . The short term thermostating range was improved to $\pm 0.02^{\circ}\text{C}$.

The final decision to abandon the air thermostat and change to a water bath system was prompted by the fact that it often took several hours, after an overnight fluctuation, to return the air bath to the correct thermostating temperature. Thus there was a considerable delay before the first point of the day could be observed and the number of equilibrium points recorded per day was often only two or three.

(b) Constant Temperature Water Bath.

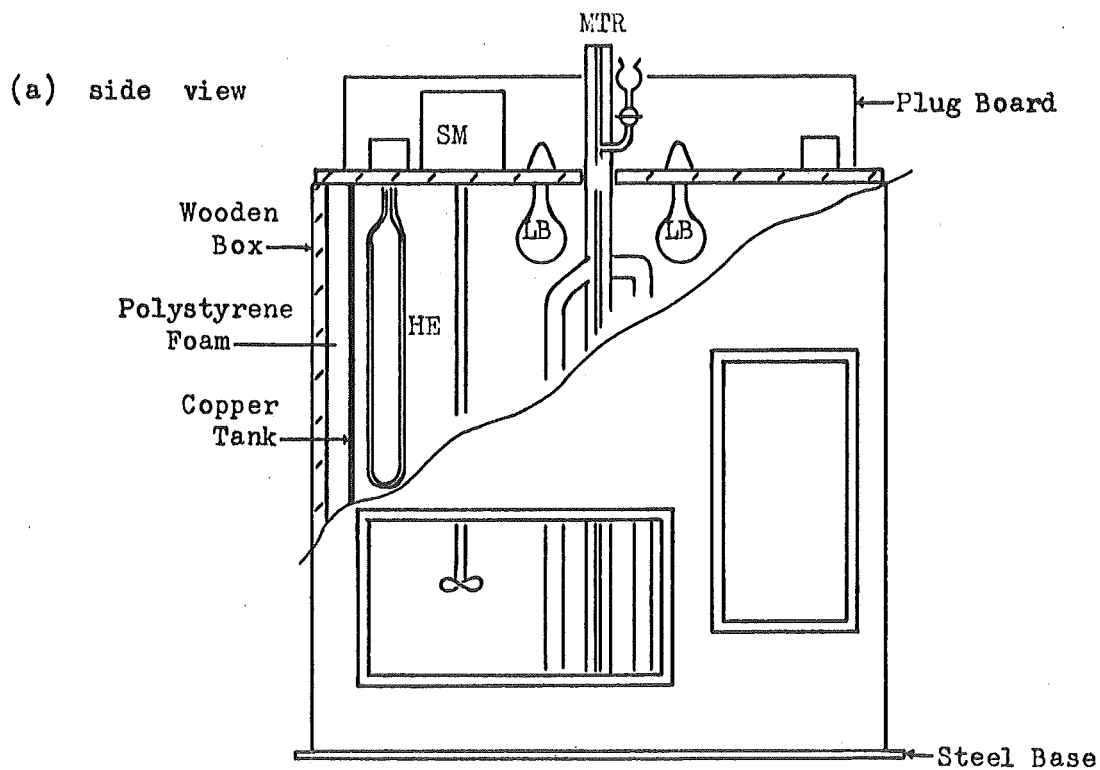
The water bath, which could be raised and lowered on a counter balance system, consisted (figure

18) of an insulated copper tank fitted with plate glass windows front and back, elements and light bulbs for heating purposes, stirrers and a mercury-toluene thermoregulator.

The tank, which when full contained about 30 gallons of water, was fabricated from 16 gauge copper sheet. All seams were riveted and soldered and the upper rim was strengthened by screwing and soldering to it lengths of angle brass ($\frac{3}{4}$ " x $\frac{1}{8}$ "). Window frames, cast from gun-metal, were screwed and soldered to the outside of the copper tank. A $\frac{3}{4}$ inch wide $\frac{1}{4}$ inch thick gasket cut from industrial rubber sheet was cemented to the inset face of each frame. One quarter inch thick plate glass windows were then glued into position followed by two further rubber gaskets before screwing on cast gun-metal retaining plates.

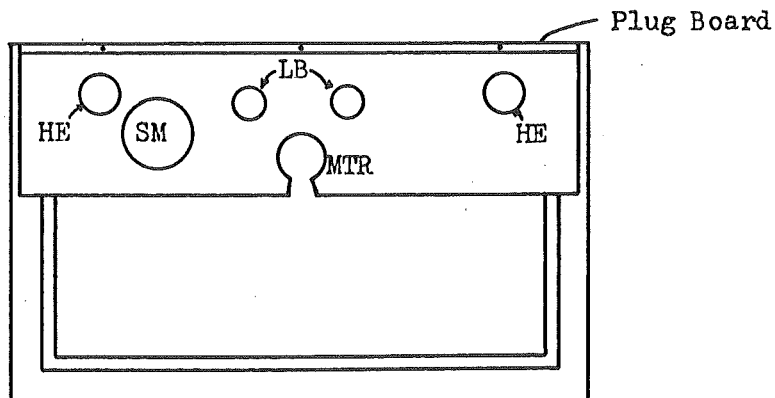
Surrounded by a layer of $1\frac{1}{2}$ inch thick expanded polystyrene foam sheet, the tank was contained inside a wooden box constructed to slide freely up and down inside ^a ~~the~~ steel framework. Screwed to the base of the box was a steel frame and to the extremities

Fig. 18 Thermostated Water Tank



- SM - stirrer motor
- LB - light bulb
- HE - heater element
- MTR - mercury-toluene regulator

(b) top view



of this frame were attached wires which passed over pulleys to the weights used to counter-balance the water bath. The bath was counter-balanced only when empty and was raised and lowered in this condition. When in operation the full tank was supported by a wooden tripod.

Auxiliary heating, stirring and temperature regulating apparatus was attached to a wooden lid fitted to the back half of the box containing the copper bath. This lid had appropriate holes cut in it to allow the necessary equipment to protrude into the bath enclosure.

The shaft of the electric motor used to drive the stirrer blade was extended by 20 inches, and careful construction, balancing and mounting of the stirrer assembly on rubber sheet was found to be necessary to reduce the effects of vibration being transmitted via the bath and framework to the vibration sensitive balance springs.

Two bar heater elements were included, one 200 watt and one 1000 watt, the smaller being included in the regulating circuit together with two 120 watt

light bulbs. For temperatures between 20°C and 30°C the heat from one light bulb was sufficient to maintain temperature, but above 30°C both bulbs were necessary. The bar heaters were used for initial warming of the water up to approximately the required temperature.

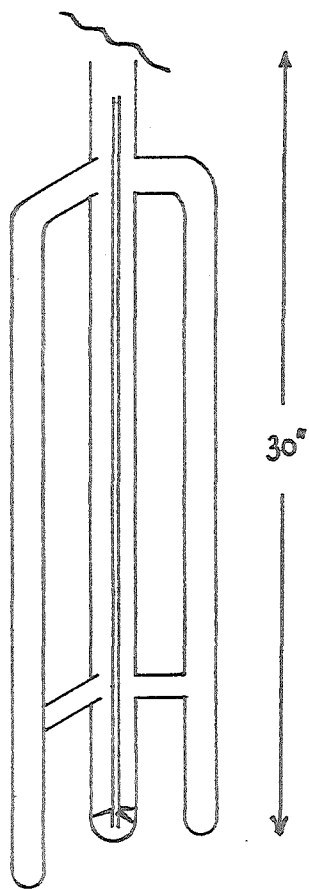
A large volume, mercury-toluene thermoregulator (figure 19b) was specially constructed for use in the water bath. The thermal expansion characteristic of the 1½ litres of liquid in the regulator, 100 ml of which was mercury, gave a linear mercury level movement in the capillary near the contact needle, of one inch per 0.05°C temperature change. With clean contacts and a clean mercury surface, this system enabled the tank to be thermostated to $\pm 0.002^\circ\text{C}$ for several days.

The contacts of the thermoregulator were contained in a circuit (figure 20) designed to reduce the contact sparking to an extremely low level. This resulted in the mercury surface and contacts remaining clean for considerable periods of time.

Fig. 19

Mercury Toluene Thermoregulators

(a) Water bath



(b) Air enclosure

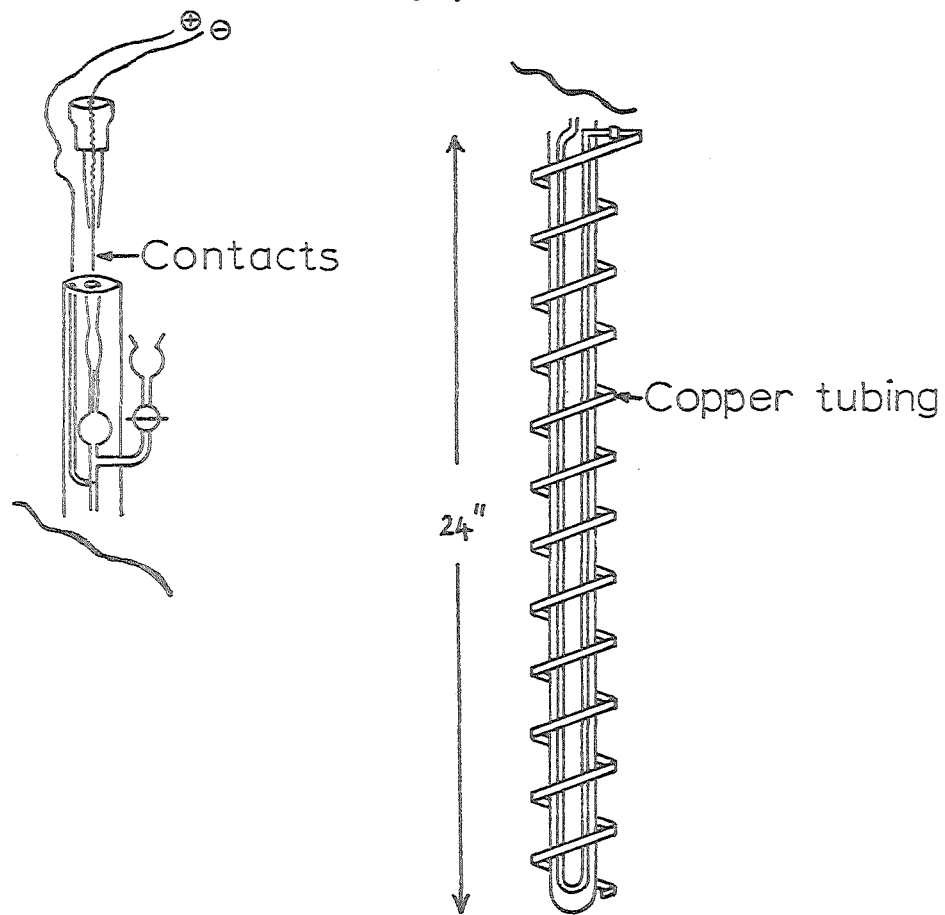
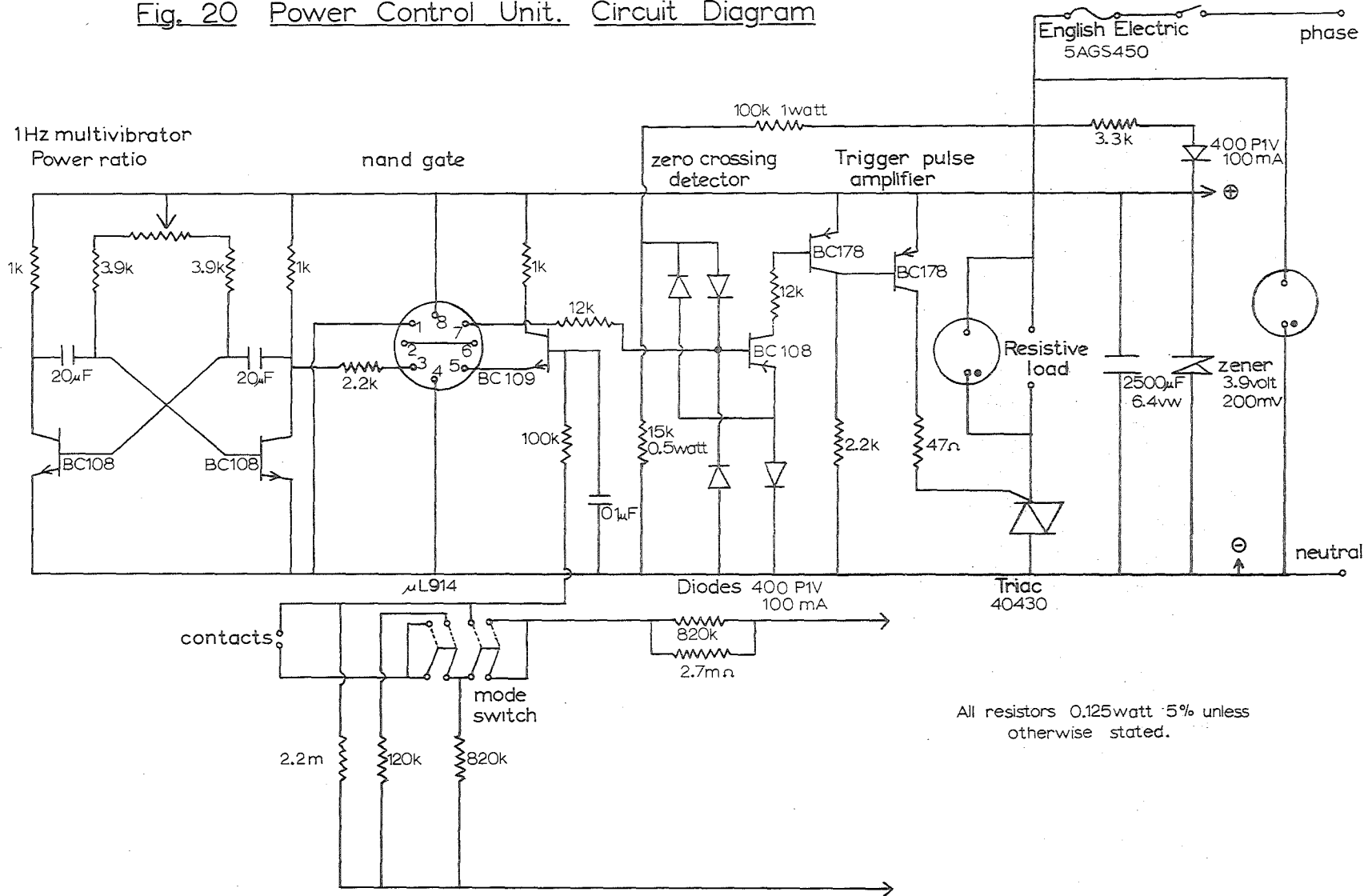


Fig. 20 Power Control Unit. Circuit Diagram



(vii) Temperature Measurement.

The thermometer used to accurately determine the isotherm temperatures consisted of a platinum resistance element (DeGussa, platinum in glass, nominal resistance 100 ohm, nominal temperature coefficient $.385 \text{ ohm}/^{\circ}\text{C}$) whose resistance was recorded by the use of a Cambridge Instruments precision decade bridge, modified to allow compensation for lead resistance effects (modified bridge circuit, figure 21). The commercially obtained, two lead resistance element was converted into a four lead element by hard soldering twin wires to each of the two original wires, making the joints as close to the element as possible. A Cambridge spot galvanometer was used as null point detector for the bridge and in this way the bridge system allowed the determination of the resistance of the element to $\pm 0.002 \text{ ohm}$, or the temperature to $\pm .005^{\circ}\text{C}$.

Accurate calibration of the resistance element, kindly done by the Physics and Engineering Laboratory of the Department of Scientific and Industrial Research, was carried out by comparison

with a standard element. The details of this calibration are included in Appendix I.

For use in the water bath, the element was completely immersed in 3 inches of distilled water contained in a 16 inch long, $\frac{3}{4}$ inch diameter glass tube sealed at one end. The element was fixed in position by forcing rubber cement around the insulated cable, connected to the element, at the point where it left the glass tube. The tube was then immersed in the bath to within $\frac{1}{2}$ inch of the top.

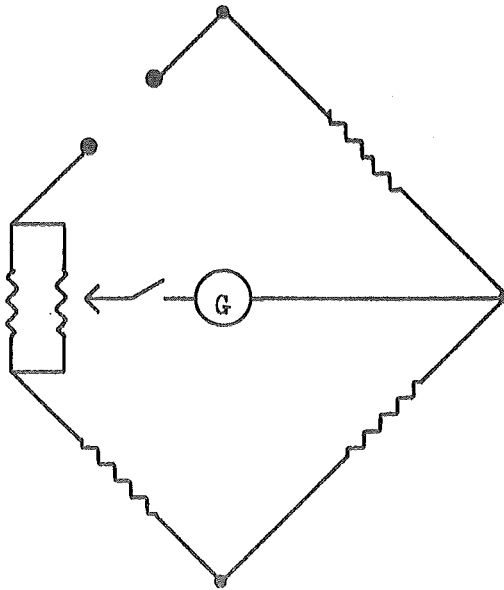
3.3.b Operation

Clay samples in the weight range 500 -700 mg, the actual weight depending on the particular spring sensitivity, were packed onto the balance pans as loose powder and suspended from the silica springs. After prolonged outgassing under high vacuum ($\leq 10^{-5}$ mmHg) at 70°C, the bath was brought to operating height and temperature and the accurate sample weights recorded by observation of spring extensions. The outgassing temperature was

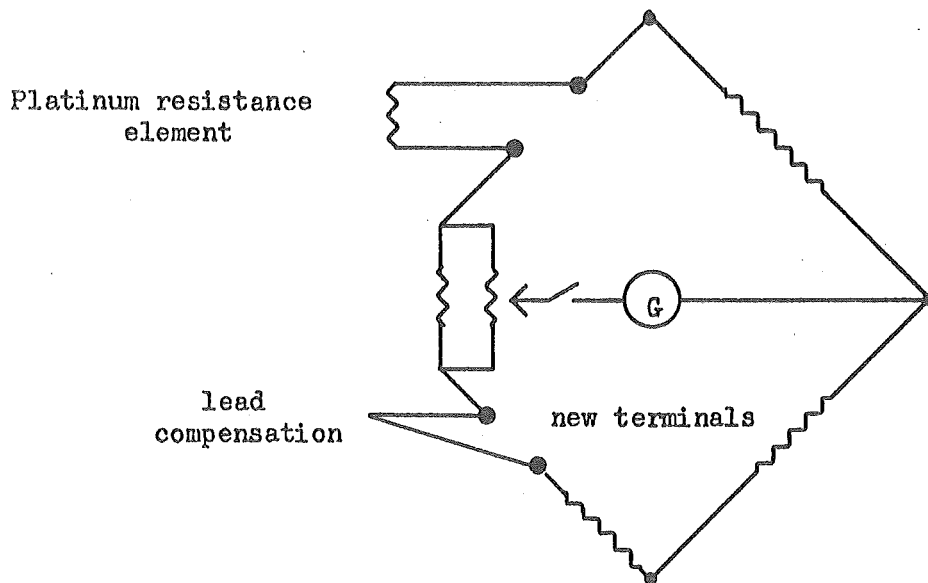
Fig. 21

Modification to Cambridge Instruments
Precision Decade Resistance Bridge

(a) Original Bridge Circuit



(b) Modified Circuit Allowing Lead Compensation



maintained by circulating water, thermostated at $70^{\circ}\text{C} \pm 2^{\circ}\text{C}$ in an external reservoir, through a copper tank placed around the adsorption tubes. Outgassing was continued until, upon isolation from the diffusion pump by closing tap G2, the pressure, as measured with the McLeod gauge, did not rise above 10^{-4} torr in 2 hours, a condition also accepted as indicating the absence of leaks in the system.

After recording the zero sample weights at the isotherm temperature, waiting 12 hours for thermal equilibrium before taking these readings, taps G2 and G3 were closed, G1 opened, and water vapour allowed to fill the dosing space of about 100ml between these three taps. Closing G1 and opening tap G2 made it possible for the vapour to pass into the adsorption tubes. After waiting a sufficient period of time for adsorption equilibrium to be reached, observations of spring extensions and system pressure were made. Subsequent points were obtained by incremental additions of water vapour to the system. Final saturation values were recorded

for a relative pressure close to 1.0 by opening taps G1 and G2, allowing the samples to come into contact with the saturated vapour.

Desorption data points were collected after very careful incremental removal of water vapour from the adsorption system by manipulation of taps G2 and G3. The dosing space was evacuated with G2 closed. After closing G3, G2 was opened slowly since too rapid water removal caused clay to be entrained in the desorbing vapour with a consequent loss of sample off the balance pans.

3.3.c Equilibrium Time

The time interval required for the attainment of the equilibrium condition, taken as no readable weight change occurring over a one hour period, varied considerably with the position of the particular point along the isotherm. Adsorption for points at low relative pressures ($P/P_0 < 0.1$) on the adsorption curve was extremely fast, essentially being completed in the first few minutes. For all points up to a relative pressure of about 0.7 on the

adsorption curve the equilibrium condition was achieved in less than one hour, while above this relative pressure a period of up to eight hours was required. Equilibrium was not attained for the last adsorption point recorded at close to the saturation pressure, the weight increasing, albeit slowly, even after a period of 24 hours. Along the desorption curve equilibrium times were somewhat longer than for points on the adsorption curve. In the higher relative pressure regions (>0.6) times of the order of 6 to 10 hours were necessary while at lower pressures up to 3 hours was sufficient.

3.3.d Errors in Water Vapour Adsorption Data

The vapour pressure of the system was read to ± 0.02 torr. As the saturated vapour pressure, appropriate to the isotherm temperature of 36.20°C , is 45 torr, the above pressure error results in an inaccuracy in relative pressure of less than 0.0005.

The spring extensions were observed

to ± 0.02 mm. Springs of various sensitivities were used during experimentation but all were nominally 25cm/gm. For this sensitivity the uncertainty in extension yields an error in the weight of water adsorbed of 0.08mg. The amount adsorbed which corresponds to a completed monolayer ranges from 8.04mg/g for lithium metahalloysite to 11.74 mg/g for magnesium metahalloysite. This accepts that the BET equation gives a reliable value for the monolayer capacity. Since the determinations were carried out on samples of about 600mg of clay the error of 0.08mg results in an uncertainty of somewhat less than 2% in the monolayer capacity for the lithium clay and somewhat over 1% in the monolayer capacity for magnesium metahalloysite.

The experimental errors are, it is noticed, considerably larger than those for the nitrogen adsorption system (section 3.2.c) and approximately encompass the errors associated with reproducibility (see table 4).

3.4 Determination of Cation Exchange Capacity

The cation exchange capacity of 'natural' (1 - 20 μ) metahalloysite was determined by two different methods, firstly by the permanganate method of Bower and Truog (303) and secondly the atomic absorption spectrophotometric determination of sodium.

3.4.a The Permanganate Method.

A sample (approximately 1g) of sodium metahalloysite, part of the bulk homoionic clay prepared as outlined in section 3.1.b, was dried in an oven at 110°C for 48 hours and placed in a tared stoppered centrifuge tube. The sodium ions were replaced with manganous ions by washing the material five times with portions (50ml) of a manganous chloride solution (0.5M) allowing a contact time of 5 minutes for each washing. Between each contact the stopper was removed, the sides of the centrifuge tube and stopper washed with ethyl alcohol (95%, pH =7) and the suspension cleared by centrifugation (1500rpm, 5 minutes). Excess manganous chloride was removed by repeatedly washing with 95% ethanol and centrifuging

until no positive silver nitrate test for chloride ions was observed with the centrifugate solution. The final settled material was oven dried at 110°C for 48 hours while in the centrifuge tube and the combination weighed.

The manganese ions, present as cation exchange ions on the resulting clay, were removed into solution by five successive washing and centrifugation procedures using 50ml. portions of 1 N ammonium acetate solution. All of the washings were retained, added together and made up to a total volume of 500ml. with distilled water. Part of this solution (⁵⁰⁰150ml.), estimated to contain about 0.3 mg of manganese, was evaporated to dryness in a 750ml. beaker. After washing the sides of the beaker with 2 - 3ml. of concentrated nitric acid, the contents were again evaporated to dryness. The acid also served to oxidise any carbonaceous material present. Concentrated sulphuric acid (5ml.) was added slowly, and cautiously diluted with distilled water (15ml.). After adding para sodium periodate (0.2g) the solution was boiled gently until the

purple colouration of permanganic acid appeared, To ensure complete oxidation, the solution was diluted to 99ml. with distilled water, the beaker covered with a watch glass and heated on a hot plate at 85-90°C for 30 minutes. After allowing to cool, the solution was diluted to 100ml. in a standard flask and the colour compared with a standard permanganate solution prepared according to the directions of Bower and Truog (303).

A Shimadzu MPS recording ultraviolet and visible spectrophotometer was used for the colour comparison, the 480 to 560 m μ region of the visible spectrum being recorded. The peak chosen for the calculation of exchange capacity was that centred at 526 m μ .

3.4.b Atomic Absorption Method

Approximately 1g of the sodium exchanged TePuke metahalloysite was placed in a tared, stoppered centrifuge tube and dried to constant weight at 110°C in an oven. After lightly crushing the dry material, calcium chloride solution (10⁻²N, 30cc) was added, the tube and contents

agitated by hand shaking and left for one hour before centrifugation (200 rpm, 10 minutes). The centrifugate was decanted and retained and a further portion of calcium chloride solution added to the sediment. A contact time of one hour, with agitation, elapsed before the contents were centrifuged as before and the supernatant separated. The two supernatant solutions were combined and poured into a 100 ml. measuring flask and made up to the mark with 10^{-2} N calcium chloride solution. Five ml. of this solution was pipetted into another 100ml. measuring flask and made up to the mark with distilled water. The final solution was then tested for sodium ion concentration by comparison with standard solutions and using a Techtron Grating Monochromator Atomic Absorption Spectrophotometer type AA4.

Solutions.

Analar sodium chloride and calcium chloride were used in the preparation of all solutions.

A 10^{-2} N solution of sodium chloride (0.5845g) was first prepared in a one litre standard flask. From this bulk solution 100ml. solutions of

Fig. 22

Visible Absorption Spectra for Permanganate Solutions
Used in Cation Exchange Capacity Determination

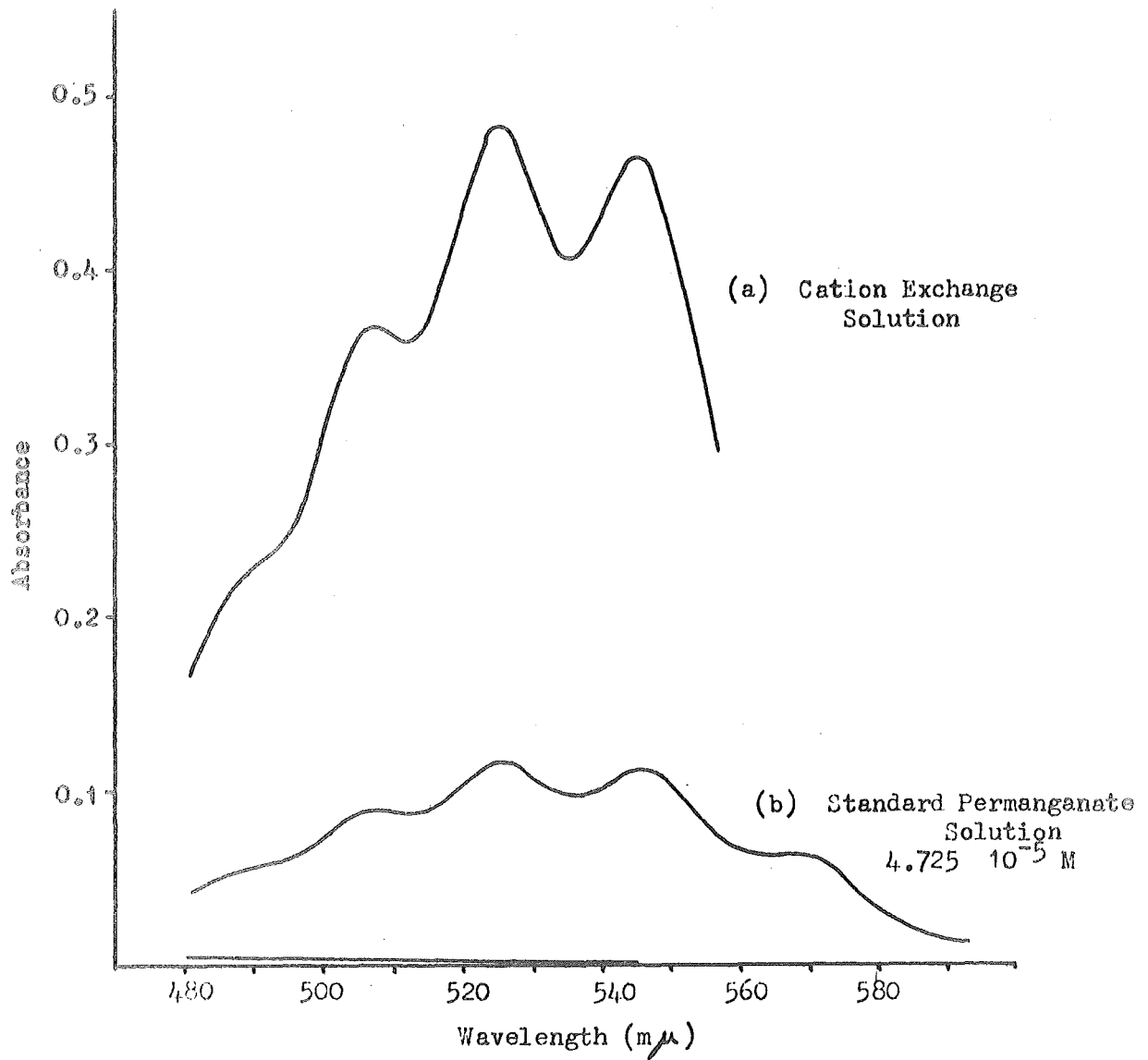
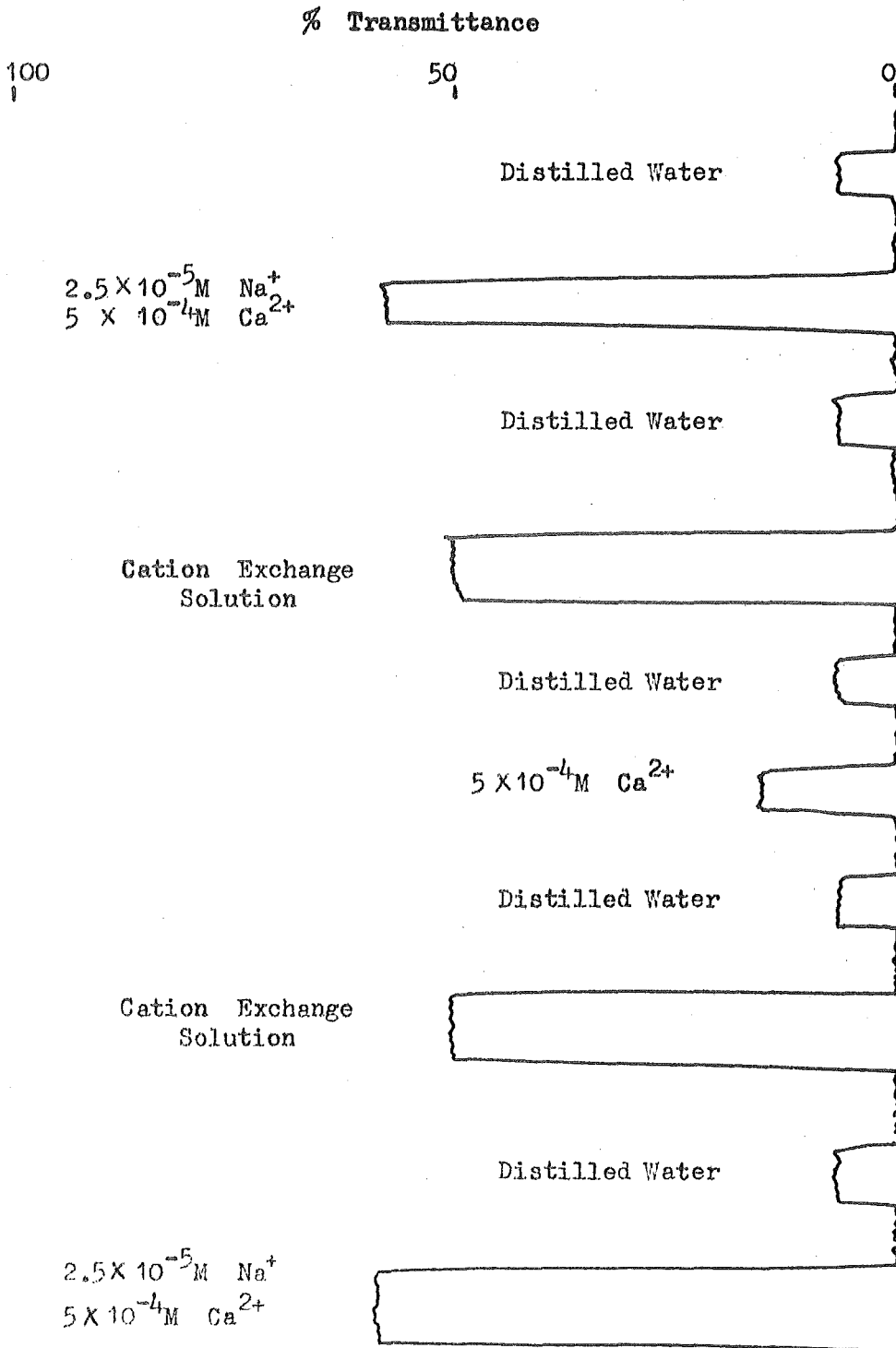


Fig. 23

Atomic Absorption Spectrophotometer Trace for the Solutions Used in the Determination of Cation Exchange Capacity



concentration 10^{-4} , 5×10^{-5} , 2.5×10^{-5} and $10^{-5}N$ were prepared by dilution. To each of these standard flasks, before completely filling up to the mark, 5ml. of a standard $10^{-2}N$ calcium chloride solution was introduced, the resulting solutions therefore being $5 \times 10^{-4}N$ in calcium chloride.

3.4.c Results.

(i) Permanganate Method

From the spectrophotometer trace, reproduced as figure 22, the absorbance values, for cation exchange and standard solutions, are $0.481 \pm .002$ and $0.114 \pm .002$ respectively. Since the concentration of the standard manganese solution was $4.72 \times 10^{-5}M$, the absorbance of the exchange solution represents a concentration of $4.72 \times 10^{-5} \times \frac{.481}{.114}M$ and contains 1.98×10^{-5} moles of Mn^{2+} or 3.96×10^{-5} equivalents of Mn^{2+} .

For a sample weight of 0.977g, this number of equivalents yields a value of cation exchange capacity equal to 4.1 ± 0.1 meq/100gm dry clay .

(ii) Atomic Absorption Method.

In this instance the output voltage of

the spectrophotometer was used as input for a Varian recorder and the percentage transmittance of the various solutions collected as traces on chart paper. A section of the chart is reproduced as figure 23. Conversion of the transmittances to absorbances and making allowance for the absorbance due to distilled water and due to calcium solution leads to values for the absorbance due to sodium ions along.

Solution	Absorbance due to sodium ions
$2.5 \times 10^{-5} \text{N Na}^+ / 5 \times 10^{-4} \text{N Ca}^{2+}$	$.305 \pm .007$
cation exchange solution	$.229 \pm .007$

The sodium ion concentration of the cation exchange solution is thus

$$2.5 \times 10^{-5} \times \frac{.229}{.305} \text{ N}$$

$$= 1.9 \pm 0.1 \times 10^{-5} \text{ N}$$

This contains 5ml. of the original exchange solution which therefore contained $1.9 \times 10^{-5} \times 20 \times \frac{100}{1000}$ equivalents Na^+ and this corresponds; for a 1.021g sample of metahalloysite,

to a cation exchange capacity of 3.8 ± 0.2 meq/100gm.

3.5 Weight Loss Determinations

The weight loss of 'natural' TePuke metahalloysite as a function of temperature was studied for both air and vacuum conditions.

(i) Heating in Air.

For the determination of weight loss in air a bottom loading Mettler balance was set up as shown in figure 24. The temperature of the wire-wound furnace was controlled to $\pm 3^{\circ}\text{C}$ by an Ether Transitrol controller and temperatures were measured with a Tinsley thermocouple potentiometer and a chromel-alumel thermocouple. Samples of the 'natural' clay ($\sim 2\text{g}$), after drying in an oven at 110°C for 8 hours, were weighed into a tared silica bucket. This bucket was then attached to the end of the silica fibre (figure 24) and lowered into the furnace enclosure. A zero weight was recorded after the material had been maintained at 110°C for four hours. The temperature was then raised to some

higher value and the weight recorded at timed intervals until constant. At this time the temperature was further increased. The range of temperatures covered was 110° to 600°C .

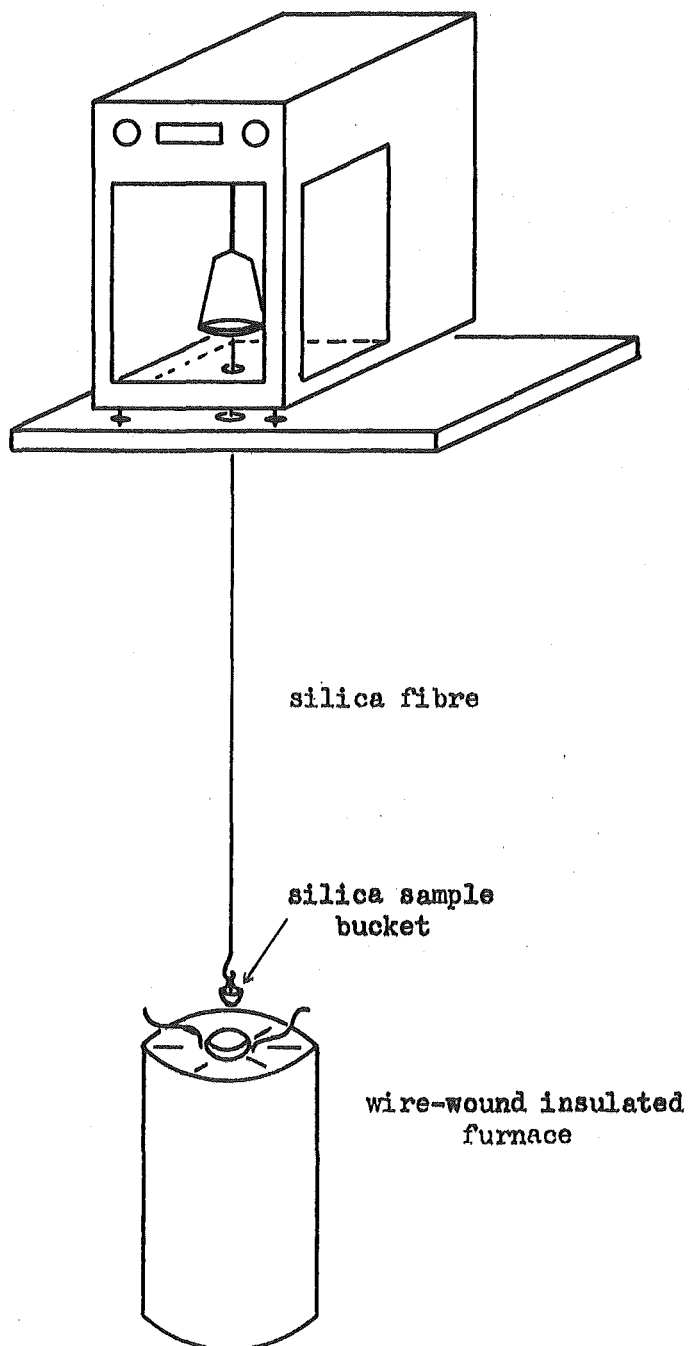
(ii) Heating in Vacuum.

Vacuum weight loss experiments were carried out on small samples ($\sim 40\text{mg}$), using a silica spiral spring balance, and on large samples ($\sim 3\text{g}$) using a bulb, fitted with a tap, which could be detached from the vacuum system and weighed.

For the small samples, a large diameter (5 cm) glass tube was included in the high vacuum adsorption system (figure 12). The tube could be detached from the system at flange joint F. When in use the joint was lightly greased with Apiezon 'N' grease and firmly clamped. The silica spring, of sensitivity 290.8 cm/g , was waxed to a glass support situated in the fixed portion of the large glass tube. A silica extension fibre was inserted between spring and sample holder so that the spring would not be in the high temperature region. Spring extensions were observed to 0.02 mm with the aid of a cathetometer,

Fig. 24

Apparatus for the Determination of Weight Loss
in Air.



this distance being the equivalent of less than 0.01 mg. Samples were contained in an aluminium pan supported, from a hook at the lower end of the spiral spring, by a nichrome stirrup. The same furnace, controller and temperature measuring equipment, used for the air weight loss experiments, were utilised again in this section.

The large clay samples were introduced into weighed sample bulbs of similar dimensions to those used for the surface area and pore size distribution studies (section 3.2.a (viii)). Bulb and contents were heated overnight in a 110°C oven, cooled in a desiccator for 10 minutes and weighed. A tap and socket joint were then glassblown on to the bulb, the tap greased and the whole attached to the high vacuum system at a cone joint, such that bulb and tap were horizontally mounted. After cautiously evacuating the contents of the bulb to 10^{-5} torr, to avoid entrainment of particles, the temperature was raised to 70°C by means of a small wire wound furnace, the temperature of which was maintained and measured as before. 60 hours later the tap was closed, the

furnace removed, and the bulb allowed to cool to room temperature. The weight loss system was then detached from the vacuum line, the grease carefully removed from the socket joint and the whole system weighed on a Mettler balance. This weight was accepted as the zero weight. Repetition of the greasing-degreasing procedure indicated that with care a reproducibility of ± 0.5 mg could be achieved. The system and contents were then subjected to a series of progressively higher outgassing temperatures each being maintained for 60 hours. Between each of these temperatures the weight was recorded after allowing the system to cool.

3.6 Infra-red Spectra

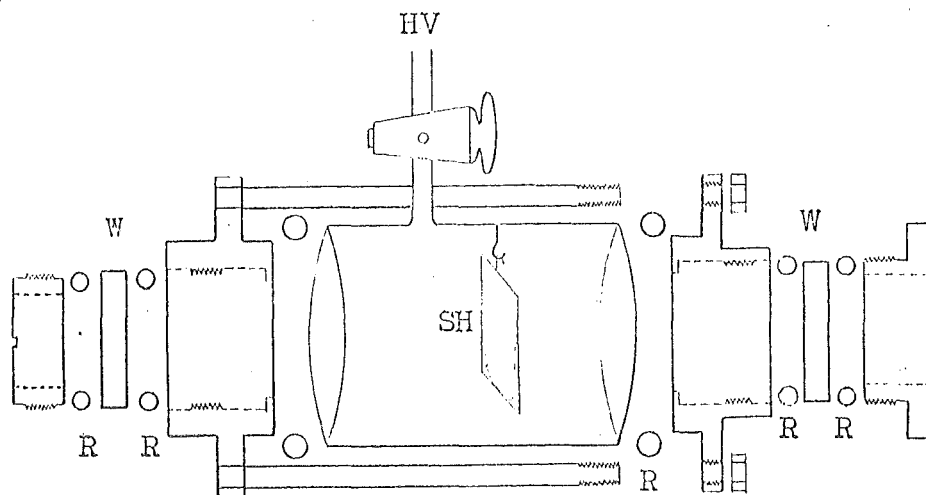
Spectra of variously treated metahalloysite samples were determined as mineral-oil (Nujol) mulls or as mulls with a halocarbon (Fluorolube). Two Perkin-Elmer grating spectrometers ^{were used} at various times, one a 421 model, the other a 337.

Some brief exploratory experiments were made to determine the possibility of following the adsorption of water vapour on metahalloysite by infra-red techniques. A vacuum cell (figure 25) was constructed which could be evacuated to 10^{-6} torr, the pressure not rising above 10^{-3} torr in one hour upon isolation from the pumps. Two methods were tried for the production of suitable mineral films (1) sedimentation directly onto the calcium fluoride windows (2) sedimentation onto various types of nylon material. Spectra were obtained using these techniques but the spectral changes observed, upon saturating the films with water vapour at room temperature, were extremely small, and for this reason it was believed that, with this apparatus, close examination of the adsorption process was not possible.

3.7 Differential Thermal Analysis Spectra

Differential thermal analysis of some samples were kindly run by the New Zealand Pottery

Figure 25 Infra-red Cell for Water Vapour Adsorption Studies
on Clay Minerals



- W Calcium fluoride window
- R "o"-ring
- HV High vacuum
- SH Sample holder

and Ceramics Research Association. These were obtained by the use of a Stone (Texas) instrument with $\alpha\text{-Al}_2\text{O}_3$ as the reference material. The samples were heated from room temperature to 1000°C at a heating rate of $10^\circ\text{C}/\text{minute}$.

CHAPTER 4 : DISCUSSION

4.1 Adsorption of Polar and Non-polar Adsorbates on Metahalloysite

4.1.1 General Observations

Complete adsorption-desorption isotherms for the adsorption of nitrogen and argon at 78°K, water vapour at 209.4°K and ethyl chloride at 273.2°K on natural metahalloysite are displayed as figures 35, 26, 33 and 29 respectively. The adsorption curves for the various systems are all of similar shape but the desorption branches differ significantly, particularly in the region of low relative pressure; those for the non-polar gases coinciding with the respective adsorption branches while the isotherms for the polar adsorbates show a narrow but persistent hysteresis down to very low pressures. A sharp decrease in the amount of adsorbate retained is indicated by a drop in the desorption isotherm which occurs at a relative pressure of 0.45 for ethyl chloride, 0.48 for nitrogen and 0.35 for argon. The

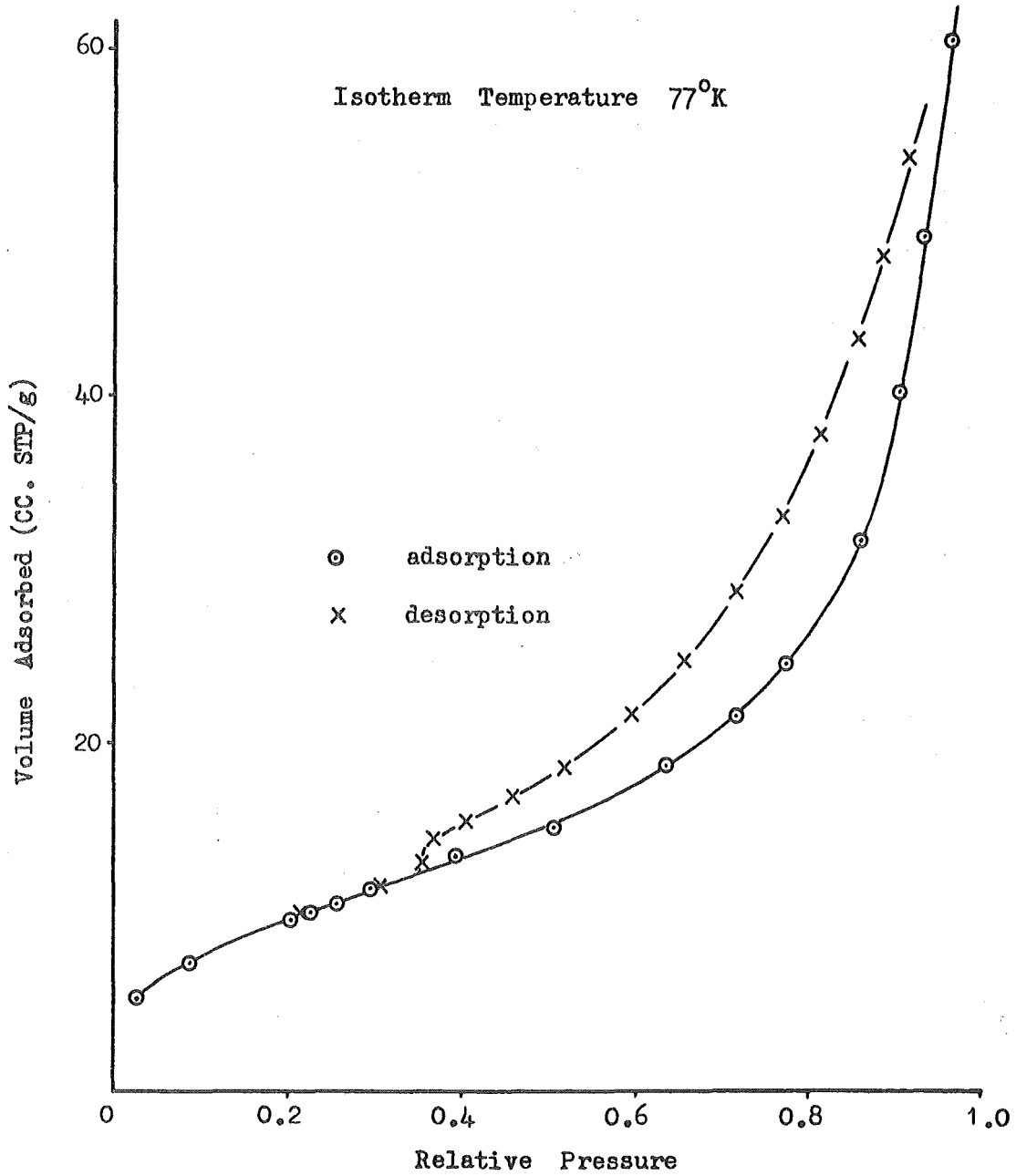
water vapour isotherm shows a small but significant decrease at 0.40.

If a capillary condensation mechanism is assumed to explain the high pressure hysteresis then the discontinuities in the various desorption curves can be related, by way of the Kelvin equation (equation 9), to the mean radius of curvature of the meniscus controlling the desorption process. The radius calculated in this manner is 11\AA for the water and argon isotherms, 12\AA for nitrogen and 14.5\AA from the ethyl chloride data. As is more fully discussed later (section 4.2), these facts, together with the overall shape of the isotherms and a knowledge of the structure of the mineral, are consistent with an adsorbent in which lamellar particles form slit-shaped pores between them.

Although the adsorption curves for the various systems appear quite similar they do, if plotted in the form suggested by Jura and Harkins (199), clearly show that the process of adsorption is quite different for polar and non-polar molecules. The curve for argon (figure 27a) is approximately

Fig. 26

Argon Sorption Isotherm For 'Natural' Te Puke
Metahalloysite Outgassed at 110°C.



linear throughout while that for nitrogen (figure 27b) has a general decrease in the negative slope from low to high amounts adsorbed (χ). The slope of the graphs for the polar molecules increases negative as the amount adsorbed increases, that for ethylchloride (figure 27c) increasing continuously and that for water (figure 27d) increasing discontinuously (see section 4.5.2). The slopes of these curves are related to the compressibility of the adsorbed film (199) and the observed differences in the curves for polar and non-polar adsorbates are presumably a reflection of the influence of the mineral surface on the adsorption of polar molecules. Strong dipole-dipole interactions, between the oxygen and hydroxyl groups regularly arranged on the mineral surface and the water or ethyl chloride molecules, should result in specific site adsorption and also in the adsorption of the molecules in a preferred orientation. Argon and nitrogen molecules are not expected to be affected by the surface in the same manner as the polar adsorbates although nitrogen has a considerable quadrupole moment (180, 187-190) and

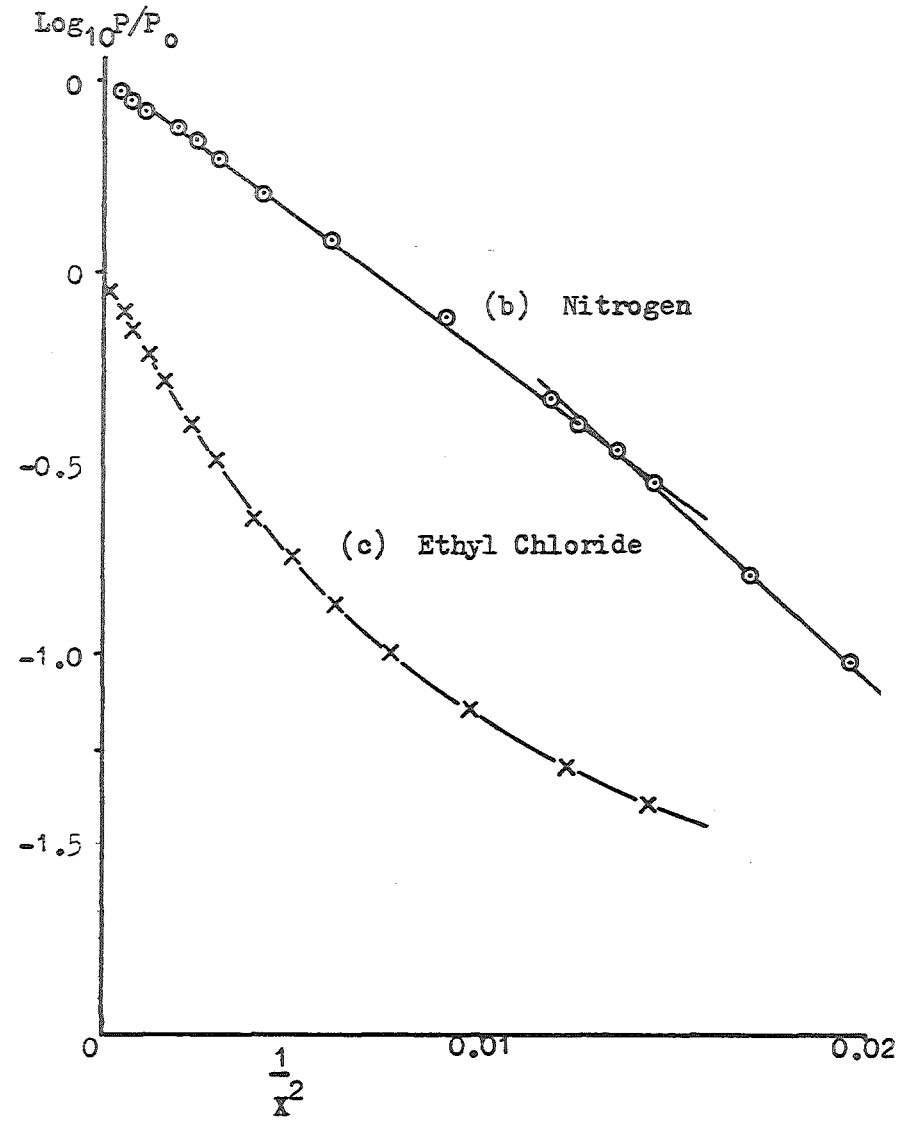
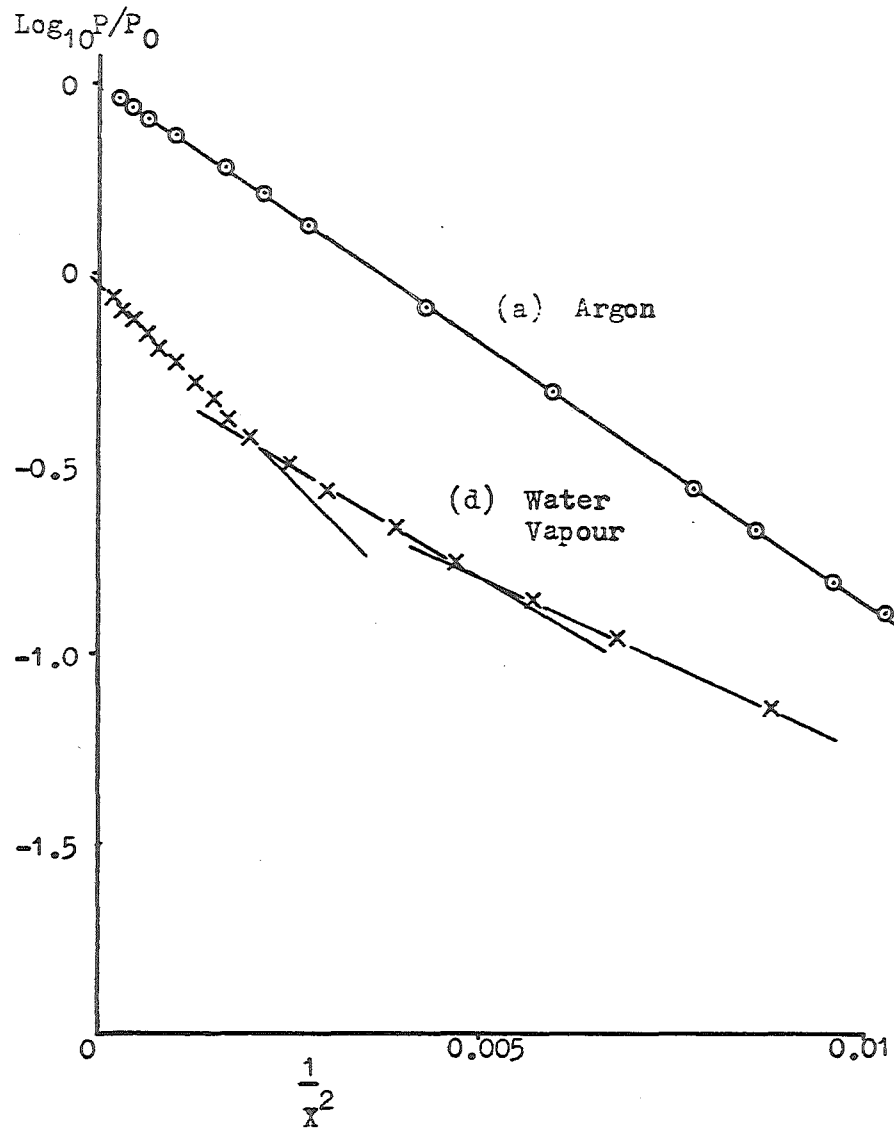
therefore should interact with the surface more strongly (187) than should argon.

4.1.2. Low Pressure Hysteresis

Hysteresis which continues to very low relative pressures, as observed in this study for ethyl chloride and water vapour adsorption on natural metahalloysite, has also been reported for many other systems, including the adsorbents graphite (265), porous glass (271), oxide gels (272,275) and clay minerals (73,87,116,117,266-270). There are also many instances of low pressure hysteresis in which chemisorption is believed to explain the observed effects (96,99,100,260-263). In the present cases however, and particularly for ethyl chloride adsorption, it seems unlikely that there should be any chemical interaction with the surface of the mineral. Usually, for the systems in which chemisorption occurs, there is, upon desorption, a residual amount of adsorbate retained which cannot be removed by outgassing at the experimental temperature. This was not observed for the water vapour isotherms obtained in this study, the amounts retained, after outgassing

Fig. 27

Jura-Harkins' Plots for the Adsorption of Argon, Nitrogen, Water Vapour and Ethyl Chloride on 'Natural' Te Puke Metahalloysite



at the isotherm temperature, being extremely small.

Low pressure hysteresis, observed for the adsorption of polar molecules on substances exhibiting a laminar structure, is most often attributed to intercalation of adsorbate between the layers of the solid (264,269). Interlayer penetration occurs, according to Everett (264), when the spreading pressure (ϕ) of the adsorbate, given by equation 18, exceeds some critical value which is dependent upon the cohesive strength of the solid. The irreversible step which results in hysteresis is probably the initial penetration as this requires the prising apart of the layers to admit the first few molecules (277).

$$\phi = RT \int_0^P n_a d \ln P \quad 18$$

n_a - amount adsorbed at P.

P - equilibrium pressure

Desorption of the intercalated molecules, which are held by powerful adsorption forces, may therefore be expected to occur at very

low relative pressures. Confirmation of this mechanism of hysteresis has been achieved in a few cases, by an X-ray study of the interlayer spacing, in particular for the adsorption of bromine on graphite (273) and for water on montmorillonite (266,274,276). The situation with the water-metahalloysite system is somewhat different since water apparently does not, to any considerable extent, penetrate the inter-layer spaces (4,65,98) except under special conditions in which the mineral has first been treated with one of certain salt solutions (15,16) or with a solution of certain organic molecules (14). The ethyl chloride molecule, less polar than water, is also unlikely to lead to intercalation of metahalloysite. This mechanism cannot, however, be completely disregarded as calculations show that interlayer penetration of about 1%, on an area basis, is all that is required to explain the width of the hysteresis loop observed, in the present study, for water vapour on natural metahalloysite.

The mechanism of irreversible capillary condensation is incapable of giving rise to hysteresis

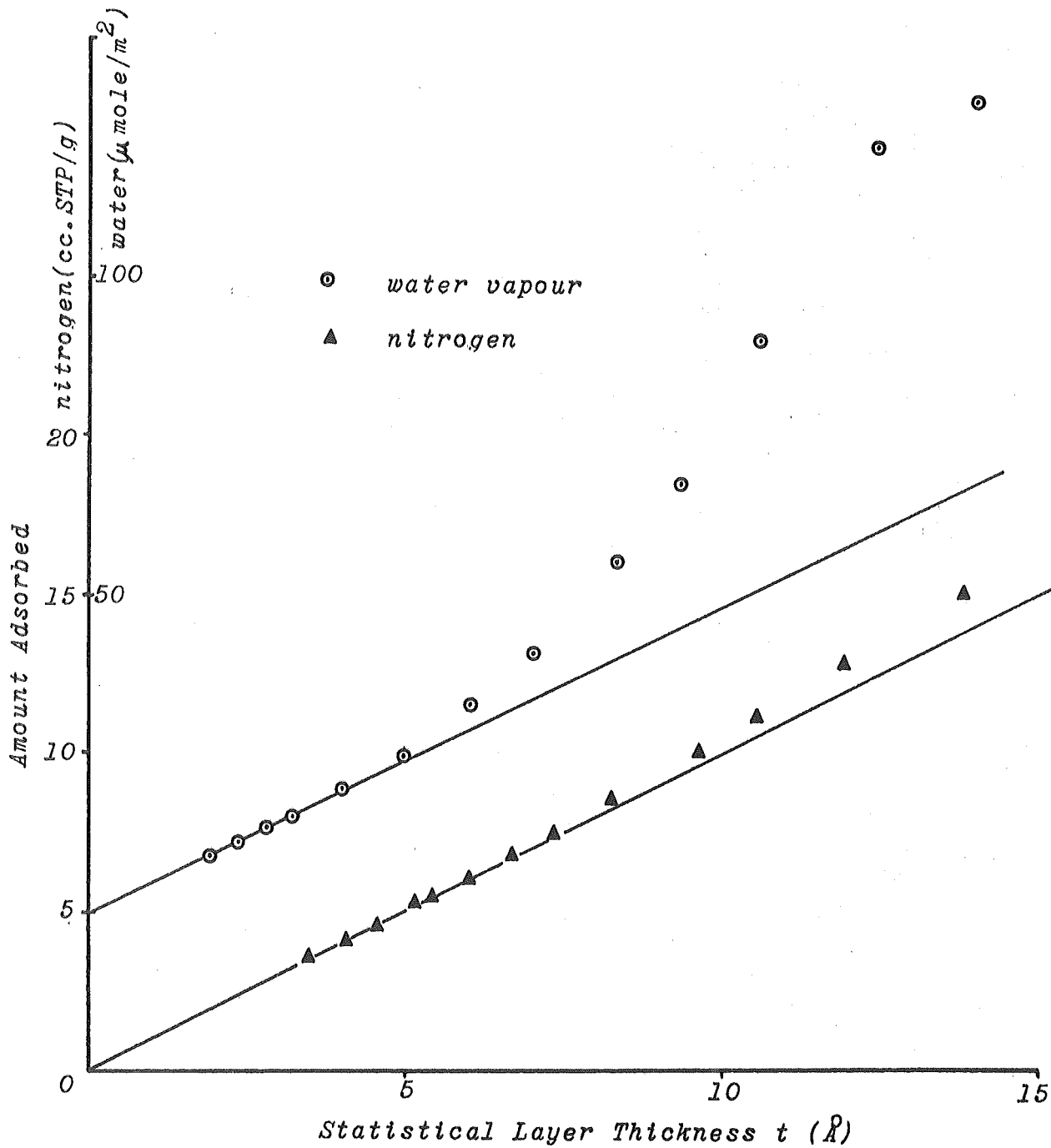
which continues down close to the zero pressure, as this requires the formation of a meniscus in pores down to radii smaller than the diameter of a single adsorbate molecule. This is clearly impossible and it has also been shown that adsorption in micropores occurs by a reversible process which is independent of the pore size (235,236). The phenomena associated with capillary condensation is incapable (225-227) of satisfactorily explaining hysteresis effects for pores of smaller than a minimum size. This lower limit has been shown (225) to be around 18\AA for nitrogen which corresponds to a relative pressure of 0.40. It is likely that a similar limit exists for water and ethyl chloride adsorption.

It has been suggested that the low pressure hysteresis, observed for the adsorption of ethylamine on silica, results from the extremely slow diffusion of adsorbate molecules trapped in fine pores (278). Plots of the volume adsorbed V_a versus the statistical thickness t (discussed in section 2.3) for the adsorption of nitrogen (figure 28(a)) and water vapour (figure 28(b)) on natural

metahalloysite, both extrapolate to the origin and indicate an absence of submicropores ($r < 5\text{\AA}$) in the sample. Thus diffusion controlled desorption is not expected to explain the low pressure hysteresis observed in the present study.

A further mechanism which may account for low pressure hysteresis is the formation of metastable adsorbed phases (279) resulting from two dimensional supersaturation (280). Adsorption may occur in a localised fashion giving rise to islands of adsorbate which coalesce at higher pressures. Desorption takes place by evaporation from a continuous liquid film. Since the vapour pressure above a small droplet is greater than that above a planar liquid surface, hysteresis should result (279). It is also possible that, during the initial adsorption the packing of molecules in the first layer is determined by the surface structure and is quite loose, while the effect of higher layers is to force further molecules into the first layer giving close packed conditions. Desorption from the surface of this closely packed layer is expected to be quite different

Fig. 28 V_a/t Plots for Nitrogen and Water Vapour Adsorbed
on 'Natural' Te Puke Metahalloysite



from the situation during adsorption. If local densely packed islands of adsorbate remain as the pressure is decreased then this mechanism can explain hysteresis to very low relative pressures. Such islands of adsorbed material might be expected to occur around the exchange cation sites on the natural metahalloysite.

Fiat, Folman and Garbatski (271), in order to explain their results for the adsorption of ammonia on porous glass, proposed that preferential desorption from the hydroxyl groups, allied with strong binding of adsorbate molecules to the oxygen sites, can lead to low pressure hysteresis.

The interaction of polar molecules with the fundamental particles of a substance during adsorption may cause alterations in the orientation of platelets. Desorption could therefore take place from a somewhat different pore geometry than that prevailing during the initial stages of the adsorption process. The result is a hysteresis which can continue to low pressures and which, it is suggested (267), is characteristic for polar adsorbates on

non-rigid adsorbents such as polymers, textile fibres and clays. This type of mechanism probably explains the hysteresis effects observed for water adsorbed on palygorskite (268) and for water on phenyl montmorillonite (270).

Although it is possible that all of the above mechanisms may operate to greater or lesser degrees for the adsorption of polar molecules on metahalloysite, the effects observed in the present study are adequately explained by the mechanism which envisages desorption from an interfacial layer more densely packed than during the initial adsorption. In this regard it is interesting to consider the adsorption data and hysteresis effects found for water and ethyl chloride adsorbed on samples of natural metahalloysite and on samples after treatment with trimethylchlorosilane (TMCS). This reagent reacts with surface hydroxyl groups and should obscure the polar surface of the mineral with a hydrocarbon layer. Because of the bulky size of the trimethylsilyl group however, it is not expected to react with every hydroxyl group, a simple weight gain experiment showing

that approximately one third of the OH groups of the natural 110°C outgassed mineral were attacked. This closely coincides with the fraction expected to react from a consideration of an atomic model of the system.

The data pertinent to this section of the discussion are contained in table 2, in the isotherms for ethyl chloride adsorption (figures 29 to 32) and in the water isotherms (figures 33 and 34).

A considerable reduction occurs in the specific monolayer capacity of a sample after treatment with TMCS, whether measured by the adsorption of water vapour, nitrogen or ethyl chloride adsorption. The decreases for nitrogen (14%) and water (10%) are approximately in the same ratio as their equivalent spherical molecular diameters (16.2\AA^2 and 10.6\AA^2 respectively from equation 6) and may reflect a change in the specific surface area of the solid of around $5\text{ m}^2/\text{g}$. Some of the decreases measured by nitrogen and water, however, may be a result of these molecules being sensitive to the nature of the surface (Section 2.1). The effective cross-sectional area of the nitrogen molecule 6N_2 was found to be larger on a

methyated silica gel surface than on the untreated gel (283). Nitrogen adsorption was reduced by trimethylsilylation of silica gel (284) or by the thermal dehydration of the gel surface (285). TMCS treatment of an amorphous silica gel, although not affecting the specific surface area, markedly decreased the water vapour adsorption (286). With these facts in mind, and also that σ_{H_2O} is dependent on the nature of the exchange cation (section 2.1), it is pointed out that the decreases in monolayer capacity for nitrogen and water vapour may be composed both of surface area changes and changes in the values of σ_{N_2} and σ_{H_2O} , due to a reduction, caused by TMCS treatment, in the number of adsorption sites available.

The reduction in the specific monolayer capacity for ethyl chloride was 33% for the TMCS treatment of a 110°C outgassed sample and 28% for treatment of a sample outgassed at 400°C. These reductions may be due in some degree to a loss of surface area but are better accounted for by a loss of adsorption sites as the result of TMCS treatment.

Fig. 29

Ethyl Chloride Sorption Isotherm for 'Natural'
Te Puke Metahalloysite Oven-heated at 110°C.

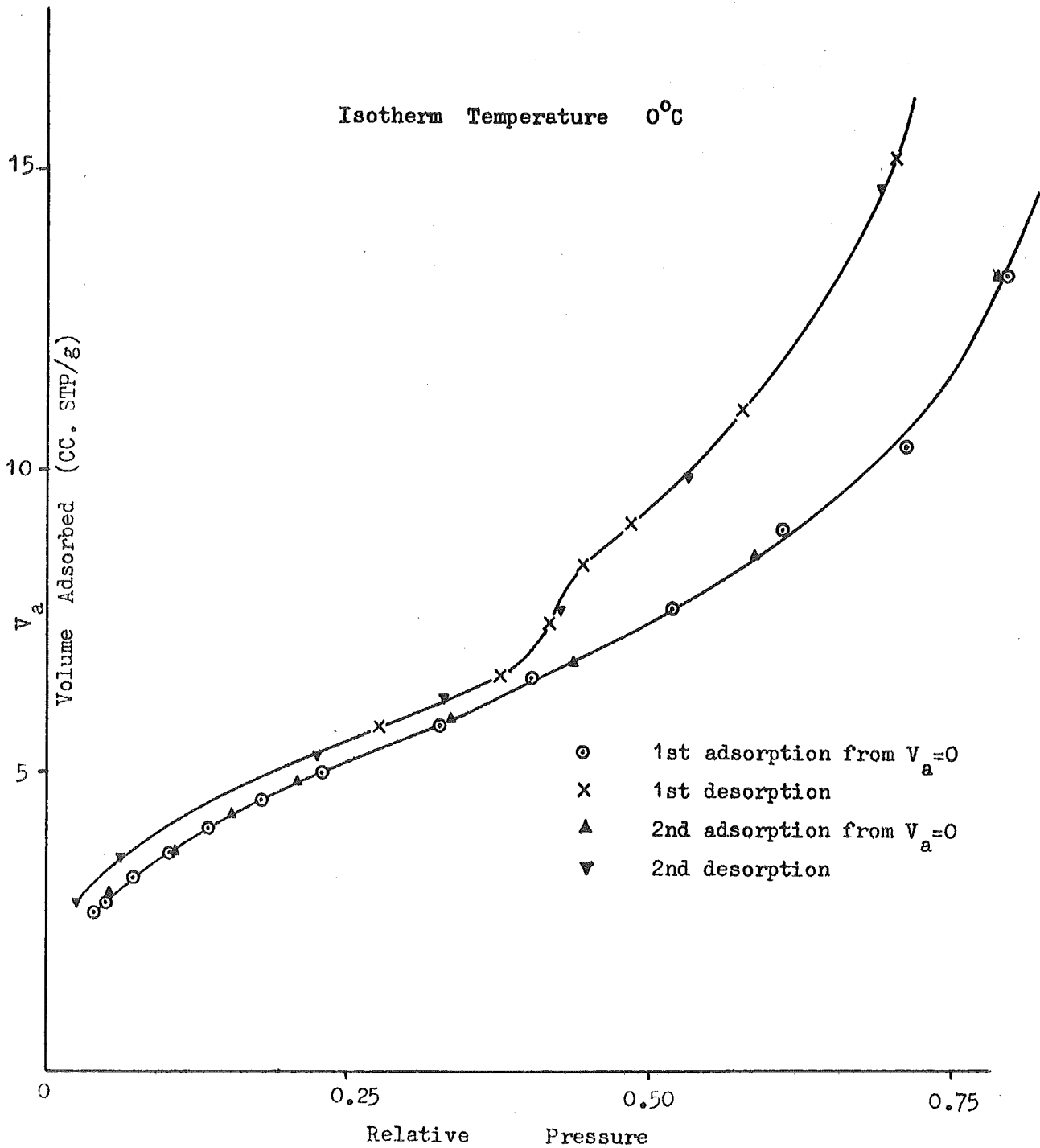


Fig. 30

Ethyl Chloride Sorption Isotherm for 'Natural
Te Puke Metahalloysite Treated with Trimethylchlorosilane

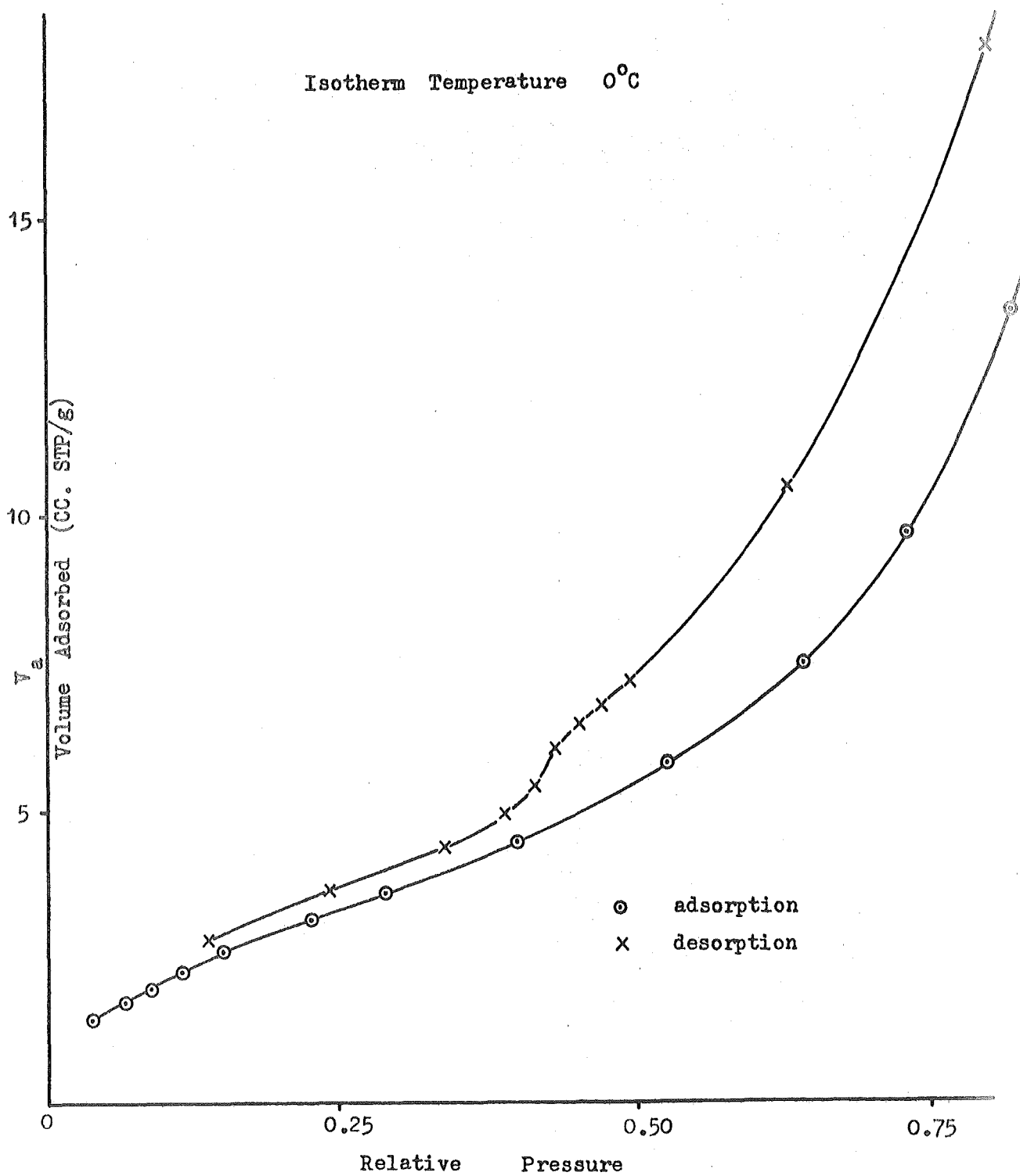


Fig. 31

Ethyl Chloride Sorption Isotherm for 'Natural'
Te Puke Metahalloysite Outgassed at 400°C.

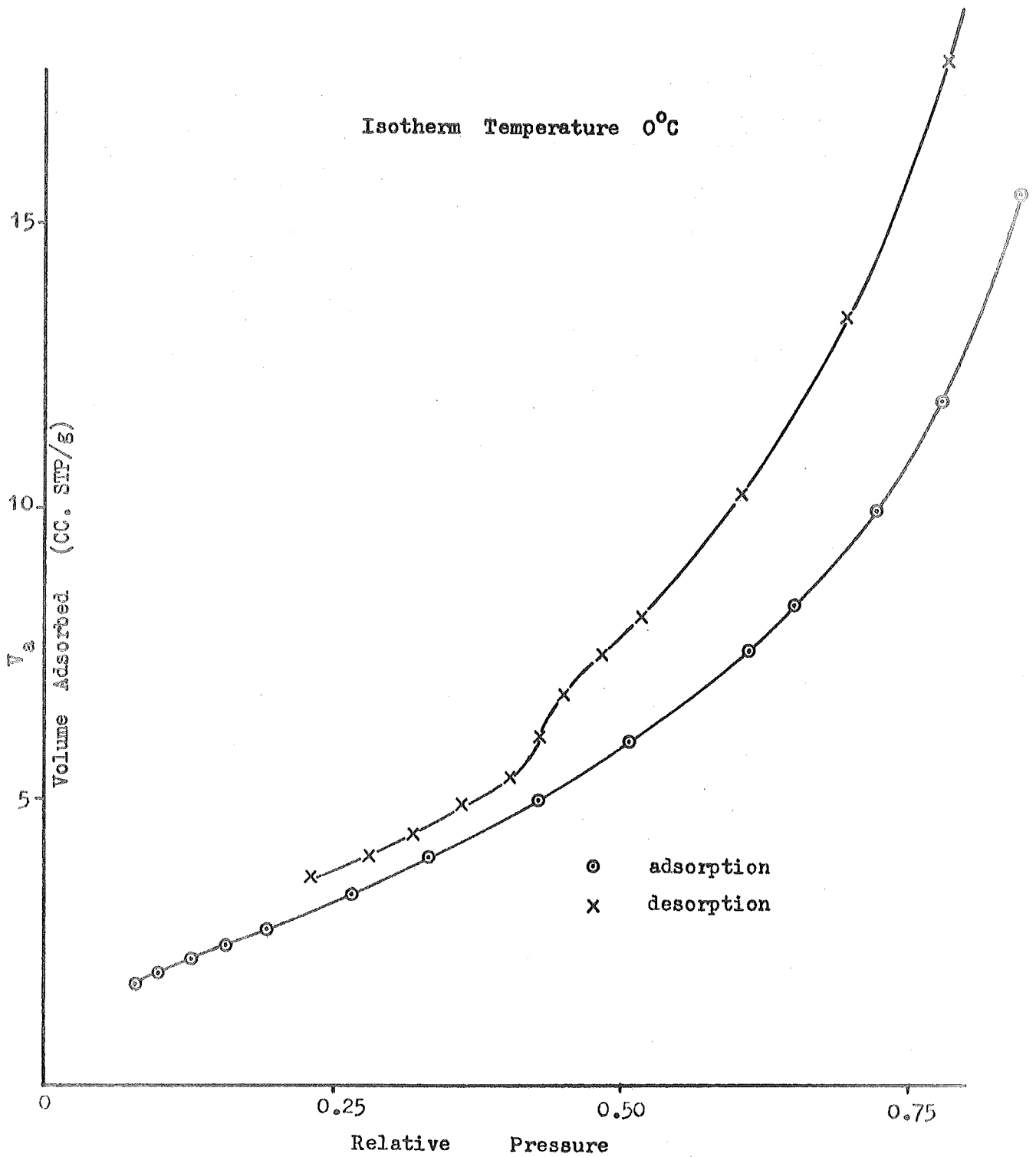


Fig. 32 Ethyl Chloride Sorption Isotherm for 'Natural' Te Puke
Outgassed at 400°C, Treated with Trimethylchlorosilane.

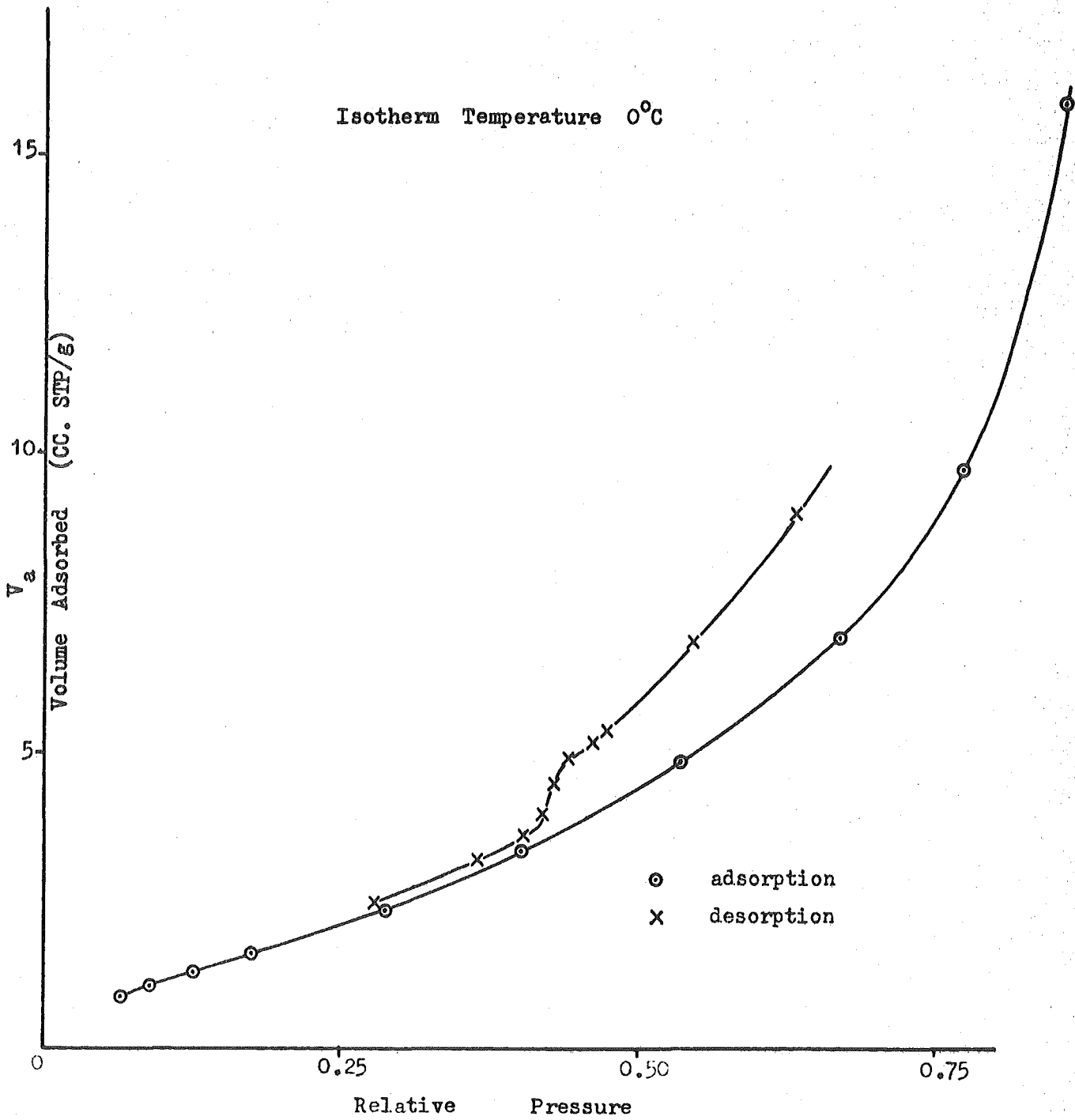


Fig. 33

Water Vapour Sorption Isotherm for 'Natural'
Te Puke Metahalloysite Oven-heated at 110°C.

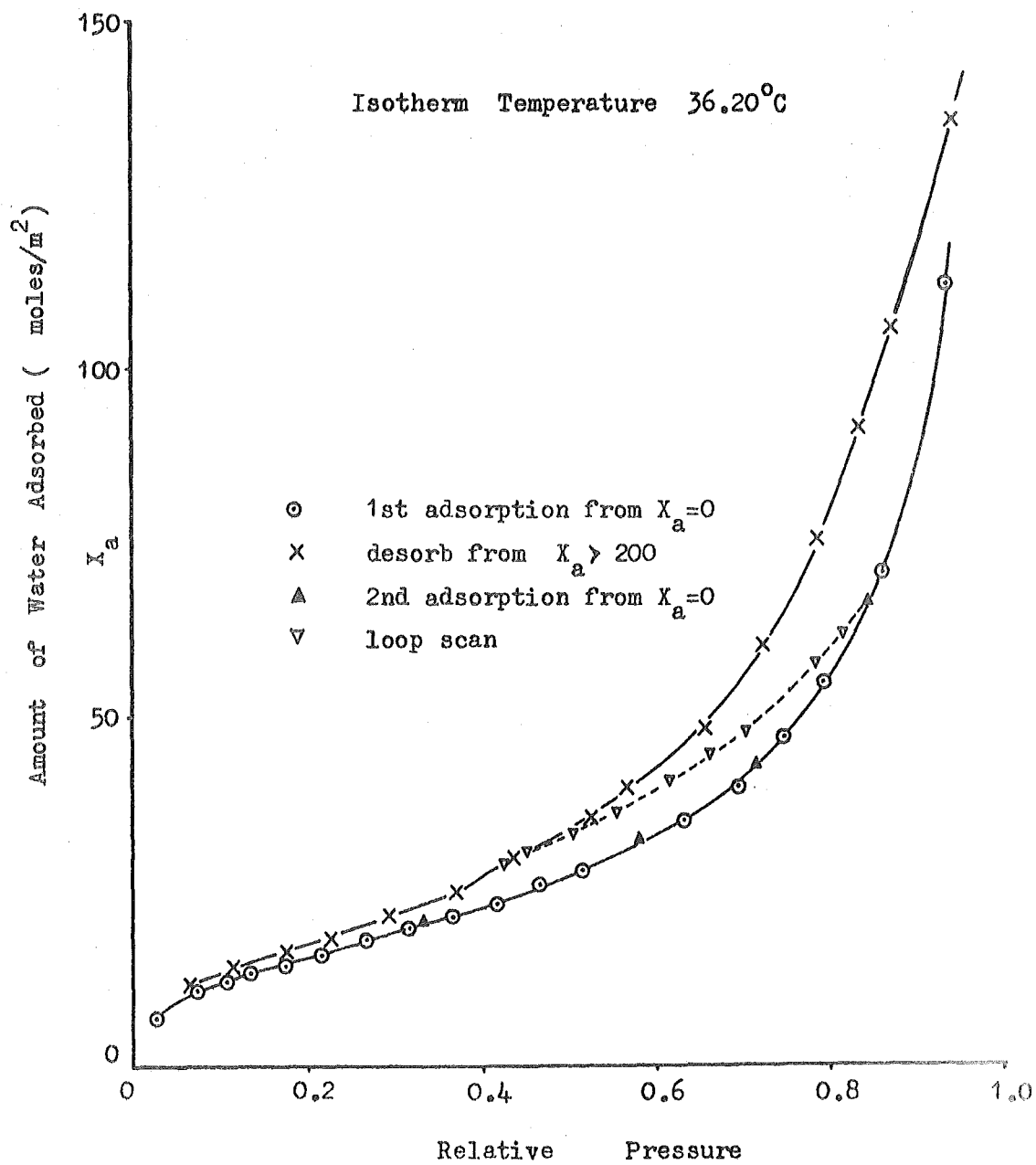


Fig. 34 Water Vapour Sorption Isotherm for Te Puke
Metahalloysite Treated with Trimethylchlorosilane.

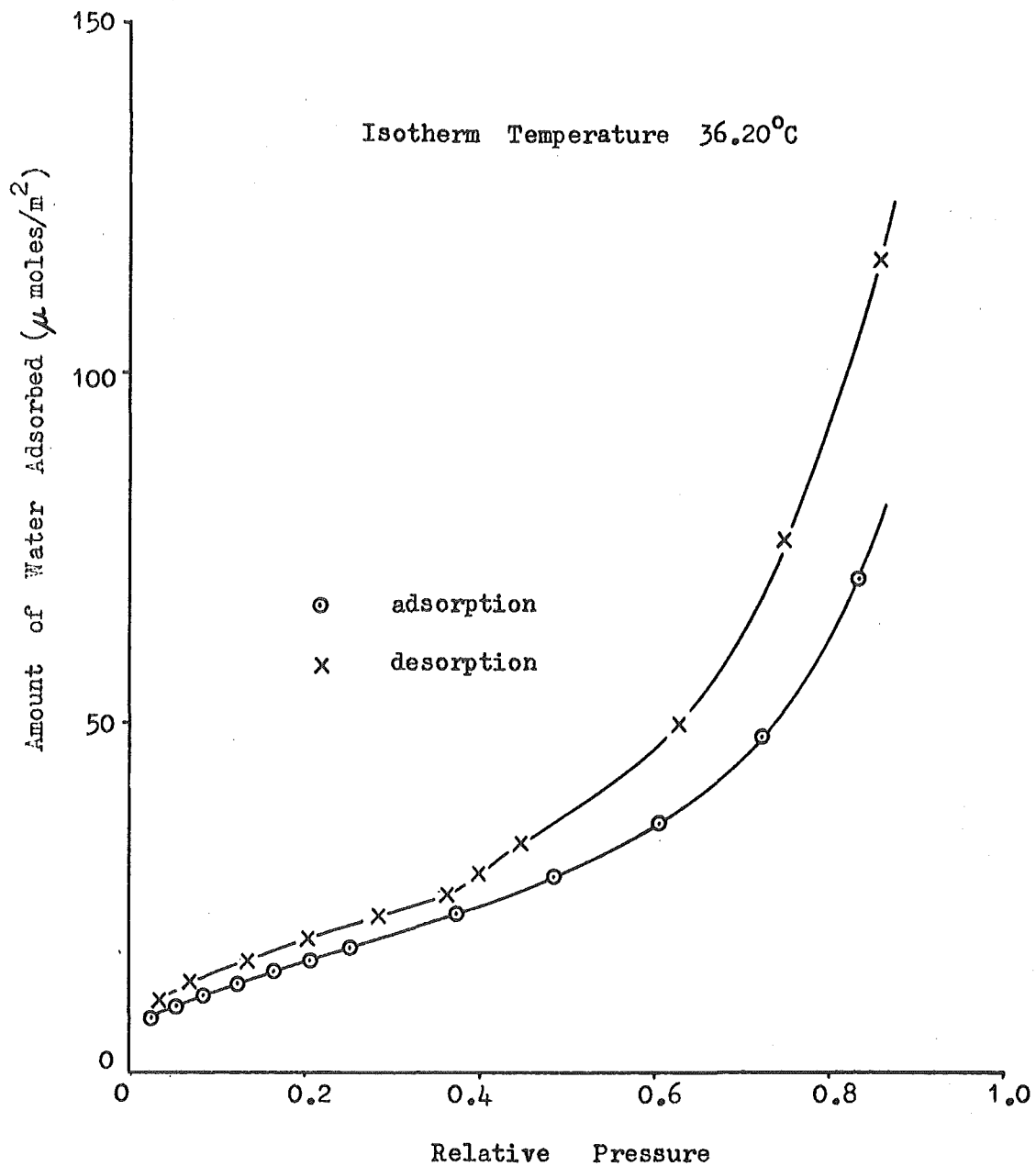


Table 2. BET Parameters Derived from the Adsorption Isotherms of Various Gases on 'Natural' Metahalloysite and Metahalloysite Treated with Trimethylchlorosilane (TMCS)

Adsorbate	Clay Treatment	BET Monolayer Capacity*	Difference %	BET C Constant
Ethyl chloride	Oven heated 110°C	4.27	33.2	29.7
	110°C heated, TMCS treated	4.22		19.3
Ethyl chloride	Outgassed 400°C	2.88	27.8	13.4
	Outgassed 400°C, TMCS treated	2.08		9.0
Water vapour	Oven heated 110°C	9.42	10.1	23.8
	110°C heated, TMCS treated	8.46		21.3
Nitrogen	Oven heated 110°C	8.25	14.4	120
	110°C heated, TMCS treated	7.06		90.7
Nitrogen	Outgassed 400°C	8.81		105

* Monolayer capacity units, for ethyl chloride and nitrogen cc.STP/g clay
for water vapour mg H₂O/g clay

Loss of surface area cannot explain the ethyl chloride specific monolayer capacity decrease from 110°C outgassed to 400°C outgassed samples, since the nitrogen monolayer capacity for the 400°C sample was 7% higher, indicating a specific surface area increase. The increased outgassing temperature caused a loss of constitutional hydroxyl groups and therefore a reduction in the surface concentration of what are presumed to be the primary adsorption sites for ethyl chloride molecules. That the ethyl chloride molecules are adsorbed on the hydroxyl groups is also indicated by reasonable agreement between the calculated value of the ethyl chloride monolayer capacity of 4.49 cc STP/gm, assuming a surface OH concentration equal to that found on kaolinites i.e. 3.4 OH/100Å² (67,287), and the experimental value of 4.27 cc STP/gm, the latter value being obtained from data uncorrected for deviations from ideality. A weight gain experiment showed that approximately one third (actually 37%) of the OH groups of the natural 110°C mineral reacted with TMCS and therefore a monolayer capacity decrease of 33%

is not unexpected. The remaining unreacted OH groups, although shielded from reaction with further TMCS molecules by the bulk of the trimethylsilyl group, are apparently available as adsorption sites for ethyl chloride molecules. Outgassing the natural clay at 400°C resulted in an hydroxyl loss equivalent to 80% of the total hydroxyl content but apparently only a 33% loss of the surface hydroxyls. TMCS treatment of the resulting material caused a further 28% loss in the number of adsorption sites. This indicates that the residual OH groups are fairly closely associated on the surface in small islands because if they were spread evenly over the entire surface each would be expected to react. It is possible that the remaining OH groups are present on the silica surface since these are thermally more stable than hydroxyls on the alumina surface (67) and can, according to Wade and Hackerman (289), form slowly on the exposed oxygens of the silicon tetrahedrons.

The non-polar nitrogen molecule and the small polar water molecule, suited to adsorption on

both oxygen and hydroxyl surfaces, are both unexpected to be affected by the loss of hydroxyl groups to the same extent as observed for ethyl chloride.

The observed low pressure hysteresis effects can be explained if the phenomenon is presumed to result from differences in the structuring of the interfacial layer during adsorption and desorption. Dipole-dipole interactions between adsorbate molecules and surface hydroxyl groups lead to specific site adsorption in the first layer. The ethyl chloride molecule on the natural 110°C outgassed sample occupies an area of approximately 30\AA^2 , while its cross-sectional area, if oriented perpendicular to the surface, should be close to that for a hydrocarbon chain, namely 20.7\AA^2 (179). As adsorption proceeds further molecules are forced into the first layer. Desorption takes place from the fully packed first layer, a situation different from the adsorption leg and therefore hysteresis results. From the ethyl chloride isotherms obtained in this study it appears that only when the surface is denuded of more than

50% of its hydroxyl groups, as in the TMCS treated 400°C outgassed sample, does the width of the hysteresis loop diminish. The presence of a greater number of hydroxyls is apparently sufficient to cause molecular ordering in the first adsorbed monolayer and to lead to hysteresis. The small hysteresis loop retained for the 400°C outgassed TMCS treated sample is probably due to local concentrations of OH groups on the surface which yield some 'islands' of structured adsorbate. These local concentrations of hydroxyl groups were necessary, as discussed above, to explain the observed monolayer capacities.

It is possible that the structuring or packing mechanism of low pressure hysteresis, outlined above for Et Cl adsorption, also explains the loop obtained for water vapour adsorption on the natural, 110°C outgassed clay (figure 33) and the undiminished loop after TMCS treatment of the sample (figure 34). Equally likely also is the possibility that the hysteresis in the water system occurs by quite a different mechanism. The phenomenon may be accounted for by an irreversible redistribution of water

molecules, during the adsorption process, from hydroxyl to oxygen sites. Adsorption by the latter sites is expected to be more stable (4,83,116) and desorption would take place from a different molecular distribution than prevailing along the adsorption leg. Redistribution of this type is supposed to occur, for example, on porous glass (271,281) and should not be markedly affected by TMCS treatment, although it may be slightly enhanced due to a reduction in the interaction energy between the adsorbed molecules and the OH surface. A molecular redistribution is also invoked to explain the hysteresis effects observed in kaolinite-water systems in terms of cation hydration (290,291). This mechanism suggests that an irreversible transition occurs between water adsorbed on the mineral surface and that intimately associated with the cations as hydration water. Retention of hysteresis after TMCS treatment might result from either the cations residing predominantly in positions where they are unaffected by the treatment and are free to hydrate, for example on the oxide surface, or

from the penetration of the organic layer by the water molecules. Both of these effects cause retardation of the desorption process and hence result in hysteresis. For various molecules, including water, it has been suggested that penetration occurs through the organic film formed by the reaction of diethyldichlorosilane with the rutile surface (282) and the same may be true for the TMCS treated clay surface.

The low pressure hysteresis loops for water adsorbed on homoionic methalloysites are fully discussed in section 4.5.2. It is noted there that the cations have a considerable effect on the width and extent of the loop, the samples saturated with large monovalent cations, for example, yielding larger hysteresis loops than those saturated with smaller univalent ions. This is opposite to the trend expected if ionic effects on the water structure were the important factors, since the larger the ion the higher its structure breaking effect, the smaller is the expected hysteresis loop. The conclusion is that although structuring effects may contribute, the low

pressure hysteresis is mainly a result of cation hydration regulated by the difference in energy between the ionic hydration energy H and the ion-clay interaction energy U . When $H - U$ is positive then cation hydration can occur and hysteresis should result (116).

4.2 Adsorption of Non-polar Molecules on Metahalloysite

The nitrogen and argon isotherms (figures 35 to 41 and 26 respectively), for the various metahalloysite samples of the present study, all display adsorption branches identified as type II of the BDDT (214) classification (figure 3). The hysteresis loops observed have a shape conforming approximately to the type B loop of the deBoer (300) classification (figure 5).

4.2.a The Type II Adsorption Isotherm

Type II adsorption isotherms are typically observed for the adsorption of non-polar adsorbates on nonporous materials or on porous materials with few micropores. This isotherm shape (figure 4) is explained (240) as due to the formation

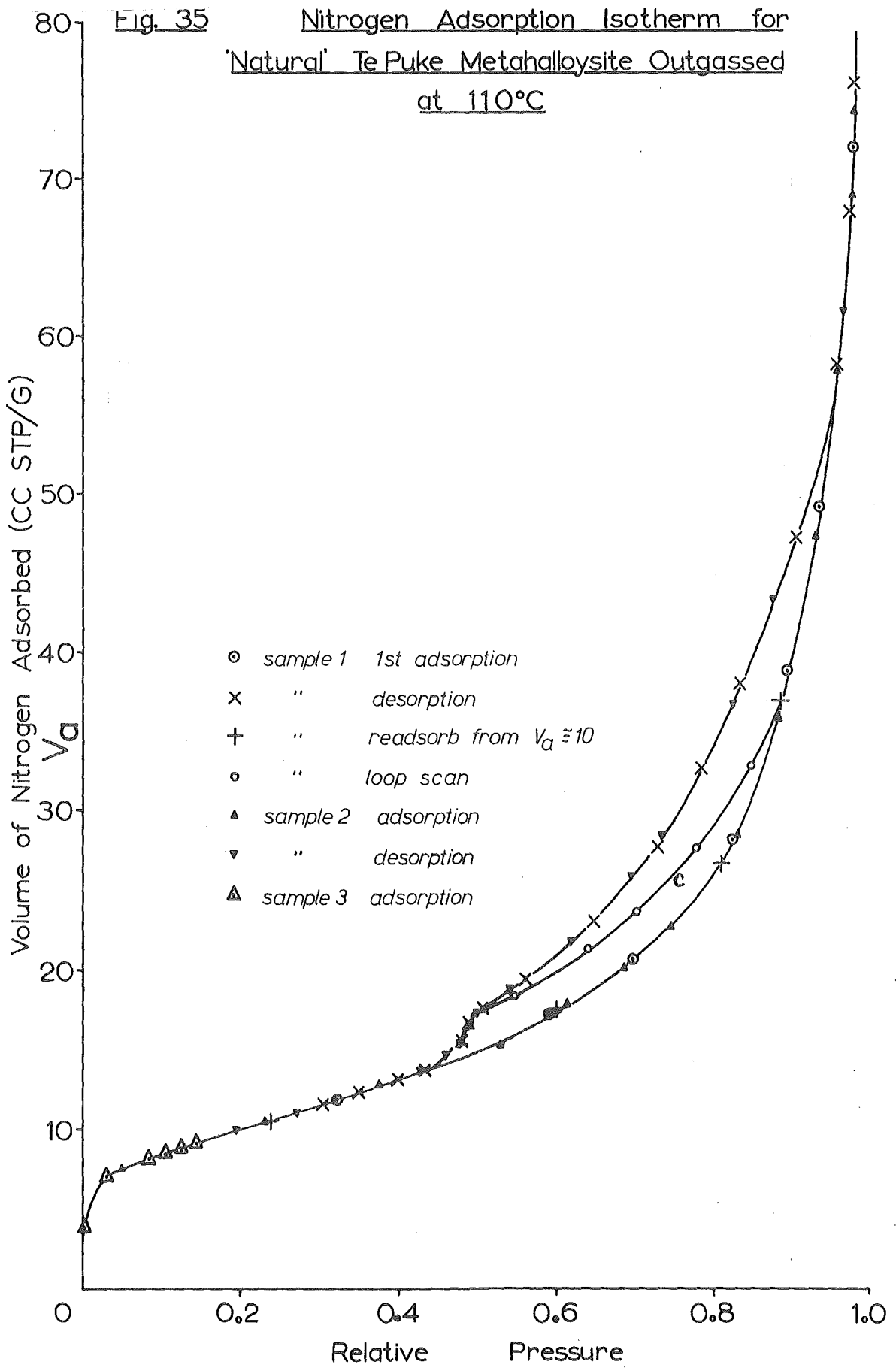


Fig. 36 Nitrogen Adsorption Isotherm for
 Natural Te Puke Metahalloysite Outgassed
 at 250°C

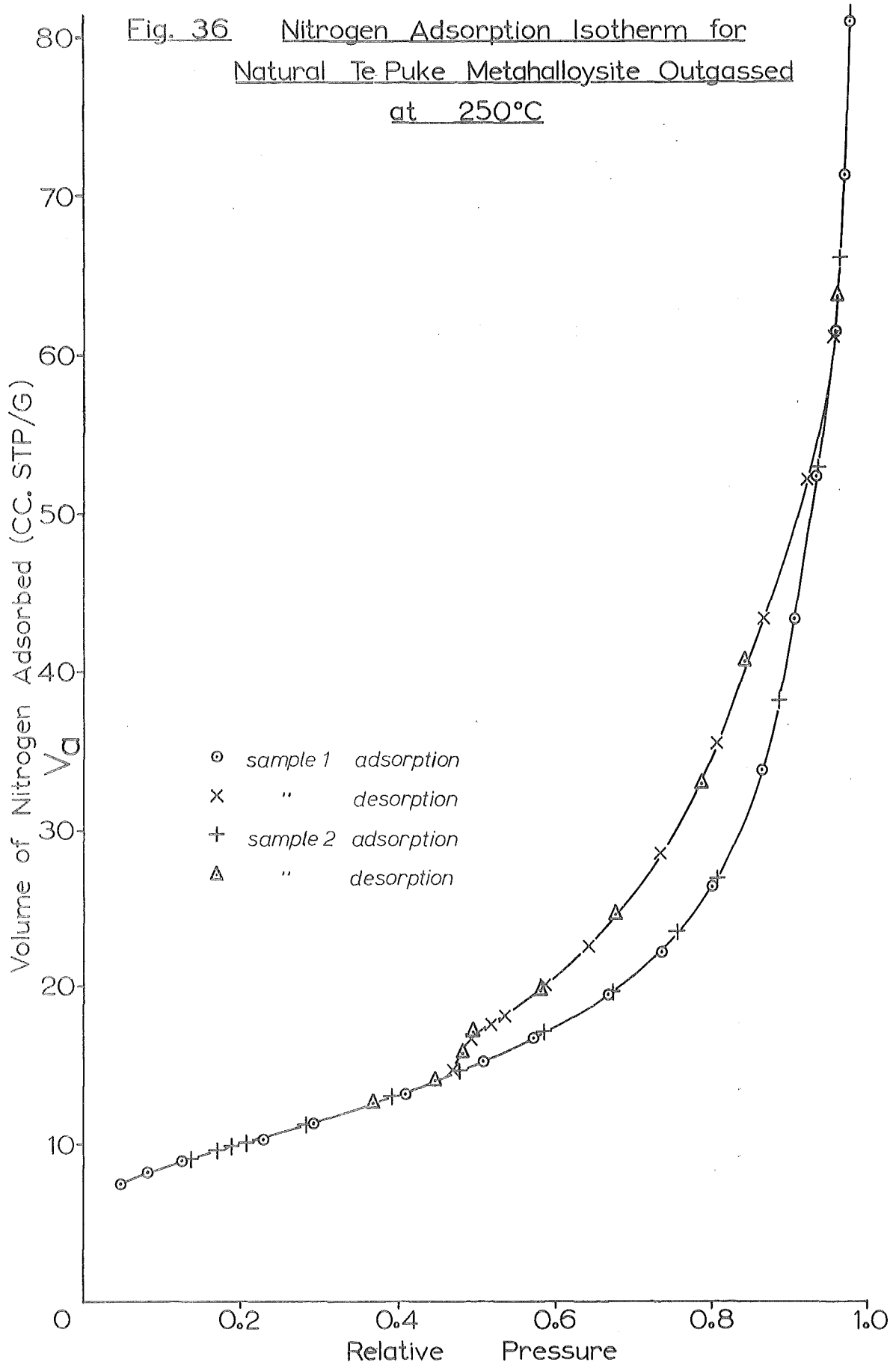


Fig. 37 Nitrogen Adsorption Isotherm for
'Natural' Te Puke Metahalloysite Outgassed
at 300°C

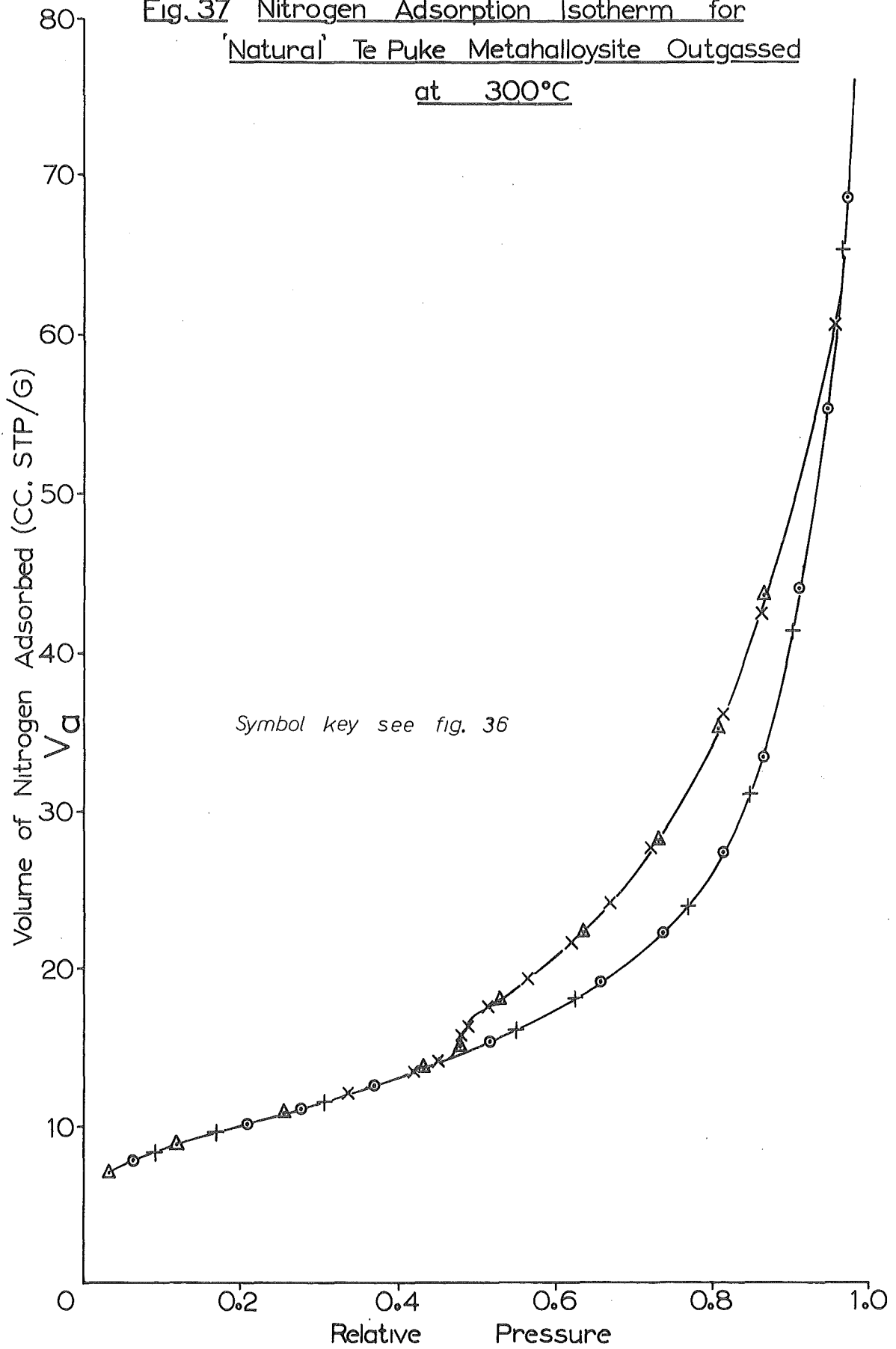


Fig. 38 Nitrogen Adsorption Isotherm for
'Natural' Te Puke Metahalloysite Outgassed
at 325°C

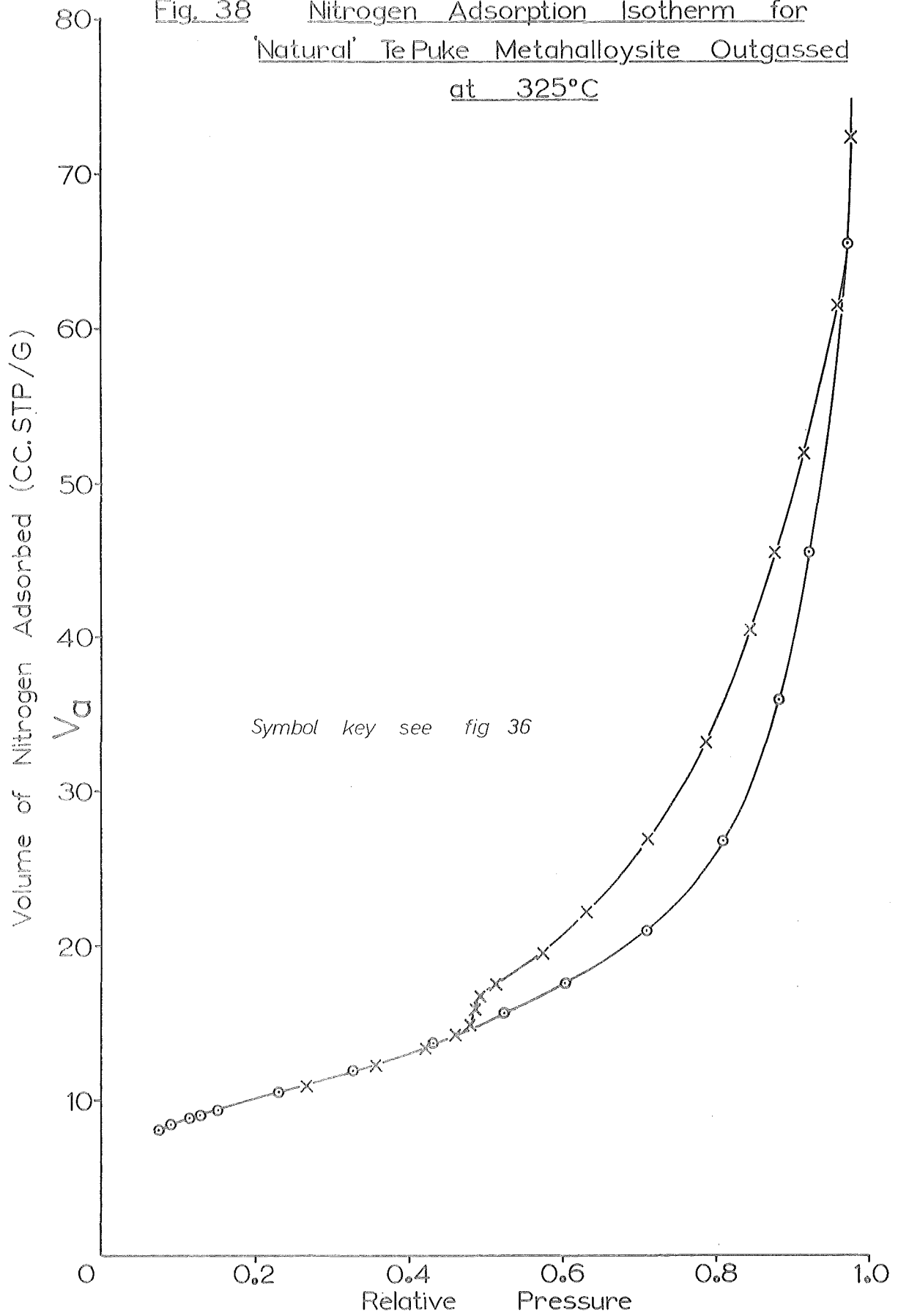


Fig. 39 Nitrogen Adsorption Isotherm for
 Natural Te Puke Metahalloysite Outgassed
 at 350°C

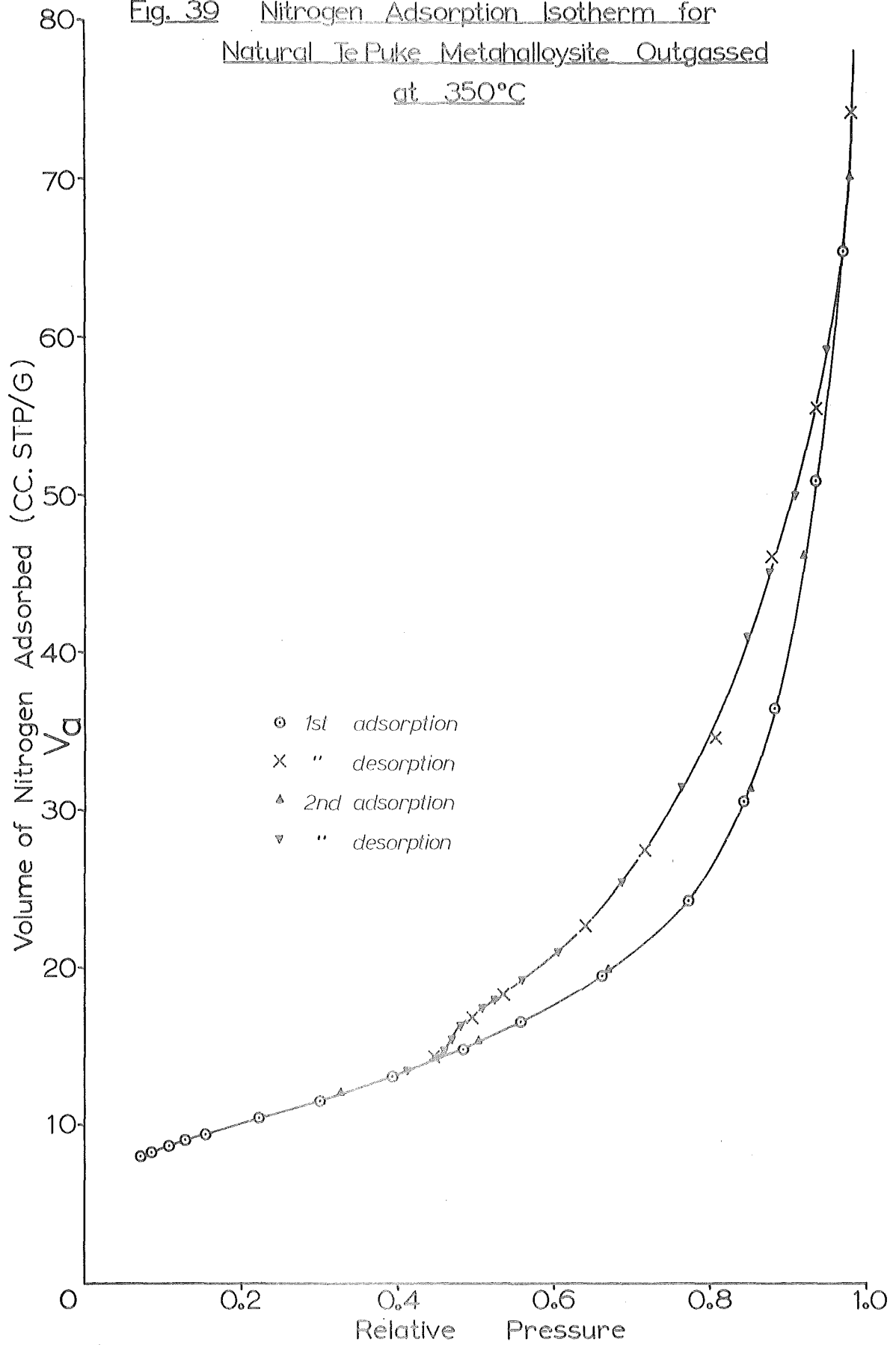


Fig. 40 Nitrogen Adsorption Isotherm for
Natural Te Puke Metahalloysite Outgassed
at 400°C

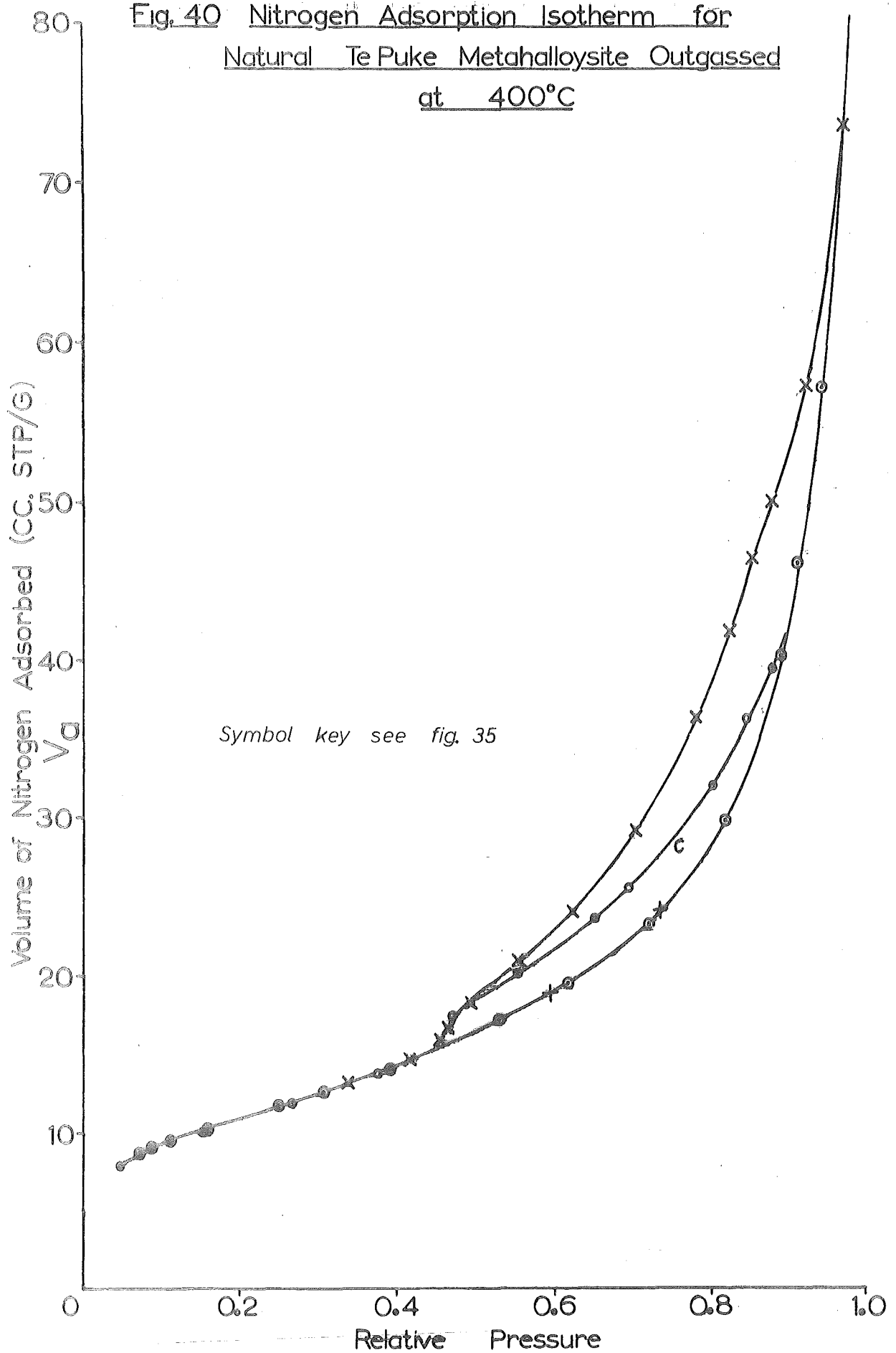
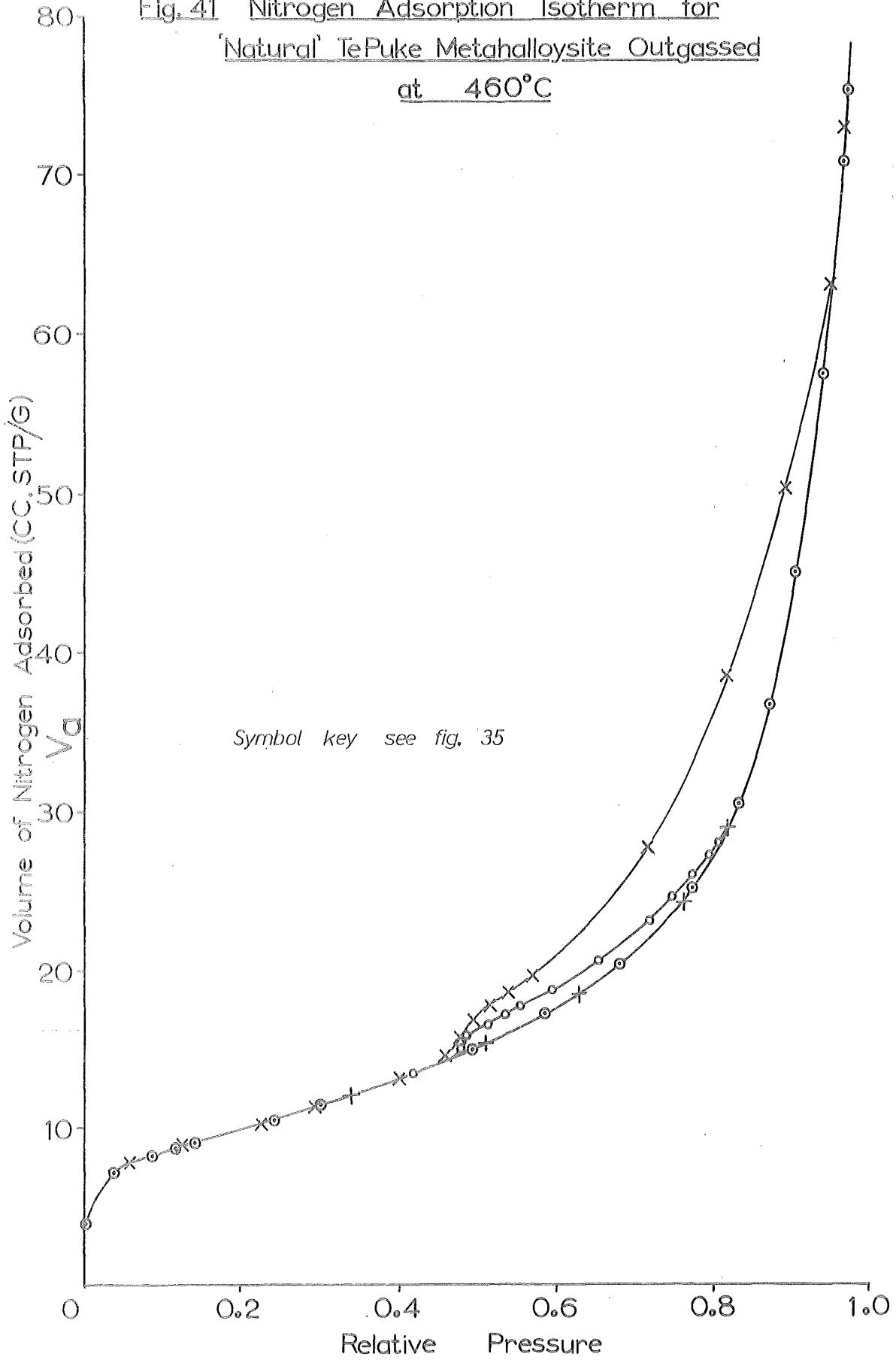


Fig. 41 Nitrogen Adsorption Isotherm for
'Natural' TePuke Metahalloysite Outgassed
at 460°C



in region A, of a monolayer over the entire exposed surface, the monolayer being completed in the region of the 'knee' K of the isotherm, followed, in relative pressure range B, by the filling of multilayers. This second approximately linear region is that to which the BET equation (equation 1) is best fitted (206). Surface areas derived from data which fall in this range of relative pressures ($0.05 < P/P_0 < 0.35$) for isotherms of type II can be regarded, as is discussed in section 2.1, as meaningful in a comparative sense, if not in an absolute sense. Region C, variable in form and extent, is ascribed to multilayer condensation modified by capillary condensation between the elementary particles and in pores if any are present (220).

4.2.b The Type B Hysteresis Loop

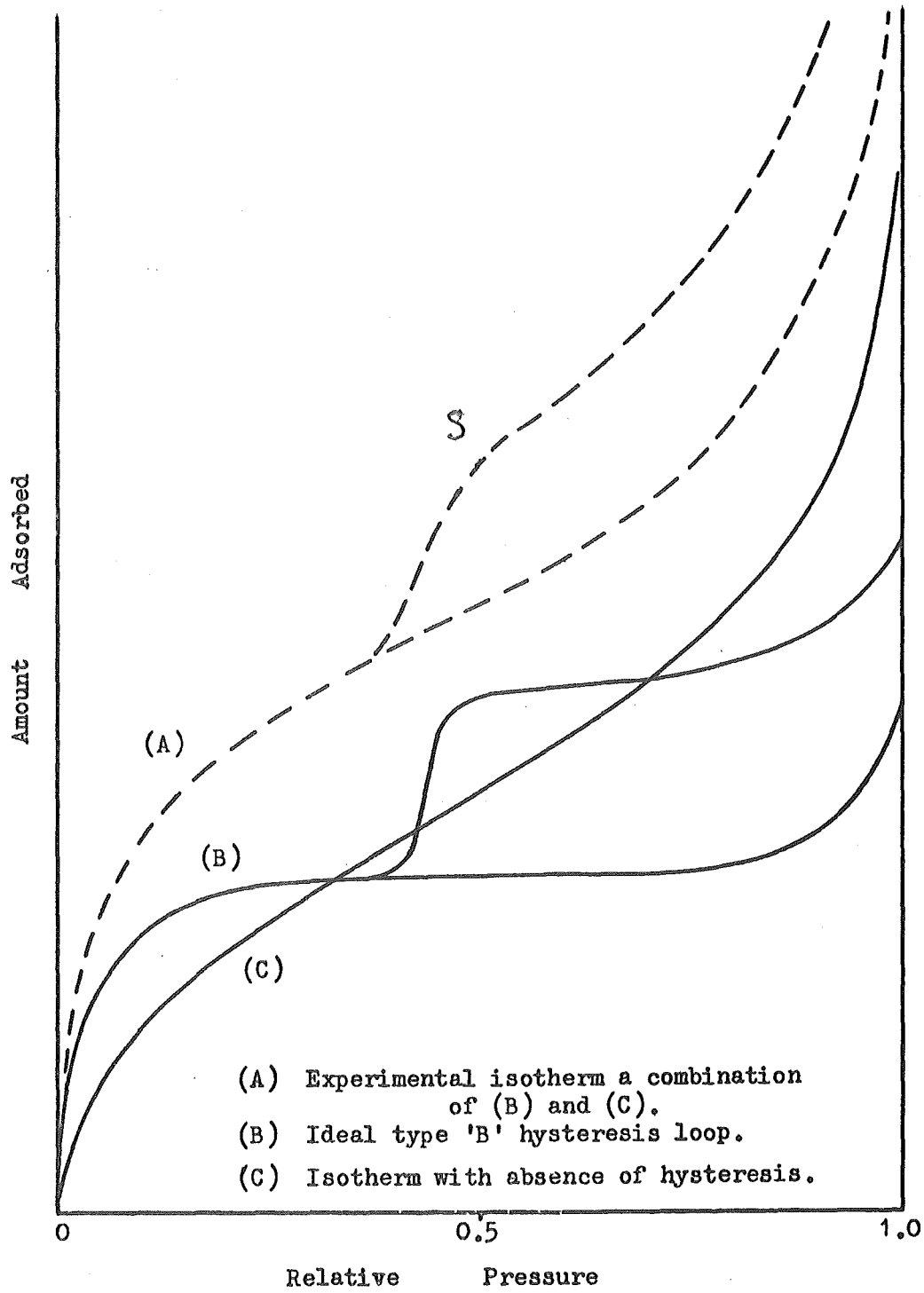
Hysteresis loops of type B have been reported for a variety of clay minerals (222,269) and for other substances with a known lamellar structure (220,247). The desorption branch of such loops (figure 42), first observed for the adsorption of oxygen, nitrogen and benzene on montmorillonite (269),

includes a shoulder S, at an intermediate relative pressure, with a sharp drop to a well-defined closure point.

Although at first ascribed to orientational changes within the matrix of the adsorbing material (269), the B type hysteresis loop is now generally associated with the porous nature of the adsorbent (304). Barrer and coworkers (269, 305) emphasized that hysteresis can arise from phenomena other than irreversible capillary condensation. They further contended that such a mechanism could not explain the considerable loss of adsorbate which occurs over a narrow range of pressures for clay minerals, as these materials are presumed to have an irregular arrangement of particles. A randomly oriented set of particles should give rise to a range of pore sizes rather than a discrete narrow range indicated by the sharp drop observed. An alternative explanation of the type B loop was put forward by these authors (269,305). Along the adsorption branch, they suggest, particles of adsorbent are oriented into a thixotropic structure

Fig. 42

The Type 'B' Hysteresis Loop



due to the influence of adsorbate surface tension forces. When, during desorption, insufficient adsorbate is left to hold the thixotropic structure together, it randomizes and the remaining adsorbate is expelled giving rise to the drop in the desorption curve. This explanation assumes that condensed adsorbate is held between clay particles and relates the position of the shoulder S to the distance between plate-like particles, using the Kelvin equation in the appropriate form (equation 20).

The evidence of adsorption studies on compacted clay minerals indicates that the above view is not entirely satisfactory and suggests that the observed hysteresis arises from the porous structure of the material formed during drying (97,136,222). In compacted systems the clay material forms a rigid matrix which is not likely to undergo significant particle rearrangement or swelling in the presence of non-polar liquids. Aylmore and Quirk (222) contend that the hysteresis loops observed are a result of intercrystal rather than interparticle condensation and present evidence (307) which leaves little doubt

that the void spaces between clay mineral crystals are of open-sided slit-shaped form. The latter observation is reasonable in view of the lamellar structure of clay minerals. By this interpretation the sharp drop in the type B hysteresis loop is to be associated with the loss of condensed liquid from a narrow discrete range of pore sizes.

DeBoer (154), in his analysis of hysteresis loop types, identified the type B loop with two pore shapes, (a) the open slit-shaped pore and (b) the ink-bottle capillary with a very wide body and a narrow short neck. As has already been stated, the slit pore is the more likely shape in the case of clay minerals. These pores could result from the interpenetration of layers or from the propping apart of plates by small mineral fragments (154).

Hysteresis, for systems containing parallel plate pores, is suitably explained (308) by a rationalisation of the general theory of hysteresis proposed by Foster (309). This theory suggests that the mechanisms of meniscus formation during adsorption, and disappearance during desorption,

are different. During adsorption multilayer formation occurs on the surface of slit pores until, at a certain high relative pressure, the void space is completely filled. For ideal parallel plates, free to move apart, this filling should not occur before the saturation pressure (154,269), there should be no capillary condensation, adsorption taking place as if on a free planar surface. The adsorption curve, in the ideal case, should therefore be extremely steep approaching saturation (as $P/P_0 \rightarrow 1$). Evaporation of the condensed liquid upon desorption is believed to take place from a hemi-cylindrical meniscus formed at the pore edges. During the initial stages of desorption the plates are drawn together by surface tension forces. If the separation cannot decrease below a certain value due to the mode of packing, and providing the range of pore sizes is relatively narrow, the desorption branch is expected to show a steep drop at a relative pressure which corresponds to the minimum plate separation. Since there is a delay in the formation of a meniscus, until complete saturation, and because the process of

capillary evaporation is controlled by this meniscus, it is believed that only the desorption branch of the isotherm is thermodynamically stable (242,310).

A large proportion of experimentally determined hysteresis loops do not conform exactly to one of the five types classified by deBoer (154), some because there is a range of pore sizes, others because the material contains pores of two or more shapes. The combination of a set of capillaries which give rise to hysteresis and a group of pores which, because of their shape, do not cause hysteresis, invariably results in a hysteresis loop which is narrower and more sloping than that for an ideal set of pores of one shape and size. Such is believed to be the case for the nitrogen and argon isotherms of the present study. Figure 42 is a diagrammatic comparison of the idealized type B hysteresis loop, and an experimental loop considered to be a combination of the ideal loop and a type II isotherm, the latter resulting from condensation in pores not giving rise to hysteresis. The combination of slit-shaped and wedge-shaped pores is the most likely to

occur in a system of plate-like crystals such as found for clay minerals. Pores of the former shape should always result in hysteresis while the latter pore type does not give a hysteresis effect. A combination of these capillary types should explain the sloping type B loops observed for the adsorption of nitrogen and argon on metahalloysite.

4.2.c Reproducibility of the Type B Hysteresis Loop.

Several authors (173,269,309,311,312) suggest that the upper part of the type B hysteresis loop, on the desorption side, is only reproducible if approached from complete saturation, the position of the desorption curve depending on the maximum amount of material adsorbed (264). The shape, point of closure and the height of the shoulder were found to be reproducible (269) indicating that these features are part of the true hysteresis loop. A similar conclusion was reached in this study from a determination of adsorption to desorption scanning loops for two different outgassed TePuke

metahalloysite samples (curve c figures 35 and 40). These scanning curves, begun at $P/P_0 \approx 0.9$, show the complete reproducibility of shoulder and drop positions. The rest of the desorption branch may however be a scanning loop. Every attempt was made in the present study to achieve a close approach to the saturation condition but, due to the nearly asymptotic approach to the $P/P_0 = 1.0$ axis, complete saturation was not reached.

The desorption branch of each of the nitrogen isotherms on vacuum heated TePuke metahalloysites is probably not a scanning curve. This is indicated by the observation that a repetition of the isotherm, for the 110°C and 300°C outgassing temperatures, making a 50% increase in the total amount adsorbed at the highest pressure reached, did not cause an appreciable shift in the position of the desorption curve.

The very steep section of the isotherms, close to the saturation pressure, is due to condensation of adsorbate in the spaces between particles or within very large pores. As these features were

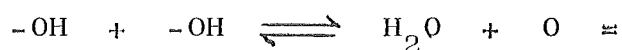
not of prime interest in the present study this portion of the isotherms was not looked at in any detail.

4.3 Weight Loss

Dehydration curves (graphs of weight loss versus temperature) for TePuke metahalloysite samples outgassed in vacuo or heated in air are displayed in figure 43, together with the data of Ross and Kerr (52) and Gallego (306) for halloysites from other localities. The curves all have the same basic shape and vary in position on the graph mainly because of variations in the initial degree of hydration of the mineral. For these minerals most of the 100 - 400°C range is taken up by a gradually increasing weight loss. This is characteristic of the mineral halloysite, other related clay minerals losing little water in this temperature range (313). Although most of the interlayer water of a fully hydrated halloysite is easily lost at room temperature by reducing the humidity, some is strongly retained and is expelled only by heating,

temperatures as high as 400°C being required for its complete removal (314). It is this water, together with small amounts of strongly adsorbed water, which is lost in the 100 - 400°C range. Adsorbed water has been shown to exist after 200°C treatment but most is lost by 300°C (315).

The position of the rapid increase in weight loss associated with the dehydroxylation of the mineral, is dependent on the origin of the sample, and presumably therefore on the degree of disorder of the lattice, and upon the conditions under which the dehydration process is carried out. The loss of structural water occurs according to the equation:



and the rate processes are dependent on the mineral, time, temperature and specimen nature, the latter including specimen size, shape, compaction and particle size distribution (62). The occurrence of the reverse reaction slows down the dehydroxylation and this is particularly found in pressed discs where entrapped water vapour can exert considerable influence on the reaction kinetics. Removal of the

Fig. 43 Dehydration Curves for Halloysites and Metahalloysites

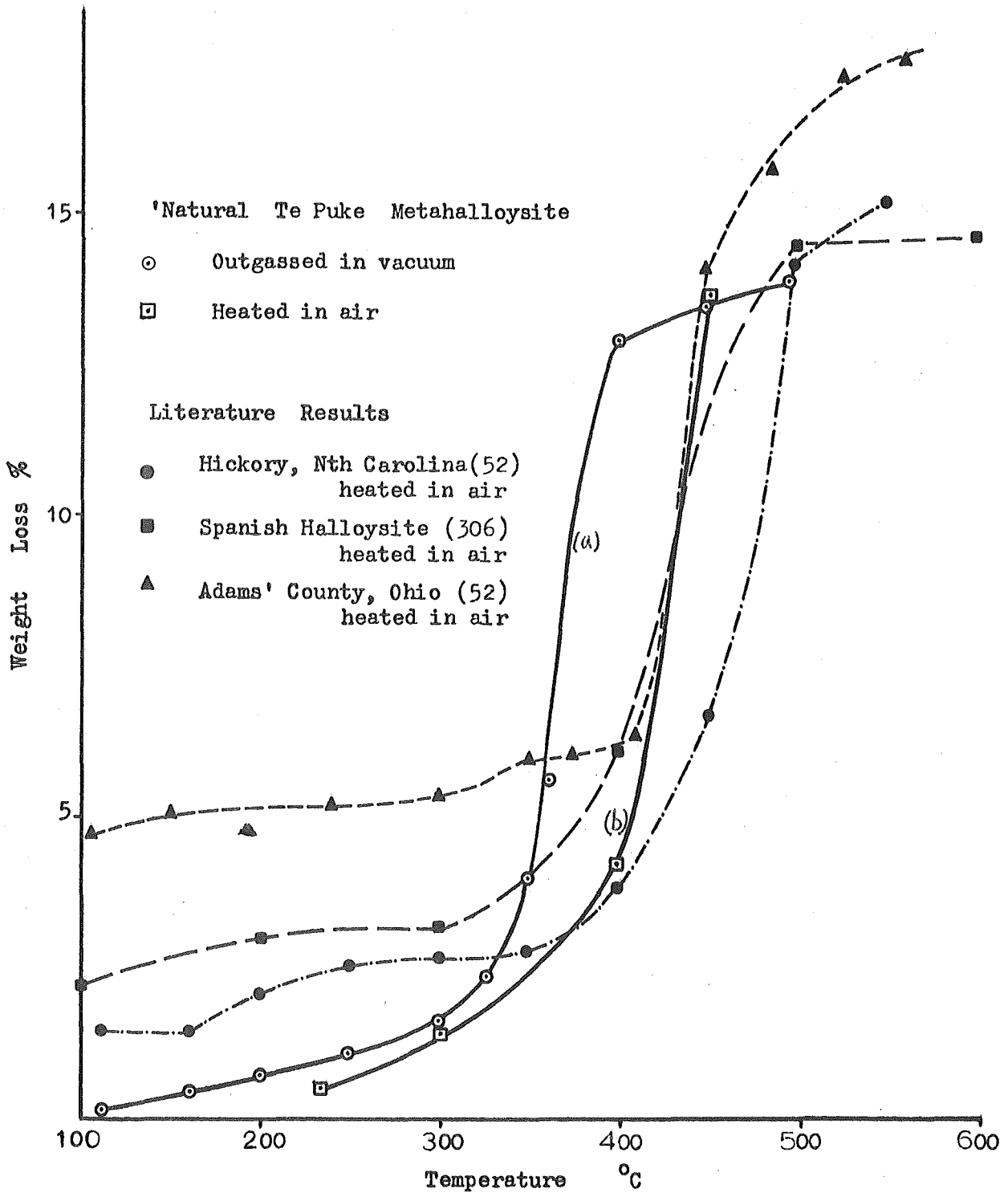


Fig. 44 Weight Loss-Temperature-Time Curves for 'Natural' Te Puke
Metahalloysite Outgassed in Vacuum and Heated in Air.

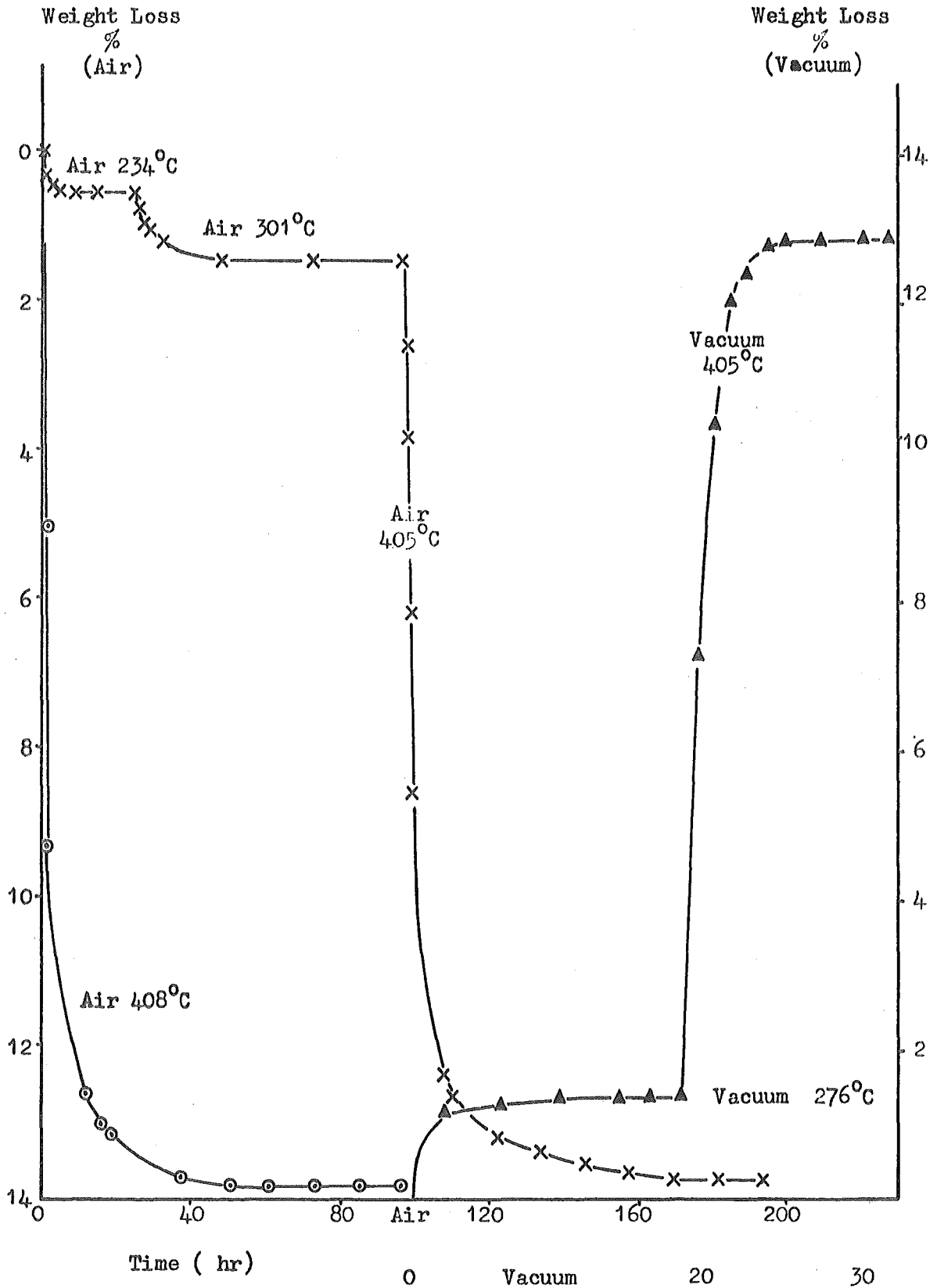


Fig. 45 IR Spectra of Te Puke Metahalloysite Vacuum
Outgassed at Given Temperatures

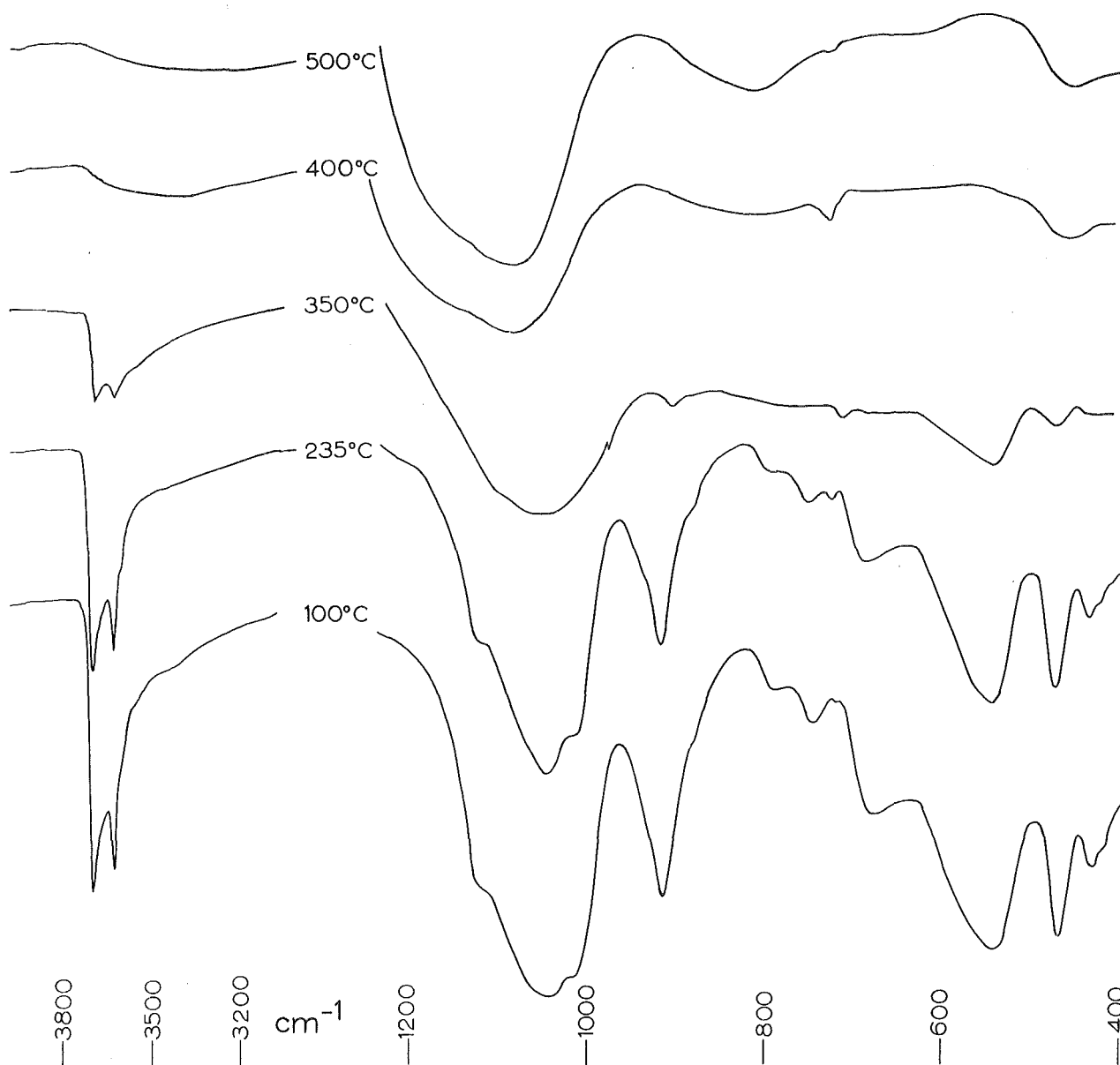


Fig.46 IR Spectra of Te Puke Metahalloysite Heated at
Given Temperatures in Air

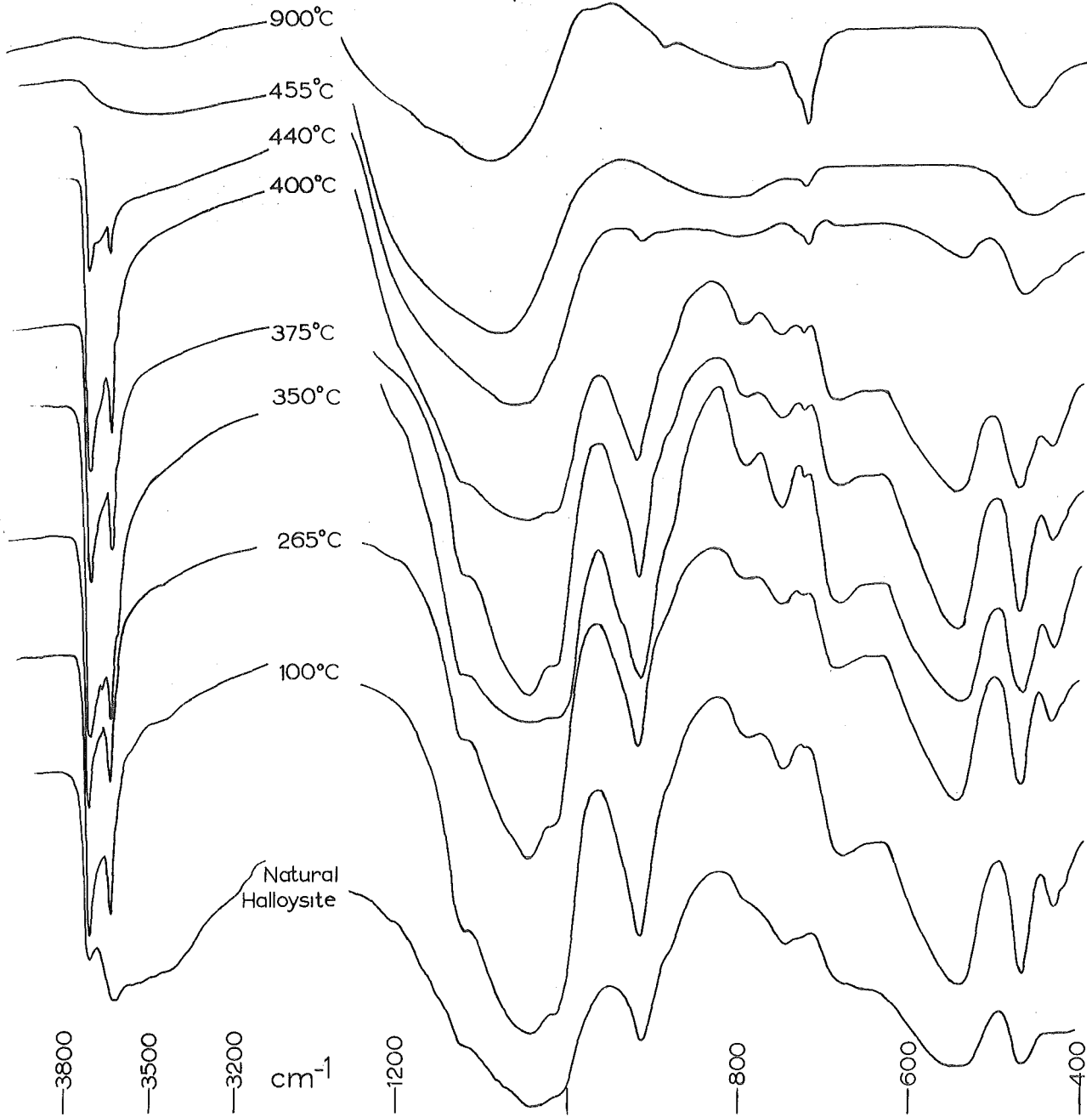


Table 3. Weight Loss in Vacuo of Te Puke Metahalloysite

Temperature °C		Time hours	Weight Loss %
Run 1. Sample weight 3.1862g			
325	± 3	60	2.44 ± 0.03
350	± 3	60	4.04
350	± 3	84	4.07
350	± 3	108	4.08
Run 2. sample weight 3.0952g			
110	± 3	48	0.16 ± 0.03
250	± 3	48	1.16
300	± 3	48	1.67
400	± 5	48	12.98
Run 3. Sample weight 3.0310g			
110	± 3	60	0.14 ± 0.03
250	± 3	60	1.17
300	± 3	60	1.75
325	± 3	60	2.31
350	± 3	60	4.05
405	± 5	60	13.03
450	± 5	60	14.04
Run 4. Sample weight 6.8989g			
160	± 3	60	0.43 ± 0.02
360	± 3	24	5.65
495	± 5	60	14.97
Run 5. Sample weight 3.2546g			
110	± 3	60	0.15 ± 0.03
250	± 3	60	1.00
250	± 3	72	1.01
300	± 3	60	1.68
325	± 3	60	2.40
400	± 5	60	13.10
Run 6. Sample weight 3.2804g			
250	± 3	60	1.11 ± 0.03
300	± 3	60	1.55
325	± 3	60	2.26
350	± 3	60	3.99
400	± 5	60	13.00
450	± 5	60	14.13

reaction product from the system should increase the rate of the dehydroxylation process. It has been found, both in this study and in others (316,317), that constant weight conditions are attained much more rapidly in vacuum than in air. A maximum of 14 hours was sufficient to achieve the steady state for vacuo outgassing while some 50 - 60 hours was required for heating in air. Time - temperature - weight loss graphs are included in figure 44 to illustrate the last point.

Comparison of the weight loss curves for vacuo and air heating conditions (figure 43, curves a and b respectively) indicates that vacuum outgassing causes dehydroxylation to take place at 50-60°C lower temperatures than in air. This was also found for the dehydration of kaolinite (316). Infra-red spectra of samples outgassed in vacuum (figure 45), and heated in air (figure 46) at different temperatures, when compared, reinforce the above conclusion. Disappearance of the hydroxyl peaks in the 3600 - 3700 cm^{-1} region occurs, to a large extent, for the vacuum condition in the range

350° - 400°C, and for the case in which de^hhydroxylation is retarded by the atmosphere, in the range 440° - 450°C. The spectra displayed by Churchman (13) for air heated samples of TePuke halloysite indicated the major fraction of lattice hydroxyl loss occurred between 475° and 500°C. The differences between Churchman's results (13) and those of the present study are probably a consequence of incomplete dehydroxylation in Churchman's samples which were heated for a period of only 8 hours. According to the present findings this is insufficient time to reach the steady state condition at a particular temperature.

Since the maximum period of time required to achieve the constant weight condition for vacuum outgassing experiments was around 14 hours for a small loosely packed sample, subsequent outgassings were carried out for 60 hours at any particular temperature. This extended treatment time should ensure steady state conditions are reached but does not necessarily ensure that the degree of dehydroxylation is uniform throughout the sample. Concentration gradients might be present in the material such as those found in pressed kaolinite

and halloysite discs (62,318). The clay mineral of the present study however was not pressed but loosely packed into the sample bulbs. The escape of product gases upon outgassing is thus facilitated, and homogeneous conditions more likely to result in the loosely packed than in the compressed state. Experimentally the absence of a concentration gradient was shown by carrying out a total weight loss to 900°C on fractions removed from the top and bottom of the sample after it had been outgassed in vacuo at a particular temperature for the 60 hour interval. Such a test was made on two samples outgassed respectively at 400°C and 450°C. For neither case was the difference in weight loss observed, between top and bottom fractions, larger than the experimental error and it is therefore believed that the outgassing procedures used yield samples which are homogeneous throughout. From this evidence it can be assumed that any alterations to the surface or porous character of the mineral, as a result of outgassing at an elevated temperature, are evenly distributed in the mass of the material.

4.4. The Effect of Pretreatments on the Specific
Surface Area and Pore Properties of Metahalloysite

4.4.1.a Maungaparerua Metahalloysite

Electron micrographs of the two particle size fractions $< 2\mu$ e.s.d. (figure 11a) and $5-10\mu$ (figure 11b) of Maungaparerua metahalloysite indicate that to a certain degree the separation techniques used have been successful in providing samples which contain respectively, mainly tabular and mainly lath-like or tubular particles. The terms 'tabular' and 'tubular' are not expected to define the real morphologies and are used only to differentiate the samples. Recent electron micrographs of fractionated Maungaparerua metahalloysite show in fact that smaller size fractions ($< 2\mu$ e.s.d.) have particles exhibiting a polygonal cross-section, as do the larger fractions. The latter material does however have much longer particles than the former. (295)

The BET specific surface areas, determined by nitrogen adsorption (table 1) are approximately 22% higher for unfired tabular samples.

than for unfired tubular samples. This is true for both dispersed and flocculated materials. Particle size fractionation of Maungaparerua halloysite is therefore seen to have a considerable effect on the specific surface area, the smaller material having the expected higher specific area. Particle size fractionation did not cause such an increase in area for TePuke metahalloysite, a $< 1\mu$ e.s.d. fraction having a specific surface area only 3.7% higher than a 1-20 μ fraction of the same mineral. The TePuke material however, is composed of small angular particles many of which are grouped together into aggregates, and few only have elongated shape (figures 7 and 8). Particle size separation of such material is not expected to give physically meaningful fractions and is not likely to lead to significant variation in specific surface area.

The increase in specific surface area on prefiring to 650°C is considerably greater for the 'tubular' than for the 'tabular' samples (table 1). This suggests that, associated with the loss of hydration water, lattice hydroxyls and remnants of

interlayer water, the 'tubular' material undergoes more thermal disintegration or pore formation than does the 'tabular' fraction. Splitting and unrolling of tubes is expected because elimination of remnants of interlayer water places strain on individual laminae (69) and is therefore likely to result in increased specific surface area (7). An increase from $38.9 \text{ m}^2/\text{g}$ to $68.7 \text{ m}^2/\text{g}$ has been observed for a metahalloysite (26) upon raising the outgassing temperature from 25 to 300°C and this is an indication of the high degree of thermal disintegration which occurs at low temperatures. In this respect metahalloysite usually differs from kaolinite, the specific area of which is almost unaffected by thermal effects in the low temperature region (26,29).

The walls of tubes observed in electron-microscopic pictures of metahalloysite materials (7) are very thin compared with the thickness of tabular particles and it is probable that the greater structural rigidity of the tabular material, due to the greater number of superposed layers, explains its lower degree of thermal fracturing in comparison with

Table 4. Specific Surface Area of Homoionic Te Puke Metahalloysite

Cation	Nitrogen Adsorption data		Water Vapour Adsorption Data							
	Specific Surface area (m ² /g)		Water Monolayer Capacity X _m (mg/g)	Specific Surface Area (m ² /g) [⊗]	Experimental error in X _m (%)	Apparent cross-sectional area of water molecule	BET 'C' constant			
Li	33.5	33.0	8.11	28.8	1.8	12.5	39.9			
Na	34.1	34.6 [*]	9.80	9.87 [*]	34.8	35.0 [*]	1.3	10.4	27.6	25.2 [*]
K	36.2	35.6 [*]	9.24	9.30 [*]	32.8	33.0 [*]	1.6	11.6	31.9	29.1 [*]
Rb	35.6		9.48	9.88 [*]	33.6	35.0 [*]	1.3	11.0	31.9	36.8 [*]
Cs	35.8		9.55		33.9		1.6	11.2	26.2	
Mg	33.8		13.32		47.2		1.2	7.6	32.3	
Ca	32.8		11.39		40.4		1.1	8.6	21.4	
Sr	33.0		10.24		36.3		1.4	9.6	23.8	
Natural (<10 μ)	35.9		9.42		33.4		1.6	9.9	23.8	
Natural (<10 μ) TMCS treated p74.	30.7		8.46		30.0		1.8	10.8	21.3	

* Determinations on separate samples.

⊗ Assuming cross-sectional area of water molecule is 10.6 Å²

tubes. If the elongated material is of polygonal cross-section with concentric fracture zones (22) then expulsion of the inner parts, at the boundaries marked by these zones, may give rise to considerable increases in specific surface area.

4.4.1.b TePuke Metahalloysite

The process of cation exchange, when applied to a 1-20 μ e.s.d. fraction of TePuke halloysite, using solutions of the chlorides of group I and II metals, caused relatively small alterations in the specific surface area (Table 4) of the metahalloysite which resulted from drying the parent mineral.

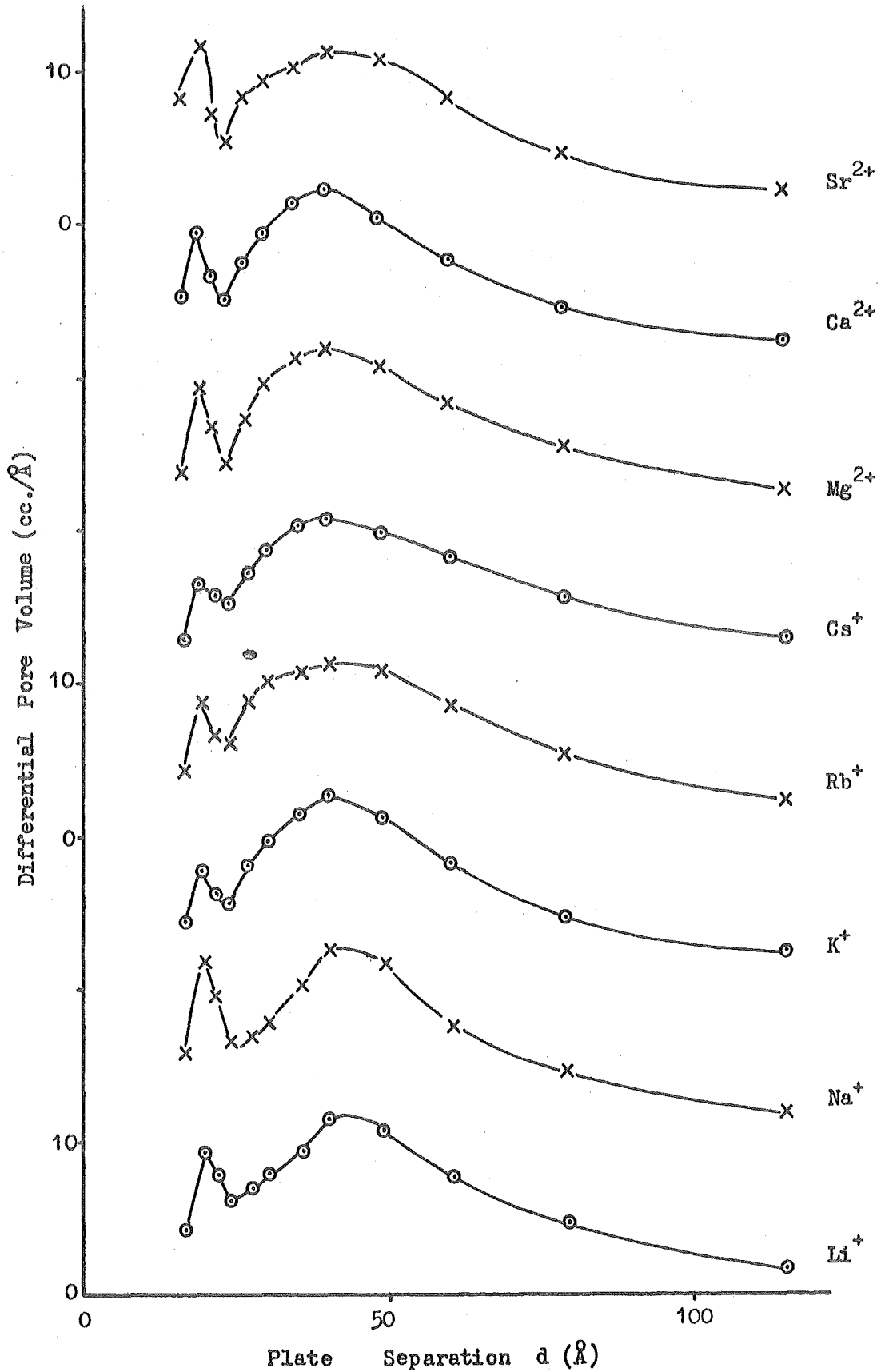
Cations may affect the specific area of a clay mineral by their effect on the submicroscopic structure (87) as a result of their effect on the arrangement and closeness of approach of the elementary clay particles; by their different tendencies to retain water of hydration; and due to size of the ion and its position on the clay surface. The last effect is likely to be a very minor one. The pore size distributions (figure 47), derived from water vapour

desorption isotherms for the different cation modifications of the TePuke clay, indicate that the various cations have little effect upon the pore system of the material. The more or less general increase in specific area, as the size of the monovalent cation increases, is consistent with a similar trend observed for kaolinite (45) but remains at present unexplained.

Treatment of a 'natural' ($\approx 10\mu$) fraction of TePuke metahalloysite with trimethylchlorosilane caused a 13% reduction in the specific surface area which is ascribed to two possible effects, steric hindrance to adsorption and energetic effects. The umbrella-like form of the trimethylsilyl group may cover sufficient surface roughness or pore openings to reduce the total adsorption. Reaction of the silane derivative with the hydroxyl surface would cause a reduction in polarity and as a result the first adsorbed layer could be more loosely packed than on a natural hydroxyl surface. Looser packing means that the effective cross-sectional area of the nitrogen molecule is larger and the calculated

Fig. 47

Pore Size Distribution of Te Puke Metahalloysite
Derived from Water Vapour Desorption Data.



monolayer capacity smaller than for the unreacted hydroxyl surface, even though it is possible that the true surface area of silylated and unreacted surfaces are the same.

4.4.2 The Effect of Vacuum Outgassing Temperature on the Specific Surface Area and Pore Properties of TePuke Metahalloysite

4.4.2.a Introduction

Initial work, discussed in the previous section, which was carried out upon Maungaparerua metahalloysite, indicated that physical and chemical treatments had marked effects on the specific surface area and porous nature of the mineral. In view of these findings it was decided to investigate systematically the influence of the vacuum outgassing temperature on the surface and porous properties of the metahalloysite prepared from TePuke halloysite. For this portion of the study three materials, derived from the bulk TePuke mineral, were used. The first two were portions of homoionic 1-20 μ e.s.d.

metahalloysite saturated respectively, with sodium and rubidium ions (section 3.1.b). The third material used was 'natural' ($< 10\mu$) metahalloysite (section 3.1.c), this being utilized for both specific surface area and pore size distribution studies.

The 'natural' clay was outgassed at a series of successively higher temperatures in the range $110 - 460^{\circ}\text{C}$ and a complete nitrogen adsorption-desorption isotherm determined after each thermal treatment. From each of these isotherms (figures 35 to 41) the BET specific surface area was computed, using data from the adsorption branch for which $0.05 < P/P_0 < 0.30$, and a differential pore size distribution calculated by applying the Kelvin equation, assuming a parallel plate pore model, to the desorption curve of the hysteresis loop. The calculated areas are contained in table 6 and depicted as figure 50. The effect of outgassing temperature on pore properties is discussed in a later section.

For the sodium and rubidium clays adsorption data was obtained only in the relative

pressure region 0.05 to 0.30 and BET surface areas calculated. The resulting values are given in table 5a and illustrated as figure 48. Assuming that the relationship of weight loss to outgassing temperature is the same for the homoionic minerals as it is for 'natural' metahalloysite (section 4.3) allows the calculation of specific surface areas for the former materials, these values being collected in table 6 and graphically in figure 50.

4.4.2.b The Specific Surface Area of Metahalloysite

Literature values of the specific surface area of metahalloysite, determined by the adsorption of nitrogen, range from 7.9 m²/g (227, p227) to 150 m²/g (87). This considerable range may be due, in part, to differences in the particle size distribution for the various mineral samples, or to the different pretreatments used. It seems more likely however that the wide range results from varying degrees of well-developed porosity among the samples. The present and other studies (26, 319,320) indicate the existence of pores of

intermediate or transitional size (15\AA - 500\AA diameter) and the present investigation further shows that these pores contribute the major fraction of the total area available for the adsorption of nitrogen molecules.

In a discussion of the specific surface area, or more precisely the BET specific surface area, of metahalloysite, it is necessary to distinguish between the total surface area and the area determined by gas adsorption, since some data (321) indicate that nitrogen does not measure the entire surface. It was shown (321), for two halloysites, that nitrogen adsorption yielded specific surface areas of $47\text{ m}^2/\text{g}$ and $67\text{ m}^2/\text{g}$, while small angle X-ray scattering experiments indicated an area of $440\text{ m}^2/\text{g}$ for both materials. The authors (321) attributed the discrepancy to the presence of micropores smaller in diameter than the nitrogen molecule, or to pore shrinkage during the dehydration which precedes low-temperature nitrogen adsorption. If the micropores of the former explanation exist in the materials of the present study then this study gives an estimation

of the effects of thermal treatments on pores, and the surface area in pores, which are larger in diameter than a nitrogen molecule.

4.4.2.c The Effect of Heating on the Specific Surface Area of Kaolins

It is generally observed for clay minerals, particularly for kaolinites and illites, that the specific surface area does not alter to any large extent on heating or upon the loss of structural water (29). This implies that dehydroxylation occurs without appreciable changes in particle size.

A small reduction in specific surface area is the more usual result of heating kaolinites to a temperature lower than that which initiates dehydroxylation, due, it is thought, to increases in particle size (322,323). The loss of hydroxyl water, which amounts to 22% by volume of the kaolinite structure (324), is accompanied by considerable structural changes leading to the depolymerization of the mineral (325). The escape of this large fraction of the mineral, in the form of water vapour, might be

expected to yield increased porosity (322), decreased particle size (327) and increased specific surface area (326).

Although an increase in specific surface area has been observed upon the dehydroxylation of kaolinite (316,323,), the magnitude of the increase was smaller than expected, because associated with the water loss was a general settling down to a structure of smaller volume. The small increase may also be explained if the holes produced by the escaping vapour are too small for the entry of nitrogen molecules (316). It also indicates that metakaolinite, the product of dehydroxylation, is relatively stable, showing little tendency to fracture into smaller crystallites (316). This stability is compatible with the structure of kaolinite.

In view of the compositional and structural similarity of metahalloysite to kaolinite, the above considerations should apply equally well to both minerals. Two studies of the influence of temperature on the specific surface area of halloysites report quite different results, Orr (227,p227) quoting

that only small changes occur while Brooks (26), for a mineral from a different source, found the comparatively large 77% increase for a change of outgassing temperature from 25°C to 300°C. These observations indicate a possible dependence of thermal behaviour on mineral origin, the properties of the materials, which are most likely to be concerned, including morphology and the degree of structural disorder. Further indications of effect of the morphology are referred to in later sections.

4.4.2.d The Surface Area of Homoionic TePuke
Metahalloysite in Relation to Outgassing
Temperature.

The effects of vacuum outgassing temperature on the surface area of cation-exchanged TePuke metahalloysite, and the similarity of the changes observed for sodium and rubidium modifications, are clearly shown in figure 48, an illustration of the data contained in table 5a.

An increase in sample surface area upon outgassing at 100°C in vacuo is ascribed to two

Table 5a Effect of Outgassing Temperature on the Surface Area (m²) of Homoionic Te Puke Metahalloysite.

Temperature °C	Surface Area (m ²) Na ⁺ - metahalloysite			Surface Area (m ²) Rb ⁺ - metahalloysite		
	25	8.58	8.65	8.62	8.49	8.54
50	-			8.48		
100	8.89	8.73 [*]		8.76	8.73	8.91 [*]
150	8.63			8.30	8.31	
200	8.43			8.13	8.20	
250	8.21			7.94	7.85	
300	8.25			7.73		
350	7.83			-		
400	7.66	7.61	7.56	7.42		
450	7.57			7.40		

*Duplicate samples (Other measurements on same samples)

Table 5b Effect of Outgassing Temperature on the Specific Surface Area of Homoionic Metahalloysites.

Cation	Specific Surface Area Σ (m ² /g)			%increase in Σ upon dehydroxylation
	Outgassed 25°C	Vacuum aged 22°C (2 years)	Outgassed 450°C	
Na ⁺	35.3 ± 0.3	34.3 ± 0.3	38.3 ± 0.4	8.5 ± 0.3
K ⁺	37.5 ± 0.3	35.9 ± 0.3	40.5 ± 0.4	8.5 ± 0.3
Rb ⁺	39.5 ± 0.3	35.6 ± 0.3	42.5 ± 0.4	9.1 ± 0.3

Fig. 48

The Effect of Outgassing Temperature on the Surface Area of Homoionic Te Puke Metahalloysite Samples

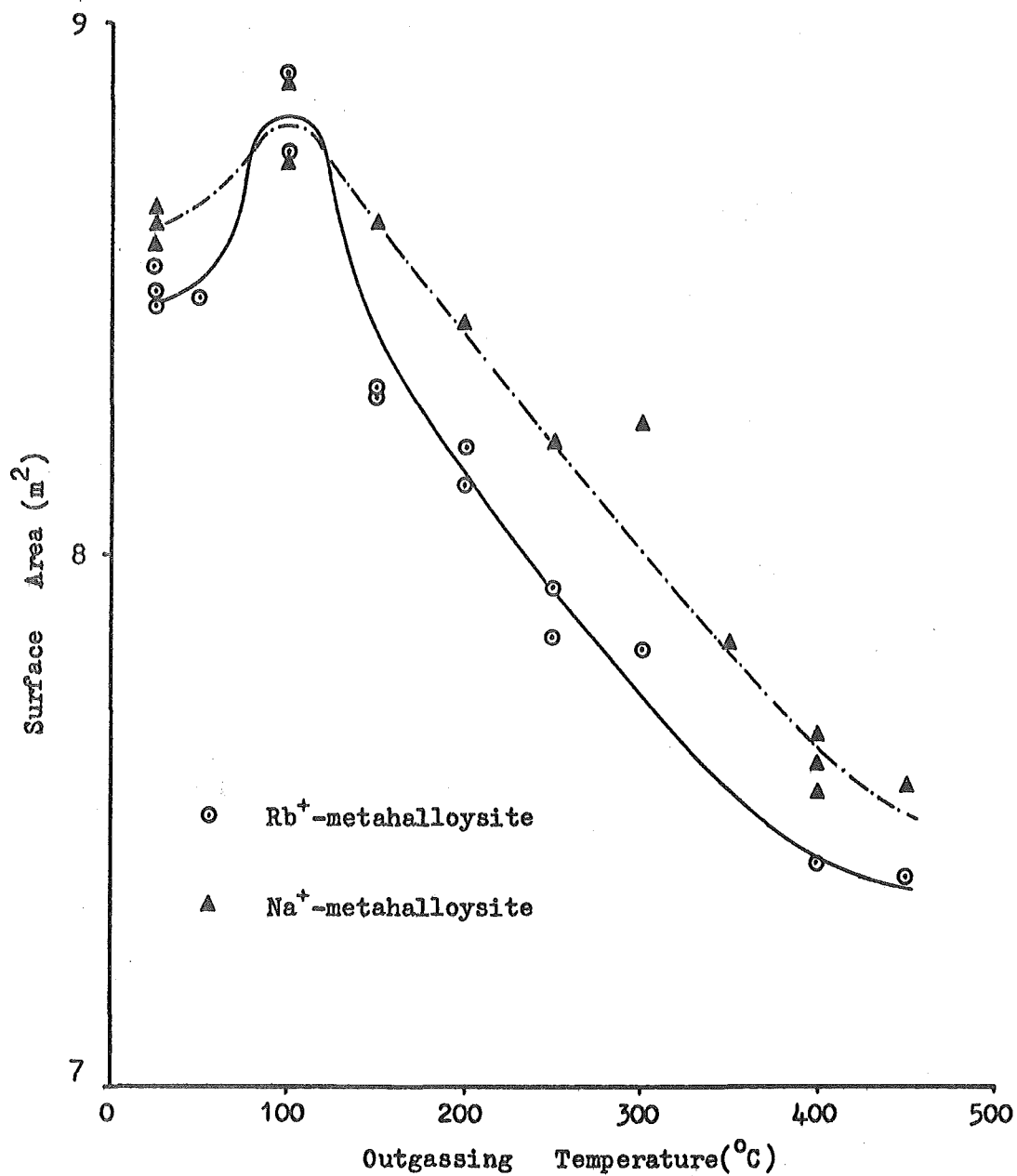
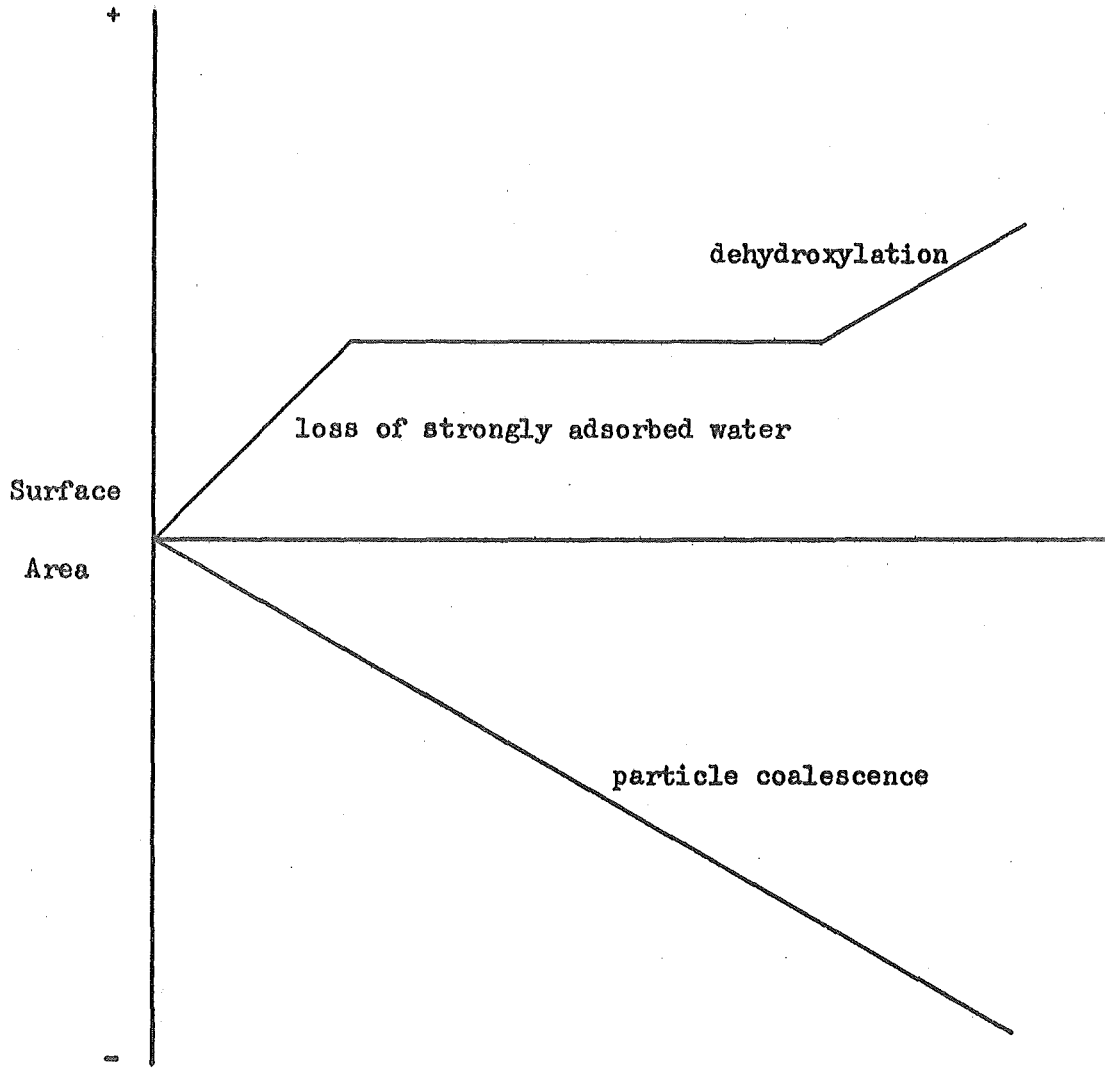


Fig. 49

Diagrammatic Representation of the Surface Area
Curves of Fig. 48



possible effects, the loss of strongly adsorbed and pore water allowing access of nitrogen molecules to a larger proportion of pore space and area, and the effects of thermal disintegration which have been found to occur in conjunction with the expulsion of remnants of interlayer water at relatively low temperatures (7,28,69). Loss of most of the interlayer water, and the occurrence of the associated thermal destruction, should however have taken place prior to the degassing experiments, while the samples were being oven dried at 110°C. Thus, particle fracturing or exfoliation are unlikely to explain the increase in surface area at low temperatures and the observed changes are best attributed to the effects of adsorbed water taken up by the samples during transfer and weighing procedures and lost on evacuation.

The decrease in surface area which occurred for outgassing temperatures in the range 100°C - 400°C is attributed to particle coalescence which, according to Martin (117), may occur by two mechanisms, twinning or cementation by amorphous

alumina. At the low temperatures involved in this study it seems unlikely that any amorphous alumina would be produced and the second mechanism is therefore not expected to contribute significantly to the surface area decreases observed. Coalescence of particles is capable of causing a large reduction in surface area, particularly if it occurs by a face to face particle interaction.

If the surface area decreases are correctly attributed to particle coalescence by twinning an accompanying change in the crystallite dimensions would be expected. Indeed, Takahashi (30) showed for a halloysite, a metahalloysite and a kaolinite, that the crystallite dimension L_c , along the direction of the crystallographic C axis, increased considerably on the temperature range 100 - 400°C. In the same range the dimension L_a , parallel to the layer plane, decreased somewhat due to thermal fracturing of the kaolin layers. In order to explain the observed decrease in area, the production of new edge area by fragmentation must be a less significant process, in the temperature range,

than the decrease in area resulting from particle coalescence.

At treatments above 400°C the surface area did not alter markedly, the effects due to coalescence presumably being offset by increases in surface area produced by the loss of hydroxyl groups in the form of vapour. As has been already mentioned, the escape of the structural water is expected to cause increased porosity and also lattice disintegration. It was found, in the present study, that the loss of hydroxyl groups from metahalloysite was considerable, under vacuum outgassing conditions, at temperatures above 350°C. A certain indication that destruction of the metahalloysite structure and particle fracturing accompanies dehydroxylation is given by the large decreases observed (30) in the crystallite dimensions both parallel to, and perpendicular to, the layer plane.

The experimental curves, relating the surface area of homoionic metahalloysite samples to the outgassing temperature (figure 48) may therefore, as a simplification, be depicted (figure 49) as being

caused by three major contributing effects:

1. loss of adsorbed and pore water,
2. particle coalescence
3. lattice destruction.

In contrast to the overall decrease in the surface area of the above samples, it was found that the specific surface areas (m^2/g) had increased by more than 8% (table 5b). The increase is a result of a combination of the effects discussed above but takes into account the weight loss of about 14% which occurs upon the dehydroxylation of the mineral (section 4.3).

4.4.2.e The Specific Surface Area of 'Natural' TePuke Metahalloysite in relation to Outgassing Temperature

The maximum change in the specific surface area of 'natural' ($<10\mu$) TePuke metahalloysite, observed for the effect of outgassing temperature in the range 110°C to 460°C , was from the minimum value of $35.2 \text{ m}^2/\text{g}$ at 250°C to the highest of $38.4 \text{ m}^2/\text{g}$ at 400°C (table 6); an overall increase of 9.4%. This

is a small change when compared with the 77% increase recorded by Brooks (26) for the 25°C to 300°C range, and with the large increases observed in the present study (section 4.4.1) for the 'tubular' fraction of Maungaparerua metahalloysite. The 'tabular' portion of the latter mineral shows a much smaller increase in area. These results indicate particle morphology has an influence upon the effects which occur upon heating metahalloysite. The elongated particles of the mineral of Brooks (26) and Maungaparerua is apparently, as was discussed earlier (section 4.4.1a), more susceptible to thermal fracturing than is the TePuke mineral, electron micrographs (figures 7 and 8) of which show little evidence of elongated particles.

It is evident from the changes in specific surface area which occur with increased outgassing temperature, that the TePuke metahalloysite behaves more like the tabular mineral kaolinite than it does the tubular or elongated morphology of halloysite. This is shown by a comparison of curve (a) in figure 50 for sodium-metahalloysite with the data of Brown and Gregg (323) for kaolinite (figure 51). The form

Table 6. Effect of Outgassing Temperature on the Specific Surface Area of Te Puke Metahalloysite.

Metahalloysite Sample	Specific Surface Area (m ² /g)				S _{des cum}
	Natural <10 μ		Homoionic 1-20 μ		
			Sodium	Rubidium	
Temperature °C					
100 ± 3	35.9	35.6* 35.2*	36.6 ± 0.6	40.1 ± 0.6	24.4
150 ± 3		-	35.6	38.1	-
200 ± 3		-	34.7	37.6	-
250 ± 3	35.0	35.3*	34.0	36.5	24.2
300 ± 3	35.3	35.8*	34.6	36.0	25.0
325 ± 3	36.3		-	-	25.4
350 ± 3	36.6		33.3	-	25.5
400 ± 5	38.4		35.8	39.0	27.2
450 ± 5		-	36.0	39.2	-
460 ± 5	35.3	35.8	-	-	26.1

* Additional determinations on separate samples

of the curves is quite similar although the rise in area due to dehydroxylation occurs at lower temperatures for the metahalloysite case, an expected result since dehydroxylation of this mineral occurs in general at 50 - 60°C below that for kaolinite (52).

The relationship between specific surface area and outgassing temperature (figure 50) is different for the 'natural' (<10 μ) TePuke clay and the homoionic (1-20 μ) fraction of the same mineral. It should be stressed that, as well as the difference in particle size of the two materials, the homoionic samples were treated with disodiummethylenediaminetetraacetic acid and 1M salt solutions while the 'natural' clay was not chemically treated in any way. The chemical treatments may or may not have altered the susceptibility of the mineral to thermal effects.

The absence of a definite specific surface area decrease for the 'natural' material, in the lower temperature range, is probably best ascribed to the fact that this mineral fraction was not subjected to outgassing in the 100 - 250°C range, the region in which the marked decrease, due to particle coalescence,

took place for the homoionic samples. It is apparent that a limited amount of particle coalescence occurs for the 250°C and 300°C treatments of the 'natural' mineral. Coalescence may indeed occur at these temperatures but the loss of surface area due to this phenomenon must be opposed by increases in area which result from the loss of structural water. At higher temperatures dehydroxylation effects are dominant and increased specific surface area results for both materials.

Electron micrographs of the 'natural' mineral taken for samples after outgassing at 110°C, 350°C and 500°C (figures 7 and 8) indicate that effects due to dehydroxylation at 350°C caused separation of aggregates into isolated particles. The 500°C treatment apparently caused reaggregation by particle coalescence. It is pointed out that the field observed in these micrographs is very small and may, because of the sampling techniques employed, not give a true indication of the actual changes which occur. The conclusions drawn from these pictures do however agree with the increase in specific surface area

Fig. 50

Effect of Outgassing Temperature on the Specific Surface Area (Σ) of Te Puke Metahalloysite

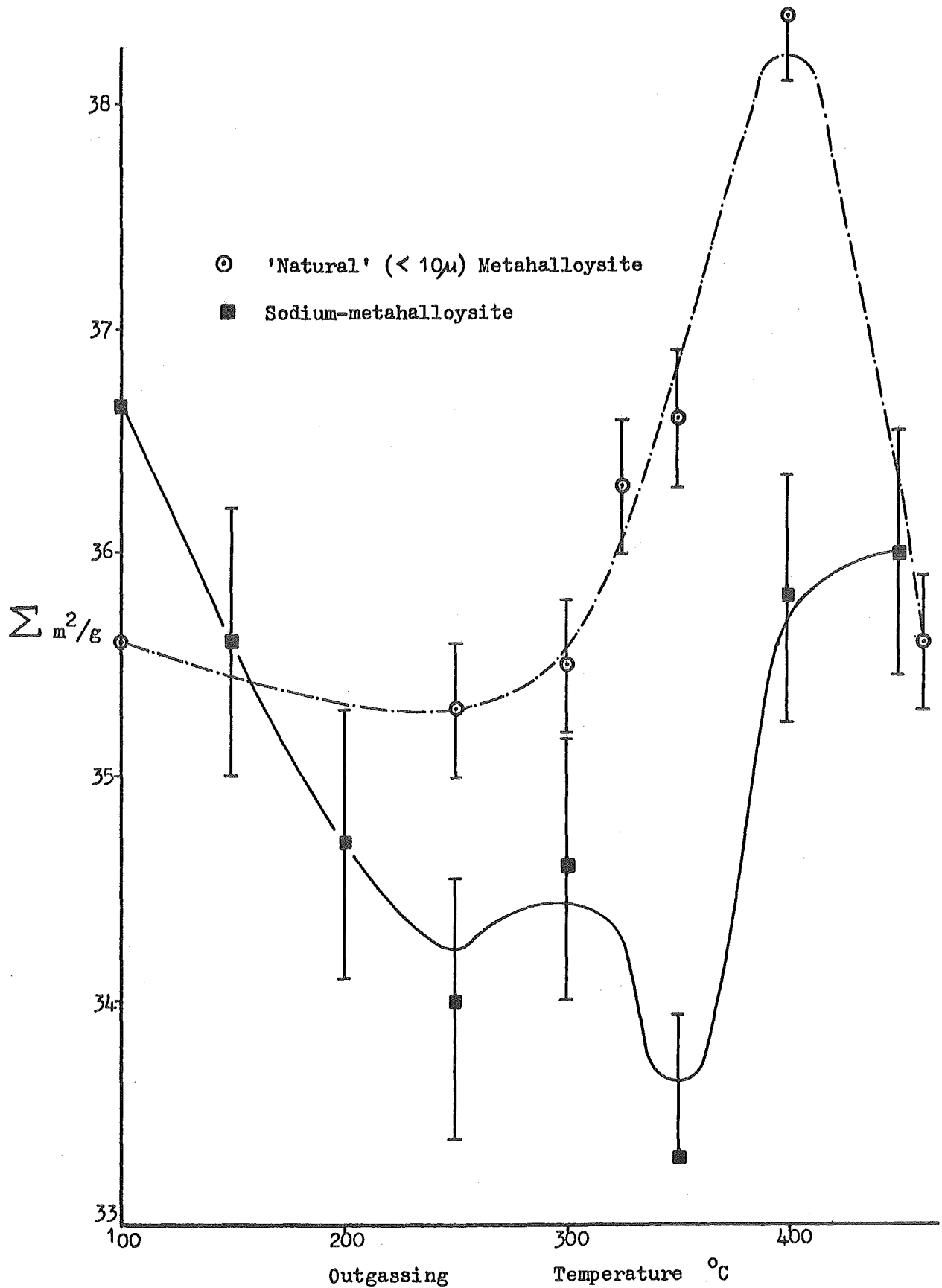
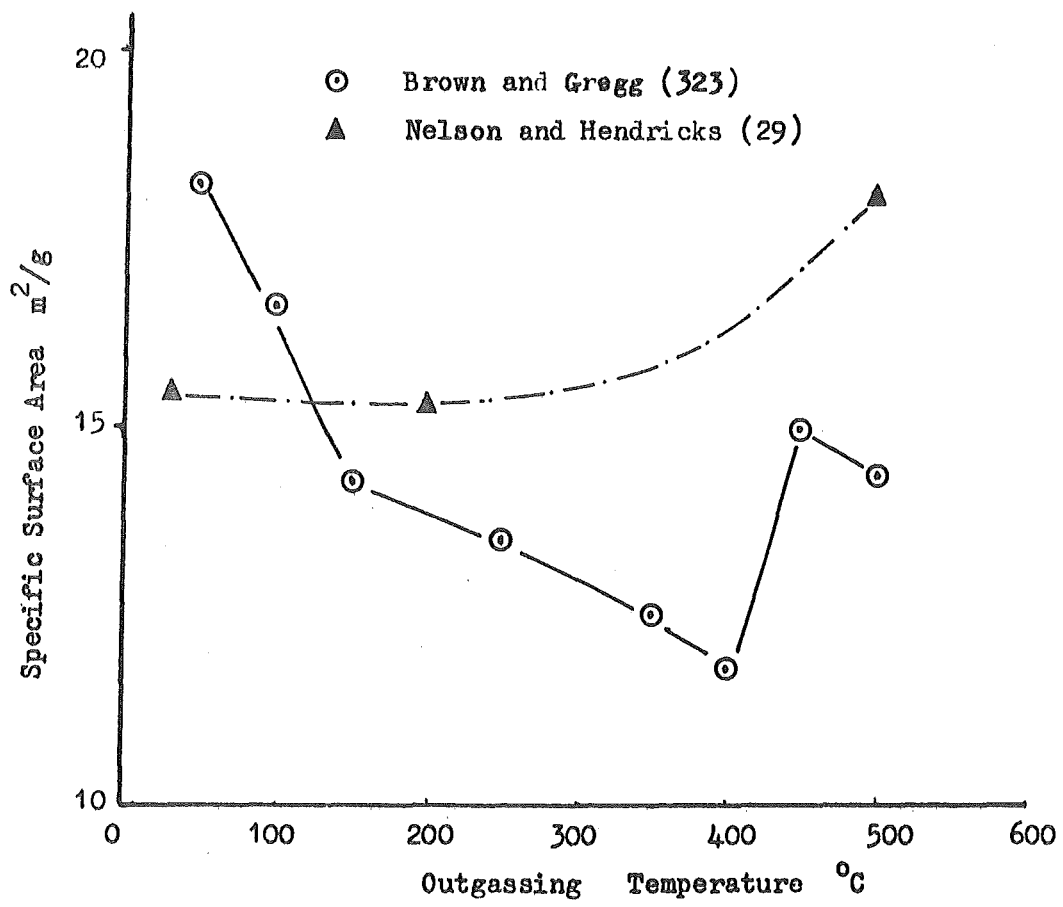


Fig. 51

Specific Surface Area of Kaolinite in Relation to Outgassing Temperature



observed at 350°C and with the decrease which is appreciable even at 460°C.

4.4.3 The Pore Size Distribution of Clay Minerals

4.4.3.a Introduction

Most natural sorbents, in particular clays and clay minerals, belong to the macro-transitional class of porous substances (203), these substances containing various amounts of pores in the size range $15\text{\AA} - 10^6\text{\AA}$. A number of important properties of clays depend on the amount and size distribution of the pores they contain, these properties including, among others, permeability, shrinkage, strength, capacity for water retention and drying properties.

Few studies have been reported which deal with the pore size distribution of clay minerals, particularly with those pore sizes amenable to determination by gas adsorption methods. As is discussed in section 2.2, such methods are, for various reasons, limited to the range of pore sizes from about 18\AA to approximately 1000\AA . The former limit is set by the apparent lack of applicability of the Kelvin

equation to the adsorption in pores of smaller than this size (225-227).

It is believed (97) that clay minerals exist in a series of structural states which depend on the history of the material and upon its water content. When dry, the internal structure and the manner in which it varies with the state of hydration can be described, at least qualitatively, by pore size distribution studies based on nitrogen adsorption (26).

The complete isotherm for the adsorption of a non-polar gas on a clay mineral very often shows a large decrease in the amount adsorbed at intermediate relative pressures on the desorption curve. This feature of the isotherm was fully discussed in section 4.2.b where it was asserted that the drop could not be explained by a random arrangement of clay particles. The narrow range of pore sizes indicated by the drop, is best explained as resulting from the nature of the packing of the fundamental clay mineral layers.

The relatively discrete ranges of pores of small diameter ($<100\text{\AA}$) observed for clay minerals are explained (97,136,222) by the formation of domains

of oriented crystals as the clay-water system dries from a gel-like state. In each domain the clay plates are in a parallel arrangement but domains are randomly oriented within the clay matrix. Relatively high separations between individual crystals in the dry state, a typical pore diameter being 30\AA (222), are possibly due to surface charge repulsions but are more likely the result of surface irregularities, interleaving of crystals, or the presence of small fragments between plates. The narrow ~~plates~~ *peaks* observed in the pore size distributions calculated for clay minerals are therefore attributed to the distance, or distances, of closest approach of clay crystals.

It has been shown, for a number of compacted clay mineral systems (222), that the major part of the total pore volume exists in pores of diameter less than 100\AA . A similar result has been quoted for a laboratory dehydrated halloysite (319). The solitary instance, for metahalloysite, of a pore size distribution derived from nitrogen desorption data, shows, as its major feature, a narrow peak

centred at $28 - 30\text{\AA}$ diameter (218). The nitrogen desorption curves of the present study (figures 35-41) have as their main feature a drop at a relative pressure around 0.50 and this is expected to give rise to a pore size distribution dominated by a single narrow peak.

4.4.3.b The Pore Size Distribution of TePuke Metahalloysite

As is pointed out in section 4.2, the isotherms for the adsorption of nitrogen on metahalloysite (figures 35 to 41) are composed of a type II adsorption isotherm and a sloping type B hysteresis loop. This combination, it was asserted, is a result of adsorption in a material containing both slit-shaped and wedge-shaped pores.

The pore size distribution is calculated by the application of the Kelvin equation (equation 9) to the desorption branch of the isotherms obtained, since this is the curve believed to be thermodynamically stable for pores of parallel plate type (242,310). In applying the Kelvin equation the tacit assumptions are made that all pores are of a uniform

idealised shape and that the adsorbed phase has the properties of the bulk liquid. Both of these assumptions are, as is discussed in section 2.2, great simplifications of the real physical situation and the conclusions drawn from pore size analysis must be regarded as qualitative rather than quantitative.

For approximate calculations the classical Kelvin equation (equation 9) can be used in the form (equation 20) appropriate to slit pores of separation d .

$$d = \frac{2\gamma V \cos \theta}{RT \ln P_0/P} \quad 20$$

(for symbol definitions see equation 9)

As is usual, the angle of contact θ is assumed to be zero, i.e. $\cos \theta = 1$. Evidence that this assumption is reasonable is given by the asymptotic approach of the adsorption curves towards the saturation axis, i.e. $P_0/P \approx 1$, this indicating complete wetting and the absence of a contact angle (224).

For more accurate calculations various

corrections must be applied to the classical Kelvin equation, in particular to allow for the thickness of the adsorbed layer which remains after a pore is emptied of its capillary condensed liquid. Making allowance for such effects results in the more complex expression (224)

$$\frac{d}{2} - t_a = \frac{\gamma V}{RT \ln P_o/P} + \int_{t_a}^{d/2} \frac{F(t) dt}{RT \ln P_o/P} \quad 21$$

R, T, P_o, P, γ, V are defined as in equation 9

F(t) - the function describing the standard adsorption isotherm and which defines the thickness of the adsorbed layer

t_a - the thickness of the adsorbed layer at pressure P/P_o

d - the plate separation for pores which empty at relative pressure P/P_o

Broekhoff and deBoer (224) solved this equation, using for the function F(t), values of the thickness t derived from nitrogen adsorption data for non-porous oxides. These authors present plate separation values for a number of relative pressures, and it is these values, or graphically interpolated values,

which are used in the present calculations. The corrections when applied substantially increase the predicted pore diameter above that given by the classical Kelvin equation.

In order to calculate a pore size distribution, the desorption curve was divided into a number of relative pressure intervals of equal size, an interval of $P/P_0 = 0.02$ being chosen. Computation was begun at $P/P_0 = 0.98$ and ended at $P/P_0 = 0.42$, the point of closure of the hysteresis loop. These limits correspond, according to equation 21, to pores of diameter 626\AA and 29\AA respectively. The volume and area of pores which are outside this range are neglected, although, as will be seen later, they must contribute significantly to the total pore volume and area. Each relative pressure interval corresponds to a decrease in the volume of liquid adsorbed (ml. per gram). The pore volume and pore surface area may be calculated by the application of expressions 22 and 23 respectively. The differential pore volume of the k th group of pores DPV_k is defined by equation 24.

$$V_k^P = \frac{d_k}{d_k - 2t_k} \left[dV_k - (t_{k-1} - t_k) \sum_{i=1}^{k-1} S_i \right] \quad 22$$

$$S_k = \frac{2V_k^P}{d_k} \quad 23$$

dV_k - liquid volume desorbed over the kth relative pressure range (ml.)

V_k^P - pore volume of the kth group of pores (ml.)

d_k - the diameter of the pores emptying at the mean relative pressure of the kth interval (Å)

S_k - the surface area of the kth group of pores (m²/g)

t_{k-1} - the thickness of the adsorbed layer at the higher relative pressure of the kth interval (Å)

t_k - the thickness of the adsorbed layer at the lower relative pressure of the kth interval (Å)

$$DPV_k = \frac{V_k^P}{dD} \quad (cc/\text{Å}) \quad 24$$

dD - the difference in diameter of the pores emptying at the higher and lower relative pressures of the kth interval (Å)

As an example the complete tabulation

of the pore size distribution calculation for the 110°C, outgassed TePuke metahalloysite is included as table 8.

The nitrogen isotherms (figures 35 to 41), for TePuke metahalloysite samples outgassed at various temperatures, are superficially very similar, an immediate indication that increasing the vacuum outgassing temperature has little effect on that part of the porous structure of the mineral which can be measured by nitrogen adsorption. Pore size distributions (figure 52), calculated from the desorption data of these isotherms, confirm this initial conclusion.

The pore size distributions (figure 52) all have essentially the same form, each containing a major peak in the 30 - 34Å region and a smaller subsidiary distribution at larger pore sizes (35 - 70Å). As the outgassing temperature is increased, a general narrowing of the subsidiary distribution takes place, being narrowest and most pronounced for the 400°C treatment. A clearer indication of the changes in pore sizes which result

on outgassing is afforded by a consideration of the cumulative pore volumes of selected pore groups. Table 7 includes the cumulative volumes for the pores in three ranges 30 - 35 \AA , 35 - 100 \AA and 100 - 626 \AA . Increased outgassing temperature up to 400 $^{\circ}\text{C}$, result in increasing higher volumes of pores in the first two ranges. The 460 $^{\circ}\text{C}$ treatment causes a reduction of the volume in these ranges. Small changes only are observed in the larger pores particularly for temperatures 300 $^{\circ}\text{C}$ and above where loss of hydroxyl water becomes important. The major change in the smallest pore range occurs upon outgassing at 250 $^{\circ}\text{C}$, a result presumably of the narrowing of large pores due to the loss of strongly adsorbed water. Pore formation is unlikely at this temperature because the degree of dehydroxylation is very small (section 4.2). A secondary increase in the volume of 30 - 35 \AA pores, and the major increase in pores of the 35 - 100 \AA range, occurs upon outgassing the mineral at 400 $^{\circ}\text{C}$. These facts, together with the minor changes in pores >100 \AA , gives rise to the general conclusion that dehydroxylation produces mainly small pores. The

Table 7. Cumulative Pore Volumes for Selected Pore Size Ranges
in Relation to Outgassing Temperature of Te Puke Metahalloysite,

Temperature °C	Plate Separation			V _{cum} ^{des}	Increase %
	30-35Å cc/g	35-100Å cc/g	100-600Å cc/g		
110	0.00580	0.0406	0.0577	0.1040	-
250	0.00864	0.0419	0.0589	0.1048	0.8
300	0.00883	0.0427	0.0633	0.1100	5.8
325	0.00885	0.0442	0.0657	0.1137	9.3
350	0.00844	0.0446	0.0664	0.1144	10.0
400	0.00937	0.0487	0.0643	0.1171	12.6
460	0.00872	0.0446	0.0654	0.1151	11.0

Table 8. Pore Size Distribution Calculation for 'Natural' Te Puke Metahalloysite Outgassed at 110°C

P/P _o	V _L _k	DVL _k	T _k	DT _k	D _k	FD _k	X _k	Y _k	V _k	Si	$\sum_{i=1}^k Si$	D	dD	DPS _k
0.98	1106.1		22.9									626		
0.96	897.3	208.8	19.8	3.1	429	1.10	-	208.8	229.7	1.07	1.07	329.5	296.0	0.775
0.94	823.8	73.5	17.5	2.3	270	1.15	2.5	71.0	81.6	0.60	1.67	228.0	101.5	0.804
0.92	765.8	58.0	16.0	1.5	199	1.19	2.5	55.5	66.0	0.66	2.33	175.5	52.5	1.26
0.90	715.5	50.3	14.94	1.06	159	1.23	2.5	47.8	58.8	0.74	3.07	143.7	31.8	1.85
0.88	669.9	45.6	13.82	1.12	131.8	1.26	3.4	42.2	53.2	0.81	3.88	121.9	21.8	2.44
0.86	630.4	39.5	12.75	1.07	113.4	1.29	4.1	35.4	45.7	0.81	4.69	105.8	16.1	2.84
0.84	594.0	36.4	11.89	0.86	99.6	1.31	4.0	32.4	42.4	0.85	5.54	93.5	12.3	3.45
0.82	560.8	33.2	11.17	0.72	88.97	1.34	4.0	29.2	39.1	0.88	6.42	84.3	9.2	4.25
0.80	529.8	31.0	10.57	0.60	80.50	1.36	3.9	27.1	36.9	0.92	7.34	76.92	7.38	5.00
0.78	499.7	30.1	10.07	0.50	73.58	1.38	3.7	26.4	36.4	0.99	8.33	70.52	6.4	5.69
0.76	473.4	26.3	9.65	0.42	67.81	1.40	3.5	22.8	31.9	0.94	9.27	65.23	5.29	6.03
0.74	447.1	26.3	9.27	0.38	62.94	1.42	3.5	22.8	32.4	1.03	10.30	60.66	4.57	7.09
0.72	423.9	23.2	8.91	0.36	58.74	1.44	3.7	19.5	28.1	0.96	11.26	56.75	3.91	7.19
0.70	403.8	20.1	8.57	0.34	55.09	1.45	3.8	16.3	23.6	0.86	12.12	53.39	3.36	7.02
0.68	385.2	18.6	8.26	0.31	51.88	1.47	3.8	14.8	21.8	0.84	12.96	50.40	2.99	7.29
0.66	367.4	17.8	8.02	0.24	49.04	1.49	3.1	14.7	21.9	0.89	13.85	47.68	2.72	8.05
0.64	351.9	15.5	7.77	0.25	46.49	1.50	3.5	12.0	18.0	0.77	14.62	45.28	2.40	7.38
0.62	337.2	14.7	7.56	0.21	44.19	1.52	3.1	11.6	17.6	0.80	15.42	43.10	2.18	8.07
0.60	324.1	13.1	7.36	0.20	42.10	1.54	3.1	10.0	15.4	0.73	16.15	41.12	1.98	7.78
0.58	312.5	11.6	7.17	0.19	40.20	1.55	3.1	8.5	13.2	0.66	16.81	39.32	1.80	7.33
0.56	300.1	12.4	6.99	0.18	38.50	1.57	3.0	9.4	14.8	0.77	17.58	37.62	1.70	8.71
0.54	289.3	10.8	6.82	0.17	36.82	1.59	3.0	7.8	12.4	0.67	18.25	36.04	1.58	7.85
0.52	280.0	9.3	6.66	0.16	35.32	1.61	2.9	6.4	10.3	0.58	18.83	34.59	1.45	7.10
0.50	270.7	9.3	6.50	0.16	33.92	1.62	3.0	6.3	10.2	0.60	19.43	33.21	1.38	7.39
0.48	239.8	30.9	6.34	0.16	32.41	1.64	3.1	27.8	45.6	2.80	22.23	31.94	1.27	35.91
0.46	225.9	13.9	6.18	0.16	31.37	1.65	3.6	10.3	17.0	1.08	23.31	30.75	1.19	14.29
0.44	215.0	10.9	6.02	0.16	30.21	1.66	3.7	7.2	12.0	0.79	24.10	29.61	1.14	10.53
0.42	208.8	6.2	5.86	0.16	29.11	1.67	3.9	2.3	3.8	0.26	24.36	28.53	1.08	3.52

$$V_{cum}^{des} = \sum V_k / 1000 = 0.1040$$

Operations carried out during computation:-

$$FD_k = \frac{D_k}{D_k - 2t_k}$$

$$Y_k = DVL_k - X_k$$

$$DPS_k = \frac{V_k}{dD}$$

$$X_k = DT_k \times \sum_{i=1}^{k-1} Si$$

$$Si = \frac{2V_k}{D_k}$$

Pore Size Distributions of 'Natural' Te Puke
Metahalloysite Outgassed at Given Temperatures

(30 - 100Å section is expanded in
Fig. 52a)

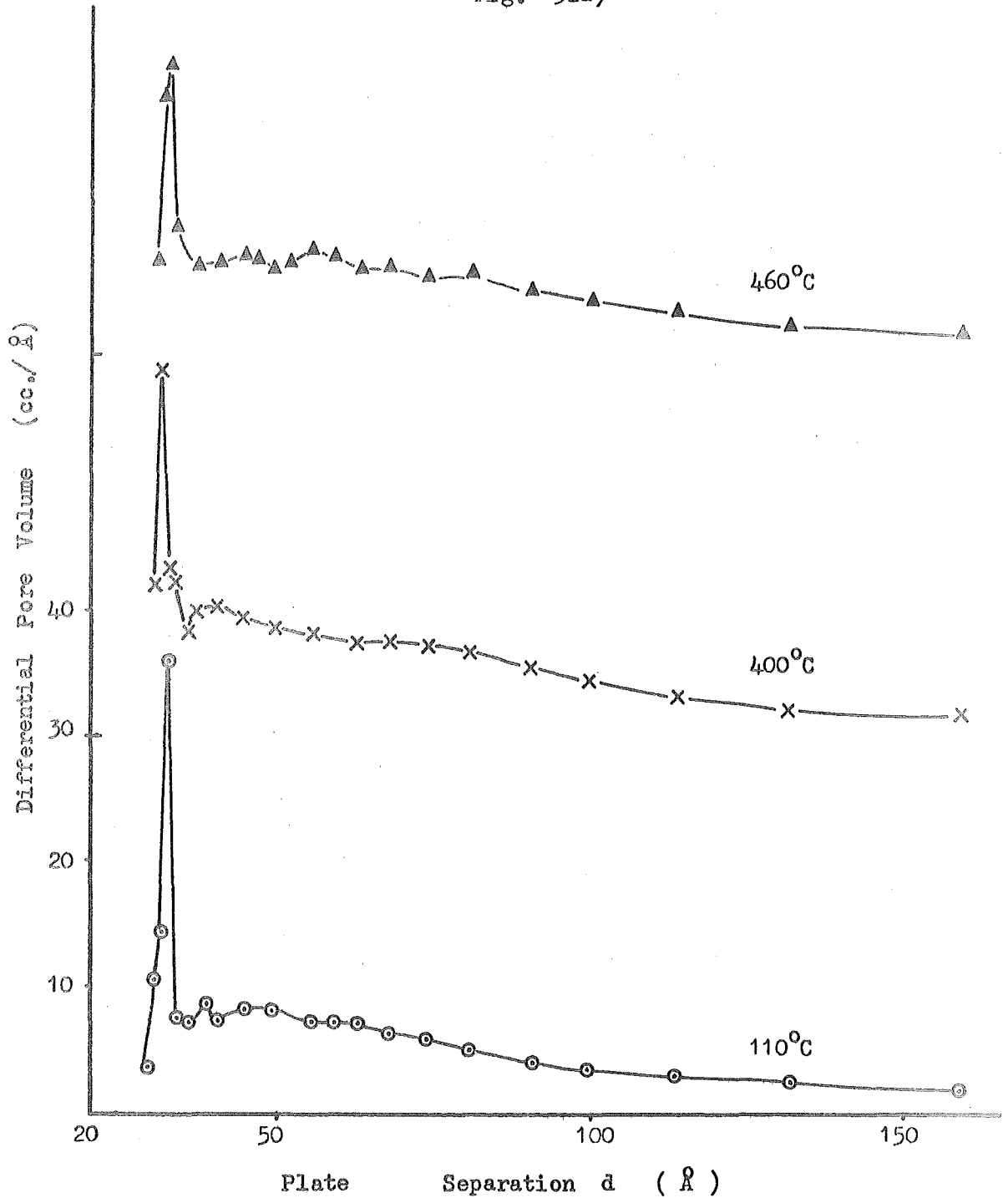
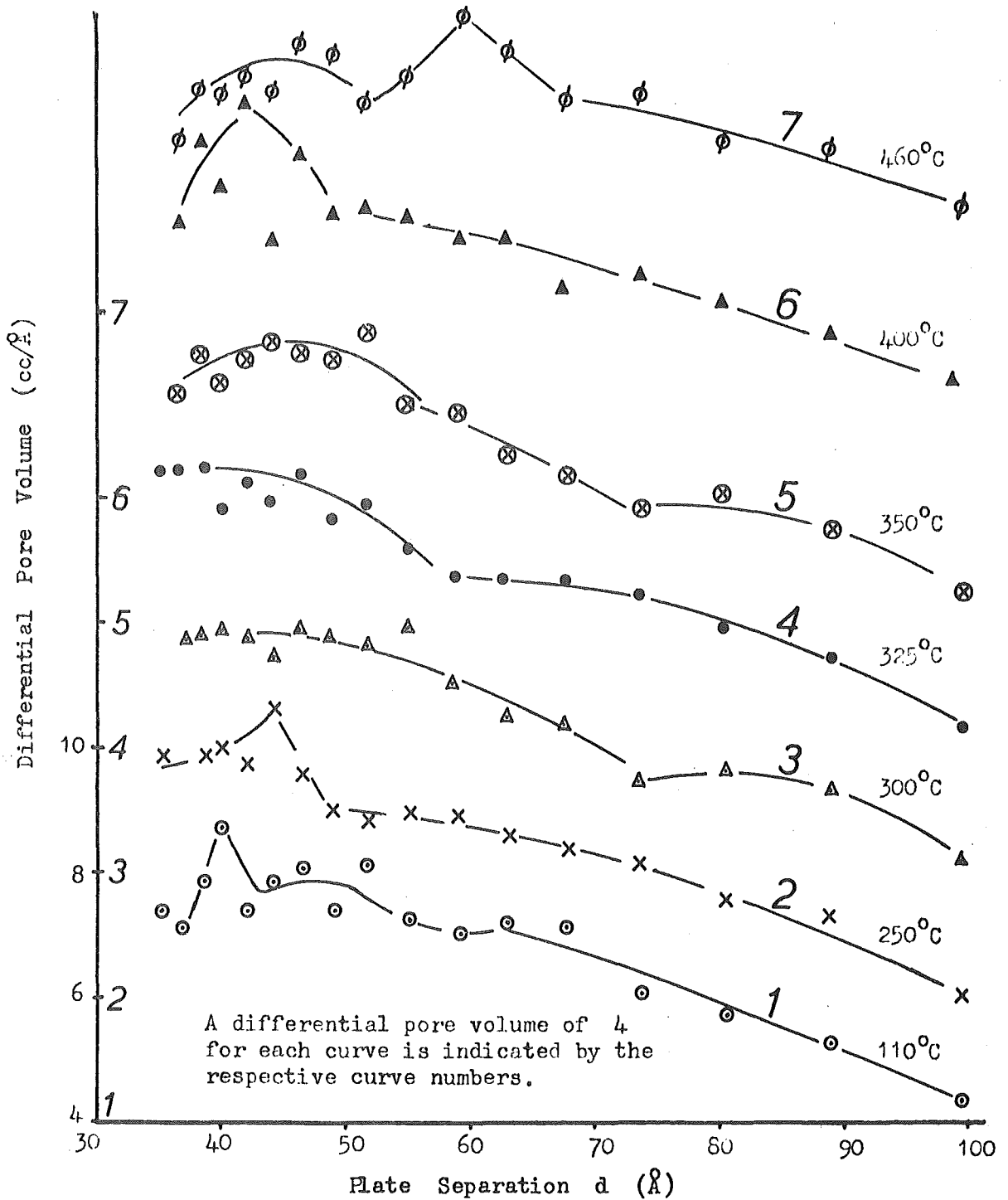


Fig. 52a

Pore Size Distributions for 'Natural' Te Puke
Metahalloysite Outgassed at Given Temperatures

(includes plate separations 30-100Å only)



reductions in pore volumes for the two smallest ranges found for the 460°C outgassing condition, and the apparent shift in the pore size distribution to pores of larger dimensions, can be ascribed to the loss of pore volume in the 30 - 100Å range due to particle coalescence.

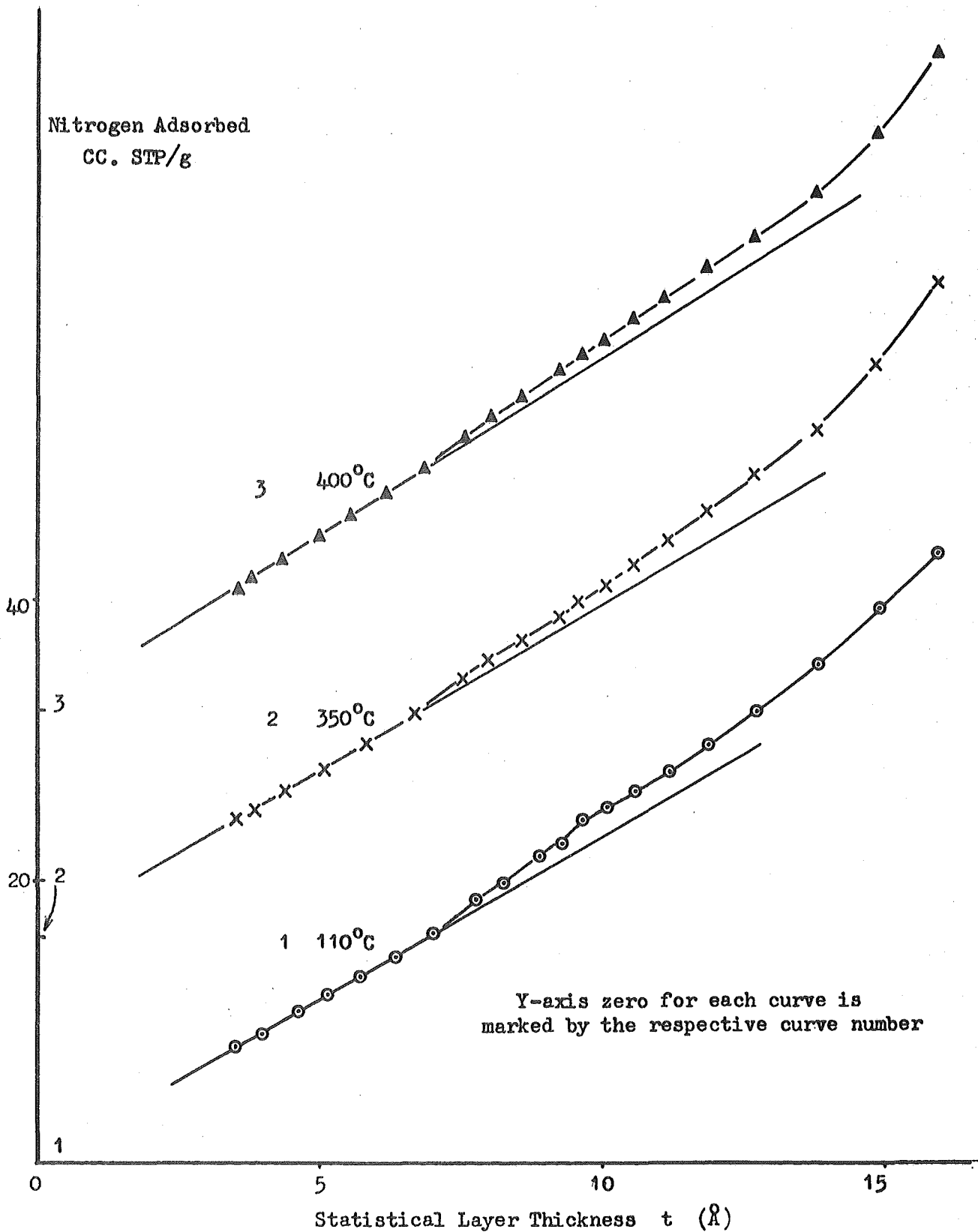
Cumulative pore specific surface areas are also calculated during the distribution calculations and these are compared in table 6, with the BET specific surface areas of the same samples. Although the cumulative areas are considerably smaller than the BET areas it is noted that there is a close correspondence between the two sets of values. This, it is believed, is evidence that changes in the specific surface area measured by nitrogen adsorption are a direct consequence of alterations in the pore area.

A criterion often accepted (244,310) as indicative of the correctness of the assumed pore shape and method of analysis, including the choice of the branch of the isotherm for analysis, is the agreement between the BET specific surface area S_{BET} and the cumulative pore specific area S_{cum} .

For slit pores the desorption branch is stable and its analysis should yield $S_{cum}^{des} = S_{BET}$. Analysis of the adsorption branch shifts the pore spectrum to wider pores and should therefore result in a cumulative area which is too small, i.e. $S_{cum}^{ads} < S_{BET}$. The use of these criteria cannot however be generally accepted, and are not satisfied in the present study, because distorted area values are expected for pores which are not of the ideal shape and because analysis leaves out the largest pores (which includes the external surface of particles) and small pores that fill or empty below the region of capillary condensation. In the present study pores of diameter greater than 626\AA and less than 29\AA are neglected, as is the particle external surface area. It is also evident from the sloping nature of the hysteresis loop that the pores are not all of the idealised shape. The existence of non-ideal pores is also shown by a positive deviation on the deBoer V_a/t plot (explained section 2.3). Such V_a/t plots are included (figure 53) for nitrogen adsorption on the TePuke mineral outgassed at 110°C , 350°C and 400°C . For the ideal parallel plate

Fig. 53

V_a/t Plots for Nitrogen Adsorption on 'Natural'
Te Puke Metahalloysite Outgassed at Given
Temperatures



system adsorption should occur as upon a free surface and the V_a/t plot should be linear. The plots for the metahalloysite-nitrogen system (figure 53) however, all show an increased slope from a thickness value $t \sim 6.5\text{\AA}$ which is associated with capillary condensation in pores of diameter $\gg 2t$, i.e. $\gg 13\text{\AA}$. The pores responsible for the slope deviation from linearity are presumed to be wedge-shaped. These pores do not give rise to hysteresis and are too small to be analysed by the application of the Kelvin equation. If there is a significant amount of wedge-shaped pores of larger sizes they could have a large effect on the cumulative surface area $S_{\text{cum}}^{\text{des}}$ as they shift the pore spectrum to higher pore sizes and thereby reduce the calculated area. The exterior surface area can be considerable for particles of small size, for example 0.2μ cubic particles of metahalloysite would have a specific area greater than $10\text{ m}^2/\text{g}$. The particles of the 'natural' TePuke mineral are quite small and must contribute a significant amount of external area. In view of the above considerations it is not unreasonable that the cumulative pore specific

surface areas are smaller than the B.E.T. areas.

4.4.3.c Pore Size Distributions from Water Desorption Data

The clay-water interaction is of much greater interest in the fields of agriculture and clay technology than is that between a non-polar gas, such as nitrogen, and a clay. For this reason, and because the water vapour desorption data was available, it was decided to calculate the pore size distributions for the 'natural' and homoionic samples of TePuke metahalloysites. The parallel plate model was again assumed and a series of calculations performed as outlined in the previous section. Since the distributions were to be simply compared the plate separations were calculated according to equation 21 neglecting the integral term. The resulting distributions are included in figure 47.

One important difficulty encountered in performing distribution calculations using water desorption data, is in the choice of the thickness (t) data to use. The isotherm for water adsorption on non-porous materials, unlike that for nitrogen, is

not universal, the amounts adsorbed depending upon the specific nature of the interaction between water and the surface. A measure of this specific interaction is given by the heat of adsorption, or approximately by the B.E.T C constant. Hagymassy et al (145) provide standard water vapour data for a number of values of the C constant. The most suitable for the present calculations is that for $C \approx 23$ which is closest to the C values calculated for the various homoionic samples 21 to 40 (table 4).

The distributions (figure 47) are all extremely similar, each with a small peak at 20\AA and a larger broad peak centred at about 40\AA . There appears to be little correspondence between the pore distributions measured by water and nitrogen adsorption experiments. The nitrogen molecule is not affected greatly by the surface and nitrogen adsorption should therefore give rise to a meaningful distribution. The water-clay system is considerably more complex however, the polar water molecule undergoing specific interactions both with the surface groups and with exchange cations. The large peak in the distributions derived from water

data could be attributed to two effects. First, it may be due to the loss of water from the clay-water system as the particles are pulled together by the strong surface tension forces of the adsorbate. The surface tension of water at 36.2°C is high (70.2 dynes/cm) compared with that for nitrogen at 78°K of 9 dynes/cm. The small value for nitrogen may indicate that the surface tension forces for nitrogen liquid are too weak to affect the arrangement of clay particles, as does water. Secondly, the water lost may be a component part of the cation hydration water.

The exchange cations in the TePuke mineral do not have a significant effect on the distribution of pores in the mineral. This is indicated by the very small differences between the pore size distributions (figure 47) derived from water-vapour data, for the various homoionic metahalloysites. This is contrary to the findings of Pansevich and Ovcharenko (87) who found quite large differences for different cationic modifications of a metahalloysite. Their curves (figure 54) have a maximum for monovalent ions at $30 - 35\text{\AA}$ and for di- and tri-valent ions at $30 - 35\text{\AA}$.

Table 9 The Effects of Exchange Cations on the Sorption Properties of Halloysite.

Ion	Specific Surface Area m^2/g (87)	Heat of Wetting Q cal/g (87)	Water Monolayer Capacity mM/g (320)	Cation Exchange Capacity $\text{meq}/100\text{g}$ (87)
K	131.0	3.63	0.60	7.4
Na	135.5	3.76	0.60	7.2
H	143.5	3.98	0.61	5.9
Al	143.5	3.98	0.61	5.7
Fe	148.0	4.10	0.63	6.3
Ca	149.0	4.14	0.67	6.4
Mg	150.0	4.15	0.70	7.3

and 50 - 100 \AA . The authors concluded that the cations affect the aggregation of the crystals and the porosity of the aggregates. No such effects occur for the TePuke mineral, the ions having very minor effects only.

Conclusions

The loss of hydroxyl water, upon vacuum outgassing, produces small changes in both pore size distribution and in specific surface area of TePuke metahalloysite. The changes in specific surface area correspond quite closely to the changes in the cumulative pore surface area which is an indication that specific surface area changes are a direct result of alterations in the pore structure. The observed changes are much less significant than might be expected from a 22% loss of constituent mineral volume and a considerable rearrangement and general settling down of the structure must take place in association with dehydroxylation.

The TePuke mineral contains both slit-shaped and wedge-shaped pores and upon dehydroxylation small pores are produced which are mainly in the 30 - 100 \AA size range.

The TePuke mineral contains both slit-shaped and wedge-shaped pores and upon dehydroxylation small pores are produced which are mainly in the 30 - 100^oÅ size range.

Exchange cations do not significantly affect the porous structure of the TePuke mineral as calculated from the water desorption data. The pore size distributions so calculated are quite different from those obtained by analysis of nitrogen desorption data, indicating that different desorption processes operate for the two adsorbates.

4.5 The Adsorption of Water Vapour on Homoionic Metahalloysite

4.5.1 Introduction

The clay-water interaction is of considerable interest in a number of industrial, agricultural and theoretical fields, and much research has been carried out in an attempt, not only to elucidate the effects of the clay mineral surface structure and its associated cations on the extent of

adsorption, but also to characterise the physical state of the adsorbed water.

It has long been accepted (8,302,311, 328) that the regular lattice of oxygen or hydroxyl groups of the clay mineral surface is likely to cause the formation of an extended net of water molecules. Several possible water structures have been postulated (8,311,328) which allow hydrogen bonding between surface groups and the adsorbed water molecules. Much of the reported evidence suggests that the initially adsorbed water is in a physical state quite different from that of normal liquid water. Reviewers (4,68,75,83) disagree however as to the nature and extent of order within the adsorbed layer. Although Martin (75) suggests a two-dimensional liquid-like model for the water layer, most evidence indicates that the initially adsorbed water exists in a quasi-crystalline state (4), the degree of structural order in the water layer decreasing quite rapidly with distance from the surface. The limit to the non-liquid water is variously considered to be at a distance of a few

molecular layers from the surface (4), one to three layers (68) and extending to a considerable distance of the order of 75 - 100Å (83).

The hydroxyl and oxide surfaces of clay minerals are considered to affect the properties of adsorbed water in different ways. Low (83), Grim (4) and Martin (116) believe that the water structure should be less stable on the hydroxyl surface. They reason that the excess electrons in the mineral lattice cause the lone pairs of the oxide oxygens to be more easily distorted and the protons of the hydroxyl groups to be less electropositive. Thus the covalent character of the bond between the water molecule and the oxide oxygen is enhanced and the stability of the water layer adsorbed on this surface increased. The stability of the layer on the hydroxyl is, according to similar reasoning, reduced. Graham (68) and Young (288) include reference to work that shows the hydrogen bonding of various adsorbates on quartz and silica gel occurs mainly at surface silanol groups and implies that the oxygen groups of

such materials are hydrophobic. Results for water adsorption on clay minerals, a bentonite whose surfaces are both oxidic (276) and a kaolinite (45), indicate however that neither type of surface is hydrophobic since for both minerals the water attributable to surface adsorption contributed more than half the total amount adsorbed.

The effect of the exchange cations, associated with the clay mineral, upon the structure and stability of the adsorbed water, generally follows the expected order, the disruptive effect of an ion of given charge being greater the larger its radius. Ions small enough to fit into the hexagonal hole in the water structure (radius 1.36\AA) should enhance the development of structure (311), while larger ions should disrupt the structure. For a given clay mineral, as the size of the exchange cation of a given charge increases, the wettability of its surface (329), the energy of water retention (126) and the amount of water adsorbed (330), all decrease.

A hypothesis which describes the water-vapour-clay mineral interaction and which

agrees with most of the available data is as follows. First, upon exposure of the surface to water, the cations hydrate if they are small enough. The initial water molecules are very strongly held, the energy of adsorption being much greater than that of a hydrogen bond. Hydration of the remaining surface then takes place with the formation of hydrogen bonds, the energy of adsorption decreasing rapidly as the surface coverage θ increases. Finally, after a few monolayers have been completed, the properties of the film become those of normal water.

Prior to the studies of Martin (116, 117) no hysteresis had been observed for the adsorption of water vapour on kaolin minerals. Such systems do however exhibit hysteresis and Martin showed the phenomenon to be best ascribed to ion hydration effects, the nature of the exchange cation determining the size and range of the hysteresis loop and the scanning behaviour observed within the loop. Martin further demonstrated that his results could be explained by an adsorption model which assumes

adsorption occurs at specific sorption sites. The active sites chosen were the exchangeable cations and holes in the surface of the kaolinite crystal at the centres of the hexagons of oxygen or triangles of hydroxyl groups.

4.5.2. Literature Results for the Metahalloysite-Water Vapour System

The reports of studies, which deal with the adsorption of water vapour by metahalloysite (87, 88, 89, 99, 331, 339), suggest that the adsorption properties of the mineral are influenced by the nature of the associated exchangeable cations, and that the observed ionic effects are slight in comparison with the effect of ions on the properties of the expanding minerals (87). The order of a series of ions, in their effect on the total amount of water vapour adsorbed, was found to be $Mg \succ Ca \succ Fe \succ H \succ Al \succ Na \succ K$ (87, 331).

Panasevich and Ovcharenko (87) concluded that cations of the ion-exchange solutions did not penetrate into the interlayer spaces of metahalloysite because insignificant changes in the

Fig. 54

Pore Size Distribution of Metahalloysite Derived from Water Vapour Desorption Data.

after Panasevich and Ovcharenko(87)

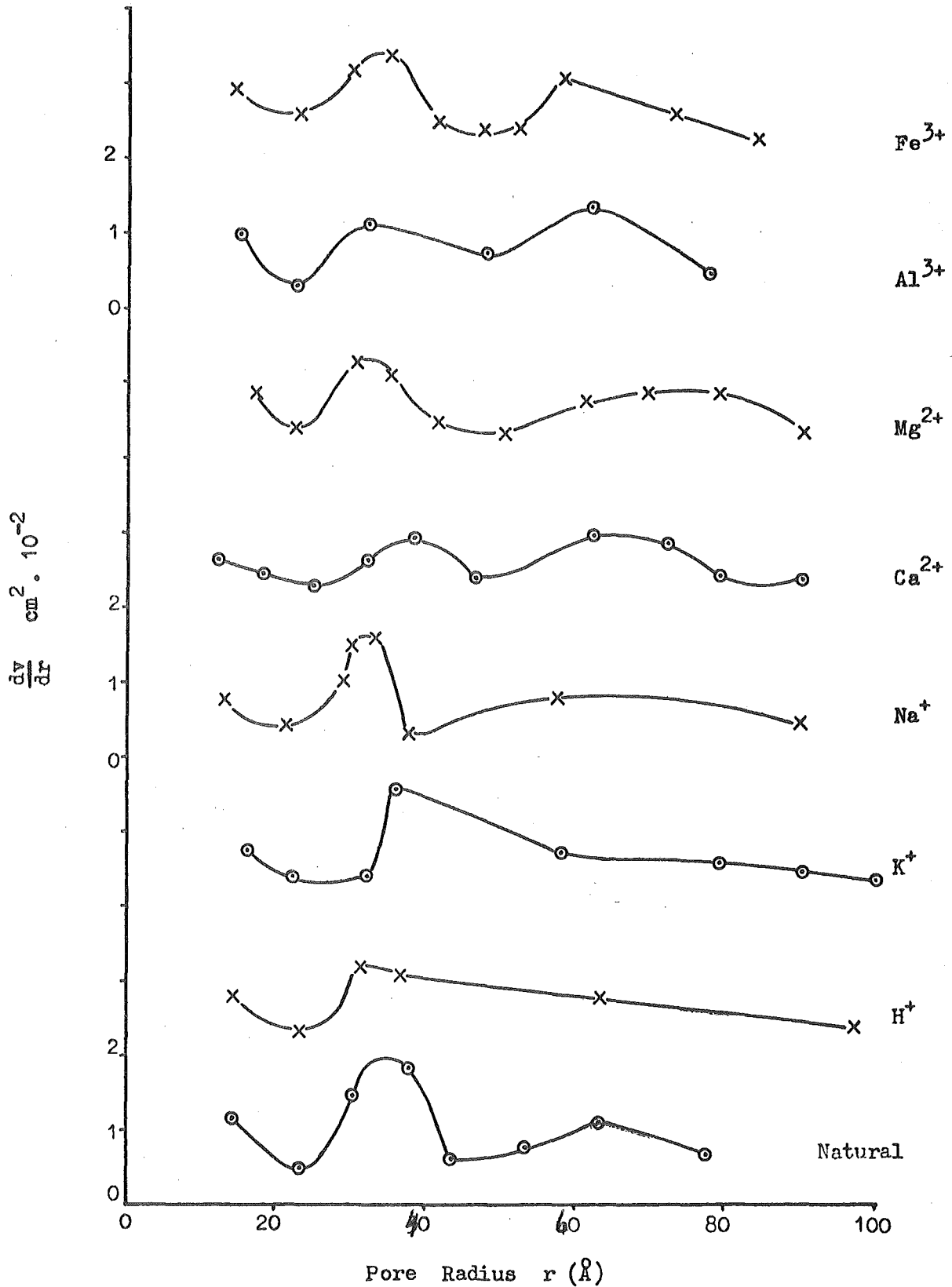


Fig. 55 Relationship of Specific Surface Area (Σ) and Water Monolayer Capacity for Homoionic Metahalloysites.

Data of Panasevich and Ovcharenko (87,88)

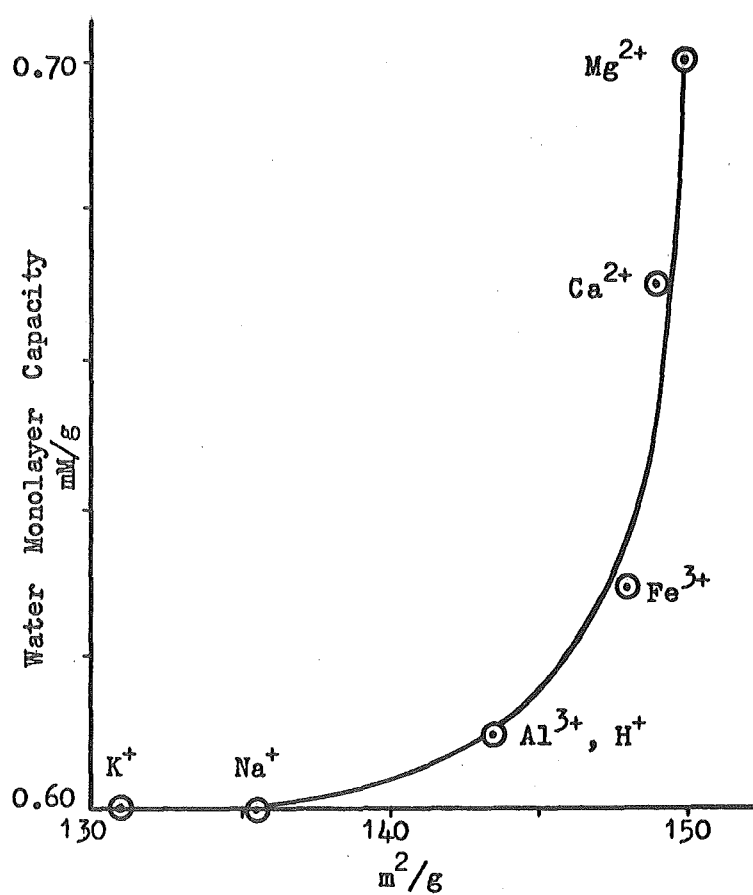


Fig. 56 Water Vapour Adsorption Isotherm
for Lithium-Metahalloysite

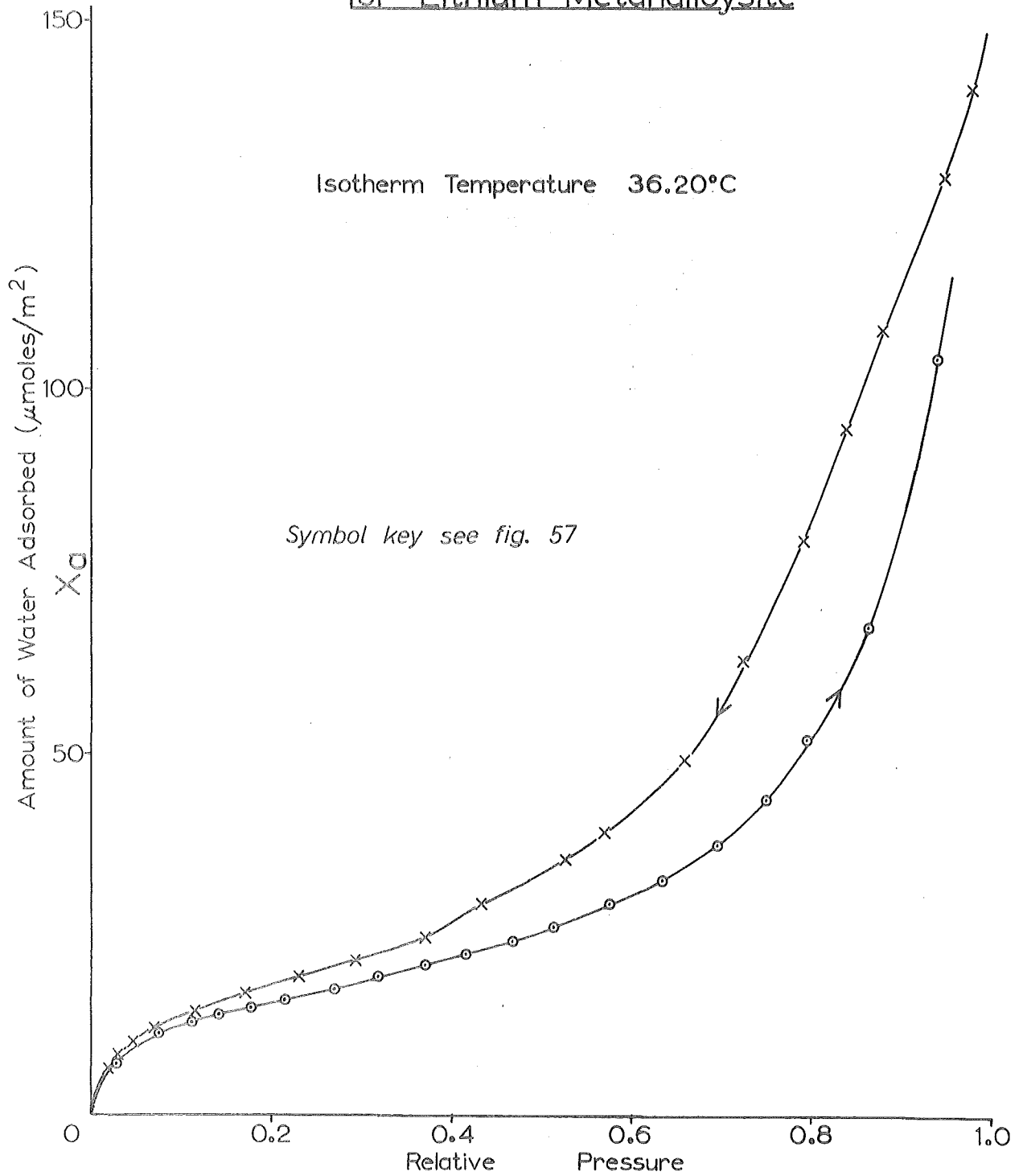


Fig. 57 Water Vapour Adsorption Isotherm for Sodium-Metahalloysite

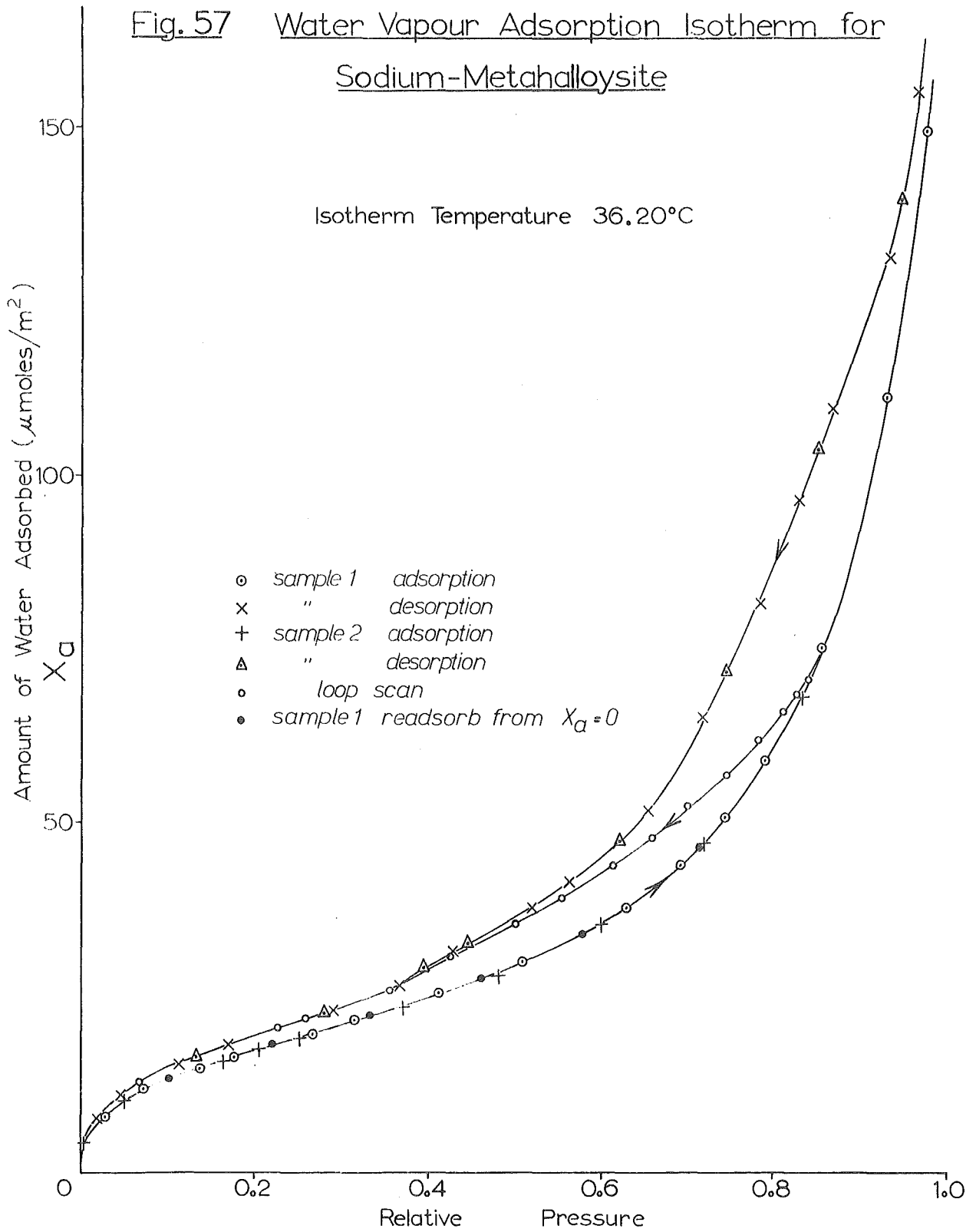


Fig. 58 Water Vapour Adsorption Isotherm
for Potassium-Metahalloysite

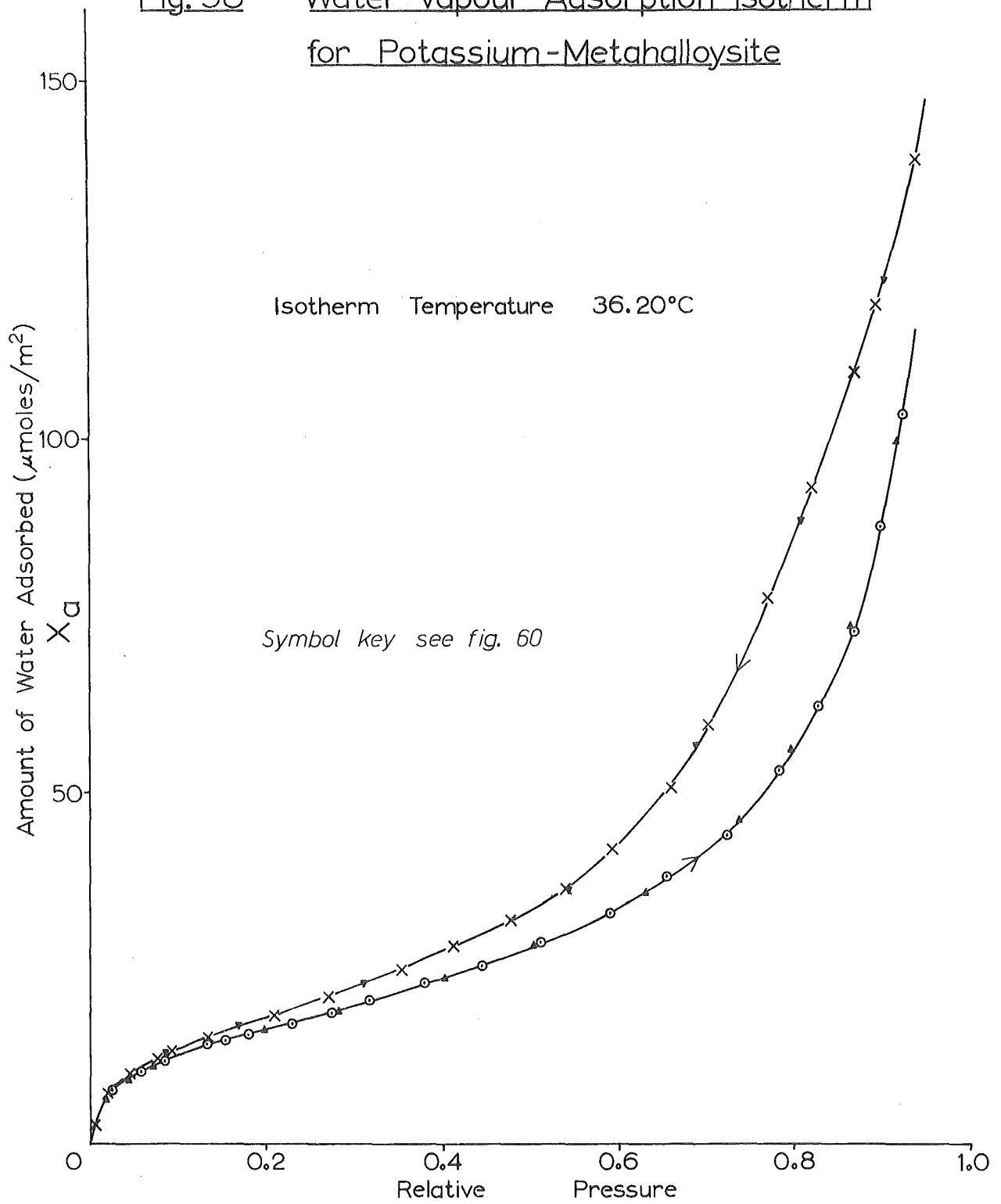


Fig. 59 Water Vapour Adsorption Isotherm
for Rubidium-Metahalloysite

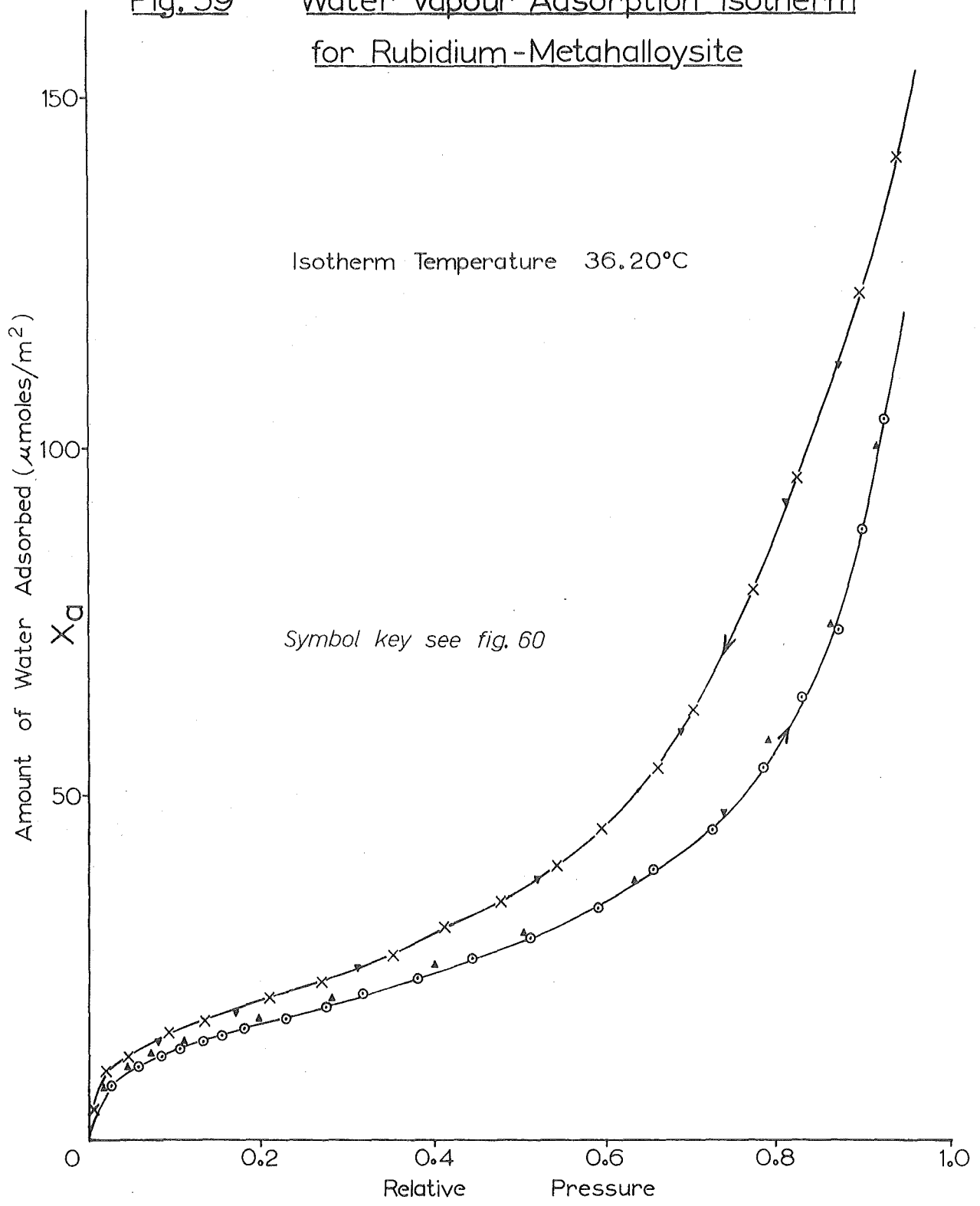


Fig. 60 Water Vapour Adsorption Isotherm
for Cesium-Metahalloysite

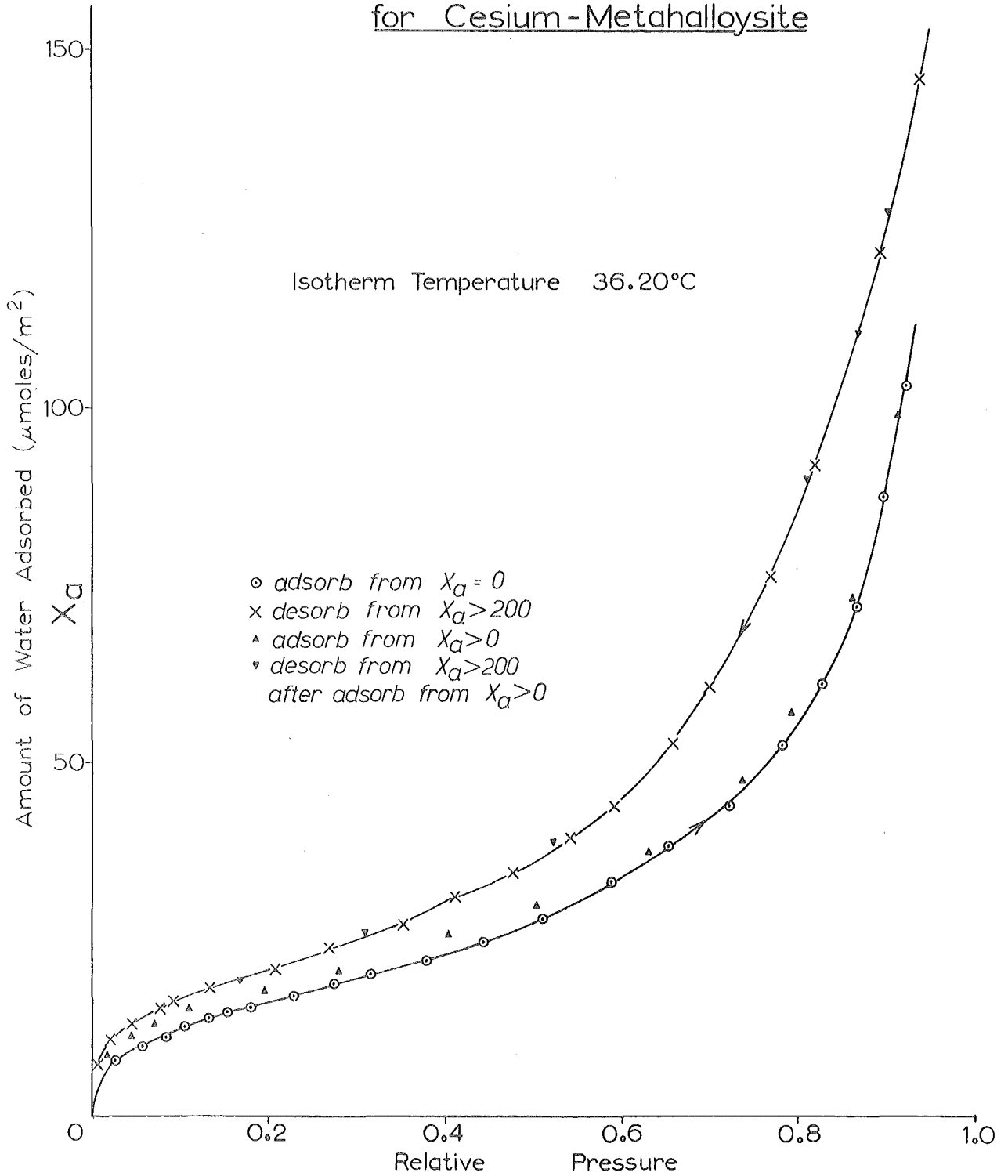


Fig. 61 Water Vapour Adsorption Isotherm for Magnesium-Metahalloysite

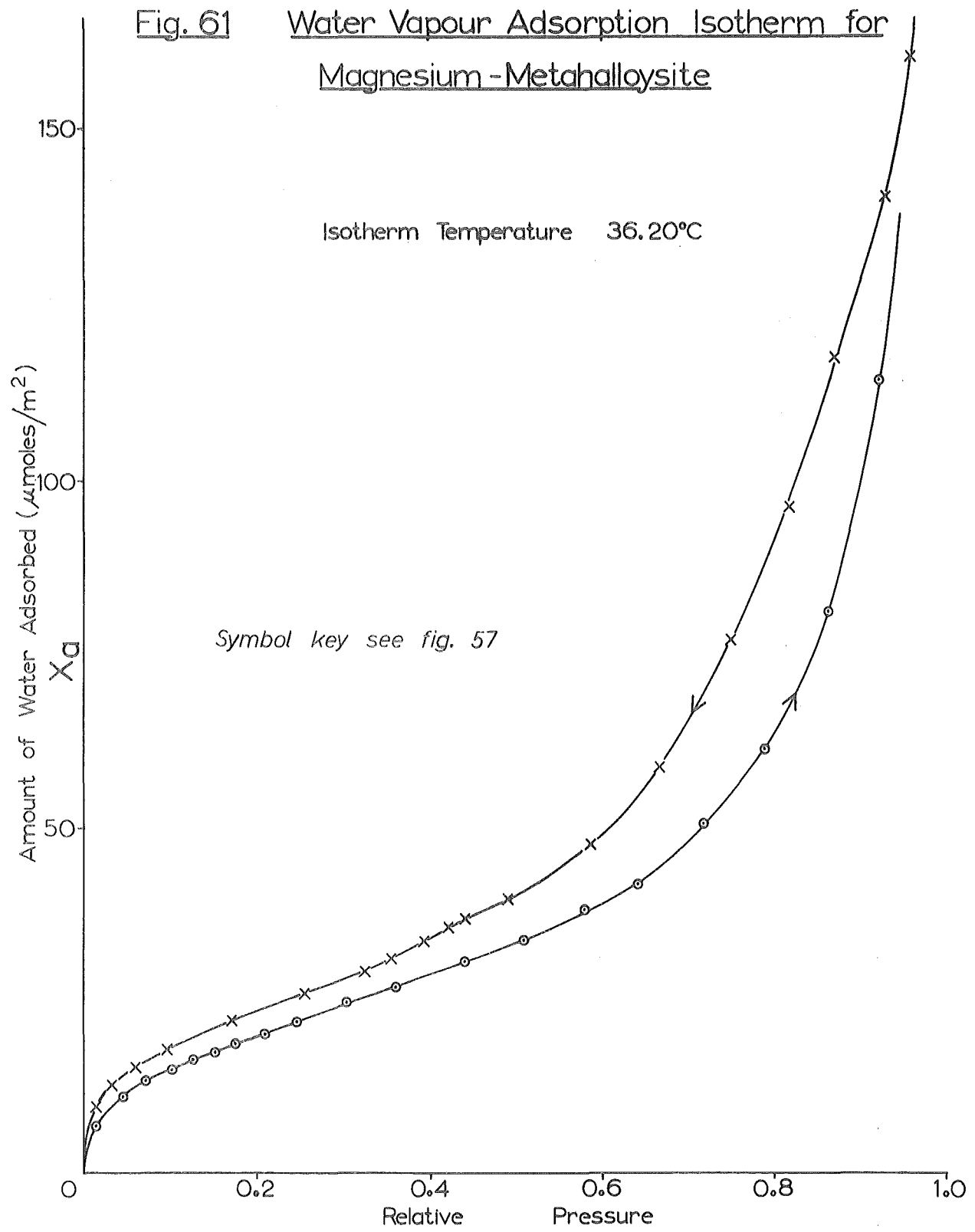


Fig. 62 Water Vapour Adsorption Isotherm for Calcium - Metahalloysite

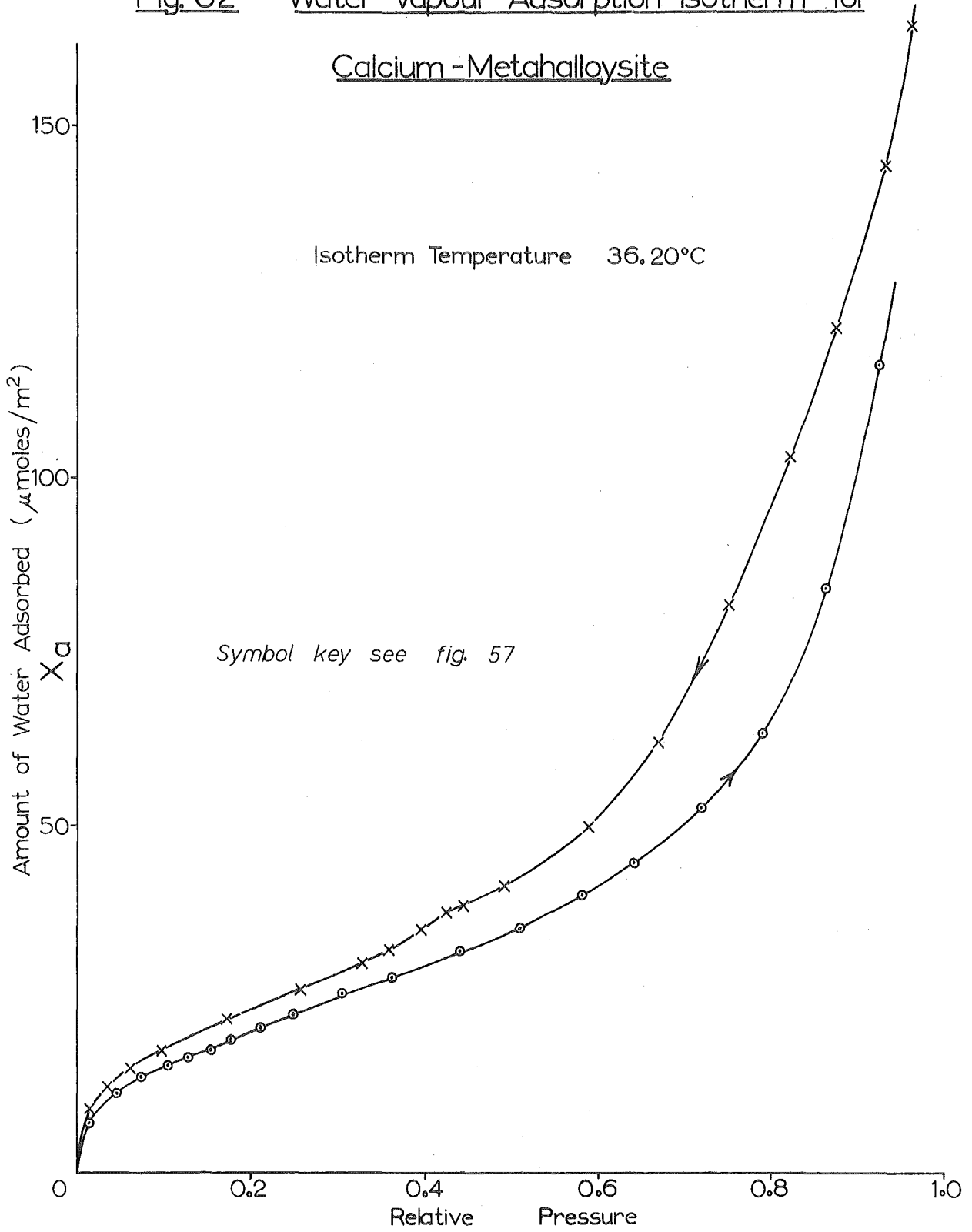
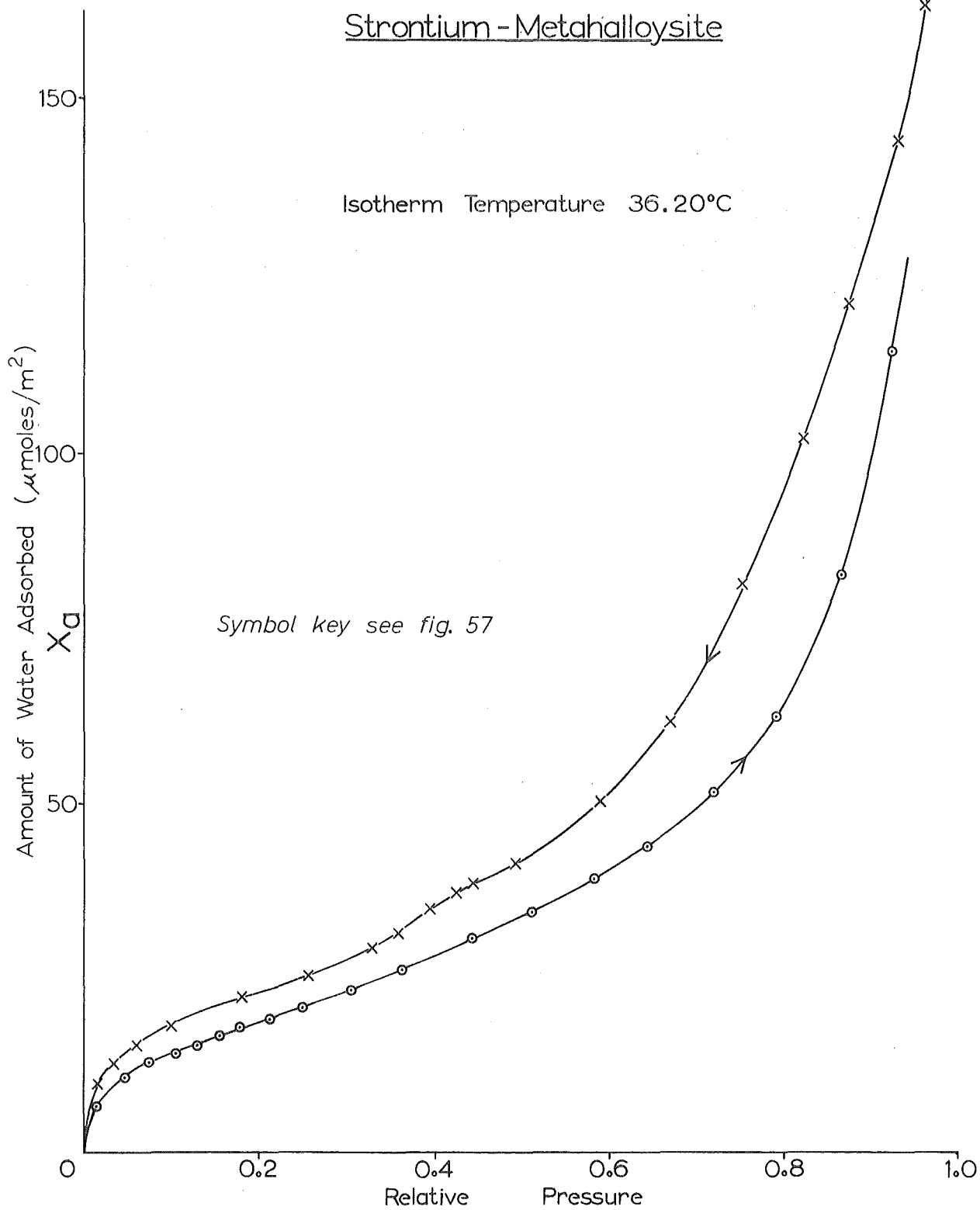


Fig. 63 Water Vapour Adsorption Isotherm for
Strontium - Metahalloysite



X-ray basal spacing took place upon cation-exchange. The exchangeable cations did however influence the water monolayer capacities (331), the heats of wetting (87) and the specific surface area of the metahalloysite (87). The results of these studies are summarized in table 9.

The order of the ions in their effect on the specific surface area from nitrogen adsorption is the same as the order for their effect on the water monolayer capacity of metahalloysite (table 9). If an alteration in specific surface area was the only result upon a change in exchange cation, a plot of water monolayer capacity X_m versus specific surface area Σ , for the data of table 9, would be linear. The curve (figure 55) is not linear and indicates that some other property of the ion-clay complex has a water-specific effect.

The specific surface areas and water monolayer capacities are identical for the Al^{3+} and H^+ modifications which is expected if the hydrogen-clay spontaneously converts into an aluminium-clay as was found to occur for other clay minerals (109-111).

4.5.3. Water- Vapour Adsorption on Homoionic
TePuke Metahalloysite

Detailed water-vapour adsorption isotherms were determined gravimetrically for various homoionic samples of TePuke (1-20 μ e.s.d) metahalloysite. The exchange positions of each sample were saturated with one of the cations Li^+ , Na^+ , K^+ , Rb^+ , Cs^+ , Mg^{2+} , Ca^{2+} or Sr^{2+} . The isotherms (figures 56 to 63) are plotted in terms of micromoles of water adsorbed per square metre of surface, in order to eliminate, from the present considerations, the effects of small changes in specific surface area which result upon cation exchange (table 4).

The complete isotherms are considered to be composed of a type II adsorption isotherm (section 4.2.a) and a narrow hysteresis loop of type B (section 4.2.b) which ends in a small discontinuity at a relative pressure of about 0.4. The lower part of the hysteresis loop is considerably modified by the presence of a narrow but persistent hysteresis 'tail' which extends down to very low pressures. There is a marked variation in the range and width

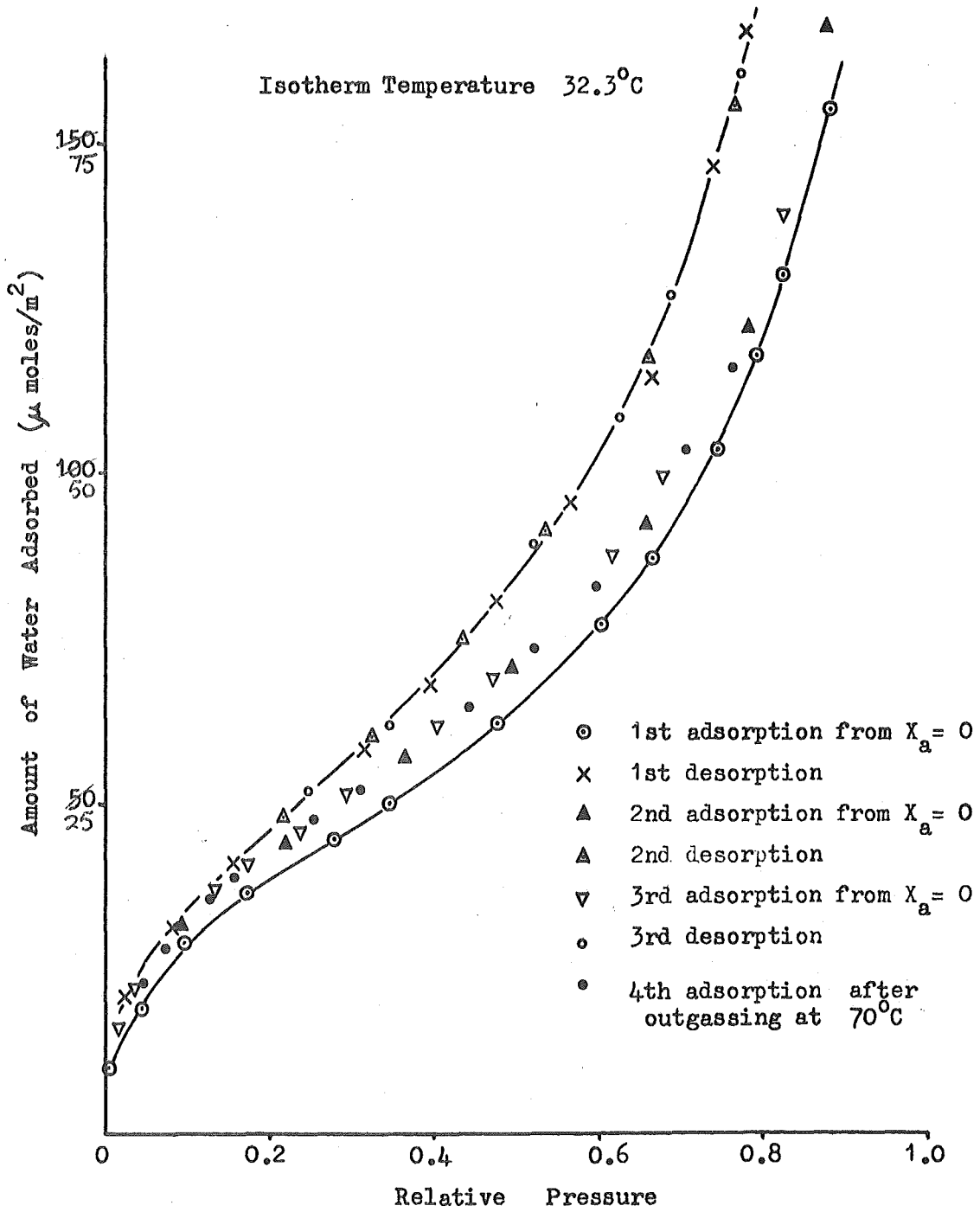
of the 'tail' region for the different homoionic samples, the hysteresis loops for some, notably Rb^+ , Cs^+ , Mg^{2+} , Ca^{2+} and Sr^{2+} , not closing until the zero pressure condition was closely approached.

The small discontinuity in the desorption isotherms for the homoionic samples of the present study was not apparent in other water-vapour isotherms reported for metahalloysite (73, 87). In the first isotherms obtained the small drop was not defined due to the few data points recorded for the intermediate region of the desorption curve. The nitrogen and argon isotherms for this clay mineral sample showed sharp drops at intermediate pressures along the desorption curve, indicating a well developed porosity (section 4.1.1), and it was thought likely that the water-vapour isotherm should contain a similar feature. Application of the Kelvin equation (equation 9), using the pore size calculated from the position of the drop in the nitrogen desorption curve, gave a predicted drop position of $P/P_0 \approx 0.4$ for the water-vapour case. When, in later experiments, more data

points were obtained around this relative pressure a small discontinuity did indeed become apparent. Adsorption to desorption scanning curves, begun at $P/P_0 > 0.8$ for Na^+ and 'natural' metahalloysites (figures 57 and 33 respectively), track across the hysteresis loop to the small drop, as did similar curves for nitrogen adsorption (figures 35 and 40). This indicates that the discontinuity is most probably the result of capillary condensation. The small drop would be more marked were it not masked by the low pressure hysteresis loop evident in the water-vapour isotherms.

Brunauer (147) recognizes two types of adsorption hysteresis, reversible or irreversible. Hysteresis is reversible if, on repetition of the experiment, the isotherm is accurately reproduced and irreversible if a different curve results. The initial hysteresis loop, for the first isotherm determined on a Rb^+ metahalloysite, was irreversible (figure 64). The first adsorption curve proved to be quite different from three succeeding adsorption traces. The final adsorption curve was obtained after

Fig. 64. Water Vapour Sorption Isotherm for Rubidium-Metahalloysite



rigorous outgassing at elevated temperatures (70°C). All of the desorption curves coincided, as did all of the adsorption curves except the first.

Reversible hysteresis after the first full cycle is an indication that the first adsorption includes contributions from irreversible processes such as particle rearrangement. All succeeding complete isotherms were recorded after first subjecting the clay sample concerned to three wetting and drying cycles which should, to a large extent, eliminate particle orientation effects. Other cases have been quoted in which second and subsequent adsorption curves have coincided while being quite different from the first adsorption, Rao (332) finding reproducible hysteresis for up to thirty cycles after the first irreversible one.

Hysteresis in the water-vapour isotherms for the homoionic metahalloysites of the present study is clearly caused by two or more effects. That part of the hysteresis loop at relative pressure greater than 0.4 (the position of the small discontinuity in the desorption curve) has been ascribed above to the

mechanism of capillary condensation. The low pressure hysteresis or 'tail' region was discussed in section 4.1.2 where it was concluded that intercalation probably does not occur for metahalloysite and that the concept of capillary condensation could not explain the existence of hysteresis down to very low pressures. Martin (116) suggested a lower limit of $P/P_0 = 0.17$ for the latter mechanism, this relative pressure corresponding to a pore the diameter of two water molecules. A curved liquid meniscus consisting of two molecules can hardly have physical meaning and therefore the limit is likely to be much higher than 0.17. The 'tail' region of the hysteresis loop, for the various homoionic samples of TePuke metahalloysite, is considerably modified by the nature of the exchange cation. This leads to the conclusion that the hysteresis in this region is directly dependent upon the cation. The same conclusion was reached by Martin (116) for water vapour sorption on kaolinite and this author attributed the hysteresis to ion hydration.

Hysteresis in surface phenomena will occur, according to Everett (342), whenever there are available to adsorbate molecules, at least two different states, the transition between the states being irreversible. A mechanism by which cations could give rise to hysteresis has been proposed by Sposito (291) and Sposito and Babcock (290). If hysteresis is due to cation hydration, the hydration water cannot continue to be taken from the vapour phase, as the amount adsorbed increases, because transfer from the vapour is prevented by multilayer formation. The excess irreversibly adsorbed water is considered to be taken from the surface water by an irreversible transition:

mineral surface water \Rightarrow cation hydration water

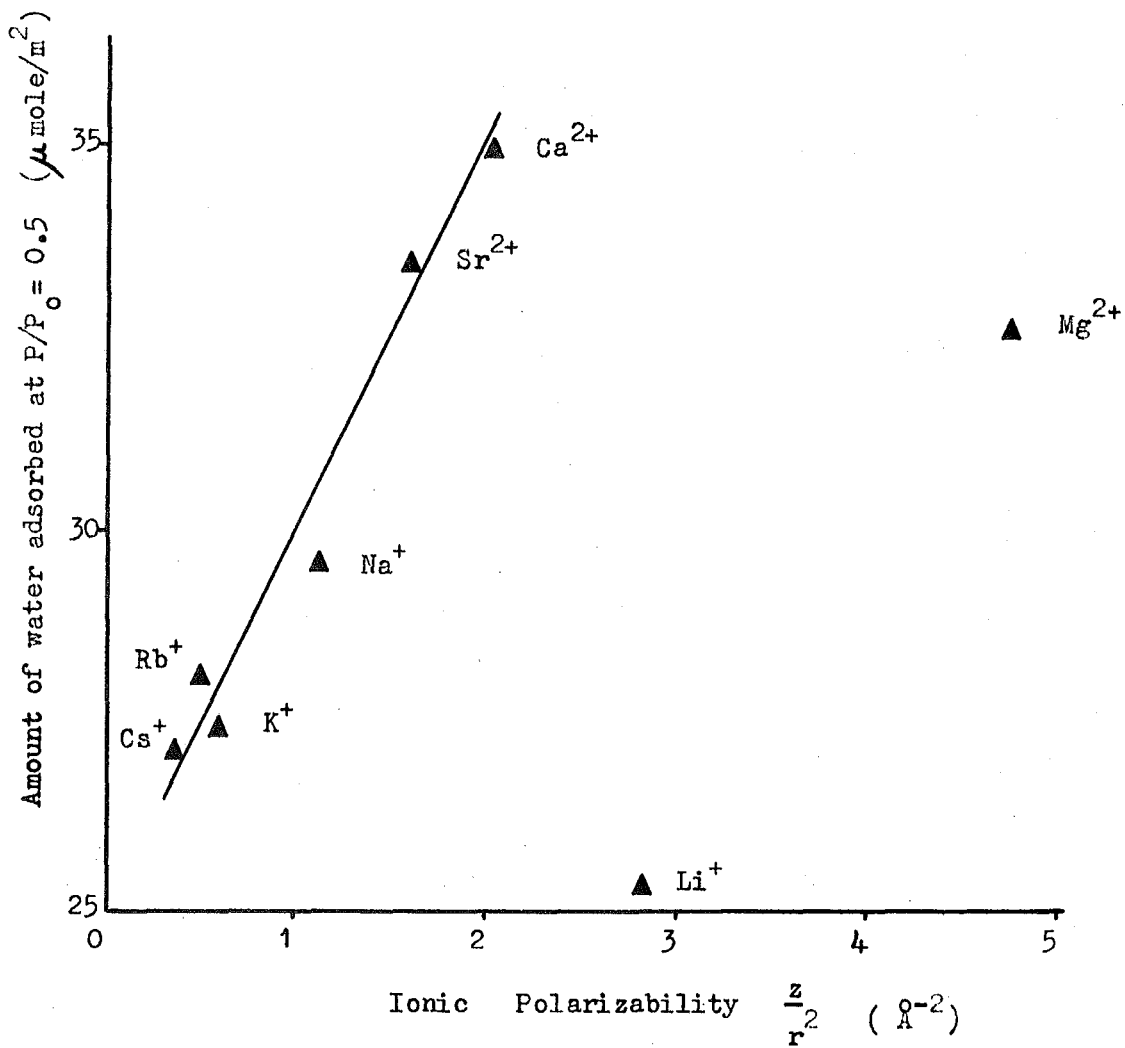
This hydration water, the authors suggest, does not return to its original state at the same relative pressure at which it was adsorbed, and therefore gives rise to hysteresis. An alternative explanation is that the cations form active sites, or activate the surface, for the initial sorption of water droplets which merge, as sorption proceeds, until a continuous

water film is formed. Desorption occurs by evaporation from the continuous film and because the vapour pressure above a small droplet is higher than over a planar liquid surface, a hysteresis loop should result (333).

A clear indication of the way in which the cations affect the adsorption properties of TePuke metahalloysite is given by a plot (figure 65) of the amount of water adsorbed at a particular relative pressure, chosen in this case to be 0.50, versus the polarizability of the exchange cation $\frac{Z}{r^2}$, where Z is the ionic charge and r the ionic radius. A reasonably linear relation is apparent for cations, Na⁺, Rb⁺, K⁺, Ca²⁺ and Sr²⁺ while the Li⁺ and Mg²⁺ data give points which are considerably off the line. It is noted that the amount of water adsorbed, for an hypothetical ion of zero ionic polarization capacity, amounted to a large fraction of that for the maximum polarization capacity. The author concludes, as did Rios and Vivaldi from similar observations for divalent and monovalent cations on kaolinite and bentonite (330), that both the

Fig. 65

Plot of Ionic Polarizability Versus The Amount of
Water Vapour Adsorbed at $P/P_0 = 0.5$ for the Homoionic
Te Puke Metahalloysites



exchangeable cations and the clay mineral surface affect the water vapour adsorption of metahalloysite.

The anomalous position of the lithium-clay in figure 65 is not unexpected, many other workers (45,116,334-337) having reported lower amounts adsorbed for various lithium-clays than expected for a small highly charged ion. This anomalous effect of the lithium ion is generally ascribed (83) to steric hindrance to hydration of the ion, which, because of its small ionic radius (0.60\AA), can fit into holes between the surface groups of the mineral lattice. Magnesium has a small ionic radius also (0.65\AA) and its anomalous position in figure 65 suggests that ions of this type also inhabit small holes in the mineral lattice.

There is no direct relationship between the nitrogen BET specific surface area and the water monolayer capacity determined for the various homoionic modifications of TePuke metahalloysites (table 4). This indicates that either the water molecule has different apparent cross-sectional areas on the surfaces of the various samples (table 4), or,

as has already been suggested, a considerable amount of water is associated directly with the cations. In any event it would appear that water vapour adsorption should not be used for the determination of the specific surface areas of metahalloysites.

4.5.4 Model for the Adsorption of Water Vapour on Metahalloysite

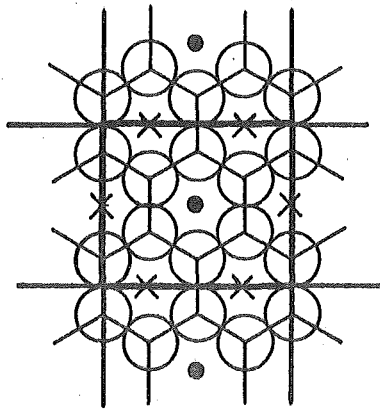
Many of the assumptions made in postulating an adsorption model for the metahalloysite-water vapour system are the same as those proposed and used by Martin (116) for the adsorption of water on kaolinite. This approach seems reasonable in view of the degree of similarity between the two mineral groups (sections 1.1 - 1.11).

Sorption is regarded as proceeding in stages, initial adsorption taking place at specific sites on the mineral surface. The total adsorption process can be conveniently divided into three component interactions: exchangeable cation hydration, oxygen surface adsorption and hydroxyl surface adsorption. All of the active adsorption sites are believed to be associated directly or indirectly

Fig. 66

Unit Sorption Cells Postulated for the Adsorption
of Water Vapour on Clay Mineral Surfaces.

(a) Kaolinite (Martin(116))



— outline of sorption unit cell

● vacant sites

X exchangeable ion sites

○ surface oxygens

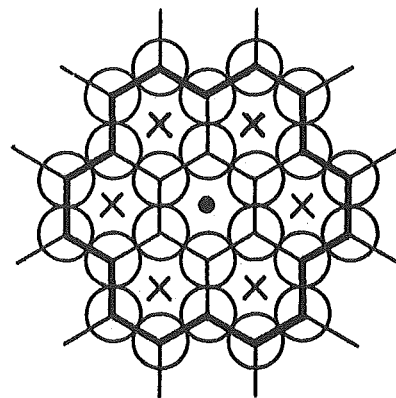
(b) Metahalloysite (Present Study)

— outline of sorption cell

● exchangeable ion sites

X activated adsorption sites

○ surface oxygens



with the exchangeable cations which, it is assumed are evenly distributed over the entire metahalloysite surface.

Even distribution of exchange sites is contrary to the general idea that the exchange cations reside at the positions of broken bonds on the crystal edges (section 1.13.b). Considerable evidence has also been reported however which indicates that isomorphous replacement is important in kaolins (82,93,119) and that charge distribution is more uniform than just residing at the edges (127).

Edge area may contribute significantly to the specific surface area of metahalloysite. This portion of the mineral surface is not however left out of consideration because it is reasonable to assume that the edges are saturated with local arrays of oxygen or hydroxyl groups, as a result of broken bonds interacting with water molecules, such that the number of adsorption sites per unit area is approximately the same as on the basal plane surfaces.

Each exchange cation is considered to have associated with it six active adsorption sites.

each of which in turn is capable of adsorbing three water molecules. The active sites are most probably situated at the holes in the mineral surface in near proximity to the site of the adsorbed cation. The sorption cell (figure 66b), consisting of one exchange cation and its associated active sites, is therefore similar to that (figure 66a) proposed by Martin (116) for the kaolinite case. The major difference is that the cations are separated by greater distances on the surface of the metahalloysite, and the individual sorption cells are therefore largely separate and do not overlap as they do for kaolinite.

The charge density of the metahalloysite surface is calculated from the cation exchange capacity value of 4.0 meq/100 gm. (section 3.4) and the nitrogen specific surface area of 35.6 m²/g, assuming a uniform distribution of exchange cations over the surface. The resulting charge density of one ion / 150Å² of surface, indicates that there is approximately one exchange cation for every three unit cells of crystal surface,

the area of a unit cell being 45.5\AA^2 (116).

Both the hydroxylic and oxidic surfaces of the present mineral are considered to be hydrophilic but the assumption is made that adsorption is greater on the oxygen surface. In presenting a microscopic theory of the kaolinite-water vapour system, Sposito (291) and Sposito and Babcock (290) indicated that the ratio of oxide surface water to hydroxyl surface water should be 2 : 1.

The adsorption process is considered to occur in a stepwise manner although it ^b pointed out that the various stages are likely to overlap to a certain degree.

Stage 1 Three water molecules are adsorbed, two per active adsorption site on the oxygen surface, one per site on the hydroxyl surface.

As the cation exchange capacity for the metahalloysite is 4.0 meq / 100gm and there are six active sites per cation, the amount of water adsorbed at the completion of this step is 6.48 mg water/g clay.

Stage 2 Adsorb three molecules at

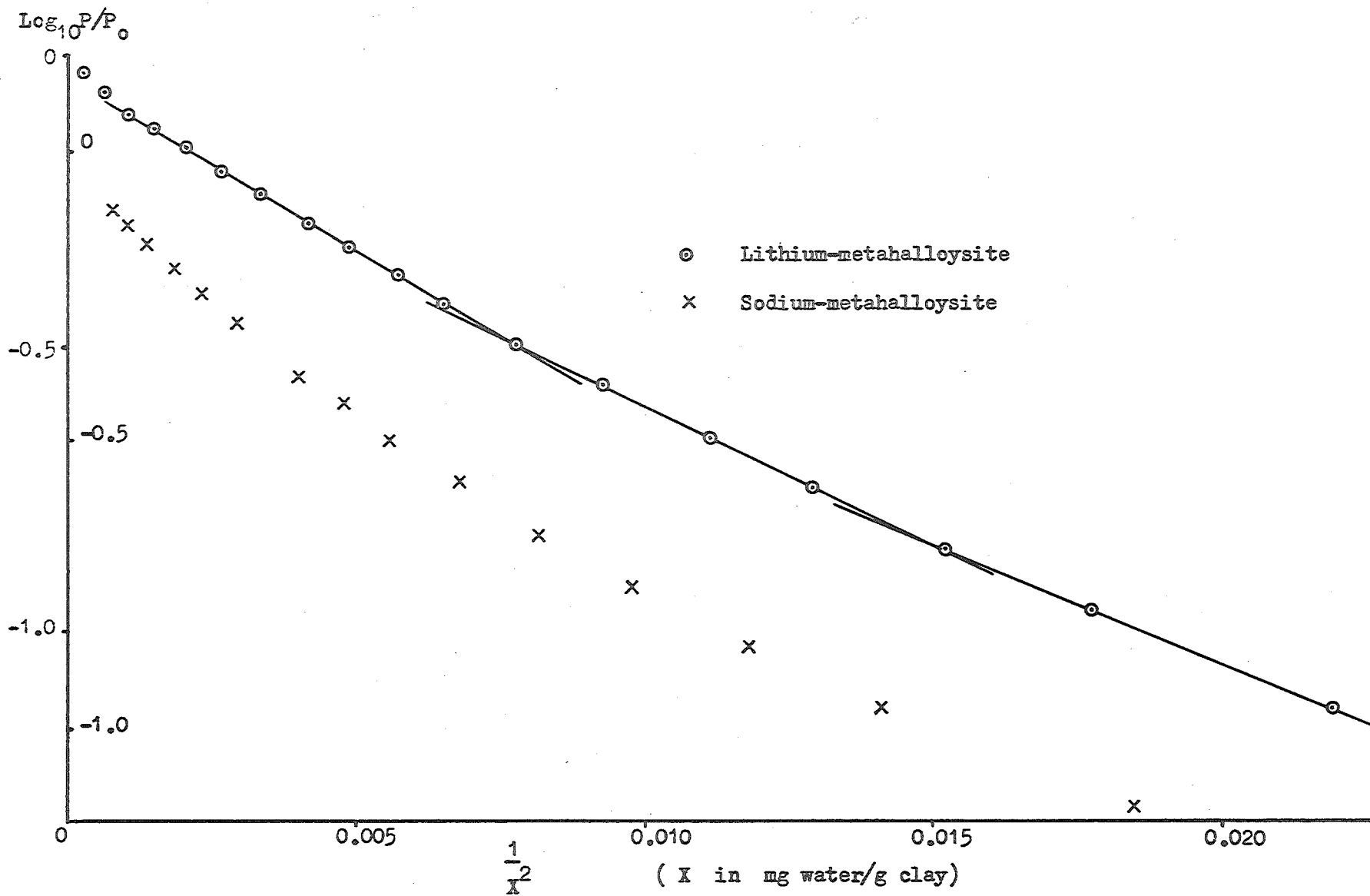
every exchangeable ion site. The amount adsorbed during this step is 2.16 mg water / g clay.

Stage 3 Adsorb sufficient water to saturate all of the available active sites. Each site finally has a triad of water molecules. A further 6.48 mg water/g clay is thus adsorbed at the completion of stage 3.

In order to test the applicability of this adsorption model, Jura-Harkins plots (graphs of the reciprocal of the amount adsorbed squared versus the logarithm of the relative pressure) were constructed (figures 67 to 70) for the water vapour adsorption data obtained for the various homoionic metahalloysites. Most of these plots show two distinct slope changes which, according to Jura and Harkins (199), signify phase changes in the adsorbed film. In the present context the alterations in slope are thought to correspond to the completion of various stages of the adsorption process. Reasonable agreement between predicted points of slope change and the experimental points observed in Jura-Harkins plots would be an indication of the acceptability of

Fig. 67

Jura-Harkins' Plots for Water Vapour Adsorption on Homionic Te Puke Metahalloysites



$\text{Log}_{10} P/P_0$

Fig. 68

Jura-Harkins' Plots for Water Vapour Adsorption on Homionic Te Puke Metahalloysites

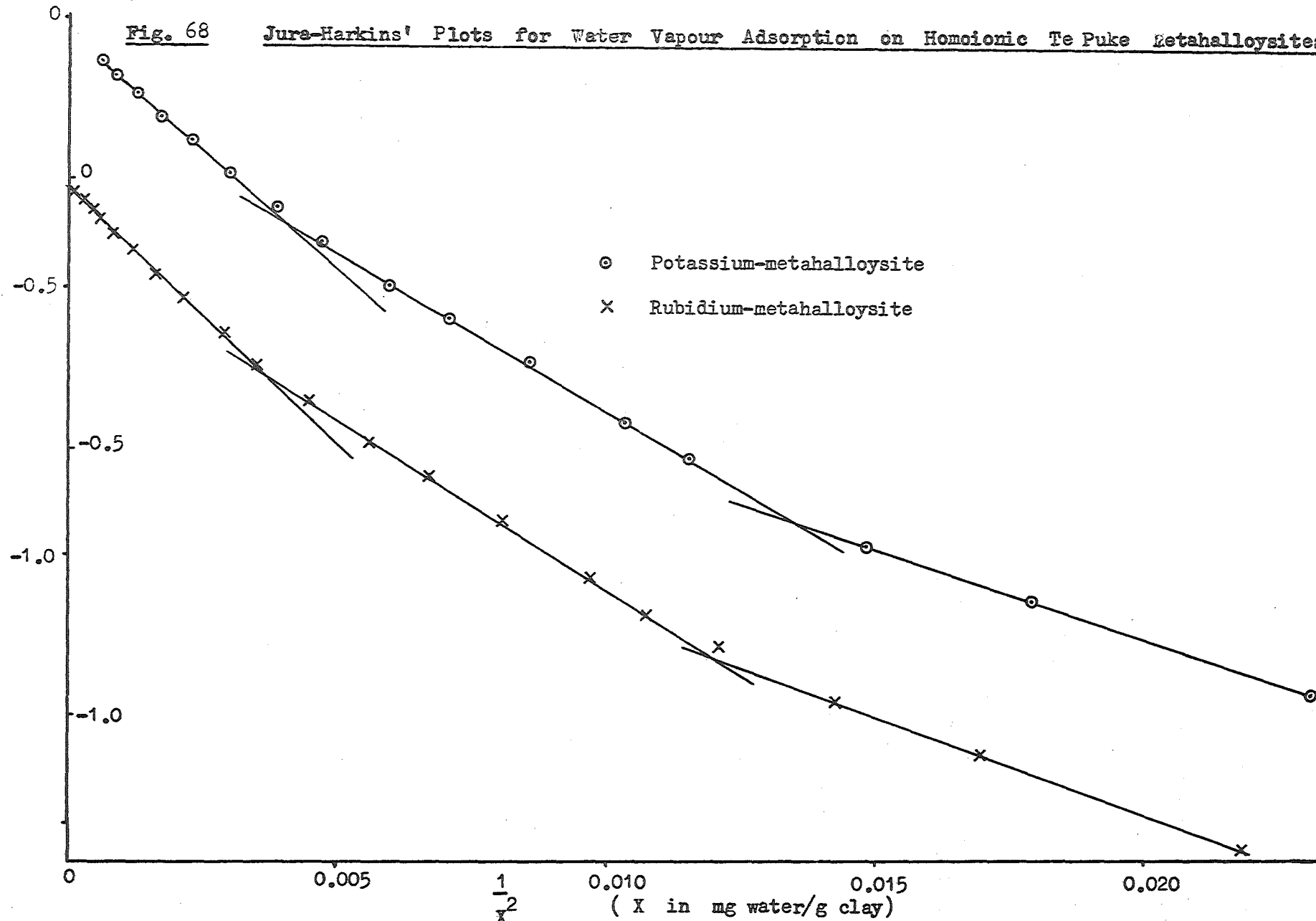


Fig. 69 Jura-Harkins' Plots for Water Vapour Adsorption on Homoionic Te Puke Metahalloysites

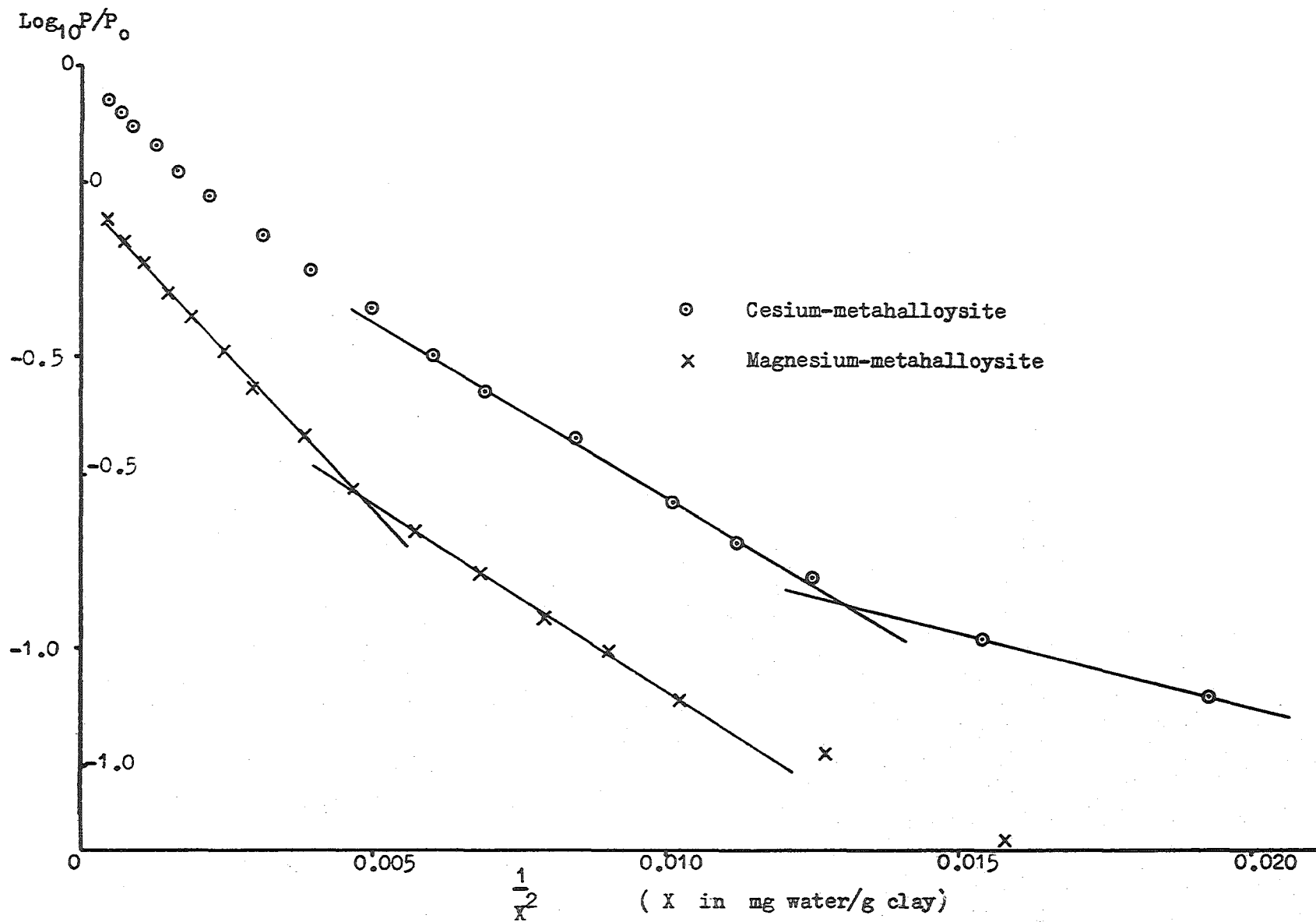
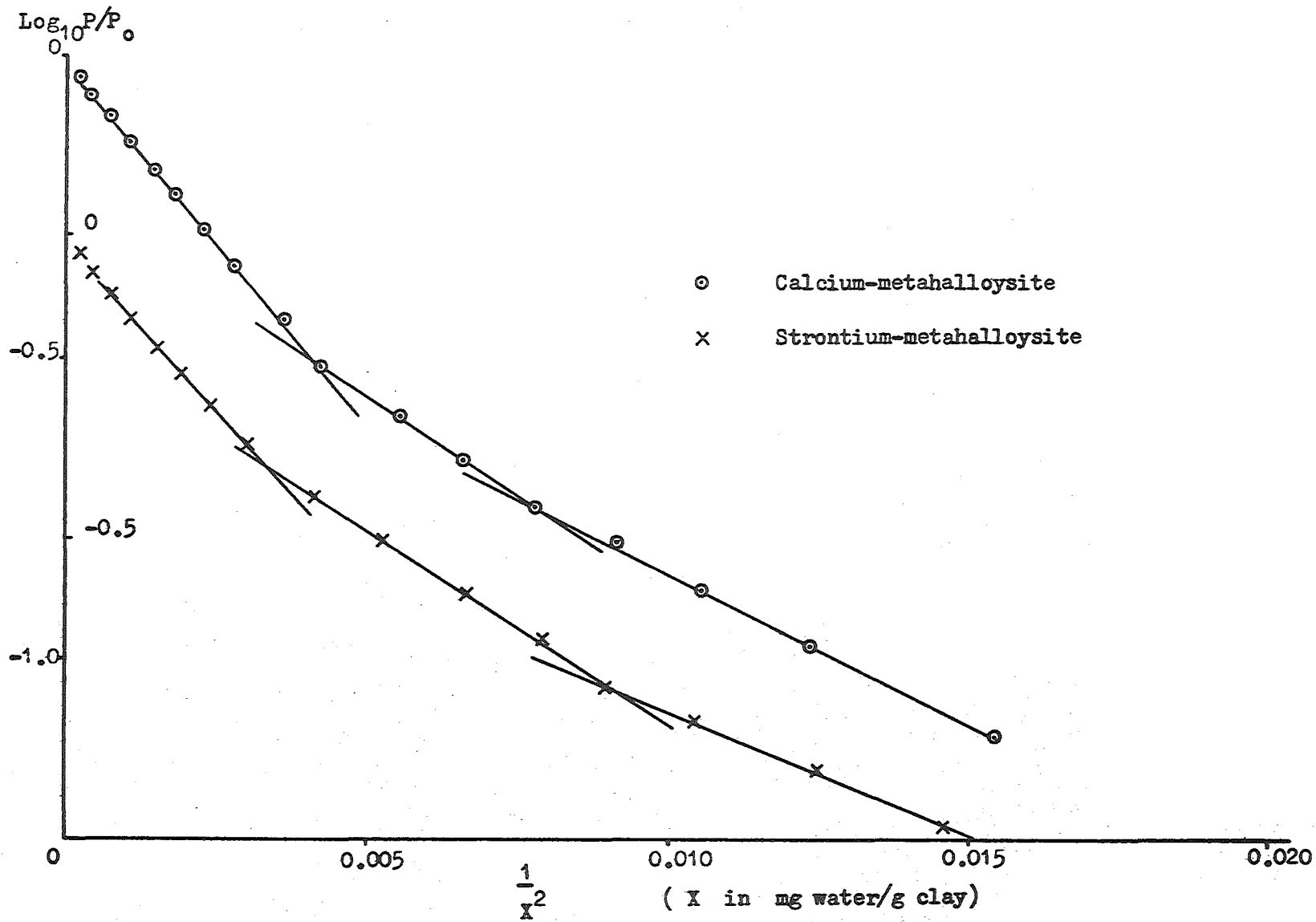


Fig. 70 Jura-Harkins' Plots for Water Vapour Adsorption on Homionic Te Puke Metahalloysites



the proposed model. Good agreement in such a test was obtained by Martin (116) for his model of the water vapour adsorption process on kaolinite.

A further effect which must be taken into account, to enable the prediction of amounts adsorbed at various relative pressures, is ion hydration. First, the generally accepted assumption (45,115,116,343) is made that the Li^+ ion is not hydrated at low relative pressures found to be below $P/P_0 = 0.8$ for kaolinite (116). Adsorption on the lithium-clay is thus thought to represent free surface hydration. The difference between the adsorption curve for the Li^+ clay and the adsorption curve for any other cation modification is ascribed entirely to ion hydration. For a cation exchange capacity of 0.04 meq/g clay, a difference of $1.2 \mu\text{moles/m}^2$ (or 0.72 mg $\text{H}_2\text{O/g}$ clay) corresponds to one molecule of ion hydration water. The number of water molecules per cation is calculated for the relative pressure at which a slope change is observed in the Jura-Harkins plot. The number, if fractional, is taken to the nearest whole number for prediction purposes.

Table 10. Experimental and Predicted Values of Jura-Harkins
'Phase' Changes

Cation	P/P ₀ [*]	Amount Adsorbed at 'Phase' change.		P/P ₀ [*]	Amount Adsorbed at 'Phase' Change	
		mg/g ⁺			mg/g ⁺	
		Predicted	Experimental		Predicted	Experimental
Li	0.316	10.8	11.3	0.174	8.6	8.8
Na		indistinct			indistinct	
K	0.403	15.8	15.3	0.115	8.6	8.5
Rb	0.432	16.6	16.6	0.124	8.6	9.0
Cs		indistinct		0.125	8.6	8.7
Mg	0.306	14.4	14.9		indistinct	
Ca	0.313	15.1	15.8	0.172	11.5	11.3
Sr	0.419	18.0	17.7	0.175	10.1	10.4

*Relative pressure at which slope changes occur in the respective Jura-Harkins plot

+ mg. water/g clay

A full tabulation of the method of predicting the amounts adsorbed according to the postulated model is included as Appendix II and the pertinent data is accumulated in table 10.

For all of the monovalent cationic modifications except sodium, there is, in the respective Jura-Harkins plots (figures 67 to 69), a distinct slope change at an amount adsorbed (x) in the range 8.5 to 9.0 mg H₂O/g clay. This closely corresponds to the amount adsorbed at the completion of the first two stages of the adsorption model, at which point 8.64 mg H₂O/g clay should be adsorbed. These slope changes occur at a relative pressure around 0.12 and the monovalent cations are apparently not hydrated at this pressure, their respective adsorption curves following closely that of the lithium-clay.

The Jura-Harkins plots for Ca²⁺ and Sr²⁺ modifications (figure 70) have two distinct points of slope alteration. The lower relative pressure 'phase' change occurs for these ions at $P/P_0 = 0.172$ and 0.175 respectively and the amounts

adsorbed are close to those predicted at the completion of stages 1 and 2, with allowance for ion hydration.

Further 'phase' changes are indicated, for Li^+ , Mg^{2+} and Ca^{2+} clays, at relative pressures 0.316, 0.306 and 0.303 respectively. The amounts adsorbed at these pressures correspond to the addition of one water molecule per active hydroxyl site after the completion of stages 1 and 2, and ion hydration water for four molecules per cation for Mg^{2+} and Ca^{2+} . The final arrangement of water molecules may be the open structure proposed by Hendricks and Jefferson (8) (figure 2), their molecular orientation requiring four molecules per unit cell which is equal to the two molecules per active site of the present model. Only small highly charged ions appear to stabilise this particular molecular arrangement, none of the 'phase' changes for the large ions K^+ , Rb^+ or Sr^{2+} being predicted by a distribution of two water molecules per adsorption site. This is consistent with the fact that larger ions are believed to have a disruptive

effect on the water structure (344). The 'phase' changes for the larger cations, which occur at $P/P_0 = 0.403$ for K^+ , 0.432 for Rb^+ and 0.419 for Sr^{2+} , are adequately predicted by the adsorption of a triad of water molecules on every active site, plus cation hydration water. It is thus observed that a 'phase' change takes place at an amount adsorbed corresponding to the completion of the three stages of the adsorption model. A triad of molecules per adsorption site is equal to six per unit cell and is, according to Grim (4, p239) sufficient to give closest packing of the adsorbed molecules.

The fact that the adsorption values for the Li^+ and Mg^{2+} modifications at $P/P_0 = 0.5$ are lower than expected from their respective polarizabilities (figure 65), was explained above as due to the small size of the ions. An alternative explanation may be found in a consideration of the difference between the ion hydration energy U and the specific ionic adsorption energy A , the latter being the energy of interaction between ion and clay lattice. An approximate value of A can be determined by the use

of equation making the

$$E = \frac{\frac{1}{2} e^2 z^2}{r} \quad 25$$

e - electronic charge

r - distance between charges

z - ionic valency

E - the work necessary to bring charges from an infinite separation to a distance r apart.

assumption that the final charge separation is twice the radius of the cation. The calculated values for the series of ions of the present study, together with the literature values (341) for U are contained in table 11. Ion hydration, it is suggested (116) will occur only if $U - A$ is positive. For the dry condition it is seen that $U - A$ is negative for Li^+ and Mg^{2+} ions while it is positive for the other cations. Thus, according to this view, all of the ions except Li^+ and Mg^{2+} are free to hydrate at all relative pressures and the observed linear relationship between polarizability and amount adsorbed is not unexpected. The ion-surface interaction is much stronger for the excepted ions and full hydration is

Table 11. Heats of Hydration (U) and Specific Ionic Interaction Energies (A) for Various Cations.

Cation	Cation Radius (340) Å	Heat of Hydration(341) Kcal/mole	Specific Ionic Interaction Energy Kcal/mole
Li	0.60	136	138
Na	0.95	114	87
K	1.33	94	62
Rb	1.48	87	56
Cs	1.69	80	49
Mg	0.65	490	508
Ca	0.99	410	333
Sr	1.13	376	292

retarded, explaining the lower than expected amounts adsorbed for these ions. The specific ionic interaction energy A is however a function of relative pressure, decreasing as water is adsorbed. $U - A$ finally becomes positive for Li^+ and Mg^{2+} and at this point true ion hydration can occur. Although this explanation obviously depends largely upon the size of the ion, it does not invoke a special position of the cation within the clay lattice as was involved in the previous explanation of the anomalous adsorptions of the Li^+ and Mg^{2+} metahalloysites.

4.5.5 Conclusion to Section 4.5

The proposed adsorption model adequately explains the slope changes observed in the Jura-Harkins plots for water-vapour adsorbed on homoionic metahalloysites. Good agreement is obtained between the amount of water adsorbed as predicted from the model and that observed experimentally for the 'phase' change points on the Jura-Harkins graphs. That this model, which is essentially the same as that used for the kaolinite-water system, also can be applied with some success to the metahalloysite-water interaction

indicates the similarity of the two mineral surfaces.

The small ions Li^+ , Mg^{2+} and Ca^{2+} stabilise a structure which is presumed to be similar to the Hendricks and Jefferson 'net' structure. The larger cations are believed to disrupt this structure with the result that a 'phase' change occurs which corresponds to the closest-packing of the adsorbed molecules.

The anomalously low adsorptions of Li^+ and Mg^{2+} on metahalloysite may be explained as due to the control of hydration by the difference between the ion hydration energy U and the specific ionic interaction energy A . The difference $U - A$ is initially negative for these ions which indicates the large effect of the surface-ion interaction.

REFERENCES

- 1 Hofmann.U., Endell.K., Wilm.D., Angew.Chem.,
47, 539 (1934)
- 2 Mehmel.M., Z. Krist., 90, 35 (1935)
- 3 Correns.C.W., Mehmel.M., ibid 94, 337 (1936)
- 4 Grim.R.E., "Clay Mineralogy". McGraw-Hill 1968, 2nd Ed.
- 5 Brindley.G.W., Clays Clay Minerals, 14, 27 (1966)
- 6 Hendricks.S.B., Am. Mineralog., 23, 295 (1938)
- 7 Hofmann.U., Morcos.S., Schembra.F.W.,
Ber. Deutsche Keram. Ges., 39, 474 (1962)
- 8 Hendricks.S.B., Jefferson.M.E.,
Am. Mineralog., 23, 863 (1938)
- 9 Lambe.L.W., Martin.R.T.,
Highway Research Board, Proc.
34, 566 (1955)
- 10 Hughes.I.R., N.Z.J. Sci., 9, 103 (1966)
- 11 Brindley.G.W., Goodyear.J.,
Mineralog. Mag., 28, 407 (1948)
- 12 Harrison.J.L., Greenberg.S.S.,
Clays Clay Minerals, 9, 374 (1962)

- 13 Churchman.G.J., Ph.D. Thesis Univ. Otago 1970
- 14 MacEwan.D.M.C., Nature, 157, 159 (1946)
- 15 Wada.K., Am.Mineralog., 44, 1237 (1959)
- 16 Wada.K., ibid 46, 78 (1961)
- 17 Brindley.G.W., Robinson.K., Goodyear.J.,
Mineralog. Mag., 28, 423 (1948)
- 18 Brindley.G.W., Robinson.K., ibid 28, 393 (1948)
- 19 Brindley.G.W., Robinson.K.,
Discs. Faraday Soc., 42B, 198 (1946)
- 20 Honjo.G., Kitamura.N., Mihama.K.,
Clay Minerals Bull., 2, 133 (1954)
- 21 Kulbicki.G., Comptes Rendus, 238, 2405 (1954)
- 22 Chukrov.F.V., Zvyagin.B.B.,
Proc.Inter.Clay Conf., Jerusalem, 1, 11 (1966)
- 23 De Souza Santos.P., de Souza Santos.H., Brindley.G.W.,
Am. Mineralog., 50, 619 (1965)
- 24 Honjo.G., Mihama.K. Acta Cryst., 7, 511 (1954)
- 25 Zvyagin.B.B., Dokl.Akad.Nauk S.S.R., 96, 809 (1954)
- 26 Brooks.C.S., Soil Sci., 79, 331 (1955)
- 27 Brindley.G.W., "The X-ray Identification and Crystal
Structures of Clay Minerals", Editor Brown.G.,
Mineralog.Soc., London 1961 2nd Ed. Chapter 2.

- 28 Kirsch.H., Pruss.W.,
Naturewissenschaften 45, 8 (1958)
- 29 Nelson.R.A., Hendricks.S.B.,
Soil Sci., 56, 285 (1943)
- 30 Takahashi.H., Bull. Chem. Soc. Japan, 32, 17 (1959)
- 31 Gastuche.M.C., Delvigne.J., Fripiat.J.J.,
Compt. Rend. Intern. Sci.
du Sol, II 439 (1954)
- 32 Oberlin.A., Tchoubar.C.,
Comptes Rendus, 244, 1524 (1957)
- 33 Hope.E.W., Kittrick.J.A.
Am. Mineralog., 49, 859 (1964)
- 34 Von Engelhardt.W., Goldschmidt.H., Heidelberger
Beitr. Mineral. U. Petrog., 4, 319 (1954)
- 35 Kunze.G.W., Bradley.W.F.,
Clays Clay Minerals, 12, 523 (1964)
- 36 de Souza Santos.P., de Souza Santos.H., Brindley.G.W.,
Am. Mineralog., 51, 1640 (1966)
- 37 Brindley.G.W., de Souza Santos.P., de Souza Santos.H.,
ibid 48, 897 (1963)
- 38 De Pablo.L., Clays Clay Minerals, 13, 143 (1966)

- 39 Bates.T.F., Hildebrand.F.A., Swineford.A.,
Am.Mineralog., 35, 463 (1950)
- 40 Bates T.F. ibid 44, 78 (1959)
- 41 Radoslovich.E.W., ibid 48, 368 (1963)
- 42 Pundsack.F.L., Natl.Acad.Sci.Publ., 566, 129 (1958)
- 43 Parham.W.E., Clays Clay Minerals, 17, 13 (1969)
- 44 Prabhakaram.P.,
Trans. Indian Ceram.Soc., 26, 57 (1967)
- 45 Keenan.A.G., Mooney.R.W., Wood.L.A.,
J.Phys.Colloid Chem., 55, 1462 (1951)
- 46 Chukrov.F.V.,
Intern. Clay Conf., Proc. Stockholm,
2, 19 (1965)
- 47 Sudo.T., Takahashi.H.,
Natl. Acad. Sci., Publ., 456, 67 (1956)
- 48 Brindley.G.W., de Kimpe.C., Nature, 190, 254 (1961)
- 49 De Kimpe.C., Gastuche.M.C., Brindley.G.W.,
Am. Mineralog., 49, 1 (1964)
- 50 Aomine.S., Wada.K., ibid 47, 1024 (1962)
- 51 Murray.H.H., ibid 39, 97 (1954)
- 52 Ross.C.S., Kerr.P.F.,
U.S. Geol.Surv., Prof.Paper 185G, 135 (1934)

- 53 Tarasevich.Yu.I., Ovcharenko.F.D.,
Kolloid Zhur., 31, 753 (1969)
- 54 Van Olphen.H., "An Introduction to Clay Colloid
Chemistry". Interscience N.Y. 1963, p72
- 55 Range.K.J., Range.A., Weiss.A.,
Z. Naturforsch., B23, 1144 (1968)
- 56 Wada.K., Am. Mineralog., 50, 924 (1965)
- 57 Chukrov.F.V., Acad.Sci.U.S.S.R., 672pp, 1955
- 58 Beutelspacher.H., van der Marel.H.W.,
Acta Univ.Carolinae, Geol.Suppl.1, 97 (1961)
- 59 Langston.R.B., Jenne.E.A.,
Clays Clay Minerals, 9, 633 (1963)
- 60 Keller.W.D., "Soil Clay Mineralogy" Editors, Rich.C.I.,
and Kunze.G.W., pp 3-76 (1964)
- 61 Jackson.M.L., Clays Clay Minerals, 6, 133 (1959)
- 62 Brindley.G.W., Nakahira.M.,
J.Amer.Ceram.Soc., 40, 346 (1957)
- 63 Keeling.P.S., Science of Ceramics, 2, 35 (1965)
- 64 Hughes.I.R., Foster.P.K., N.Z.J.Sci., 13, 89 (1970)
- 65 Roy.R., Osborn.E.F., Am. Mineralog., 39, 853 (1954)
- 66 Harrison.J.L., Greenberg.S.S.,
Clays Clay Minerals, 9, 102 (1962)

- 67 Fripiat.J.J., ibid 12, 327 (1964)
- 68 Graham.J., Rev.Pure Applied Chem., 14, 81 (1964)
- 69 Hampel.B.F., Cutler.I.B.,
 J. Amer.Ceram.Soc., 36, 30 (1953)
- 70 Nemetschek.Th., Holmann.U.,
 Z. Naturforsch., 166, 620 (1961)
- 71 Range.K.J., Range.A., Weiss.A.,
 Intern. Clay Conf., Proc., Stockholm 1969,
 vol I, pp 3-14. Israel Univ.Press Jerusalem.
- 72 White.W.A., Illinois Geol.Survey Rept.Invest.208 (1958)
- 73 Valitskaya.V.M., Tarasevich.J.I., Ovcharenko.F.D.,
 Dzhus.E.V., Vlason.A.I., Sharkina.E.V.,
 Ukr. Khim. Zh., 34,1120 (1968)
- 74 Grim.R.E., "Applied Clay Mineralogy". McGraw-Hill
 N.Y. 1962
- 75 Martin.R.T., Clays Clay Minerals, 9, 28 (1962)
- 76 Aylmore.L.A.G., Quirk.J.P.,
 Soil Sci., 102, 339 (1966)
- 77 Ormsby.W.C., Shartsis.J.M., Woodside.K.H.,
 J. Am. Ceram. Soc., 45, 361 (1962)
- 78 Wey.R., Sieskind.O., Leiberguth.V.P.,
 Bull. Assoc. Franc. Etude Sol 1959

- 79 Fripiat.J.J., Gastuche.M.C., Vancompernelle.G.,
Trans. 5th Intern. Congr.
Soil Sci., 2, 401 (1954)
- 80 Deuvel.H., Clay Minerals Bull., 1, 207 (1952)
- 81 Russell.E.W., "Soil Conditions and Plant Growth",
9th Edition Longmans 1961
- 82 Schofield.R.K., Samson.H.R.,
Clay Minerals Bull., 2, 45 (1953)
- 83 Low.P.F. Adv. Agronomy, 13, 269 (1961)
- 84 Garrett,W.G., Walker.G.F.,
Clay Minerals Bull., 4, 75 (1959)
- 85 Uchiyama.N., Onikura.Y.,
Tohoky J. Agr. Research, 9, 213 (1959)
- 86 Green-Kelly.R., Clay Minerals Bull., 5, 1 (1962)
- 87 Panasevich.A.A., Ovcharenko.F.D.,
Dopovidi Akad. Nauk. Ukr.RSR.1964, 349
- 88 Panasevich.A.A., Ovcharenko.F.D.,
Bentonit. Gliny Chekh.Ukr., Tr.Ukr.-
Chekh Konf. Bentonitam, Uzhgorod, Ukr.SSR
1965, 75 (Pub.1966)
- 89 White.W.A., Ph.D. Thesis, Univ.Illinois (1955)
- 90 Garrett.W.G., Walker.G.F., Proc.2nd Aust.Conf.Soil
Sci. 1, 1(1957)

- 91 Weiss.A., Z.Anorg. Allgem. Chem., 297, 232 (1958)
- 92 Jurinak.J.J., J.Phys. Chem., 65, 1853 (1961)
- 93 Robertson.H.S., Brindley.G.W., Mackenzie.R.C.,
Am.Mineralog., 39, 118 (1954)
- 94 Burford.J.R., Despande.T.L., Greenland.D.J.,
Quirk.J.P., J. Soil Sci., 15, 192 (1964)
- 95 Orchiston.H.D., Soil Sci., 88, 159 (1959)
- 96 Asher.R.C., Goodman.J.F., Gregg.S.J.,
Proc. Brit. Ceram.Soc., 5, 125 (1965)
- 97 Aylmore.L.A.G., Quirk.J.P.,
Clays Clay Minerals, 9, 104 (1962)
- 98 MacEwan.D.M.C., Trans. Far. Soc., 44, 359 (1948)
- 99 Ferguson.C.B., Wade.W.H.,
J. Coll. Interf. Sci., 24, 366 (1967)
- 100 Isirikyan.A.A., Kazmenko.I.A., Kiselev.A.V.,
Koll. Zhur., 26, 675 (1964)
- 101 Brindley.G.W., Clay Minerals Bull., 2, 60 (1953)
- 102 Gregg.S.J., ibid 2, 61 (1953)
- 103 Takahashi.H., Clays Clay Minerals, 6, 279 (1959)
- 104 Churchman.G.J., Private Communication
- 105 Kelley.W.P., Jenny.H., Soil Sci., 41, 367 (1936)
- 106 Fernandez Alvarez.T., An.Edafol.Agrobiol.,
28, 285 (1969)

- 107 Komarov.V.S.; Povoroznyuk.L.I., Plyushchevskii.N.I.,
Zonov.Yu.G., Dokl.Akad. Nauk Belarusk SSR.,
9, 450 (1965)
(CA.63:17701f)
- 108 Chuzo.K., Suzuki.T., Ohashi.A.,
Mem.Sch.Sci.Eng. Waseda Univ.
Tokyo, 30, 25 (1966)
- 109 Coleman.N.T., Craig.D., Soil Sci., 91, 14 (1961)
- 110 Cashen.G.H., Nature, 197, 349 (1963)
- 111 Uskova.E.T., Vasil'ev.N.G.,
Ionity Ionnyi Obmen, Akad. Nauk SSR
Sb. Statei 1966, 53 (CA.67:85311h)
- 112 Low.P.F., Clays Clay Minerals, 8, 170 (1960)
- 113 Gerei.L., Agrokem, Talajtan Suppl., 14, 203 (1965)
- 114 Huang.P.H., Jackson.M.L.,
Soil Sci. Soc. Amer. Proc., 29, 661 (1965)
- 115 Jurinak.J.J., J. Phys.Chem., 65, 62 (1961)
- 116 Martin.R.T., Clays Clay Minerals, 6, 259 (1959)
- 117 Martin.R.T., ibid 5, 23 (1958)
- 118 Jacobs.T.H., Nature, 199, 481 (1963)
- 119 Cashen.G.H., Trans. Far. Soc., 55, 477 (1959)
- 120 Ovcharenko.F.D., Proc. Int. Clay Conf. Tokyo,
1, 585 (1969)

- 121 Douglas.L.A., Soil Sci., 103, 191 (1967)
- 122 Orchiston.H.D., ibid 87, 276 (1959)
- 123 Martin.R.T., Clays Clay Minerals, 8, 102 (1959)
- 124 Yoshinaga.N., Soil Sci., Plant
Nutr. (Tokyo), 12, 1 (1966)
- 125 Brusset.H., Ann.Chim.(Paris), 9, 477 (1954)
- 126 Mackenzie.R.C., Mineralog Soc.Gr.Brit.
Clay Mineral Bull., 115 (1950)
- 127 Jurinak.J.J., Volman.D.H.,
J. Phys.Chem., 65, 150 (1961)
- 128 Greenland.D.J., Quirk,J.P.,
Trans.Joint Meeting Comm.IV and V
Intern. Soc.Soil Sci.,79 (1962)
- 129 Kutilek ibid 88 (1962)
- 130 Emmett.P.H., Brunauer.S., Teller.E.,
J.Amer.Chem.Soc., 60, 309 (1938)
- 131 Halsey, Jr.G.D.Official Digest,
J.Paint TechnolEngl.,36, 544 (1964)
- 132 Schram.A., Trans.9th Natl.Vacuum Symp.
Amer.Vac.Soc., 301 (1962)
- 133 Lloyd.I.O., "Surface Chemistry",
Reinhold Publ.Corp.,N.Y. 1963

- 134 Gregg.S.J., Sing.K.S.W.,
"Adsorption, Surface Area and
Porosity". Academic Press
London and N.Y., 1967
- 135 Langmuir.I., J.Amer.Chem.Soc., 38, 2221 (1916)
- 136 Quirk.J.P., Aylmore.L.A.G.,
Trans.7th Intern.Congr.
Soil Sci., 2, 378 (1960)
- 137 Flood.E.A., Editor "The Solid-Gas Interface".
Edward Arnold Ltd., London.
Vol.1, 1967
- 138 Hill.T.L. J.Chem.Phys., 14, 263 (1946)
- 139 Gregg.S.J., Jacobs.J.,
Trans.Far.Soc., 44, 574 (1948)
- 140 Smith.R.N., Pierce.C.,
J.Phys.Coll.Chem., 52, 1115 (1948)
- 141 Cook.M.A. J.Amer.Chem.Soc., 70, 2925 (1948)
- 142 Barrer.R.M., Mackenzie.N., McLeod.D.,
J.Chem.Soc., 1736 (1952)
- 143 Singleton.J.H., Halsey.G.D.,
Can.J.Chem., 33, 184 (1955)
- 144 Bangham.D.H., Saweris.Z.,
Trans.Far.Soc., 34, 554 (1938)

- 145 Hagymassy, Jr. J., Brunauer. S., Mikhail. R. Sh.,
J. Coll. Interf. Sci., 29, 485 (1969)
- 146 Maggs. F. A., "Progress in Coal Science".
Editor. D. H. Bangham,
Interscience, New York, 148 (1949)
- 147 Brunauer. S., "Physical Adsorption of Gases and
Vapours", Vol. 1.
Oxford University Press 1945
- 148 Emmett. P. H., Brunauer. S.,
J. Amer. Chem. Soc., 59, 1553 (1937)
- 149 Brunauer. S., Deming. L. S., Deming. W. E., Teller. E.,
J. Amer. Chem. Soc., 62, 1723 (1940)
- 150 Voigt. E. M., Tomlinson. R. H.,
Can. J. Chem., 33, 215 (1955)
- 151 De Boer. J. H., Linsen. B. G., Osinga. Th. J.,
J. Cat., 4, 643 (1965)
- 152 De Boer. J. H., Linsen. B. G., Osinga. Th. J.,
ibid 7, 135 (1967)
- 153 Frennet. A., Disc. Far. Soc., 41, 114 (1966)
- 154 De Boer. J. H., In "The Structure and Properties of
Porous Materials". Editors
D. H. Everett, F. S. Stone, Butterworth,
London 1958, p68

- 155 Sing.K.S.W., Swallow.D.,
Proc.Brit.Ceram.Soc., 39 (1965)
- 156 Mannweiler.U., Chimia (Aarau), 20, 363 (1966)
- 157 Harris.M.R., Chem.Ind., 1295 (1967)
- 158 Beeck.O., "Advances in Catalysis", Academic
Press,N.Y. 1950 Vol.II, p.151
- 159 Haul.R.A.W., Angew.Chem., 68, 238 (1956)
- 160 Mainwaring.J., Stock.R.,
Lab.Pract., 15,752,758(1966)
- 161 Adams.T.J., Sherwood.J.N., Swinton.F.L.,
J.Chem.Soc., A, 1195 (1966)
- 162 Pierce.C., Ewing.B., J.A.C.S., 84,4070 (1962)
- 163 Pierce.C., Ewing.B.,J.Phys.Chem., 68,2562 (1964)
- 164 Campbell.K.C., Duthie.D.T.,
Trans.Far.Soc., 61, 558 (1965)
- 165 Schay.G., Periodica Polytech., 9, 187 (1965)
- 166 Koder.K., Onishi.Y.,
Bull.Chem.Soc.Japan, 33, 338 (1960)
- 167 Cannon.W.A., Nature, 197,1000 (1963)
- 168 Gaines,Jr.G.L., Cannon.P.,
J.Phys.Chem., 64, 997 (1960)
- 169 Chessick.J.J.,Sturm.J.E., J.Chem.Ed. 39, 580 (1962)

- 170 Sing.K.S.W., Swallow.D.,
J.Appl.Chem., 10, 171 (1960)
- 171 Walker.W.G., Zettlemyer.A.C.,
J.Phys.Chem., 57, 182 (1953)
- 172 Harris.M.R., Sing.K.S.W.,
Chem. and Ind., 757 (1967)
- 173 Barrer.E.P., Joyner.L.G.
Anal.Chem., 23, 791 (1951)
- 174 Isirikyan.A.A., Kiselev.A.V.,
J.Phys.Chem., 66, 205 (1962)
- 175 Kini.K.A., Lahiri.A. Fuel 39, 515 (1960)
- 176 Muller.J., Regner.A.,
Coll.Czech.Chem.Commun.30, 3399 (1965)
- 177 Kaganer.M.G., Dokl.Akad.Nauk.S.S.R., 138, 405 (1961)
- 178 De Boer.J.H., Houben.G.M.M., Lippens.B.C.,
Meys.W.A., Walrave.W.K.A. J.Cat., 1, 1 (1962)
- 179 Rao.K.S. Das.B., Current Science, 37, 274 (1968)
- 180 Bassett.D.R., Boucher.E.A., Zettlemyer.A.C.,
J.Coll.Interf.Sci., 27, 649 (1968)
- 181 Brunauer.S., Kantro.D.L., Weise.C.H.,
Can.J.Chem., 34, 729 (1956)
- 182 Brunauer.S., Kantro.D.L. Copeland.L.E.
J.A.C.S., 80, 761 (1958)

- 183 Harkins.W.D., Jura.G.,
J.Chem.Phys., 11, 430 (1943)
- 184 Harkins.W.D., Jura.G., J.A.C.S., 66,1362 (1944)
- 185 Brunauer.S., Mikhail.R.Sh., Bodor.E.E.,
J.Coll.Interf.Sci., 24, 451 (1967)
- 186 Orchiston.H.D., Soil Sci., 79, 71 (1955)
- 187 Aristov.B.G., Kiselev.A.V.,
Zhur.Fiz.Khim., 37,2520 (1963)
- 188 Kiselev.A.V., Disc.Far.Soc., 40, 205 (1965)
- 189 Aristov.B.G., Kiselev.A.V.,
Zhur.Fiz.Khim., 38,1984 (1964)
- 190 Barrer.R.M. Proc.Brit.Ceram.Soc., 5, 120 (1965)
- 191 Brennan.D., Graham.M.J., Hayes.F.H.,
Nature, 199,1152 (1963)
- 192 Malden.P.J., Marsh.J.D.
J.Phys.Chem., 63,1309 (1959)
- 193 Ainscough.J.B., Nature, 195,1089 (1962)
- 194 Haynes.J.M., J.Phys.Chem., 66, 182 (1962)
- 195 Rhodin.T.N., J.A.C.S., 72,5691 (1950)
- 196 Lopez-Gonzalez.J.DeD., Carpenter.F.G., Deitz.V.R.,
J.Phys.Chem. 65,1112 (1961)
- 197 Emmett.P.H. "Catalysis" Reinhold N.Y. 1954,vol.I

- 198 Voet.A., Colloq.Nationaux Centre
Natl.Rech.Sci. 24, 72 (1963)
- 199 Jura.G., Harkins.W.D., J.A.C.S., 68, 1941 (1946)
- 200 Thomas.J.M., Nature 189, 134 (1961)
- 201 Wolfe.R., Sams.J.R.,
J.Phys.Chem., 69, 1129 (1965)
- 202 Dubinin.M.M., Zhukovskaya.E.G., Murdmaa.K.O.,
Russ.J.Phys.Chem., 37, 218 (1963)
- 203 Dubinin.M.M., Adv.Coll.Interf.Sci., 2, 217 (1968)
- 204 Dubinin.M.M., J.Coll.Interf.Sci., 23, 487 (1967)
- 205 Bering.B.P., Dubinin.M.M., Serpinsky.V.V.,
J.Coll.Interf.Sci., 21, 378 (1966)
- 206 Dollimore.D., Heal.G.R., Nature, 208, 1092 (1965)
- 207 Lamond.T.G., Marsh.H., Carbon, 1, 281 (1964)
- 208 Bye.G.C., Robinson.J.G., Sing.K.S.W.,
J.Appl.Chem., 17, 138 (1967)
- 209 Kini.K.A., J.Phys.Chem., 68, 217 (1964)
- 210 Ganguli.N.C., Mukherjee.P.N., Lahiri.A.,
Fuel, 40, 525 (1961)
- 211 Anderson.R.B., Hofer.L.J.E., Bayer.J.,
Fuel, 41, 559 (1962)
- 212 Kini.K.A., Fuel, 42, 103 (1963)

- 213 Dellyes.R., J.Chim.Phys., 60, 1008 (1963)
- 214 Marsh.H., Wynn-Jones.W.F.K.,
Carbon, 1, 269 (1964)
- 215 Atkins.J.H., Carbon, 3, 299 (1965)
- 216 Moreau.C., C.R.Acad.Sci.(Paris), 253, 2044 (1961)
- 217 Barrett.E.R., Joyner.L.G., Halenda.P.H.
J.Amer.Chem.Soc., 73, 373 (1951)
- 218 Delon.J., Dellyes.R.,
C.R.Acad.Sci.(Paris) D265, 1661 (1967)
- 219 Lippens.B.C., Linsen.B.G., de Boer.J.H.,
J.Cat., 3, 32 (1964)
- 220 De Boer.J.H., Lippens.B.C., ibid, 3, 38 (1964)
- 221 De Boer.J.H., Lippens.B.C., ibid, 3, 44 (1964)
- 222 Aylmore.L.A.G., Quirk.J.P.,
J.Soil Sci., 18, 1 (1967)
- 223 Anderson.R.B.,
Ed."Experimental Methods in
Catalytic Research", Academic Press
N.Y., 1968
- 224 Broekhoff.J.C.P., de Boer.J.H.,
J.Cat., 10, 391 (1968)
- 225 Harris.M.R., Chem.Ind., 268 (1965)

- 226 Orr.R.G., Branion.R., Lielmezs.J. ibid 1250 (1968)
- 227 Orr.Jr.C., Dallavale.J.M.,
"Fine Particle Measurement",
MacMillan Co.N.Y. 1959
- 228 Fedyakin.N.N., Zh.Fiz.Khim., 36, 1450 (1962)
- 229 Spencer.D.H.T., Fereday.F.,
Chem.Ind., 847 (1968)
- 230 Broekhoff.J.C.P., de Boer.J.H.,
J.Cat., 10, 153 (1968)
- 231 Broekhoff.J.C.P., de Boer.J.H.,
ibid 10, 368 (1968)
- 232 Broekhoff.J.C.P., de Boer.J.H.,
ibid 10, 377 (1968)
- 233 Broekhoff.J.C.P., de Boer.J.H.,
ibid 9, 15 (1967)
- 234 Broekhoff.J.C.P., de Boer.J.H.,
ibid 9, 8 (1967)
- 235 Derjaguin.B.V.,
Proc.Intern.Congr.Surface
Activity, 2nd London 1957,2, 153 (1957)
- 236 Derjaguin.B.V.,
Acta Physicochem.U.S.S.R.12, 18 (1960)

- 237 Irving.J.P., Butt.J.B.,
J. Appl. Chem., 15, 139 (1965)
- 238 Emig.G., Hofmann.H., J. Cat., 8, 303 (1967)
- 239 Pierce.C., J. Phys. Chem., 72, 3673 (1968)
- 240 Codenhead.D.E., Everett.D.H.,
S.C.I., Conf. Industrial Carbon
and Graphite, London 1957
- 241 Brunauer.S., Mikhail.R.Sh., Bodor.E.E.,
J. Coll. Interf. Sci., 25, 353 (1967)
- 242 De Boer.J.H.,
Proc. Brit. Ceram. Soc., 5, 114 (1965)
- 243 Foster.A.G., J. Phys. Coll. Chem., 55, 638 (1951)
- 244 De Boer.J.H., van den Heuvel.A., Linsen.B.G.,
J. Cat., 3, 268 (1964)
- 245 Mikhail.R.Sh., Brunauer.S., Boder.E.E.,
J. Coll. Interf. Sci. 26, 45 (1968)
- 246 De Boer.J.H., Linsen.B.G., van der Plas.Th.,
Zondervan.G.J., J. Cat., 4, 649 (1965)
- 247 De Boer.J.H., Proc. Brit. Ceram. Soc. 5, 5 (1965)
- 248 De Boer.J.H., Lippens.B.C., Linsen.B.G.,
Broekhoff.J.C.P., van den Heuvel.A.,
Osinga.Th.J.,

- J. Coll. Interf. Sci. 21, 405 (1966)
- Lippens. B.C., de Boer. J.H.,
J. Cat., 4, 319 (1965)
- 250 Ernsberger. F.M., Rev. Sci. Instr., 24, 998 (1953)
- 251 Sing. K.S.W., Chem. Ind. 829 (1967)
- 252 Payne, D.A., Sing. K.S.W., ibid 918 (1968)
- 253 Carruthers. J.D. ibid 1772 (1968)
- 254 Bye. G.C., Sing. K.S.W., ibid 1139 (1967)
- 255 Mikhail. R.Sh., Copeland. L.E., Brunauer. S.,
Can. J. Chem., 42 426 (1964)
- 256 Mikhail. R.Sh., J. Chem. U.A.R., 6, 27 (1963)
- 257 Sing. K.S.W., Chem. Ind., 44, 1520 (1968)
- 258 Cutting. P.A., Sing. K.S.W.,
Chem. Ind., 268 (1969)
- 259 Harris. M.R., Sing. K.S.W.,
Proc. Intern. Congr. Surface
Activity, 3rd Cologne 1960 2, 42 (1960)
- 260 Kuchkaeva. I.K.,
Vesta Akad. Navuk Belarusk. SSR
Ser. Khim. Navuk, 3, 22 (1966)
(CA 66: 49538h)
- 261 Ermolenko. N.F., Efros. M.D. ibid 1, 21 (1966)
(CA 65: 288f)

- 262 Sing.K.S.W., Madeley.J.D.,
J.Appl.Chem., 4, 365 (1954)
- 263 Holmes.H.F., Fuller.E.L.Jr., Secoy.C.H.,
J.Phys.Chem., 72, 2293 (1968)
- 264 Everett.D.H., "The Solid-Gas Interface",
Editor E.A.Flood, volume II,
chapter 36. Edward Arnold, London 1967
- 265 Holmes.J.M., Beebe.R.A.,
J.Phys.Chem., 61, 1684 (1957)
- 266 Van Olphen.J., J.Coll.Sci., 20, 882 (1965).
- 267 Brooks.C.S., Soil.Sci., 99, 182 (1965)
- 268 Ovcharenko.F.D., Tarasevich.Yu.I., Valitskaya.V.M.
Koll.Zhurn. 29, 712 (1967)
- 269 Barrer.R.M., McLeod.D.M.,
Trans.Far.Soc., 50, 980 (1954),
51, 1290 (1955)
- 270 Barrer.R.M., Reay.J.S.S.,
Clay Minerals Bull. 3, 214 (1957)
- 271 Fiat.D., Folman.M., Garbatski.U.,
Proc.Roy.Soc., A260, 409 (1960)
- 272 Thorp.J.M.,
Trans.Far.Soc., 55, 442 (1959)

- 273 Saunders.G.A., Ubblehode.A.R., Young.D.A.,
Proc.Roy.Soc., A271, 499 (1963)
- 274 Mering.J., Trans.Far.Soc., 42B, 205 (1946)
- 275 Day.R.E., Parfitt.G.D., *ibid*, 63 708 (1967)
- 276 Mooney.R.W., Keenan.A.G., Wood.L.A.,
J.A.C.S., 74, 1371 (1952)
- 277 Hirst.W., Discs.Far.Soc., 3, 26 (1948)
- 278 Ross.R.A., Taylor.A.H.,
Proc.Brit.Ceram.Soc., 5, 167 (1965)
- 279 Arnell.J.C., McDermot.H.L.,
Proc.2nd Intern.Conf.Surface Activity
1957, 113
- 280 De Boer.J.H., 'The Dynamical Character of
Adsorption' Oxford. 1953, 224
- 281 Folman.M., Yates.D.J.C.
Trans.Far.Soc., 54, 1684 (1958)
- 282 Isirikyan.A.A., Kiselev.A.V., Ushakova.E.V.,
Koll.Zhurn., 27, 690 (1965)
- 283 Ganichenko.L.G., Dubinin.M.M., Zaverina.E.D.,
Kiselev.A.V., Krasil'nikov.K.G.,
Izv.Akad.Nauk SSSR, Otd.Khim.
Nauk 1535 (1960) (CA56: 14957h)

- 284 Kiselev.A.V., Shcherbakova.K.D.,
Abhandl.Deut.Akad.Wiss.Berlin,
Kl.Chem.,Geol.,Biol., 207 (1962)
(CA 59: 8151d)
- 285 Aristov.B.G., Kiselev.A.V.,
Zh.Fiz.Khim., 37,2520 (1963)
- 286 Shcherbakova.K.D., Kataliz v Vysshei Shkole,
Min.Vysshego i Srednego Spets. Obrazov.
SSSR, Tr. 1-go (Pervogo) Mezhvuz.
Soveshch. po Catalizu 1958, Pt 2, 31 - 7
(CA 59:12210e)
- 287 Uytterhoeven.J.,
Bull.Groupe Franc.Argiles.10, 69 (1963)
- 288 Young.J.E., 'Clay-Water Systems'.
Editor W.G. Lawrence. Alfred University,
Alfred, New York, 1965. Chapter 15
- 289 Wade.W.H., Hackerman.N.,
J.Phys.Chem., 63,1639 (1959)
- 290 Sposito.G., Babcock.K.L.,
Clays Clay Minerals, 14, 133 (1966)
- 291 Sposito.G., Ph.D. Thesis Univ.California,
Berkeley 1965

- 292 Linzey.J., Pers. Comm.
- 293 Jackson.M.L., 'Soil Chemical Analysis'
Constable and Co.Ltd., London, 1958
p.294
- 294 Fiegl.F., 'Qualitative Analysis by Spot Tests'.
Second Edition 1939 p.179
Elsevier, London
- 295 Linzey.J., Pers.Comm.
- 296 Percival.H.J., Ph.D. Thesis. Univ.Victoria
New Zealand 1969
- 297 Emmett.P.H., Adv.Colloid Sci. 1, 3 (1942)
- 298 Salman.T., Robertson.R.F.,
Can.Mining Met.Bull., 1088 (1965)
- 299 Melville.H., Gowenlock.B.G.,
'Experimental Methods in Gas Reactions'
p 198 (1964). Macmillan, London
- 300 Nelson.S.M., Huang.H.H., Sutton.L.E.,
Trans.Far.Soc., 65, 225 (1969)
- 301 Loebenstein.W.V., Deitz.V.R.,
J.Chem.Phys., 15, 687 (1947)
- 302 Macey.M.H.,
Trans.Brit.Ceram.Soc., 41, 73 (1942)

- 303 Bower.C.A., Truog.E.,
Ind.Eng.Chem., Anal.Ed., 12, 411 (1940)
- 304 McDermot.H.L., Arnell.J.C.,
Can.J.Chem., 34, 1114 (1956)
- 305 Barrer.R.M., Reay.J.S.S.,
Proc.2nd Intern.Conf.Surface Activity,
vol.II, p.79 Butterworth, London 1957
- 306 Gallego.A., I.O.N., 27, 61 (1967)
- 307 Aylmore.L.A.G., Quirk.J.P.,
Nature, 187, 1046 (1960)
- 308 Foster.A.G., J.Chem.Soc., 1806 (1952)
- 309 Foster.A.G., Trans.Far.Soc. 28, 645 (1932)
- 310 Linsen.B.G., van den Heuvel.A.,
'The Solid-Gas Interface'
Editor E.A. Flood, vol.2, chapter 35,
Edward Arnold, London, 1967.
- 311 Forslind.E., Trans. 1st Intern.Ceram.
Congr., 98 (1948)
- 312 Sing.K.S.W., Proc.Brit.Ceram.Soc. 5, 114 (1965)
- 313 Murray.P., White.J.,
Trans.Brit.Ceram., 54, 137 (1955)
- 314 Brindley.G.W., Goodyear.J.,
Mineralog.Mag. 28, 203 (1948)

- 315 Alexanian.C., Morel.P., Le Bouffant.L.,
Bull.Soc.Franc.Ceram. 71, 3 (1966)
- 316 Gregg.S.J., Stephens.M.J.,
J.Chem.Soc., 156, 3951 (1953)
- 317 Mellor.J.W., Holdcroft.A.D.,
Trans.Brit.Ceram.Soc., 10, 94 (1911)
- 318 Brindley.G.W., Nakahira.M.,
Clays Clay Minerals, 5, 266 (1958)
- 319 Zalevskii.N.I., Prir.Sorbenty, Sb.Dokl.Sess.
Nauch.Sov.Sin., Izuch.Primen.
Adsorbentov Akad.Nauk SSR, Vladivostok
112 (1966) (CA69:90132w)
- 320 Ovcharenko.F.D., Panasevich.A.A., Kazansky.V.M.,
Dokl.Akad.Sci.Ukr.SSR, 1492 (1963)
- 321 Brusset.H., Le Rat.B., Makki.M.,
Annales de Chim., 19, 31 (1954)
- 322 Vaughan.F., Brit.CeramRes.Assn.Spec.Publ.13(1956)
- 323 Brown.M.J., Gregg.S.J.,
Clay Min. Bull., 1, 228 (1952)
- 324 Freund.F., Ber.Deutsch.Keram.Ges. 44, 5 (1967)
- 325 Butt.Yu.M., Stroit Materiali Silikat
Prom., 6, 4 (1965)
(CA63:10780b)

- 326 Gregg.S.J., 'Surface Chemistry of Solids'.
Chapman and Hall, London. 1951 Chap.IV
- 327 Roy.R., Roy.D.M., Francis.E.E.,
J.Amer.Ceram.Soc., 38, 198 (1955)
- 328 Barshad.I., Am.Mineralog., 34, 675 (1949)
- 329 Enright.D.P., Weyl.W.A.,
J.Appl.Phys. 21, 338 (1950)
- 330 Rios.E.G., Vivaldi.J.L.M.,
Trans. 4th Intern.Cong.Soil Sci.,
vol.2, 67 (1950)
- 331 Ovcharenko.F.D., Panasevich.A.A., Kazansky.V.M.,
Dokl.Akad.Sci.Ukr.SSR, 1492 (1963)
- 332 Rao.K.S., J.Phys.Chem., 45, 500, 513 (1941)
- 333 Pierce.C., Smith.R.N. ibid 54, 784 (1950)
- 334 Low.P.F., Soil Sci.Soc.Amer.Proc., 22, 395 (1958)
- 335 Hendricks.S.B., Nelson.R.A., Alexander. L.T.,
J.A.C.S., 62, 1457 (1940)
- 336 Anderson.D.M., Low.P.F.,
Soil Sci.Soc.Amer.Proc. 22, 99 (1958)
- 337 Rowland.R.A., Weiss.E.J., Bradley.W.F.,
Clays Clay Minerals, 4, 85 (1956)
- 338 Grtner.J.W., Z.Krist. 83, 75 (1932)

- 339 White.W.A., Pichler.E.,
Illinois State Geol.Survey Circ.266
(1959)
- 340 Bingham.E.C., J.Phys.Chem., 45, 885 (1941)
- 341 Bernal.J.D., Fowler.R.H.,
J.Chem.Phys., 1, 515 (1933)
- 342 Everett.D.H., Whitton.W.I.,
Trans.Far.Soc., 48, 749 (1952)
- 343 Jurinak.J.J., Soil Sci.Soc.Amer.Proc.,
27, 269 (1963)
- 344 Lawrence.W.G., 'Clay-Water Systems',
Editor Lawrence.W.G. Alfred University,
Alfred, New York. 1965 Chapter III

APPENDIX I

Details of Platinum Resistance Element Calibration

All correspondence to be
addressed to:
THE DIRECTOR

In reply please
Quote Ref No

PEL 131/8/-
ZSG/AC



DEPARTMENT OF SCIENTIFIC AND INDUSTRIAL RESEARCH
PHYSICS AND ENGINEERING LABORATORY

Telephone 699 199
Cables and Telegrams: PHYSICAL.

Private Bag,
Lower Hutt, New Zealand.

14 October 1969

Report on: Platinum resistance thermometer element.
Forwarded by: University of Canterbury, Department of Chemistry.
Particulars: Platinum wound element, glass insulated.
Nominal resistance at 0°C, 100 ohms.

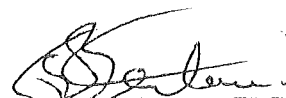
The element was calibrated by comparisons with a Laboratory Standard platinum resistance thermometer in a well stirred water bath, and at 0°C in melting ice.

The figures tabulated below lie on a quadratic curve computed from the observed values of resistance at various temperatures between 0° and 100°C.

Temperature °C	t ₆₈	Resistance ohms
0		99.970 ± 0.005 ohms
5		101.926
10		103.878
15		105.827
20		107.772
25		109.714
30		111.652
35		113.587
40		115.518
45		117.446
50		119.370
55		121.291
60		123.209
65		125.122
70		127.033
75		128.940
80		130.843
85		132.743
90		134.640
95		136.533
100		138.423

The Scale in use at the Laboratory is the International Practical Temperature Scale of 1968.


Z.S. Garvitch
Senior Technical Officer


W.S. Bertaud
for Director

The quadratic curve from which the above points were calculated is:-

$$\frac{R_t}{R_0} = 1 + At + Bt^2$$

where $A = 3.9159 \times 10^{-3}$ and
 $B = -6.95 \times 10^{-7}$.

APPENDIX II

Prediction of 'Phase' Changes According to the Adsorption Model Proposed for Metahalloysite.

Stages of the Adsorption Model

Stage 1 - two water molecules per active site on the oxygen surface and one per site on the hydroxyl surface corresponds to 6.48 mg water/g clay.

Stage 2 - three water molecules per cation site corresponds to 2.16 mg. water/g clay.

Stage 3 - a triad of water molecules is completed at each active site. A further 6.48 mg water/g clay is adsorbed.

Let the oxygen surface active site be defined as OS, the hydroxyl surface site as HA and the cation site as CS.

Lithium - metahalloysite.

1st slope change at $P/P_0 = 0.174$

Stage 1 + stage 2 = 8.64 mg water/g clay

2nd slope change at $P/P_0 = 0.316$

Stage 1 + Stage 2 = 8.64 " " "

add 1 water molecule/HA = 2.16 " " "

10.80 " " "

Potassium-metahalloysite.

1st slope change at $P/P_0 = 0.115$

Stage 1 + Stage 2 = 8.64 " " "

2nd slope change at $P/P_0 = 0.403$

Stage 1 + Stage 2 = 8.64 " " "

Stage 3 = 6.48 " " "

ion hydration 1 molecule/cation = 0.72 " " "

15.84 " " "

Rubidium-metahalloysite

1st slope change at $P/P_0 = 0.124$

Stage 1 + Stage 2 = 8.64 mg water/g clay

2nd slope change at $P/P_0 = 0.432$

Stage 1 + stage 2 = 8.64 " " "

Stage 3 = 6.48 " " "

ion hydration 2 molecules/cation = 1.44 " " "16.56 " " "

Cesium -metahalloysite

1st slope change at $P/P_0 = 0.125$

Stage 1 + Stage 2 = 8.64 " " "

Magnesium-metahalloysite

2nd slope change at $P/P_0 = 0.306$

Stage 1 + Stage 2 = 8.64 " " "

add 1 water molecule/HA = 2.16

ion hydration 10 molecules/cation = 3.60 " " "14.40 " " "

Calcium-metahalloysite

1st slope change at $P/P_0 = 0.172$

Stage 1 + Stage 2 = 8.64 " " "

ion hydration 8 molecules/cation = 2.88 " " "11.52 " " "2nd slope change at $P/P_0 = 0.313$

stage 1 + stage 2 = 8.64 " " "

add 1 water molecule/HA = 2.16 " " "

ion hydration 12 molecules/cation = 4.32 " " "15.12 " " "

Strontium-metahalloysite

1st slope change at $P/P_0 = 0.175$

stage 1 + stage 2	=	8.64	mg	water/g	clay
ion hydration 4 molecules/cation	=	<u>1.44</u>	"	"	"
		10.08	"	"	"
		<hr/>			

2nd slope change at $P/P_0 = 0.419$

stage 1 + stage 2	=	8.64	"	"	"
stage 3	=	6.48	"	"	"
ion hydration 8 molecules/cation	=	<u>2.88</u>	"	"	"
		18.0	"	"	"
		<hr/>			

The model also predicts slope changes for sodium, cesium and magnesium clays as follows:-

Sodium metahalloysite

1st slope change at $P/P_0 \sim 0.14$

stage 1 + stage 2	=	8.64	mg	water/g	clay
ion hydration 1 molecule/cation	=	<u>0.72</u>	"	"	"
		9.36	"	"	"
		<hr/>			

2nd slope change at $P/P_0 \sim 0.35$

stage 1 + stage 2	=	8.64	"	"	"
stage 3	=	6.48	"	"	"
ion hydration 3 molecules/cation	=	<u>2.16</u>	"	"	"
		17.28	"	"	"
		<hr/>			

Cesium metahalloysite

2nd slope change at $P/P_0 \sim 0.48$

stage 1 + stage 2	=	8.64	"	"	"
stage 3	=	6.48	"	"	"
ion hydration, 2 molecules/cation	=	<u>1.44</u>	"	"	"
		16.56	"	"	"
		<hr/>			

Appendix II, cont.

Magnesium metahalloysite

1st slope change at $P/P_0 \sim .16$

stage 1 + stage 2 = 8.64 mg water/g clay

ion hydration, 6 molecules/cation = 2.16 " " "

10.80 " " "

APPENDIX III

MODEL 44 PS VERSION 3, LEVEL 3 DATE 70237

```
C            GENERAL PROGRAMME FOR THE CALCULATION OF ISOTHERM DATA
C            *****
          INTEGER D,E
          DIMENSION PB(90),PEQM(90),TV(90),TVEQM(90),PO(90),VOL(90),VOLEQM(9
          20),VA(90),VAT(90),VG(90),TCTN2(90),VOLACD(90),DELN2(90),VD(90),VL(
          390),PR(90),Y(90),L(90),D(90),T1(90),T2(90),HGFAC1(90),HGFAC2(90),P
          4TC(90),PTC(90),SVP(90),VDOS(90),TITLE(20),AMOLS(90),X(90),Z(20),F(
          520),G(20),GG(20),FG(20),DY(20),DYY(20)
565 WRITE(6,665)
665 FORMAT(////40(' *'))
      READ(5,666,END=13)TITLE
666 FORMAT(20A4)
      WRITE(6,667)TITLE
667 FORMAT(//20A4)
165 READ(5,99,END=13)A,TB,SAM,WS,N,FT,VDOSAD,VFS,TA,PZERO
99  FORMAT(F5.2,2F6.1,F7.4,I3,F7.4,F8.3,F6.3,F6.1,F6.3)
      WRITE(6,97)A,TB,SAM,WS,N,FT,VDOSAD,VFS,TA,PZERO
97  FORMAT(/F5.2,2F6.1,F7.4,I3,F7.4,F8.3,F6.3,F6.1,F6.3)
      WRITE(6,52)
52  FORMAT(/7CH            P            DELN2            TOTN2            PR            VG            P/V(PO-P)
      1                            )
      K=0
      SUMX=0.0
      SUMXX=0.0
      SUMXY=0.0
      SUMY=0.0
      SUMYY=0.0
      SUMGG=0.0
      SUMDYY=0.0
C
C            HELIUM CALIBRATION
252 READ(5,252)DCSV,PTCHE,PTOHE,THE1,THE2,HGFAC3,HGFAC4,PZHE
      FORMAT(F8.3,2F7.3,2F5.1,2F8.5,F7.3)
      PT1=(PTCHE-PZHE)*HGFAC3
      PT2=(PTOHE-PZHE)*HGFAC4
      VOLHE1=(DOSV/TB+VFS/(THE1+TA))*PT1*FT
      VOLHE2=(DOSV/TB+VFS/(THE2+TA))*PT2*FT
      FD=(VOLHE1-VOLHE2)/PT2
C
      DO 5 J=1,N
      READ(5,115)T1(J),T2(J),HGFAC1(J),HGFAC2(J),PTC(J),PTO(J),SVP(J),VD
105  OS(J),L(J),D(J)
115  FORMAT(2F5.1,2F8.5,3F7.3,F8.3,2I2)
      VOL(J)=VDOS(J)/(TB+VFS/(TA+T1(J)))
      VOLEQM(J)=VDOS(J)/TB+VFS/(TA+T2(J))
      VOLACD(J)=VDOSAD/TB+VFS/(TA+T1(J))
      PB(J)=(PTC(J)-PZERC)*HGFAC1(J)
      PEQM(J)=(PTC(J)-PZERC)*HGFAC2(J)
      PO(J)=SVP(J)*HGFAC2(J)
```

Appendix III cont.

MODEL 44 PS VERSION 3, LEVEL 3 DATE 70237

```
TV(J)=VOLADD(J)*PB(J)*FT
TVEQM(J)=VCLEQM(J)*PEQM(J)*FT
TOTN2(1)=TV(1)
IF(J-1)27,26,27
27 IF(D(J)-1)28,24,29
28 DELN2(J)=(PB(J)-PEQM(J-1)*VOLEQM(J-1)/VCL(J))*VOL(J)*FT
GO TO 25
29 DELN2(J)=(PB(J)-PEQM(J-1)*VCLEQM(J-1)/VCLACD(J))*VOLADD(J)*FT
GO TO 25
24 DELN2(J)=0.0
25 TOTN2(J)=TOTN2(J-1)+DELN2(J)
26 CONTINUE
DELN2(1)=TOTN2(1)
VD(J)=FD*PEQM(J)*(1.0+A*PEQM(J)/76.0)
VU(J)=TVEQM(J)+VD(J)
VA(J)=TOTN2(J)-VL(J)
VG(J)=VA(J)/hS
PR(J)=PEQM(J)/PO(J)
IF(L(J)-1)41,40,41
41 WRITE(6,95)J,PEQM(J),DELN2(J),TOTN2(J),PR(J),VG(J),Y(J)
95 FORMAT(1X,I2,F7.3,2F9.3,F7.4,F8.3,F11.7,            'CES')
GC TO 5
40 IF(PR(J)-0.05) 42,150,150
150 IF(PR(J)-0.30)151,151,42
151 Y(J)=PR(J)/(VG(J)*(1.0-PR(J)))
K=K+1
SUMX=SUMX+PR(J)
SUMY=SUMY+Y(J)
SUMYY=SUMYY+Y(J)*Y(J)
SUMXY=SUMXY+PR(J)*Y(J)
SUMXX=SUMXX+PR(J)**2
GO TO 10
42 Y(J)=0.0
10 WRITE(6,98)J,PEQM(J),DELN2(J),TOTN2(J),PR(J),VG(J),Y(J)
98 FORMAT(1X,I2,F7.3,F9.3,F9.3,F7.4,F8.3,F11.7,            'ADS')
5 CONTINUE
WRITE(6,96)K
96 FORMAT(' K=',I2)
IF(K-2)15,15,14
C
C    CALCULATION OF SURFACE AREA
14 B=(SUMXY-(SUMX*SUMY)/K)/(SUMXX-(SUMX**2)/K)
XBAR=SUMX/K
YBAR=SUMY/K
A=YBAR-B*XBAR
WRITE(6,30)B
30 FORMAT('/' SLOPE='',F9.6)
WRITE(6,32)A
32 FORMAT(' INTERCEPT='',F9.6)
```

Appendix III cont.

MODEL 44 PS VERSION 3, LEVEL 3 DATE 70237

```
CAPMCN=1.0/(A+B)
SAADS=SAM*CAPMCN*6.023/22.414
WRITE(6,114)CAPMCN
114 FORMAT(/' NITROGEN MONDLAYER CAPACITY=',F6.2'CC STP/GM')
WRITE(6,12)SAADS
12 FORMAT(' ADSORPTION SURFACE AREA =',F9.2,'SQ METRES/GRAM')
CADS=(A+B)/A
WRITE(6,11)CADS
11 FORMAT(' BET CONSTANT CADS =',F7.2)

C
C CALCULATION OF CORRELATION COEFFICIENT
TL=(SUMXY/K)-XBAR*YBAR
BL1=(SUMXX/K)-XBAR**2
BL2=(SUMYY/K)-YBAR**2
R=TL/(SQRT(BL1)*SQRT(BL2))
WRITE(6,144)R
144 FORMAT(' CORRELATION COEFFICIENT=',F6.3)
DO 60 J=1,N
IF(L(J)-1)60,65,60
65 IF(PR(J)-0.05)60,66,66
66 IF(PR(J)-0.30)67,67,60
67 G(J)=PR(J)-XBAR
GG(J)=G(J)**2
SUMGG=SUMGG+GG(J)
DY(J)=Y(J)-YBAR
DYY(J)=DY(J)**2
SUMDYY=SUMDYY+DYY(J)
60 CONTINUE
SS=(SUMDYY-B**2*SUMGG)/(K-2)
P=SS*(1.0/(K-2)+XBAR**2/SUMGG)
Q=SS/SUMGG
PERRS=100*Q/B
PERRI=100*P/A
WRITE(6,7)
7 FORMAT(/' ERROR ESTIMATES')
WRITE(6,111)PERRS
111 FORMAT(' PERCENT ERROR IN SLOPE=',F6.4)
WRITE(6,112)PERRI
112 FORMAT(' PERCENT ERROR IN INTERCEPT=',F6.4)
ERRSA=((P+Q)/(A+B))*SAADS
PERRSA=((P+Q)/(A+B))*100.0
WRITE(6,23)ERRSA
23 FORMAT(' ERROR IN SPECIFIC SURFACE AREA=',F9.3'SQ METRES/GM')
WRITE(6,113)PERRSA
113 FORMAT(' PERCENT ERROR IN SPECIFIC SURFACE AREA=',F8.4)
15 GO TO 565
13 STOP
END
```

Appendix III cont.

Explanation of names used

PB	- Pressure in burette-free space system (cm.Hg) upon addition of gas
P0	- Saturation vapour pressure
PEQM	- Pressure in system at equilibrium
VA	- Volume of gas adsorbed (cc at S.T.P.)
VU	- " " " unadsorbed (cc at S.T.P.)
VD	- Volume of gas in the dead space at equilibrium(cc at S.T.P.)
VG	- Volume adsorbed per gram solid (cc at S.T.P./g)
VFS	- Calibrated volume of the free space (cc)
PR	- Relative vapour pressure
Y	- B.E.T. function
TB	- Burette temperature °K
T1	- Free space temperature at time of gas addition(°C)
T2	- " " " " " " equilibrium (°C)
A	- Van der Waals correction factor
WS	- Sample weight (g)
SAM	Molecular cross-sectional area (\AA^2)
N	- Total number of data cards
VDOS	- Volume of burette not filled with mercury
CAPMON	- Monolayer capacity (cc. S.T.P./g)
SAADS	- Specific surface area (m^2/g)
HGFAC	- Correction factor to correct observed pressures to standard values at 0°C
TA	273.2°K
PZERO	- Zero reading of manometer (cm)
PTC	- Pressure in burette-free space with sample bulb tap closed
PTO	- As above, tap open
FD	- Dead space correction factor
DELN2	- Increment(or decrement) in volume of gas (cc.S.T.P.)
TOTN2	- Total amount of gas in adsorption system(cc S.T.P.)
L	- Numeral to signify whether adsorption or desorption point, L = 1 for adsorption, L = 0 for desorption
D	- Numeral to denote whether gas addition or subtraction was carried out or not. D = 0, gas addition or subtraction, D = 1, no gas added or subtracted D = 2, gas added or subtracted from the system together with a change in the volume of dosing bulbs filled with mercury.

APPENDIX IV

Water Vapour Sorption Data for 'Natural' and Homoionic Metalloxyites
at 36.20°C

P/P_0	Lithium $X^* \mu\text{m}/\text{m}^2$	Sodium $X^* \mu\text{m}/\text{m}^2$	'Natural' ($< 10\mu$) $X^* \mu\text{m}/\text{m}^2$
<u>Adsorb from $X=0$</u>			
0.027	7.0	7.8	6.9
0.073	11.4	11.9	10.7
0.109	12.6	13.7	12.2
0.140	13.7	15.0	13.2
0.177	14.8	16.4	14.6
0.216	16.0	18.0	16.1
0.269	17.5	19.8	18.2
0.317	19.1	21.8	19.9
0.369	20.9	23.5	22.5
0.415	22.3	25.8	24.1
0.467	24.1	28.0	25.8
0.512	26.0	30.2	28.3
0.574	29.3	33.8	31.6
0.633	32.6	38.0	35.3
0.694	37.3	44.3	39.8
0.748	43.5	51.0	47.2
0.793	51.7	59.1	54.7
0.861	67.2	75.5	71.0
0.936	104.4	111.6	112.1
0.984	142.8	149.8	158.0
0.996	176.4	205.4	230.3
<u>Desorb from $X > 150$</u>			
0.972	141.5	155.4	171.5
0.941	129.0	131.7	135.7
0.874	108.3	110.0	106.4
0.835	94.7	96.8	91.2
0.789	79.2	81.9	75.3
0.722	62.8	65.6	59.9
0.659	49.0	51.9	47.9
0.568	39.0	41.9	39.1
0.525	35.4	38.0	35.7
0.432	29.2	31.7	29.8
0.370	24.6	26.7	24.8
0.292	21.4	23.2	21.2
0.229	19.0	20.7	18.5
0.171	16.9	18.3	16.4
0.114	14.3	15.4	13.6
0.068	11.7	12.6	11.3
0.046	10.0	10.8	9.6
0.031	8.1	9.1	8.0
0.018	6.5	7.6	6.2

* micromoles/metre²

Appendix IV cont

<u>P/P₀</u>	Lithium	Sodium	'Natural' (< 10 μ)
<u>Readsorb from X = 0</u>			
0.105		13.2	11.8
0.222		18.5	17.0
0.335		22.7	21.0
0.461		27.8	26.2
0.579		34.4	32.1
0.718		46.8	43.4
0.857		74.5	70.5
<u>Desorb from X \approx 75</u>			
0.846		70.9	66.6
0.831		68.6	63.8
0.816		66.1	61.8
0.787		62.0	57.6
0.749		57.2	53.1
0.704		52.6	48.3
0.663		48.0	44.5
0.614		44.1	40.5
0.557		39.2	36.5
0.504		35.5	33.2
0.451		32.3	30.6
0.428		30.8	29.3
0.402		29.4	27.8
0.378		27.5	25.7
0.359		26.1	24.3
0.261		22.1	20.7
0.168		18.4	16.9
0.072		13.0	12.3
0.028		9.5	8.2
<u>Readsorb from X \approx 10</u>			
0.060		11.7	10.3
0.130		15.4	14.0
0.294		21.8	20.6
0.348		24.0	22.5
0.482		30.0	28.3
<u>Desorb from X \approx 30</u>			
0.430		28.1	26.2
0.385		26.3	24.6
0.330			22.9
0.276		22.2	21.0
0.225		20.6	18.8

Appendix IV cont.

P/P ₀	Potassium	Rubidium	Cesium
<u>Adsorb from X=0</u>			
0.025	7.4	7.6	7.7
0.057	10.2	10.5	9.7
0.084	11.5	12.0	11.2
0.106	12.7	13.1	12.5
0.133	13.7	14.1	13.9
0.154	14.3	15.0	14.7
0.180	15.3	15.7	15.4
0.230	16.7	17.3	16.9
0.276	18.3	19.0	18.7
0.319	20.0	20.8	20.0
0.382	22.5	23.2	21.9
0.447	24.8	26.1	24.6
0.514	28.2	28.9	27.8
0.592	32.3	33.4	33.0
0.657	37.3	38.7	38.1
0.727	43.3	44.5	43.6
0.787	52.3	53.5	52.2
0.832	61.4	63.6	60.8
0.873	71.9	73.6	71.8
0.903	86.9	87.8	87.4
0.928	102.6	103.7	102.9
0.943	138.7	141.6	146.0
<u>Desorb from X > 200</u>			
0.899	118.2	121.9	121.8
0.875	108.7	111.6	110.2
0.824	92.4	95.3	91.8
0.775	76.5	79.1	76.1
0.705	59.0	61.9	60.2
0.663	50.1	53.5	52.6
0.596	41.3	44.9	43.7
0.545	36.2	39.5	39.1
0.479	31.4	34.4	34.2
0.413	27.8	30.5	31.1
0.355	24.3	26.6	26.9
0.271	20.6	22.8	23.8
0.209	18.0	20.4	20.8
0.135	14.8	16.9	18.0
0.093	13.0	15.4	16.1
0.076	11.7	13.8	14.9
0.045	9.6	12.1	12.7
0.019	7.9	10.1	10.7
0.007	2.6	4.5	7.3
<u>Readsorb from X > 0</u>			
0.017	6.0	7.2	8.8
0.044	8.7	10.4	11.4
0.072	10.6	12.2	12.8
0.111	12.7	14.2	15.2
0.198	15.9	17.2	17.6

Appendix IV cont

P/P ₀	Potassium	Rubidium	Cesium
0.283	18.4	20.2	20.4
0.406	23.2	25.0	25.7
0.507	27.7	29.6	29.9
0.635	35.0	40.0	36.9
0.742	45.4	47.1	47.0
0.798	55.3	57.3	56.8
0.866	72.3	74.1	73.0
0.919	98.7	100.0	98.9
<u>Desorb from X > 200</u>			
0.971	164.1	166.5	171.1
0.908	121.6	125.3	127.4
0.813	87.8	91.7	89.9
0.690	56.2	58.6	58.2
0.524	35.7	37.6	39.0
0.312	22.5	24.9	26.2
0.169	16.6	18.1	18.9
0.087	12.7	13.6	15.4

P/P ₀	Sodium	Natural < 10 μ TMCS treated, p74	P/P ₀	Lithium
<u>Adsorb from X = 0</u>			<u>Adsorb from X=0</u>	
0.004	4.2	3.5	0.011	5.0
0.027	7.9	7.6	0.032	7.8
0.051	10.1	9.3	0.056	9.4
0.088	12.4	11.1	0.083	11.2
0.125	14.0	12.7	0.104	12.3
0.166	15.8	14.6	0.128	13.4
0.206	17.5	16.1	0.156	14.1
0.254	19.3	18.3	0.193	15.4
0.375	23.3	22.9	0.232	16.8
0.486	28.4	28.6	0.330	20.3
0.605	35.6	35.8	0.469	25.3
0.723	47.2	47.8	0.586	30.9
0.838	68.4	70.8	0.680	37.1
			0.762	46.9
			0.826	57.5
<u>Desorb from X > 200</u>			0.908	84.5
0.955	140.0	170.3	0.944	119.2
0.859	104.2	116.3		
0.749	72.0	76.4		
0.625	47.4	49.6		
0.449	32.8	32.2		
0.399	29.5	28.4		
0.352	26.0	26.0		
0.283	22.4	22.3		
0.203	18.8	18.8		
0.134	16.2	15.5		
0.070	12.6	12.6		
0.034	9.8	9.8		
0.014	6.6	7.2		

Appendix IV cont.

P/P ₀	Magnesium	Calcium	Strontium
<u>Adsorb from X = 0</u>			
0.013	6.6	6.9	6.5
0.046	10.4	11.3	10.4
0.073	13.0	13.6	12.7
0.103	14.6	15.2	13.9
0.128	16.2	16.6	15.0
0.155	17.3	17.7	16.4
0.177	18.4	19.3	17.7
0.212	19.9	20.9	18.8
0.250	21.7	22.8	20.6
0.306	24.5	26.2	23.2
0.364	26.6	28.2	26.1
0.444	30.3	32.1	30.5
0.513	33.4	35.4	34.2
0.584	37.8	40.2	38.9
0.645	42.6	44.8	43.4
0.723	50.3	52.6	51.3
0.794	60.9	63.4	62.1
0.867	81.0	84.5	82.5
0.927	114.1	116.5	114.1
0.995	239.3	237.9	231.6
<u>Desorb from X > 200</u>			
0.976	185.0	188.9	185.7
0.963	160.7	165.1	163.2
0.933	140.6	145.0	110.2
0.876	117.5	121.8	120.7
0.824	98.4	103.3	101.7
0.755	76.8	73.6	81.0
0.672	58.5	62.2	61.3
0.592	47.2	50.2	50.0
0.494	39.1	41.5	41.0
0.446	36.5	38.5	38.1
0.426	35.2	37.6	37.4
0.397	33.2	35.0	34.6
0.360	30.8	32.2	31.1
0.330	38.9	30.3	29.1
0.258	25.7	26.5	25.0
0.174	21.7	22.2	22.0
0.099	18.0	17.6	18.0
0.060	14.7	14.8	15.0
0.033	12.2	12.2	12.4
0.014	9.1	9.1	9.4